

University of Strathclyde

Department of Pure and Applied Chemistry

Development of Lysine-Targeted Irreversible Inhibitors of PI3K δ

Thesis submitted to the University of Strathclyde in fulfilment
of the requirements for the degree of Doctor of Philosophy

by

Samuel E. Dalton

2018



Declaration of Copyright

This thesis is the result of the author's original research. It has been composed by the author and has not been previously submitted for examination which has led to the award of a degree.

The copyright of this thesis belongs to the author under the terms of the United Kingdom Copyright Acts as qualified by University of Strathclyde Regulation 3.50. Due acknowledgement must always be made of the use of any material contained in, or derived from, this thesis.

Samuel E. Dalton

Signed:

Date:

Abstract

Targeted covalent inhibition of poorly conserved cysteine residues for kinase inhibition has increased in popularity over recent years. Whilst these inhibitors are often highly successful, studies have shown that only ~40% of human kinases are amenable to this approach. Furthermore, cysteine point-mutations present common resistance mechanisms to these drugs. This thesis explores the concept of targeting the catalytically essential lysine of the kinase, which is conserved throughout the human kinome, for selective covalent inhibition. The validity of this approach is exemplified with the lipid kinase phosphoinositide 3-kinase delta (PI3K δ), as it has been implicated in a range of diseases, and is not amenable to traditional cysteine-targeting.

An activated ester motif was identified that was able to covalently modify this lysine residue, on non-selective scaffolds. These scaffolds were then optimised by exploration of the hinge-binder, back-pocket, and electrophilic warhead to afford a series of indazole-based inhibitors that showed nanomolar potency and >100-fold selectivity in biochemical assays. The best series of inhibitors were then progressed to a full kinetic analysis to understand the mechanism of binding to PI3K δ . The lead inhibitor, possessing a *para*-fluorophenolic ester warhead, showed evidence of target engagement in CD4+ T-cells in the sub-nanomolar range with an extended duration of action. Additionally, this inhibitor showed minimal off-target engagement in chemoproteomic studies in Ramos cells.

In summary, this thesis discloses the development of the first selective irreversible inhibitor of PI3K δ . This supports the hypothesis that covalent inhibition of kinases can be achieved by targeting a highly conserved lysine residue, opening the door to covalent targeting of kinases not possessing reactive cysteine residues. Additionally, this inhibitor may have applications in the design of long-acting therapeutics for kinase-mediated diseases. Finally, this concept may also offer a way of overcoming cysteine point-mutations as an acquired resistance mechanism to currently available targeted covalent inhibitors.

Acknowledgements

A significant number of people have provided support to me throughout this PhD, both scientifically and personally, and I am incredibly grateful to all of them, even if I have not been able to name them explicitly here.

Firstly, I would like to thank my GSK-based PhD supervisor Dr Sébastien Campos (GSK) for his commitment to my training, enthusiasm, support, wit, and scientific rigour. In a similar vein, I also thank Prof John Murphy (UoS) for his academic supervision and advice throughout the project. Your combined contributions have led me to produce a piece of work that I am immensely proud of. Additionally, the co-authors of the paper associated with this work have been key to its scientific progression throughout – thank you to Lars Dittus, Daniel Thomas, Máire Convery, Joao Nunes, Jacob Bush, John Evans, Thilo Werner and Marcus Bantscheff.

Outside of the direct science, I would like to thank several other individuals at GSK and UoS for their impact on my PhD experience, professionally. Firstly, Prof Harry Kelly and Prof William Kerr, for setting up this collaborative scheme, offering me a position, and supporting my development throughout. Additionally, I would like to thank Andrea Malley for her administrative support. I am also very grateful to Vipul Patel for having me in his department, providing ample opportunities for scientific and professional development, and allowing me to venture out and explore the more biological aspects to this project. Thanks also go to Nicole Hamblin, Zoe Henley, David House, Eric Talbot, Sophie Bertrand and Ken Down for providing scientific input and advice throughout this project, especially for external presentations and for reviews of the paper.

On the technical side, there are numerous individuals who have invested time and effort in training me, as well as answering the many questions I had as a chemist attempting biology. I am incredible grateful for the time these individuals have been able to spare, and the skills and knowledge that they have taught me. In particular (in no particular order), Nick Barton, Collette Chitty, Peter Francis, Laurie Gordon, Neil Hodnett, Sandra Kumper, Sean Lynn, James Rowedder, Emma Sherriff, Helen Taylor, Darren Poole, Andrew Cansfield, Jon Hutchinson, Henrik Johansson and Ali Roberts.

There are many individuals that have made this an enjoyable experience, and kept my spirits up during stressful times. Firstly, I'd like to thank the rest of my PhD cohort - Julien

Vantourout, Joe Dixon, Jason Williams, Rob Griffiths, Jonathan Spencer, Julia Hyslop, James Sanderson and Marie-Pierre Dreanic. It's been a pleasure working alongside all of you, and I hope our paths cross again. Many of the graduate employees, industrial placement students, and apprentices at GSK have also contributed to an enjoyable workplace that I have enjoyed coming to for the last 3.5 years. Particular individuals of note include Jack Coward, Andrew Baxter, Grant McGonagle, Henry Blackwell, Vikki Clayton, Luke Green, and all members of the Flexible Discovery Unit in labs 2S110 and 2S156 from 2014-2018 that are too numerous to name individually.

I have been very fortunate over this PhD to undertake two secondment opportunities. The first was to the Murphy Lab at UoS for 4 months. I would like to thank the members of the Murphy Lab that I interacted with whilst I was there for making it a thoroughly enjoyable experience - Giuseppe Nocera, Andrew Smith, Anthony McDonagh, Florimond Cumine, Simon Rohrbach, Jude Arokianathar, Katie Emery, Allan Young, Mark Allison, and Josh Barham. The Mac Robertson Travel Scholarship then funded another 3-month secondment to the Cravatt Lab at The Scripps Research Institute in La Jolla, California. I am incredibly grateful to the University of Glasgow for providing this funding through the Scholarship, and to Prof Ben Cravatt for welcoming me into his lab for this time. Additionally, I would like to thank particular members of his lab and the TSRI community for scientific advice, training, beach trips and surfing lessons – Chris Parker, Micah Niphakis, John Teijaro, Melissa Dix, Kim Masuda, Chris Joslyn, Ektarina Vinogradova, Esther Kemper, Armand Cognetta, Liron Bar-Peled, Kenneth Lum, and Thomas Wucherpennig.

I would also like to thank my parents, Julie and Simon Dalton, for your pride and providing of endless support to my endeavours, despite not having a clue what I really do! My final acknowledgment is reserved for my other half, Georgina. Without your support throughout this process – from writing my initial application, through two secondments, one paper, plenty of practice presentations, ranting about my scientific problems, and many late nights and weekends on my laptop – I would not have made it to where I am.

Contents

ABSTRACT	II
ACKNOWLEDGEMENTS	III
CONTENTS	V
ABBREVIATIONS	VII
1. INTRODUCTION	1
1.1 COVALENT BONDS IN DRUG DISCOVERY AND CHEMICAL BIOLOGY	1
1.1.1 <i>Background</i>	1
1.1.2 <i>Achieving Covalent Inhibition</i>	5
1.2 KINASES IN COVALENT DRUG DISCOVERY	10
1.2.1 <i>The Kinome</i>	10
1.2.2 <i>Phosphoinositide 3-Kinases</i>	13
1.3 <i>Project Aims</i>	16
2. DISCOVERY OF COVALENT PI3Kδ PROBES	18
2.1 PI3K δ INHIBITOR CHEMOTYPES	18
2.1.1 <i>Reversible Binders</i>	18
2.1.2 <i>Covalent Binders</i>	24
2.2 INVESTIGATION OF HINGE-BINDING GROUPS	27
2.2.1 <i>DHP vs Indazole Hinge Binders</i>	28
3. OPTIMISATION OF IRREVERSIBLE BINDERS	44
3.1 EXPLORING THE SELECTIVITY POCKET WITH A BASIC AMINE.....	44
3.1.1 <i>Molecular Modelling</i>	45
3.1.2 <i>Synthesis</i>	47
3.1.3 <i>Biological Characterisation</i>	52
3.2 EFFECTS OF VARYING THE ELECTROPHILIC CENTRE.....	57
3.2.1 <i>Molecular Modelling of Sulfur Electrophiles and Synthesis</i>	58
3.2.2 <i>Medicinal Chemistry of Sulfur-based Electrophiles</i>	62
3.3 VARIATION OF THE BACK-POCKET BINDING GROUP	64
3.3.1 <i>Synthesis of Indole-containing Activated Esters</i>	66
3.3.2 <i>Medicinal Chemistry of the Indole Compounds</i>	68
3.4 VARIATION OF THE ELECTRONICS OF THE PHENYL LEAVING GROUP	70
3.4.1 <i>Medicinal Chemistry Data for Varying of the Leaving Group</i>	71
4. FURTHER BIOLOGICAL CHARACTERISATION	76
4.1 KINETIC ANALYSIS OF BINDING, AND MECHANISTIC IMPLICATIONS	76
4.2 SPECIFICITY OF THE COVALENT INTERACTION	83

4.3	SELECTIVITY PROFILE OF ESTER 60	87
4.3.1	<i>Kinetic Selectivity Analysis at Closely Related Isoforms</i>	87
4.3.2	<i>Wider Kinome Selectivity Analysis Under Biochemical Conditions</i>	92
4.3.3	<i>Proteome-wide Determination of Off-Targets of Compound 60</i>	93
4.3.4	<i>Phenotypic Consequences of Covalent PI3Kδ Inhibition</i>	105
5.	CONCLUSIONS AND FUTURE DIRECTIONS	109
5.1	CONCLUSION	109
5.2	FUTURE WORK.....	112
6.	EXPERIMENTAL	115
6.1	SUMMARY OF BIOLOGICAL ASSAYS USED	115
6.1.1	<i>Biochemical TR-FRET Assay</i>	115
6.1.2	<i>Human Whole-blood Assay</i>	117
6.1.3	<i>Kinetic Assay</i>	118
6.1.4	<i>Proteomics</i>	119
6.2	BIOLOGY AND COMPUTATIONAL	122
6.2.1	<i>Isolated Enzyme Assay</i>	122
6.2.2	<i>Human Whole-blood Assay</i>	123
6.2.3	<i>HPLC Reactivity Assays</i>	123
6.2.4	<i>X-Ray Crystallography</i>	125
6.2.5	<i>Kinetic Binding Assay at PI3Kδ</i>	126
6.2.6	<i>Intact Protein Mass Spectrometry</i>	131
6.2.7	<i>Jump Dilution Experiment</i>	132
6.2.8	<i>Kinetic Binding Assay at PI3Kα and PI3Kβ</i>	134
6.2.9	<i>Wider-kinome Selectivity Screening</i>	135
6.2.10	<i>In-lysate Binding Assay for Probe 131</i>	139
6.2.11	<i>Proteomic In-cell Selectivity Analysis of Compound 60</i>	140
6.2.12	<i>Cellular Washout Experiment</i>	143
6.2.13	<i>Computational Modelling</i>	144
6.3	SYNTHETIC CHEMISTRY	146
7 –	REFERENCES	204

Abbreviations

σ_p	Hammett substituent constant
ABPP	Activity-based protein profiling
AcOH	Acetic acid
ADP	Adenosine diphosphate
AlCl ₃	Aluminium trichloride
Arg, R	Arginine
Asp, D	Aspartic acid
ATM	Ataxia telangiectasia mutated serine/threonine protein kinase
ATP	Adenosine triphosphate
Bpin	4,4,5,5-Tetramethyl-1,3,2-dioxaborolane
BSA	Bovine serum albumin
BTK	Bruton's tyrosine kinase
CDK	Cyclin dependent kinase
CHAPS	3-[(3-Cholamidopropyl)dimethylammonio]-1-propanesulfonate
COPD	Chronic obstructive pulmonary disease
COX-2	Cyclooxygenase 2
CPME	Cyclopentyl methyl ether
CuAAC	Copper-catalysed azide-alkyne cycloaddition
Cys, C	Cysteine
DBCO	Dibenzocyclooctyne
DCC	<i>N,N'</i> -Dicyclohexylcarbodiimide
DCDMH	1,3-Dichloro-5,5-dimethylhydantoin
DCM	Dichloromethane
DDM	<i>N</i> -dodecyl- β -D-maltoside
DHP	Dihydropyran
DIPEA	<i>N,N</i> -Diisopropylethylamine
DMAP	4-Dimethylaminopyridine
DMF	<i>N,N</i> -Dimethylformamide
DMSO	Dimethylsulfoxide
DNA-PK	DNA-dependent protein kinase
DTT	Dithiothreitol
EDTA	Ethylenediaminetetraacetic acid
EGFR	Epidermal growth factor receptor
ELISA	Enzyme-linked immunosorbent assay
ERK	Extracellular signal-related kinases
EtOAc	Ethyl acetate
EtOH	Ethanol
FAAH	Fatty acid amide hydrolase
FAC	Final assay concentration
FAD	Flavin adenine dinucleotide
FBS	Foetal bovine serum

FDA	United States Food and Drug Administration
FGFR	Fibroblast growth factor receptor
FP	Fluorophosphate
FRET	Förster resonance energy transfer
FSBA	5'-(4-Fluorosulfonylbenzoyl)adenosine
Glu, E	Glutamic acid
GPCR	G-coupled protein receptor
GRP	General receptor of phosphoinositides
GSH	Glutathione
GST	Glutathione S-transferase
HATU	1-[Bis(dimethylamino)methylene]-1H-1,2,3-triazolo[4,5-b]pyridinium 3-oxid hexafluorophosphate
HEPES	4-(2-Hydroxyethyl)-1-piperazine ethanesulfonic acid
His, H	Histidine
HMBC	Heteronuclear multiple bond correlation spectroscopy
HOBt	Hydroxybenzotriazole
HPLC	High-performance liquid chromatography
HRMS	High-resolution mass spectrometry
HSQC	Heteronuclear single quantum correlation spectroscopy
hWB	Human whole-blood
IA	Iodoacetamide
IEDDA	Inverse electron-demand Diels-Alder
IFN γ	Interferon gamma
Ile, I	Isoleucine
IPA	Isopropanol
Itk	Interleukin-2-inducible tyrosine kinase
JAK	Janus kinase
KHF ₂	Potassium bifluoride
K_i	Concentration of irreversible inhibitor required to achieve the half-maximal rate of covalent inactivation under the applied conditions
K_i	Thermodynamic inhibition constant for rapid reversible binding, corrected for ATP concentration
K_i^{app}	Apparent thermodynamic inhibition constant for rapid reversible binding, not corrected for ATP concentration
k_{inact}	Rate constant for inactivation
K_M	Michaelis constant that describes the concentration of substrate required to achieve half the maximal enzyme turnover rate
k_{off}	Rate of dissociation of a ligand from an enzyme-ligand complex
k_{on}	Rate of association of free ligand and enzyme to form the reversibly bound enzyme-inhibitor complex
LCMS	Liquid chromatography-mass spectrometry
LC-MS/MS	Liquid chromatography-tandem mass spectrometry
LiAlH ₄	Lithium aluminium hydride
Lys, K	Lysine
MDAP	Mass directed automated preparative HPLC

Me	Methyl
MeOH	Methanol
Met, M	Methionine
MS	Mass spectrometry
MSD	Mesoscale Discovery
mTOR	Mammalian target of rapamycin
MudPIT	Multidimensional Protein Identification Technology
NaHCO ₃	Sodium bicarbonate
NaOH	Sodium hydroxide
<i>N</i> -Boc-Lys	<i>N</i> _α -(tert-Butoxycarbonyl)-L-lysine
NH ₄ OH	Ammonium hydroxide
NHS	<i>N</i> -Hydroxysuccinimide
nM	Nanomolar
NMM	<i>N</i> -Methylmorpholine
NMP	<i>N</i> -Methyl-2-pyrrolidone
NMR	Nuclear magnetic resonance
PAGE	Polyacrylamide gel electrophoresis
PBMC	Peripheral blood monocyte
PBS	Phosphate-buffered saline
PdCl ₂ (dppf)	[1,1'-Bis(diphenylphosphino)ferrocene]dichloropalladium(II)
PEG	Polyethylene glycol
Perm	Permeability
PFP	Pentafluorophenol
PH	Pleckstrin homology
Ph ₂ SiH ₂	Diphenylsilane
PI	Phosphoinositides
PI3K	Phosphatidylinositol-3-kinase
pIC ₅₀	Negative natural log of the half maximal inhibitory concentration
PIPkins	Phosphatidylinositolphosphate kinases
PKC	Protein kinase C
Plk	Polo-like kinase
pM	Picomolar
PMHS	Polymethylhydrosiloxane
Pro, P	Proline
PtdIns	Phosphatidylinositol
PtdIns(3,4,5)P ₃	Phosphatidylinositol-3,4,5-trisphosphate
PtdIns(4)P ₁	Phosphatidylinositol-4-phosphate
PtdIns(4,5)P ₂	Phosphatidylinositol-4,5-bisphosphate
PTEN	Phosphatase and tensin homolog
pX	Negative natural logarithm of X
PyBOP	Benzotriazol-1-yl-oxytripyrrolidinophosphonium hexafluorophosphate
RhH(CO)(PPh ₃) ₃	Tris(triphenylphosphine)rhodium carbonyl hydride

rmsd	Root-mean-square deviation
RPMI 1640	Roswell Park Memorial Institute 1640 medium
RSK2	p90 Ribosomal S6 kinase-2
rt	Room temperature
s.d.	Standard deviation
s.e.m	Standard error of the mean
SAR(s)	Structure Activity Relationship(s)
SCX	Strong cation-exchange
SDS	Sodium dodecyl sulfate
Ser, S	Serine
SHIP1/SHIP2	SH2-containing inositol phosphatase 1/2
SILAC	Stable Isotope Labelling in Culture
SM	Starting material
SNAr	Nucleophilic aromatic substitution
SPAAC	Strain-promoted azide-alkyne cycloadditions
Strep-APC	Streptavidin-allophycocyanin
STP	Sulfotetrafluorophenyl
T3P®	Propylphosphonic anhydride
TBTA	Tris[(1-benzyl-1H-1,2,3-triazol-4-yl)methyl]amine
TCEP	Tris-(2-carboxyethyl)phosphine
TCO	<i>trans</i> -Cyclooctene
TCP	2,4,6-Trichlorophenol
TEAB	Tetraethylammonium bicarbonate
TFA	Trifluoroacetic acid
THF	Tetrahydrofuran
THP	Tetrahydropyran
Thr, T	Threonine
TMSCl	Trimethylsilyl chloride
TMT	Tandem mass tag
TR-FRET	Time-resolved Förster resonance energy transfer
TrkA	Tropomyosin receptor kinase A
Trp, W	Tryptophan
Ts	Tosyl
Tyr, Y	Tyrosine
Val, V	Valine
XPhos palladacycle	Chloro(2-dicyclohexylphosphino-2',4',6'-triisopropyl-1,1'-biphenyl)[2-(2-aminoethyl)phenyl]palladium(II)
ZAK	Sterile alpha motif- and leucine zipper-containing kinase
Zn(OAc) ₂	Zinc acetate

1. Introduction

1.1 Covalent Bonds in Drug Discovery and Chemical Biology

1.1.1 Background

Covalent inhibition is not a novel concept. The well-known analgesic, Aspirin **1**, is arguably the first covalent inhibitor in modern medicine, originally marketed in 1899, followed by the penicillin antibiotics **2** in the mid-1940s (**Figure 1**).¹ These drugs act by covalently binding to a serine residue of their target enzymes, however their mechanisms are subtly different. **1** acetylates serine 530 (Ser530) near the active sites of cyclooxygenase-2 (COX-2), with loss of the salicylic acid backbone of the drug,² whilst the β -lactam of **2** covalently attaches to a serine residue (Ser36) in the active site of penicillin binding protein 1B, disrupting efficient bacterial cell wall synthesis.^{3,4} Both modifications prevent binding of the natural substrate to the active site, inactivating the enzymes. Acetylation of COX-2 is irreversible, thus the enzyme is permanently inactivated, whilst the ester formed by penicillins is reversible, and is slowly hydrolysed to an inactivated β -lactam and the active enzyme.^{2,3} This illustrates the difference between *reversible* covalent inhibition, and *irreversible* covalent inhibition. Irreversible covalent inhibition forms the focus of this thesis, due to the early proof-of-concept nature of the project. (*i.e.* Proving the existence of an irreversible covalent bond is far more facile than proving a transient reversible bond.) Nevertheless, there are notable advantages to the reversible targeting approach,^{5,6} which are expanded on in the context of lysine-targeting PI3K δ inhibitors in the conclusion of this thesis, and may warrant further investigation.

One of the main advantages of the irreversible covalent approach in drug discovery is duration of action.^{1,7} An irreversible inhibitor will maintain its pharmacological effect until the target protein is resynthesised, which may be advantageous if this rate is slow.¹ This can lead to a very long duration of action due to decoupling of pharmacokinetics (how the body affects the drug) and pharmacodynamics (how the drug affects the body), and therefore less frequent, lower doses for patients.^{1,8} Other advantages of covalent targeting include prevention of drug resistance when targeting catalytic residues, as mutation of the residue will often offer no biological advantage, and exquisite potency and selectivity when targeting isoform-specific residues.^{9,10} However, there is also a risk of toxicity associated with unselective covalent binding of the reactive, often electrophilic, functional groups^{6,10-15}.

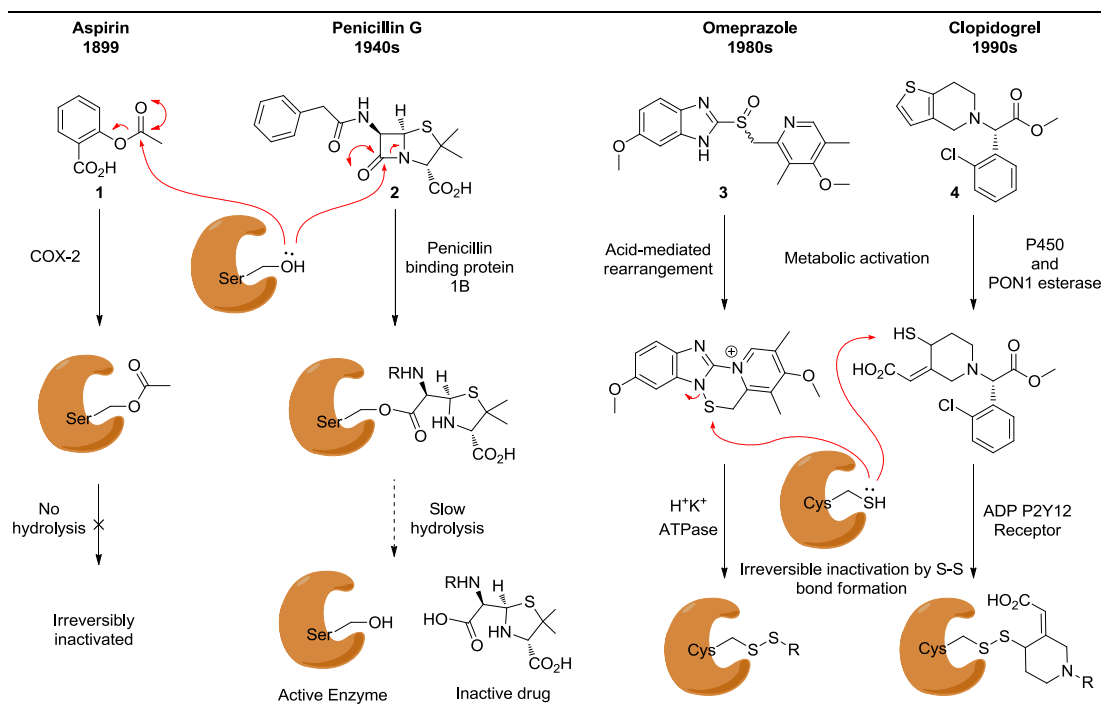


Figure 1 – Blockbuster irreversible drugs Aspirin, Penicillin, Omeprazole and Clopidogrel. Aspirin and Penicillin antibiotics react with serine residues at their target enzymes. For Aspirin, this results in irreversible acetylation of this residue, whereas the penicillin modification is reversible, and slowly hydrolysed to release the active enzyme. Omeprazole and Clopidogrel are both metabolically converted into a reactive metabolite that forms an irreversible disulfide bond with the target enzyme. Importantly, the covalent mechanisms of action of these drugs were discovered after the drugs were marketed.

Despite trepidation, numerous covalent inhibitors are being discovered and entering the market.¹⁴ Recent blockbuster drugs include the proton pump inhibitor omeprazole **3**,¹⁶ and the antiplatelet clopidogrel **4** (**Figure 1**).¹⁷ In both of these cases, the administered drug is converted into a reactive metabolite which reacts with a cysteine residue in the target enzyme (**Figure 1**) (H⁺K⁺ ATPase for omeprazole,¹⁸ and the ADP P2Y₁₂ receptor for clopidogrel^{10,19}). Importantly, a considerable number of these historic covalent drug molecules were discovered by serendipity and their mode of action was only elucidated years after their discovery.^{1,20} Recent advances in the design and development of covalent drugs have contributed to understanding the factors required to achieve selective irreversible inhibition of a biological target.^{1,8,9,21,22} This approach to targeted covalent inhibitors has proved successful with the recent approval of two covalent kinase inhibitors, Afatinib **5** and Ibrutinib **6**, to treat patients with metastatic non-small cell lung cancer, and mantle cell lymphoma, respectively.^{23–26} Both target active site cysteine residues near the ATP binding site of the kinases - **5** targets the receptor tyrosine kinase epidermal growth factor receptor (EGFR),²⁷ and **6** targets Bruton’s tyrosine kinase (BTK).²⁸ Additionally, covalent inhibition can provide a method of binding to typically “undruggable” targets, such as the oncogenic

protein KRAs which is implicated in a significant proportion of non-small-cell lung cancer patients.^{29–31}

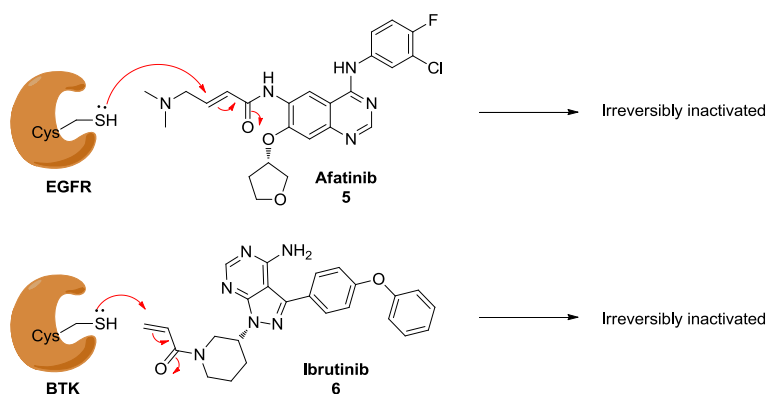


Figure 2 – Structures and targets of Afatinib and Ibrutinib, the two first “targeted covalent inhibitors”. In both cases, a cysteine residue near the ATP binding pocket of the targeted kinases reacts with the α,β -unsaturated system of the inhibitor to afford a covalent adduct.

In addition to the pharmacological benefits of covalent inhibitors, the ability to form covalent bonds with proteins is of immense importance in the development of chemical probes (**Figure 3**). These compounds are often not suited to use as a drug, but find themselves as tools to further understand the biology of a specific protein, such as cyclin dependent kinases (probes **7** and **8**),^{32,33} ATP-binding proteins (probes **10** and **11**)³⁴ and epigenetic proteins (probe **12**).^{35,36} In addition, chemical probes can be used to rapidly access target selectivity by competition binding assays. A notable example of this is the KiNativ platform developed by Patricelli and Cravatt.³⁷ This platform utilises lysine-reactive ATP and ADP probes (compounds **10** and **11**, respectively) that bind to almost all kinase active sites covalently. Using this approach, two probes can identify and quantify kinome selectivity of a compound using chemoproteomics.^{38,39} Furthermore, this technology has been expanded to other classes of enzymes, such as the serine hydrolase family by invoking a similar concept of pan-hydrolase inhibitor that has a serine-reactive covalent warhead (probe **13**).^{40,41} Finally, broader methods aimed at identifying reactive lysine (probes **14** and **15**),⁴² methionine (probe **16**),⁴³ and cysteine (probe **17**)⁴⁴ residues in entire proteomes, have also been disclosed in the literature.

A common theme with the above techniques is the presence of a reactive functional group, that could, in theory, covalently bind non-specifically to multiple proteins. This may be desired, in the case of profiling reactive amino acids and entire families of proteins, however it may cause toxic effects if applied to drug discovery. Additionally, particular protein targets may not be prone to forming covalent bonds with a reactive inhibitor due to a lack of a

suitable amino acid. This may prevent observation of an off-target interaction by typical gel or chemoproteomic readouts. To circumvent this, photoaffinity probes present another viable method of introducing covalency in the chemical biology and chemical probe arena (**Figure 3**). These molecules contain unreactive functionalities such as diazirines (general probe **18**), which become activated upon exposure to UV light, forming a carbene which inserts into nearby bonds.⁴⁵ This provides a snapshot of that compound's interactions at a particular moment in time, and can be used to elucidate off-target binding, protein targets of phenotypic screening hits, and novel binding pockets on proteins using fragments for lead discovery.^{46–48}

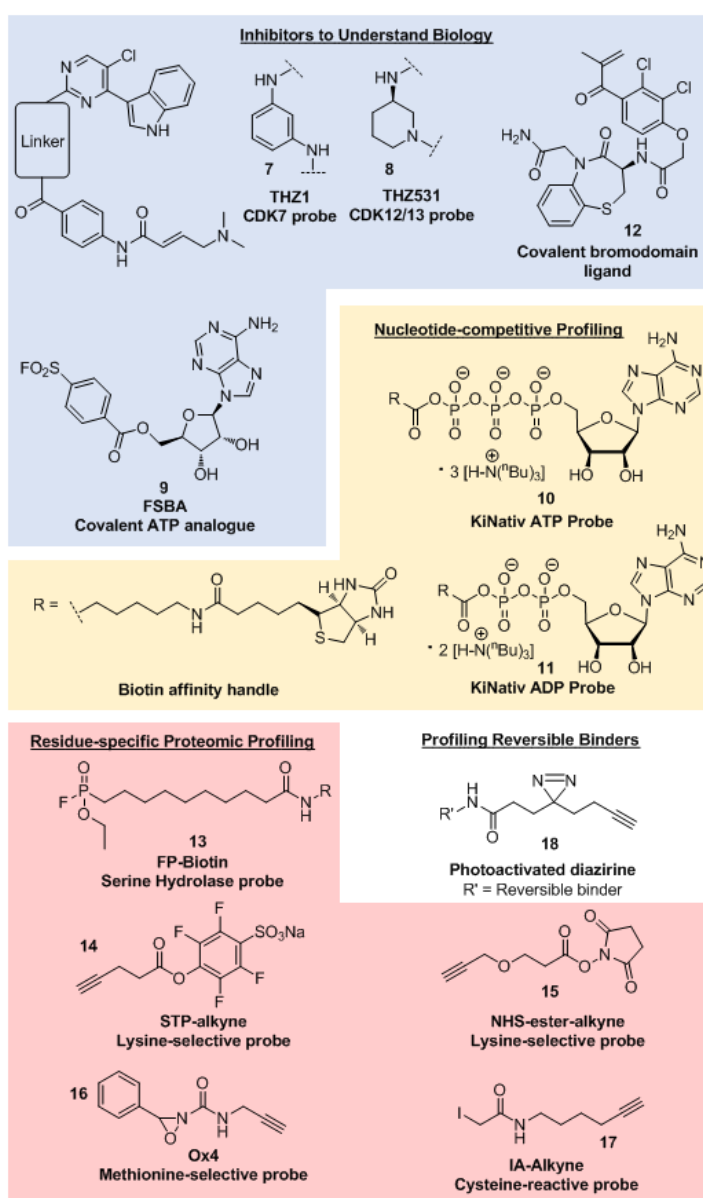


Figure 3 – Selected examples of small molecules that form covalent bonds to proteins, and their applications to chemical biology.

This thesis focusses on the application of electrophilic warheads to specifically target one amino acid in one protein, amongst the milieu of biological nucleophiles. The aim is initially to demonstrate that this is possible at the desired target, and then optimise this compound into a probe, and potentially a drug-like molecule. As the final compound may eventually be used *in vivo*, photoaffinity-based methods were not pursued.

1.1.2 Achieving Covalent Inhibition

In the context of selective probe development, and drug discovery, covalent inhibition is regarded as a two-step process.⁴⁹ First, non-covalent interactions are integral to forming a reversibly bound enzyme inhibitor complex (E-I) from the free inhibitor and enzyme (E + I). These interactions include typical binding forces such as van der Waals interactions, hydrogen bonds, through-water interactions, π -stacking, and lipophilic interactions.⁵⁰ This is described by the equilibrium constant K_i , which itself is made up of the microscopic rate constants k_{on} and k_{off} , depicting the on and off-rates of reversible binding.^{10,49} The second step is the covalent binding step, which is governed by the reactivity of the electrophile and the nucleophilic amino acid. This step can be irreversible ($k_{-2} = 0$) or reversible ($k_{-2} \neq 0$), depending on the nature of the chemical reaction forming the bond.^{1,10,35} In the irreversible case focussed on here, the rate constant governing this step reduces to k_{inact} , where “inact” means “inactivation of the enzyme”.³⁵ This is summarised in **Figure 4**.

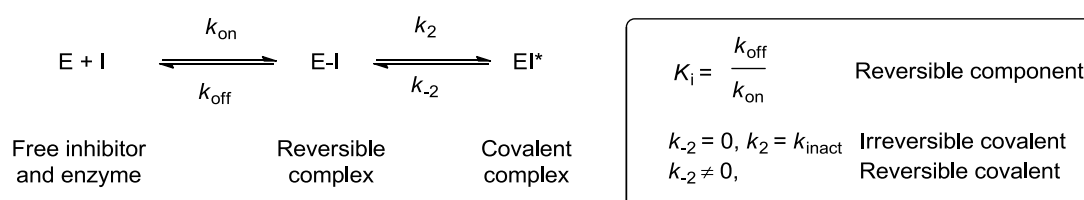


Figure 4 – General kinetics of covalent inhibition.

Potency and selectivity of an irreversible inhibitor can therefore be modulated by four factors:⁵¹ careful selection of a non-conserved amino acid residue at the target can greatly improve selectivity; fine tuning of the non-covalent interactions that govern K_i ; optimisation of the position of the electrophilic warhead with relation to the targeted amino acid; and tuning of the reactivity of the electrophilic warhead.^{1,10,12,35} Potent reversible binding of an inhibitor increases the effective concentrations of the reactive partners, forcing a reaction to occur.^{52,53} Achieving this with successful optimisation of the non-covalent interactions allows the use of mildly reactive electrophiles to initiate the covalent bond-forming reaction, which should reduce the risk of promiscuous reactivity.^{7,14}

In addition to good design of the inhibitor, the local environment around the amino acid can significantly increase its reactivity, allowing even milder electrophiles to be used. A well-known example of this occurs in the protease family of enzymes. These enzymes use a catalytic amino acid (typically serine, threonine or cysteine) to cleave amide bonds.⁵⁴ Taking the enzyme trypsin, from the serine protease family, as an example, it is clear from chemical intuition that serine would be unable to efficiently cleave an amide bond at neutral pH in solution. For this reaction to occur in the enzyme active site, interactions with a nearby histidine and aspartic acid residue render the serine residue more nucleophilic. This is known as the catalytic triad, and is a prevalent motif in structural biology that confers heightened reactivity to specific amino acids.^{54,55} Outside of the protease family, and more generally, buried amino acids are known to show heightened reactivity. For example, lysine residues are typically protonated at physiological pH ($pK_{aH} \sim 11$), however buried lysine residues in active sites have been shown to have pK_{aH} values as low as 5.^{56,57} This renders the lysine “hyper-reactive”, and therefore more likely to engage in a covalent bond-forming reaction with a weak electrophile.⁴² Additionally, certain cysteine residues have been identified as hyper-reactive, and are thought to be highly “ligandable”, or redox-active and involved in redox-mediated cellular processes.^{44,58,59}

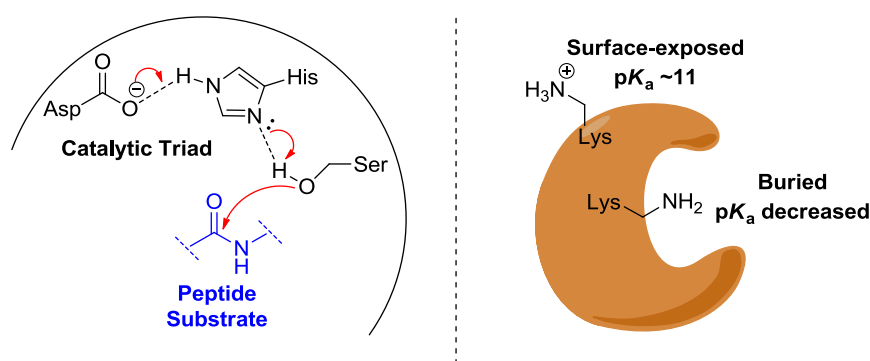


Figure 5 – Buried amino acids can exhibit uniquely different reactivities. Protease enzymes cleave amide bonds of peptides using an active-site amino acid that is rendered more nucleophilic by its local environment. An example of the serine protease family is shown, where the catalytic triad of aspartic acid, histidine, and serine facilitate a heightened nucleophilicity of the catalytic serine. Buried lysines can also exhibit greater reactivity due to pK_a changes in hydrophobic regions.

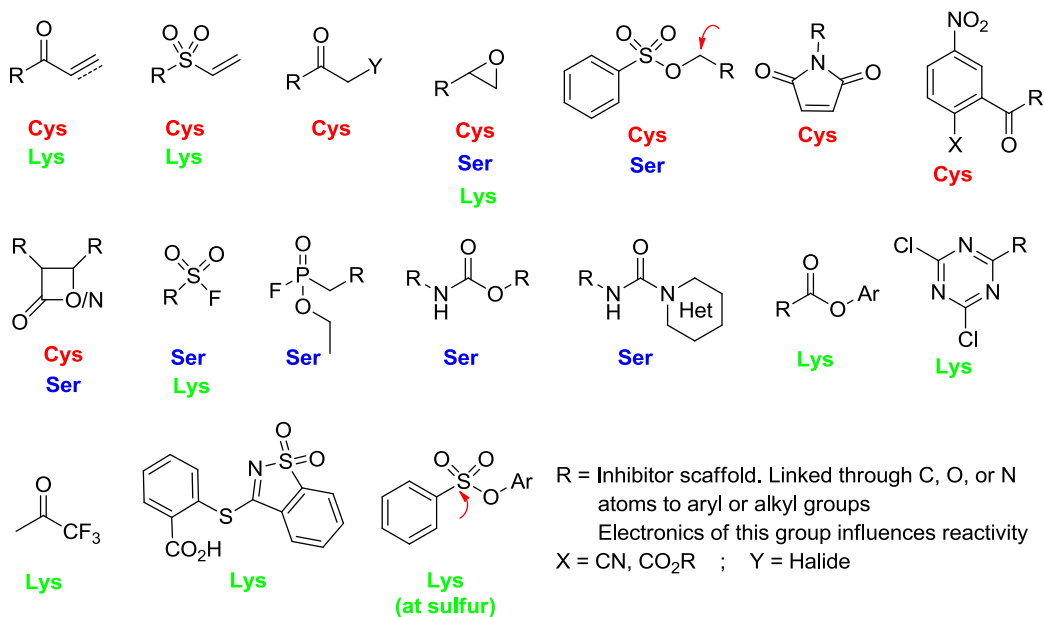
Many reactive groups exist for covalent conjugation of biological macromolecules, with varying degrees of applicability to covalent drug and probe discovery. **Figure 6** gives selected examples of warheads that are commonly seen in covalent drug candidates and chemical probes, along with their residue-reactivity profiles. It is clear that a truly residue-specific electrophile is difficult to identify, however efforts can be made to select a warhead that has

a favourable reactivity profile with the targeted amino acid. The section below discusses these warhead chemotypes in greater detail.

Often, especially in drug discovery, the reactive partners for covalent ligands take the form of a thiol (*i.e.* cysteine residue) and a Michael acceptor such as an acrylamide,^{9,13,60} cyanoacrylamide⁶¹, α,β -unsaturated ketone or ester,^{62,63} or more reactive sulfur-based derivatives.^{63–65} Indeed, many theoretical and experimental investigations into the chemical reactivity of these groups have been carried out, with the aim of improving understanding to better facilitate covalent drug discovery.^{66–72} Owing to cysteine's relatively low abundance in the proteome,⁷³ this approach can facilitate the generation of exquisitely selective compounds. Furthermore, cysteine is well suited to 1,4-addition due to the soft polarisable nature of the nucleophilic sulfur atom, which reacts preferentially with the β -carbon, over the carbonyl or sulfone centre.⁷⁴ Many other electrophiles exist to target cysteine residues, including α -halocarbonyls,^{44,58,75} epoxides,^{76,77} sulfonate esters (sulfonate anion leaving group),^{78,79} maleimide groups,^{80,81} and *p*-NO₂ S_NAr substrates.^{82,83} Furthermore, addition of a second electron-withdrawing group onto the α -carbon of the Michael acceptor generates a reversible covalent binding group, which can be beneficial for minimising the effects of off-target covalent interactions.^{5,84,85}

Outside of the cysteine-targeting realm, alcohol groups have been identified as tractable nucleophiles for covalent inhibition, exemplified by aspirin,² and β -lactam antibiotics (**Figure 1**).^{3,4} Additionally, inhibitors of the serine hydrolase enzyme superfamily have proven rich in their chemotypes for targeting the active site serine residue.⁸² Electrophiles to achieve this include fluorophosphonate,⁴⁰ β -lactams⁸⁶ and -lactones,⁸⁷ sulfonyl fluorides,⁸⁸ carbamates,⁴¹ *N*-heterocyclic ureas,^{89,90} boronic acids and nitriles (reversible addition).⁹¹ Cross-reactivity can be an issue in covalent drug design, and indeed many of these electrophiles are also applicable to targeting the alcohol functionalities of threonine and tyrosine residues. In particular, sulfonyl fluorides and sulfonate esters (with loss of the sulfonate anion) react well with tyrosine residues.^{92–94} Methods of targeting less reactive amino acids such as glutamic acid,⁹⁵ and even methionine,⁴³ have emerged recently in the literature also (**Figure 3**).

Irreversible Covalent



Reversible Covalent

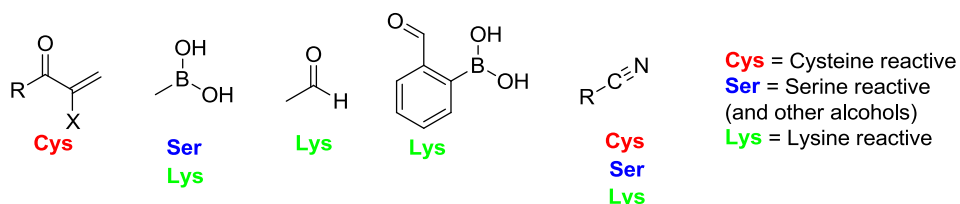


Figure 6 – Selected examples of irreversible and reversible-covalent warheads for targeting cysteine, alcoholic residues (such as serine, tyrosine and threonine), and lysine.

Lysine residues present a unique opportunity for covalent targeting, as they are unlikely to be reactive when solvent-exposed, yet their reactivity may be heightened in the active site of proteins due to pK_a differences (**Figure 5**). At the outset of this project, lysine-reactive warheads were limited in their availability, yet considerable interest has developed in this field since. Indeed, a recent review has been published summarising lysine-targeting as an approach to covalent inhibitor discovery,⁹⁶ and reactivity studies building on cysteine-reactivity investigations have begun to appear in the literature for lysine-reactive warheads.⁹⁷ Historically, sulfonyl fluorides were used for targeting lysine residues, when appended to the ATP mimetic 5'-(4-fluorosulfonylbenzoyl)adenosine (FSBA) (compound **9**, **Figure 3**),³⁴ however these have also been shown to exhibit cross-reactivity with alcohol-bearing amino acid side chains. Nevertheless, sulfonyl fluorides have gained interest rapidly over recent years for lysine modifications.^{98–100} Very recently, the concept of alternative S(VI) reactive centres, such as fluorosulfonates ($-OSO_2F$),^{101–103} has emerged due to better hydrolytic

stability than sulfonyl fluorides (-SO₂F). Additionally, reports of α,β -unsaturated systems, such as the archetypal acrylamide and vinyl sulfonamide warheads used for cysteine targeting, reacting with lysine residues have been disclosed.^{97,104} In addition, the harder nature of the reactive nitrogen lone pair, compared to the softer and more polarisable sulfur lone pair, facilitates efficient 1,2-addition to carbonyl centres. For example, lysine residues are commonly shown to form reversible covalent imine adducts with aldehydes and ketones, which can be chemically reduced to form an irreversible amine bond.^{7,91,105,106} Furthermore, these adducts have been shown to be efficiently stabilised by donation of the resulting imine lone pair into a vacant p-orbital on an adjacent boron atom.^{91,107} This reactive nature also facilitates efficient amidation reactions with activated esters,^{42,108,109} and residue-selective S_NAr-mediated reactions with dichlorotriazine groups.^{83,110}

Research into residue-selective warheads for covalent modification is a very active area, with a vast number of articles being published. Protocols to screen these groups computationally for incorporation into drug-like scaffolds are emerging,^{111,112} yet the determinants of residue selectivity are not yet known. Significant effort has been made in the literature towards understanding the intrinsic chemical reactivity of drug-like warheads (often Michael acceptors), however these studies are by no means comprehensive. Often, a particular warhead class is thoroughly studied (*e.g.* the electronic effects of various aryl groups appended to acrylamides) against one amino acid mimetic (*e.g.* *N*-acetyl cysteine).⁶⁹ Whilst these studies are thorough for the specified system, they are limited in their descriptions of the chemical reactivities of these groups with different amino acid mimetics. Furthermore, these analyses only consider the chemical reactivity of the warhead, which is not fully representative of a protein's active site, and also neglects the contribution of reversible binding to covalent inactivation (**Figure 4**). Indeed, reports of conflicting chemical and proteomic reactivities exist,^{83,94} highlighting the need to fully profile reactive warheads, and optimised covalent binders, in native biological systems. Together, these points show the need to optimise both reversible binding and chemical reactivity for covalent inhibitor design.

1.2 Kinases in Covalent Drug Discovery

1.2.1 The Kinome

Kinases are a class of proteins that catalyse the transfer of a phosphate group from adenosine triphosphate (ATP) to a specific substrate, forming a phosphorylated product and adenosine diphosphate (ADP). They are one of the largest enzyme classes in nature, with over 500 distinct members, comprising roughly 1.7% of the human genome.¹¹³ Their activity modulates key cellular events such as cell growth, cell migration, cell survival, metabolism, differentiation and apoptosis.^{114–116} Kinases form a superfamily of proteins that can be classified depending on their substrates. For example, protein and lipid kinases phosphorylate protein substrates and lipid substrates, respectively.¹¹⁷ There are 518 protein kinases, of which 478 share a common eukaryotic protein kinase (ePK) catalytic domain.¹¹⁶ The remaining 40 form the atypical kinome, which show biochemical kinase activity, yet lack high sequence homology with the ePK.¹¹⁶ Additionally, there are roughly 20 lipid kinases that show reasonable homology with the ePK (**Figure 7**).¹¹³ Owing to their involvement in multiple cellular processes, and disease-specific dysregulation, selective inhibition of kinases has become a common strategy for drug discovery.¹¹⁸

The first documented kinase inhibitors date back to the 1950s and 1960s, with identification of kinase-mediated signalling pathways through protein phosphorylation.^{119,120} However, there was scepticism from the drug discovery world over the possibility for ATP-competitive kinase inhibition to be therapeutically useful. This was due to the high intracellular concentrations of ATP, high sequence homology of kinase ATP binding sites, and therefore expected difficulty in obtaining selective inhibition without off-target toxic effects.¹²¹ In the 1980s, the discovery that staurosporine inhibited Protein Kinase C (PKC)¹²² dispelled some of these concerns, and the concept of ATP-competitive kinase inhibition was developed further with the disclosure of inhibitors of Epidermal Growth Factor Receptor (EGFR) and other protein kinases.^{123,124} The breakthrough success of Gleevec (Imatinib) as a Bcr-Abl tyrosine kinase inhibitor for the treatment of chronic myelogenous leukaemia¹²⁵ proved the remaining concerns unwarranted, and paved the way for selective kinase inhibition by targeting the ATP binding site as a viable strategy for drug discovery.^{126,127} Since Gleevec's approval in 2001, there has been an overwhelming explosion of research into kinase signalling pathways, and the development of kinase inhibitors for the treatment of disease. This has been further fuelled by the sequencing of the human kinome,¹¹⁶ improvements in

genetic validation of kinase targets, and an increase in biochemical and cellular assay throughput.¹²⁸ Indeed, two reviews in 2015 by Wu *et al.*¹²⁹ and Fabbro *et al.*¹²⁸ identified roughly 30 small molecule kinase inhibitors that are approved for various indications by the US Food and Drug Administration (FDA), and 130 kinase inhibitors in Phase 2 and 3 clinical trials. However, only around 80 kinases have been targeted by these therapies, and the overwhelming majority are in the oncology space;¹²⁸ thus there is considerable room for further development.

Covalent kinase inhibition has been harnessed as a unique way of overcoming high intracellular concentrations of competing ATP.⁹⁶ By targeting poorly conserved cysteine residues in the vicinity of the ATP binding site, researchers have been able to achieve more complete and sustained target engagement, by virtue of the covalent reaction proceeding to completion rather than equilibrium.^{60,130} As discussed earlier, this targeted covalent inhibition approach led to the clinical successes of the kinase inhibitors Afatinib and Ibrutinib (**Figure 2**). This approach has since been used with multiple other cysteine-containing kinases such as the cyclin dependent kinases (CDKs),^{32,33} janus kinases (JAKs),^{112,131} p90 ribosomal S6 kinase-2 (RSK2),¹¹² fibroblast growth factor receptor (FGFR),¹³² and extracellular signal-related kinases (ERKs),¹³³ amongst others.

Computational efforts have identified 18 unique cysteine locations in protein kinases that are amenable to this targeting approach,¹³⁴ and are indeed targeted by the inhibitors detailed above.^{134–137} Whilst this approach has proven highly successful in some cases, these studies showed that it is limited to ~200 kinases that possess a suitable cysteine, of which covalent inhibitors are known for less than 50 of them.¹³⁷ Therefore, development of alternative methods of achieving selective covalent kinase inhibition, that can be more generally applied, are needed.

Due to the functional similarity of kinases, they possess highly structurally similar ATP binding pockets, with a conserved ATP-chelating lysine residue that is non-covalently involved in the ATP transfer reaction of kinases.¹³⁸ ATP and ADP mimetics possessing reactive warheads were shown to covalently modify this lysine, in a non-selective manner.³⁷ The wide coverage (~300 endogenous kinases in the 2007 initial disclosure)³⁷ obtainable from this reactivity has been exploited in the generation of activity-based probes to profile the selectivity of kinase inhibitors for drug discovery (**Figure 8**).^{37,39} In addition, these probes modify non-kinase ATP

binding proteins such as heat-shock proteins.³⁷ However, these probes are not cell-permeable therefore can only be used in cell lysates.

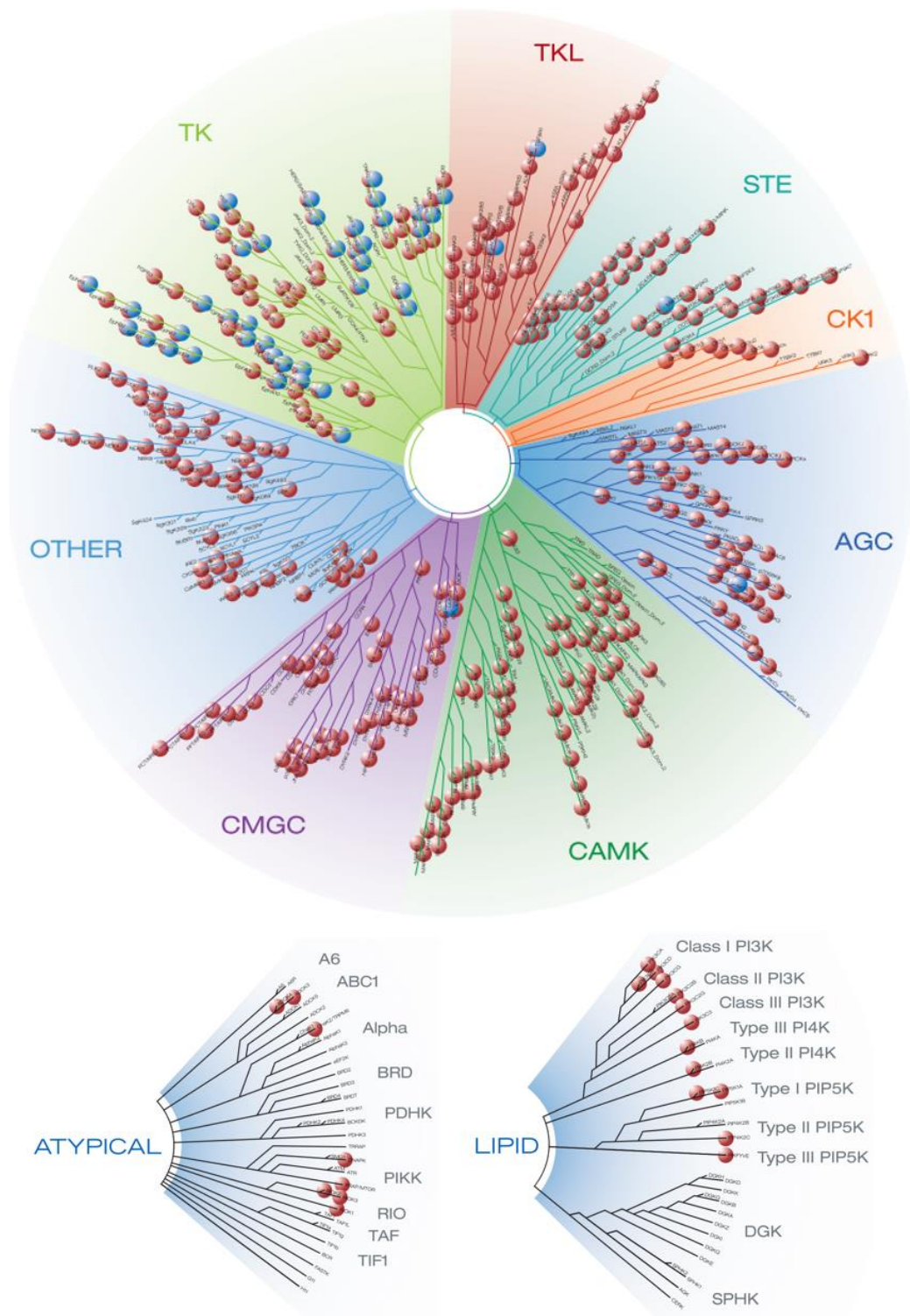


Figure 7 – The human kinome phylogenetic tree. The top circle depicts the protein kinome, and the bottom two sections the atypical kinome and the lipid kinome. At the end of each branch is a functionally unique kinase. The figure is adapted from DiscoverRx (<https://www.discoverrx.com/tools-resources/document-resource-library/documents/the-human-kinome>) where the blue and red circles denote the assay formats available for each kinase.

Since beginning this project, a second report of cell-permeable promiscuous covalent inhibitors reacting with this lysine residue through a sulfonyl fluoride warhead has been disclosed by Taunton *et al* (**Figure 8**).⁹⁸ In a similar manner to the ATP/ADP probes, this probe identified 133 endogenous kinases, from live cell treatments, which were covalently labelled at this conserved lysine residue.⁹⁸ The authors only investigated one cell line in this study, whereas the KiNativ ADP/ATP probe targets were identified from 4000 proteomic experiments across multiple cell lines and tissue sources.^{37,98} Therefore, it is expected that the Taunton probe will be able to label a greater number of kinases in different cell lines with different expression profiles.

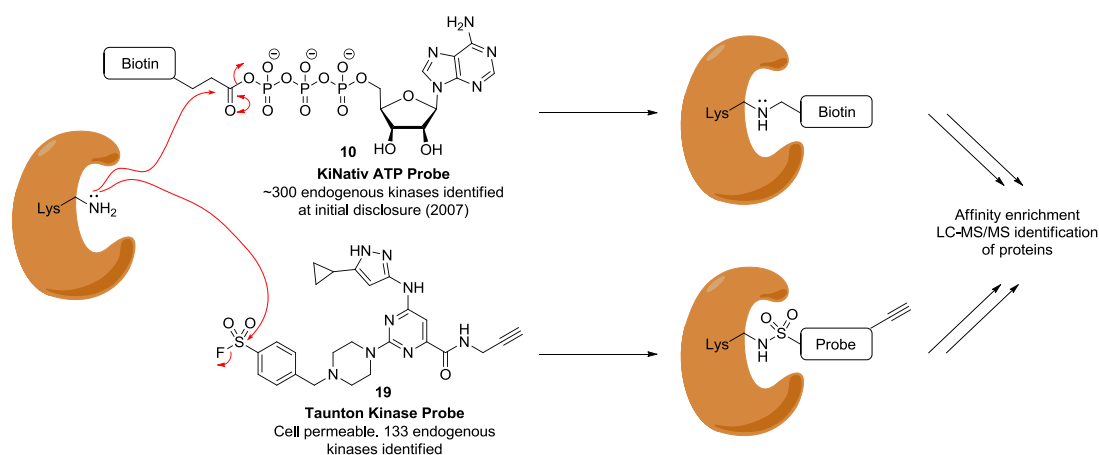


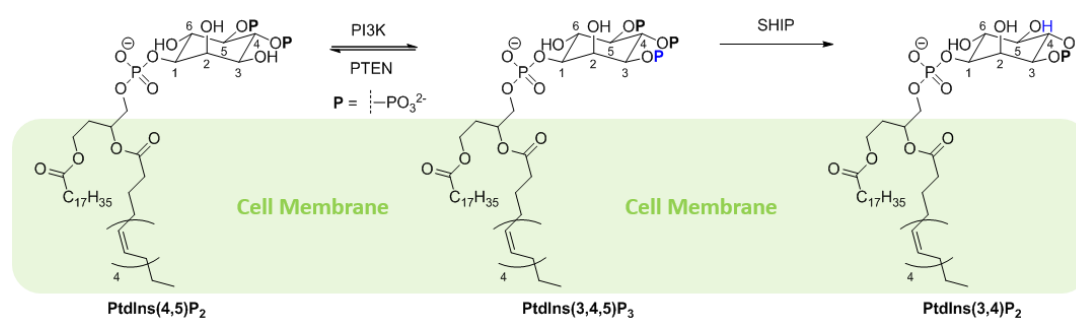
Figure 8 – Structure of promiscuous kinase probes that have been used for chemoproteomic experiments. Covalent binding to a significant number of kinases is achieved through reaction with the conserved ATP-anchoring lysine residue.

Together, these reports posit the question of whether this lysine residue could be selectively modified in one kinase, as a general approach to covalent kinase inhibition that is orthogonal to cysteine targeting. This thesis explores this question, through modulation of the catalytic lysine of the lipid kinase phosphoinositide 3-kinase delta (PI3K δ). Furthermore, if this approach is successful, it could theoretically be applied to any kinase which has been shown to be covalently engaged through this residue in the studies above.

1.2.2 Phosphoinositide 3-Kinases

Discovered in the 1980s,¹³⁹ phosphoinositide 3-kinases (PI3Ks) are a particular type of lipid kinase that catalyse the phosphorylation of phosphoinositide lipids (PIs) at the 3-hydroxyl position.¹⁴⁰ Mammalian PI3Ks can be divided into three classes based on their structure and substrate specificity. Class I PI3Ks are dimeric proteins made up of one catalytic, and one regulatory domain that preferentially phosphorylate phosphatidylinositol-4,5-bisphosphate

(PtdIns(4,5)P₂) to phosphatidylinositol-3,4,5-trisphosphate (PtdIns(3,4,5)P₃).¹⁴¹ Multiple effectors are able to bind the secondary messenger PtdIns(3,4,5)P₃, that are involved in many cellular functions. The level of PtdIns(3,4,5)P₃ is therefore tightly regulated in the cell by the opposing action of PI3Ks and phosphatases such as SH2-containing inositol phosphatase (SHIP1 and SHIP2) and phosphatase and tensin homolog (PTEN). These phosphatases catalyse the reverse reaction of PI3K by dephosphorylating the inositol ring at the 5 and 3 positions, respectively, to maintain the level of PtdIns(3,4,5)P₃ in the cell (**Scheme 1**).^{142–145}



Scheme 1 – Action of PI3K to convert PI[4,5]P₂ into PI[3,4,5]P₃ and the action SHIP and PTEN phosphatases to control the level of PtdIns(3,4,5)P₃ in the cell.^{143–145}

Within the Class I PI3Ks are the isoforms of interest to this thesis: PI3Ks alpha (PI3K α), beta (PI3K β), gamma (PI3K γ) and delta (PI3K δ). PI3K α , PI3K β and PI3K δ belong to Class IA, characterised by association of the catalytic subunits p110 α , p110 β and p110 δ to the p85 adaptor subunit.¹⁴¹ This adaptor subunit facilitates activation of the kinase by interaction with receptor tyrosine kinases, and localises the dimer at the membrane.¹⁴² PI3K γ belongs to Class IB, and contains the p110 γ catalytic subunit bound to the p101 adaptor subunit, that allows activation by G-protein coupled receptors (GPCRs).^{140,146,147} The PtdIns(3,4,5)P₃ product is responsible for multiple downstream pathways, including B-cell migration, T-cell differentiation, macrophage accumulation, and neutrophil trafficking into inflamed tissues during the inflammatory response.^{142,148,149} In addition, pathways responsible for actin polymerisation, protein synthesis, cell survival and cell cycle entry are affected by these transformations (**Figure 9**).^{114,150} Class II PI3Ks phosphorylate phosphatidylinositol (PtdIns) and phosphatidylinositol-4-phosphate (PtdIns(4)P₁), whereas Class III PI3Ks only phosphorylate PtdIns.¹⁴⁰

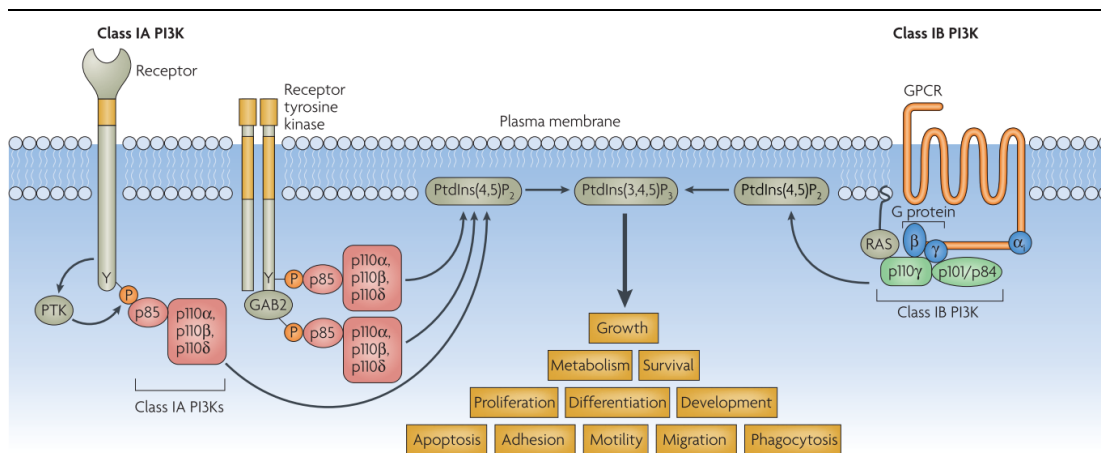


Figure 9 – Generalised locations of Class I PI3K proteins, and downstream pathways that the product of their reaction, PtdIns(3,4,5)P₃ modulates.¹⁵⁰ Reprinted with permission from Rommel *et al.*¹⁵⁰ Copyright 2007 Nature Publishing Group.

1.2.2.1 Class I PI3Ks in Disease

Studies on the Class I PI3Ks have shown them to be involved in various different diseases.^{141,145,151} Importantly, localisation of the PI3K proteins in specific cell types throughout the body is key for the disease-relevance of each isoform.

PI3K α activation has been observed in cancers, where mutations in the gene coding for the p110 α catalytic domain (PIK3CA) caused overexpression of PI3K α in tumours.¹⁵² PI3K β has also been linked to cancer by its involvement in carcinogenesis.¹⁵³ Inhibiting the activity of these isoforms is therefore a target for cancer therapy. However, both are expressed ubiquitously and knockout studies in mice have shown that removal of the genes coding for either kinase is fatal.^{154,155}

PI3K γ and PI3K δ are preferentially expressed in leukocytes in the immune system, and have been identified as key players in macrophage accumulation during inflammation.¹⁵⁶ Their involvement in T-cell receptor signalling, B-cell development,¹⁴⁸ and neutrophil trafficking into inflamed tissue¹⁴⁹ make them attractive targets for the treatment of inflammatory and autoimmune diseases such as asthma, chronic obstructive pulmonary disease (COPD), rheumatoid arthritis, lupus erythematosus, and activated PI3K δ syndrome.^{142,147,157,158} In contrast to PI3K α and β , PI3K δ and γ knockout mice remain viable, suggesting that lower toxicity may be associated with inhibition of these enzymes, relative to PI3K α and β .^{142,147,148,156,159}

Many of the diseases that PI3K δ is associated with are chronic in nature,^{142,158,160} and may therefore benefit from the prolonged duration of action attainable by a covalent targeting

approach. Moreover, unpublished work from our laboratories has determined a long resynthesis half-life for PI3K δ in primary human T-cells. This suggests that a single dose of an irreversible inhibitor could suppress PI3K δ over-activation, with an extended duration of action. Additionally, a proteome-wide study of cysteine reactivity conducted by Backus *et al.*,⁴⁴ and bioinformatic approaches conducted by multiple groups^{135–137,161} did not identify PI3K δ as a protein possessing a ligandable cysteine residue. However, being a member of the kinase family of proteins, it does possess the conserved, ATP binding lysine.¹³⁸ Together these points justify PI3K δ as an ideal target to investigate the possibility of developing selective covalent kinase inhibitors targeting the kinome conserved lysine.

1.3 Project Aims

This research project aims to engage the conserved catalytic lysine residue covalently with an electrophilic inhibitor (**Figure 10**). As mentioned above, this has been achieved in the literature using promiscuous probes based on ATP/ADP, and commercialised into a selectivity assay for kinase inhibitors in clinical development.^{37,39} However, reports of this approach being used to selectively target the conserved residue in one kinase have not been disclosed. Furthermore, this approach should then be applicable to the kinome, and may facilitate generation of covalent inhibitors of any given kinase, particularly those without isoform-specific targetable cysteine residues. The general aims of this project, and where these aims are explored, are summarised below.

- Explore lysine-targeting electrophiles to covalently inhibit PI3K δ through binding to the conserved lysine (Sections 2 and 3)
- Optimise inhibitor design using published, and internally generated knowledge to maximise potency and selectivity (Section 3)
- Achieve criteria fit for purpose as a chemical probe,¹⁶² and a potentially a drug-like molecule. Initial criteria include: nanomolar potency in biochemical assays, selectivity >100-fold over off-target enzymes under biochemical conditions, <1 μ M potency in a cell-based assay, and evidence of covalent selectivity in a cell-based system (Section 4).
- Develop synthetic methods to access these compounds efficiently
- Provide a thorough biological characterisation of the lead compound(s), justifying their development as either chemical probes or drugs (Section 4)

The general work-flow presented in this thesis is shown below. Firstly, structures are modelled using a crude non-covalent binding approximation to assess the potential for covalent binding of the inhibitors (*i.e. in silico* potency, reactive centre alignment, trajectory of nucleophile attack). Promising structures are then progressed through to synthesis, and initial biological characterisation in isolated enzyme assays and a phenotypic assay carried out in human whole-blood, that measures secretion of the inflammatory cytokine interferon gamma (IFN γ), after stimulation with CytoStim.¹⁶³ Crystallography is then invoked for promising compounds to assess their binding mode. This process generates SAR to establish the next series of compounds to enter the cycle.

Towards the end of the thesis, the most promising set of compounds is taken forward to further biological characterisation including intact protein mass-spectrometry, external kinase panel selectivity assays, target engagement experiments in cell lysates, binding kinetics, and chemoproteomic analysis of proteome-wide selectivity.

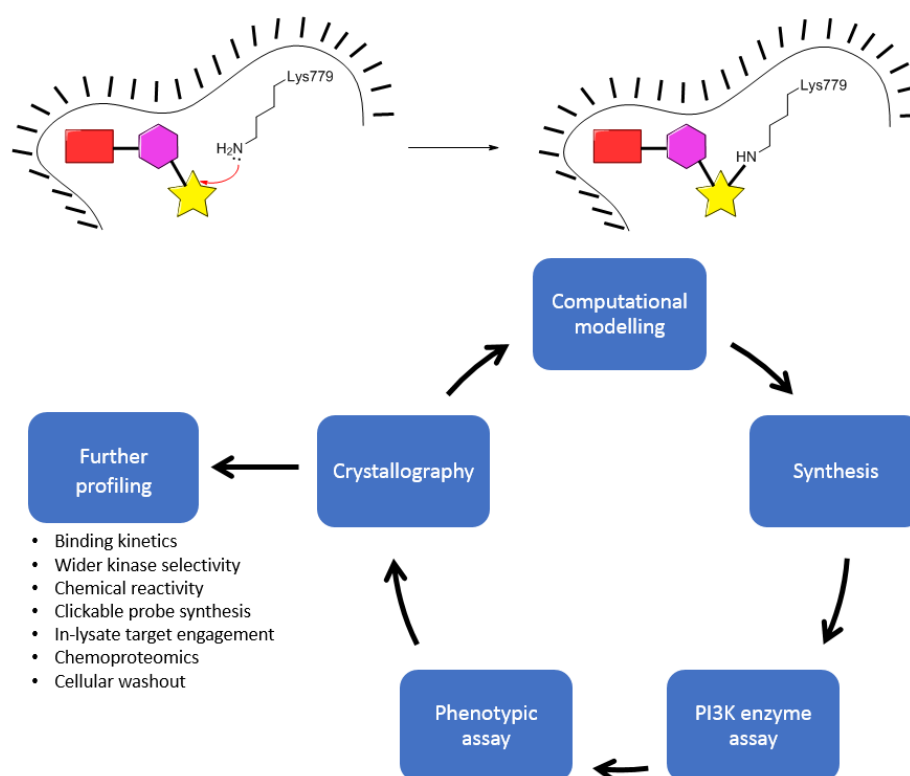


Figure 10 – Cartoon representation of the aim of this research and work flow. The overall aim of this research is to achieve covalent inhibition by reaction between Lys779 and the electrophilic centre. The workflow utilises structure-based design, synthesis, isolated enzyme assays, a phenotypic assay and crystallography as the core process. The best compound(s) are then taken forward for further analysis involving the methods listed. The red, purple, and yellow boxes depict different parts of the inhibitor structure, such as a hinge-binder, back-pocket group and reactive centre.

2. Discovery of Covalent PI3K δ Probes

As discussed in **Figure 4**, to establish a covalent bond, the inhibitor must be reversibly bound in the active site by favourable interactions, which align the electrophilic centre with the nucleophilic amino acid residue. To achieve this, knowledge of the ATP binding site, and relevant PI3K δ chemotypes is required.

2.1 PI3K δ Inhibitor Chemotypes

2.1.1 Reversible Binders

With the PI3K pathway being involved in so many diseases, and mortality dependent on which kinase is inhibited, achieving isoform selectivity is crucial in drug design. However, the structure of the Class I PI3K ATP binding sites is highly conserved between the isoforms,^{164–166} making this task difficult for medicinal chemists. The crystal structure of ATP bound in PI3K δ is shown below in **Figure 11**, highlighting key interactions and pockets that are relevant to inhibitors discussed in this section. All amino acid numbering is relative to the PI3K δ crystal structure.

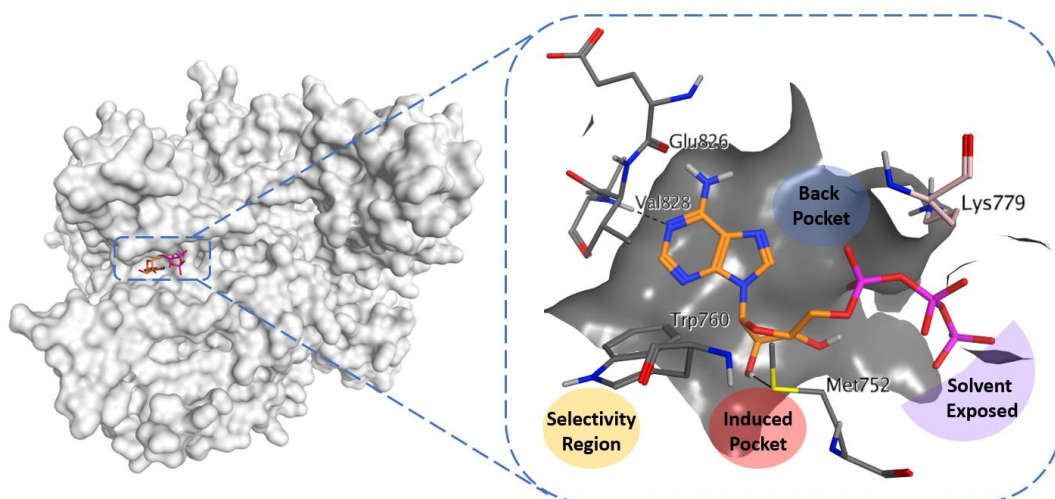


Figure 11 – Crystal structure obtained in-house of ATP bound to murine PI3K δ . Left shows the van der Waals surface for the entire protein, with the ligand highlighted in colour. Right shows a zoomed in image of the ATP binding pocket. Key residues and interactions are shown, as well as key binding regions for inducing potency and selectivity for PI3K δ inhibitors.

Consistent with the structure of protein kinases, the ATP binding site of PI3K δ sits between the N and C terminal lobes of the kinase domain.^{117,128} Key interactions with backbone N-H

and C=O groups at the “hinge” region between these lobes are highly conserved. For PI3K δ , the adenine ring of ATP interacts through hydrogen bonds with valine 828 (Val828) N-H, and glutamic acid 826 (Glu826) C=O.^{165,167} The ribose sugar and triphosphate motifs of ATP then extend off this structure, towards the solvent-exposed region, where the PtdIns(4,5)P₂ substrate will bind for the phosphorylation reaction to occur. This reaction is catalysed by magnesium coordination between the β and γ phosphates (not shown in the above structure) as a general Lewis acid to activate the phosphoryl group, and the terminal amine of the conserved lysine (Lysine 779, Lys779) between the α and β phosphates to orient the triphosphate chain towards the substrate.^{113,128,138,167,168} Three key regions for potency and selectivity are the solvent-exposed selectivity region next to Tryptophan 760 (Trp760), an induced selectivity pocket next to Methionine 752 (Met752), and the hydrophobic back-pocket region near Lys779.¹⁶⁵ These regions are illustrated below with key inhibitors.

Two selective inhibitors of PI3K δ , TGR-1202 (compound **20**),¹⁶⁹ and Idelalisib (formerly CAL-101, compound **21**),¹⁷⁰ are presented in **Figure 12**. **20** is currently in Phase I Clinical Trials for patients with relapsed or refractory hematologic malignancies.¹⁶⁹ Idelalisib **21** has recently been approved as a First in Class PI3K δ inhibitor by the United States Food and Drug Administration (FDA) to treat patients with relapsed chronic lymphocytic leukaemia, relapsed follicular B-cell non-Hodgkin lymphoma, and relapsed small lymphocytic lymphoma.^{170–172}

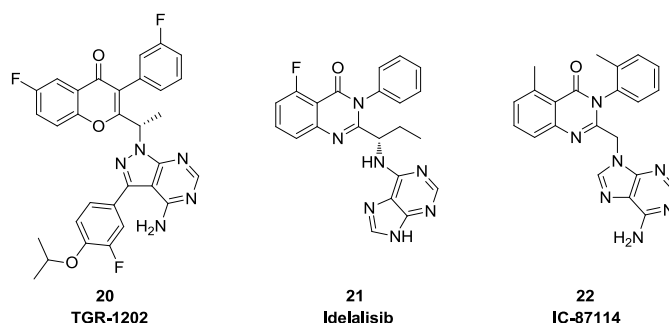


Figure 12 – Selective, reversible PI3K δ inhibitors that target the induced selectivity pocket

Structure activity relationships (SARs) describing how inhibitors **20** and **21** achieve isoform selectivity were originally developed with Idelalisib’s predecessor, IC-87114 (compound **22**). Its structure is similar to compounds **20** and **21**, which allowed a hypothesis to be drawn about how these compounds achieve selectivity for PI3K δ .¹⁶⁵ This hypothesis was recently confirmed, by crystallography, for compound **21**.¹⁷² Key binding interactions at the hinge between Valine 828 (Val828), Glutamic acid 826 (Glu826) and the purine ring of compound **21** are satisfied, mimicking the interactions ATP makes with this region (**Figure 13**).^{172,173} An

induced hydrophobic selectivity pocket exists between Tryptophan 760 (Trp760) and Isoleucine 777 (Ile777) on one side, with Methionine 752 (Met752) and Proline 758 (Pro758) on the other, sandwiching the quinazolinone rings. This pocket arises from a conformational change in PI3K δ where Met752 switches from an “in” position resting next to Trp760, to an “out” position.^{165,172,173} Modified PI3K δ constructs, where Met752 has been mutated to a β -branched amino acid (Valine or Isoleucine), are resistant to the δ -selective inhibitor **22**, but retain sensitivity to non-specific isoform inhibitors,¹⁷³ indicating that occupying this pocket is critical to achieving isoform selectivity for these types of compounds.

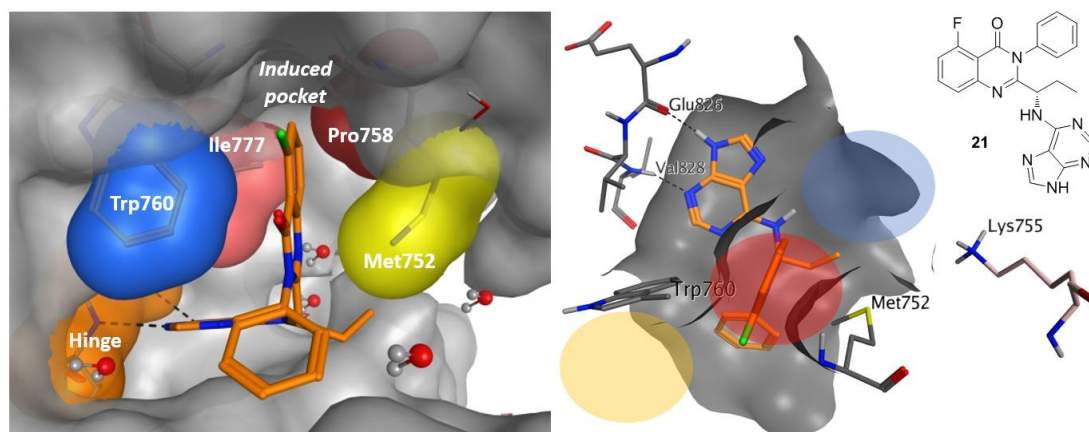


Figure 13 – Binding mode of Idelalisib (compound **21**)¹⁷² in PI3K δ (PDB: 4XE0). Key residues at the hinge (Val828 and Glu826) are highlighted in orange, and residues defining the selectivity pocket are highlighted in blue (Trp760), yellow (Met752), pink (Ile777) and red (Pro758). The structure is shown in the ATP orientation from **Figure 11**, including the colour-coded binding pockets, for reference.

The “affinity” or “back” pocket exists much deeper into the enzyme. ATP does not bind here (**Figure 11**), but inhibitors such as PIK-90 (compound **23**) do (**Figure 14**).¹⁷³ Compound **23** is a non-selective PI3K inhibitor, as it is flat and does not interact with the specificity pocket like the propeller shaped **21**. Instead, its potency is achieved by projecting a pyridine ring into this back pocket, forming a hydrogen bond to the conserved lysine, and increasing its number of hydrophobic interactions. Exchange of the pyridyl nitrogen for a carbon reduces its potency by 100-fold,¹⁷³ highlighting the importance of this hydrogen bond for this series of inhibitors. The only available crystal structure for **23** is bound in PI3K γ , however due to the similarities of the ATP binding sites, and the unselective nature of the inhibitor, comparisons to PI3K δ can be drawn.¹⁷³ The labelled residues in **Figure 14** therefore correspond to the labelled residues in **Figure 13**. For example, Val828 in PI3K δ corresponds to Val882 in PI3K γ , Glu826 to Glu880, and the conserved Lys779 in PI3K δ to Lys833 in PI3K γ .

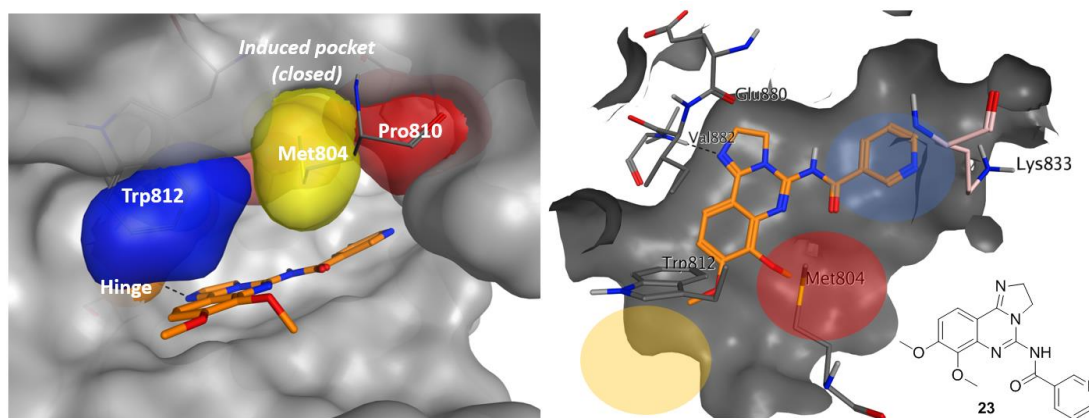


Figure 14 – Binding mode of PIK-90 (compound **23**) (PDB: 2CHX). The compound is flat in structure, and does not occupy the induced selectivity pocket like **21**. As a consequence, it does not show selectivity over any PI3K isoform.¹⁷³

Extensive prior research in our laboratories has targeted PI3K δ selectively for the treatment of inflammatory respiratory conditions such as COPD and allergic asthma.^{163,174} The most advanced molecules belong to a series of indazole-based compounds that are suitable for inhaled administration.¹⁶³ The two most prominent of these are the clinical candidates **24** and **25** (**Figure 15**).

Both compounds utilise an indazole hinge binder, that forms the key hydrogen bonds to the hinge residues Val828 and Glu826. The compounds do not cause the induced pocket to form, but instead extend a pendant amine off the 4-position of the indazole ring. This group gives selectivity for the δ isoform by packing the basic amines into a selectivity region next to Trp760.¹⁷⁵ It is important to note that this region is different to the induced selectivity pocket exploited by compounds **20** - **22**, and does not require a conformational change in the protein to accommodate the inhibitor. **Figure 16A** illustrates this, by overlaying the crystal structures of compounds **21** and **24**. The surface of the active site for compound **24** is shown, and the absence of space for the quinazolinone rings of compound **21** (black structure) is clearly visible. The different locations of Met752 side-chain are also clearly shown. In both compounds **24** and **25**, the oxazole ring does not show any particular interactions with the receptor, and most likely acts as a flat spacer unit.

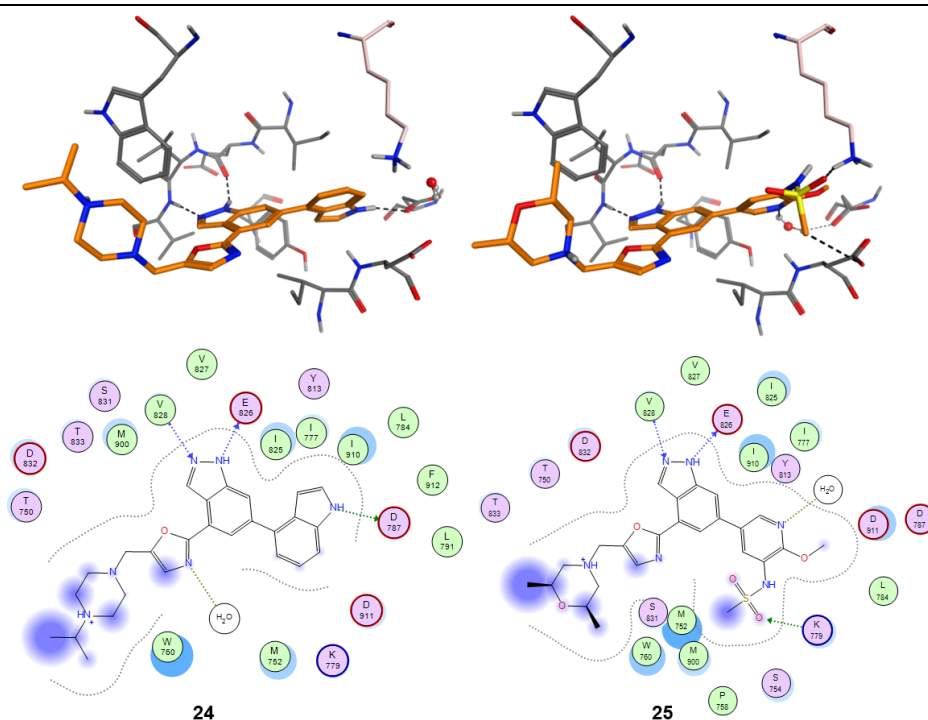


Figure 15 – Top left: Crystal structure of compound **24** in the ATP binding site of PI3K δ (PDB: 5AE8).¹⁶³ **Bottom left:** Two dimensional interaction map of the crystal structure above. Key hinge interactions to Val828 and Glu826 are shown, as well a back pocket hydrogen bond to Asp787. **Top right:** Crystal structure of compound **25** in the ATP binding site of PI3K δ (PDB: 5AE9).¹⁶³ **Bottom right:** Two dimensional interaction map of the crystal structure above. Hydrogen bonds to hinge residues Val828 and Glu826 are shown, with water interactions to the pyridyl nitrogen and sulfonamide interaction with Lys779 evident in the back pocket.

The compounds generate potency and selectivity at PI3K δ by exploiting the differences in amino acid residues between the isoforms that pack against the conserved Trp760 residue **Figure 16B**. PI3K α possesses an arginine residue,¹⁷⁶ PI3K β and γ a lysine residue, whereas PI3K δ has a much smaller and less cationic threonine residue.¹⁷⁵ Introduction of a lipophilic amine in this region is tolerated at PI3K δ , and the protonated nature of the amine at physiological pH mimics the favourable cation- π interaction observed between the basic residue and Trp760 in the other three isoforms. For the amine to engage in this interaction with the other three isoforms, it would have to overcome a steric penalty, and also an electrostatic penalty, which is highly disfavoured and therefore induces selectivity for PI3K δ .¹⁷⁵

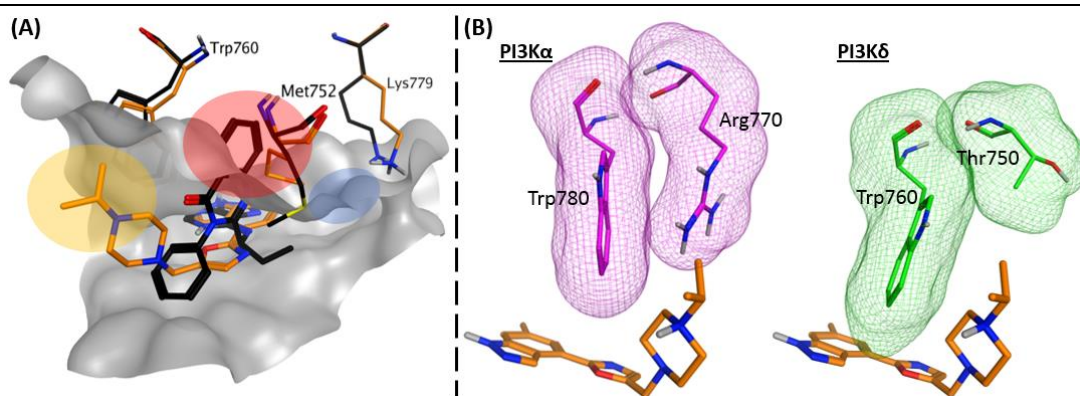


Figure 16 – Distinguishing the induced selectivity pocket, and the selectivity region. **(A)** Receptor and inhibitor structures for **21** (black), and **24** (orange) are presented. The receptor surface for compound **24** is shown, with pocket colours from **Figure 11**. The "closed" nature of the induced selectivity pocket is clear from the clash with Idelalisib, and the change in location of Met752 from "in" (orange, closed pocket) to "out" (black, open pocket) is also evident. **(B)** Selectivity is achieved from the solvent-exposed selectivity region due to differences in the amino acid which packs next to Trp760 between the isoforms. PI3K α is shown as an example (PDB: 4JPS),¹⁷⁶ which has a bulky arginine residue (Arg770) that engages Trp760 in a cation- π interaction. PI3K β and γ possess large, cationic lysine residues in this region.¹⁷⁵ The structure for compound **24** is shown in this region, truncated after the hinge binding region for clarity.

The back-pocket region is where these two compounds differ greatly, and different interactions can be seen in **Figure 15**. Compound **24** makes a hydrogen bond to aspartic acid 787 (Asp787) through the indole N-H, whereas compound **25** interacts with Lys779 through one of the oxygens of the sulfonamide group, and the sulfonamide N-H. Additionally, compound **25** interacts with a water molecule via the pyridyl nitrogen, that forms a solvent bridge to Asp787. Both of these structural features are well tolerated in the enzyme, and the two back-pocket groups therefore present different vectors for including an electrophilic warhead to target Lys779.

Research within our laboratories then turned towards developing PI3K δ inhibitors for oral delivery. To this end, Peace *et al.*¹⁷⁷ investigated inhibitors possessing different hinge binding motifs. The group discovered the currently unpublished dihydropyran (DHP) series, which were effective at binding in the PI3K δ ATP active site. Compound **26** (**Figure 17**) is a representative example from this series. It binds to the PI3K δ hinge via a monodentate interaction between Val828 and the oxygen of the DHP ring. The methoxypyridyl sulfonamide binds in the back-pocket region of the ATP binding site. This group makes similar interactions to compound **25**, through the nitrogen of the pyridyl ring to the key water molecule, and through the oxygen of the sulfonamide to Lys779. Additionally, the other sulfonamide oxygen interacts with Trp760 which has switched orientation compared to the crystal structures for compounds **24** and **25** presented in **Figure 15** (from a position denoted as "out" to "in").

Finally, the pyrrolidine ring is positioned in the solvent-exposed selectivity region next to Trp760 to achieve selectivity over α , β and γ . This extension from the sulfonamide is used in the DHP series to achieve selectivity, in a similar manner to the pendant arms previously described in the indazole series. This side chain is solvent-exposed, and therefore allows modulation of the physicochemical properties of the molecule.

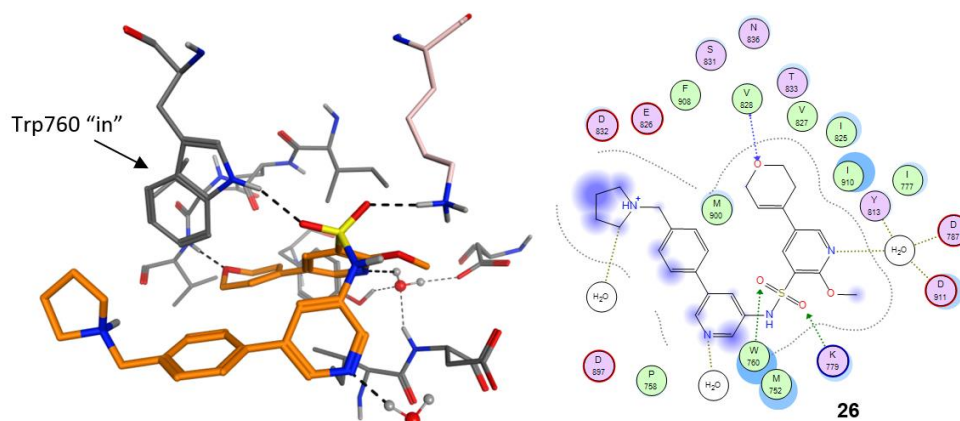


Figure 17 – Left: Crystal structure of compound **26** in PI3K δ . Right: Two-dimensional interaction map of this structure.

2.1.2 Covalent Binders

Discovered in 1957 by isolation from *Penicillium wortmanni*,¹⁷⁸ Wortmannin (compound **27**, **Figure 18**) became one of the first known inhibitors of PI3K enzymes and was instrumental in determining the role of the PI3K pathway.^{179,180} Crystal structures of Wortmannin bound to PI3K α ¹⁸¹ and PI3K γ ¹⁷⁹ were elucidated and were important in determining the mode of its inhibition. The C₁ carbonyl engages the hinge Val residue via a hydrogen bond interaction, and the furan ring is opened by covalent reaction at C₁₅ with the conserved lysine residue^{140,182} (Lys802 in α , Lys833 in γ). This results in covalent inhibition of PI3K isoforms, by blocking the ATP binding site, as detailed in **Figure 18**.

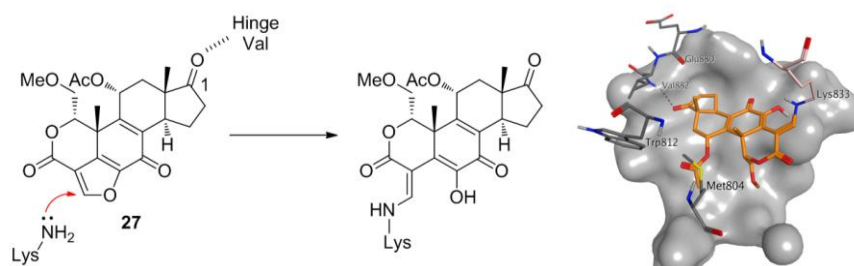


Figure 18 – Covalent bond-forming reaction of Wortmannin **27** with the conserved lysine. The crystal structure of **27** bound covalently to PI3K γ is also shown (PDB: 1E7U).^{179,183}

Despite no absolute evidence of covalent reaction with the β and δ isoforms, Wortmannin is believed to covalently inhibit these isoforms as the lysine is conserved. *In vitro* assays have shown that Wortmannin displays similar potency for the class I, II and III PI3Ks, as well as the PI3K related enzymes mammalian target of rapamycin (mTOR), DNA-dependent protein kinase (DNA-PK), ataxia telangiectasia mutated serine/threonine protein kinase (ATM) and type II phosphatidylinositolphosphate kinases (PIPKins) α and β .¹⁸⁴ It also covalently inhibits Polo-like kinases 1 and 3 (Plk1 and Plk3) by targeting the conserved lysine residues in their active sites.^{185,186} This promiscuity further supports the postulate that Wortmannin covalently inhibits the β and δ isoforms by targeting this conserved lysine residue. Despite its biological importance, Wortmannin was never developed in the clinic due to its instability in biological systems and toxicity, probably resulting from its promiscuous covalent nature.^{187,188}

PX-866 (compound **28**, **Figure 19**) has been developed as a Wortmannin-like PI3K inhibitor. In comparison, it displays a 10-fold increase in potency, improved stability in biological systems, reduced hepatotoxicity, and improved pharmacokinetics.^{187,188} It engages the conserved lysine of the PI3K isoforms in a covalent, non-selective manner.^{187,189} This is achieved due to the reversible nature of the furan ring opening.¹⁸³ Compound **28** acts as a prodrug to Wortmannin, with cyclization by the hydroxyl group and expulsion of diallylamine reforming the reactive furan ring of Wortmannin.^{183,190} Less clinically successful Wortmannin analogues PWT-458 (compound **29**)¹⁹¹ and WAY-176 (compound **30**) have also been developed.¹⁹⁰ PX-866 is currently in Phase II clinical trials to treat patients with recurrent or metastatic castration-resistant prostate cancer.¹⁹²

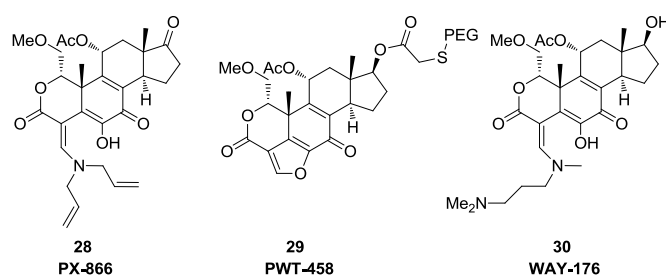


Figure 19 – Structures of PX-866, **28**, PWT-458, **29**, (PEG = polyethylene glycol) and WAY-176, **30**.

It is also worth noting that, recently, selective covalent inhibition of PI3K α has been achieved by Nacht *et al.*⁶² Their compound targets Cys862, an amino acid near the ATP binding site which is specific to the α isoform, with nanomolar potency and 25-fold selectivity against the

other isoforms in biochemical assays. The compound utilises a Michael acceptor as the electrophilic warhead, and shows no off-target reactivity with glutathione (GSH). Whilst this compound is claimed as a selective inhibitor of PI3K α , the reported 25-fold selectivity is modest at best. Other than this, Wortmannin and its synthetic analogues, no further examples of covalent Class I PI3K inhibitors are known.

Table 1 below summarises the biochemical pIC₅₀ values for compounds **21**, and **24-27** when tested in the PI3K isolated enzyme assay (see Section 6.1.1 Biochemical TR-FRET Assay). Higher pIC₅₀ values indicate a more potent compound, with the value increasing logarithmically. Compound **24** demonstrates excellent levels of PI3K δ activity (pIC₅₀ = 9.0) and selectivity over the other three isoforms (>1000-fold selectivity achieved). The structurally related indazole inhibitor **25** displays a similar activity profile, albeit slightly poorer selectivity over α , β and γ . It should be noted that above a pIC₅₀ of 9.0 is in the tight-binding limit, as the potency of the inhibitor is comparable to the concentration of enzyme in the assay,⁴⁹ thus these values may not be completely accurate. As the compound is competitive with ATP binding, increasing the concentration of ATP (2 mM) in the experiment facilitates accurate measurement of a “desensitised” pIC₅₀. This pIC₅₀ is then converted into the reversible binding constant pK_i, which represents the true binding affinity of the compound, using the Cheng-Prusoff equation (see Section 6.2.1 Isolated Enzyme Assay).¹⁹³ The pK_i values obtained from this assay for inhibitors **24** and **25** are shown in parenthesis in **Table 1**.

Compound **26** is less active in the PI3K δ assay compared to the indazole inhibitors and presents ~100-fold selectivity. Wortmannin **27** shows a pIC₅₀ value of ~10 nM at each of the four isoforms, reflecting its documented non-selective nature. It is important to note at this stage that irreversible covalent inhibition is a time-dependent process, as the reactions proceed to completion, rather than equilibrium.^{1,8} As a consequence of this, pIC₅₀ values can be highly variable for the same inhibitor-enzyme system if measured at different time points. Indeed, after infinite time, the pIC₅₀ should approach the tight-binding limit of the assay, and reflect the concentration that is equal to 50% of the initial enzyme concentration in the assay. To provide some contextualisation of the data presented, the isolated enzyme assays have all been quenched and measured after a 1 h incubation.

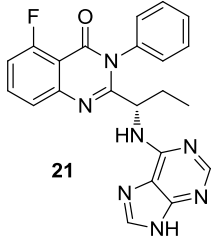
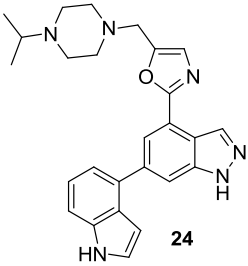
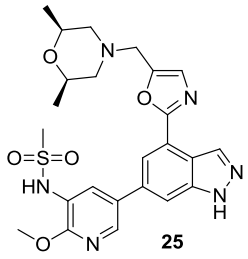
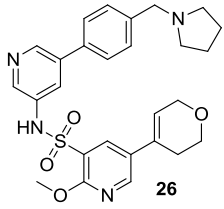
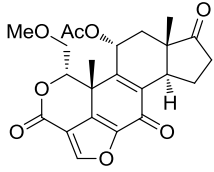
Compound	pIC ₅₀ (pK _i)			
	δ	α	β	γ
 21	8.1	5.0	5.8	6.6
 24	9.0 (9.9)	5.3	5.8	5.2
 25	9.1 ^a (10.1)	6.3	6.2	6.3
 26	8.3	5.5	6.2	5.0
 27	8.3	8.1	8.0	8.2

Table 1 – pIC₅₀ (pK_i) values for compounds **21** and **24-27**, obtained by isolated PI3K enzyme assay. ^a Data reported from N = 17, with one additional empty value.

2.2 Investigation of Hinge-Binding Groups

The different hinge binding motifs presented provide methods of optimising the spatial location of the electrophilic centre in relation to Lys779, whilst also altering the non-covalent interactions that are crucial to achieving selectivity and potency, prior to formation of the covalent bond. Structures based on the propeller shaped inhibitors shown in **Figure 13** were

not pursued, due to the lack of back-pocket occupying group. Initial efforts to establish a covalent bond focussed on using the indazole and DHP hinge binders, due to their success in compounds **24** – **26**, with the methoxypyridine back-pocket group as an initial starting point. Indeed, as presented in **Figure 20**, these different hinge binding motifs position the pyridyl back pocket units, into which the electrophilic centre will be incorporated, in slightly different positions in relation to the potentially nucleophilic nitrogen of Lys779 (distances from the nitrogen to the potential electrophilic sites are noted in green). Whilst the lysine is likely to be highly flexible, the difference in distance, and reaction trajectories could have a significant impact on the covalent binding potential of the inhibitors. In addition, activated esters used by Choi *et al.* were initially investigated as the reactive partner,¹⁰⁸ as these were shown to chemoselectively label one lysine in a complex biological fluid.

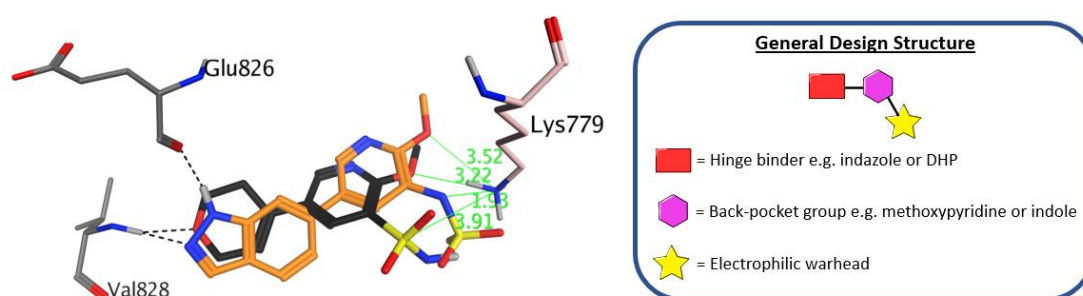


Figure 20 – Overlay of the crystal structures of compounds **25** (orange) and **26** (black) to illustrate movement of the potential electrophilic centre with different hinge-binding groups. All active site residues are removed except for the key hinge residues Val828 and Glu826, and the targeted Lys779. Basic amine side-chains, and interactions in the back pocket have been removed for clarity. Distances from the nucleophilic nitrogen of Lys779 to the potential electrophilic sites are given in angstroms.

2.2.1 DHP vs Indazole Hinge Binders

2.2.1.1 Computational modelling

Throughout this thesis, compounds are computationally modelled to assess their suitability for covalent inhibition. This is done by first modelling the compounds non-covalently, and assessing the position of Lys779 in relation to the electrophilic centre, and comparing the calculated affinity of the compound relative to compound **24** (10.88 kcal·mol⁻¹). Next, the covalent bond is forced and the energy of the structure minimised again (see Section 6.2.13 Computational Modelling for full protocol). The resulting structure is investigated for anything untoward, such as irregular bond lengths and angles or distortion of the protein,

which may indicate that covalent inhibition by the compound is unlikely to occur. Results of computational modelling dictate which compounds are synthesised.

Based on the crystal structures of the DHP and indazole inhibitors **24** - **26** described above, and the evidence of covalent bonding to lysine described by Choi *et al.* by activated esters,¹⁰⁸ six compounds were initially proposed as potential covalent PI3K δ inhibitors (**Figure 21**). These compounds consisted of a DHP or indazole hinge binder, with the methoxynicotinic acid core and an activated ester electrophile. The overlay of the crystal structures presented above (**Figure 20**) identified that Lys779 was in close proximity to the sulfonamide unit once the inhibitors were non-covalently bound in the ATP active site. Replacement of the sulfonamide present in compounds **25** and **26** with the esters developed by Choi *et al.*¹⁰⁸ could result in covalent PI3K δ inhibitors. This initial design is summarised below in **Figure 21**.

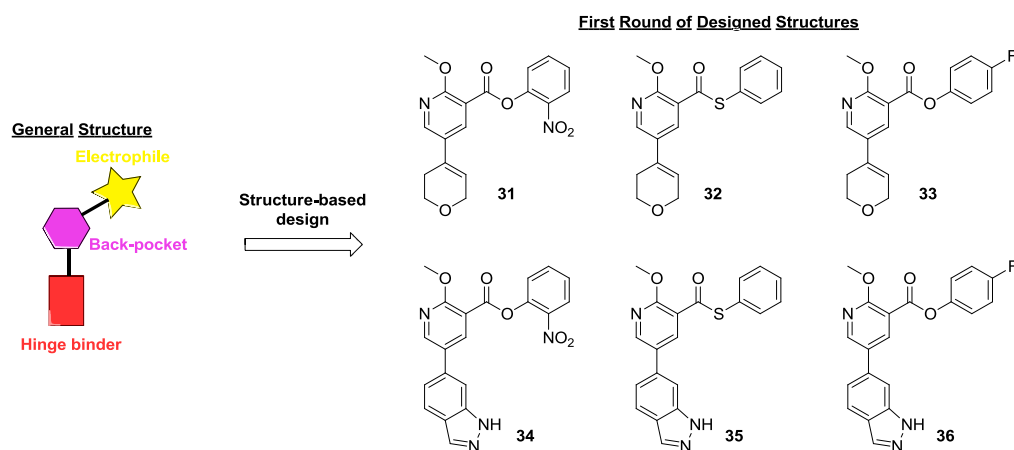


Figure 21 – Six compounds in total were designed based on the general structure shown - three aromatic esters with the DHP motif (**31** - **33**), and three with the indazole motif (**34** - **36**).

The six esters were computationally modelled in the active site of PI3K δ , and the results of this investigation are shown in **Table 2**.

Entry	Hinge	Ester	Calculated Affinity / kcal·mol ⁻¹
1		Compound 24	10.88
2		<i>o</i> -NO ₂ (31)	9.25
3	DHP	thioester (32)	8.51
4		<i>p</i> -F (33)	8.27
5		<i>o</i> -NO ₂ (34)	8.78
6	Indazole	thioester (35)	8.48
7		<i>p</i> -F (36)	8.42

Table 2 – Calculated affinity values for the proposed esters (compounds **31-36**). Compound **24** was also modelled, and its affinity value is used as a benchmark for a potent non-covalent compound.

With the exception of compound **31**, the esters showed similar calculated affinities across the selection, with 0.51 kcal·mol⁻¹ difference between the most and least affinitive compounds. Based on this approach alone, all compounds should therefore be synthesised, as the similar calculated affinities for the PI3K δ ATP binding site should translate to similar non-covalent potencies. However, covalent interactions will alter the observed potency in a time-dependent manner. Therefore, if these inhibitors proved to be covalently bound, it would be expected that different pIC₅₀ values would be observed, which may correlate with the reactivity of the electrophilic centre.

Figure 22 shows the energy minimised models for the six esters bound non-covalently in the PI3K δ ATP active site. As expected from the crystal structures of compounds **24 - 26**, the pyranyl oxygen, and the indazole N and N-H engage the hinge through monodentate and bidentate hydrogen bonds, respectively. The key solvent bridge between a single water molecule and the pyridyl nitrogen, Tyr813, Asp787 and Asp911 was also evident in both series.

Interestingly, in the DHP series, the carbonyl of the ester group interacted with Lys779, directing the electrophilic carbon centre away from Lys779 whilst pulling the nucleophilic amine centre closer to the ligand. In contrast, the indazole series did not show this interaction, exposing the electrophilic carbon to nucleophilic attack by Lys779. However, here the Lys779 side-chain was directed away from the ligand. The residue is clearly flexible, therefore in solution it may move to engage the carbonyl centre covalently in the indazole series. However, for the DHP ligands, rotation of the pyridyl-carbonyl C-C bond was required to expose the electrophilic centre to Lys779.

Modelling the DHP series with the carbonyl groups pointing away from Lys779 gave small changes in calculated affinity, with a slight increase for the thioester (**Table 3**). This showed another possible conformation of the ligand, in which the carbonyl was better aligned for nucleophilic attack. The *o*-NO₂ group also clearly interacted with Lys779, as well as the methoxy group and the carbonyl of the ester, which may have resulted in the notably higher calculated affinity of compound **31**. However, this may be detrimental for covalent inhibition by locking the DHP ligand in this conformation where the carbonyl is directed towards the nucleophilic amine.

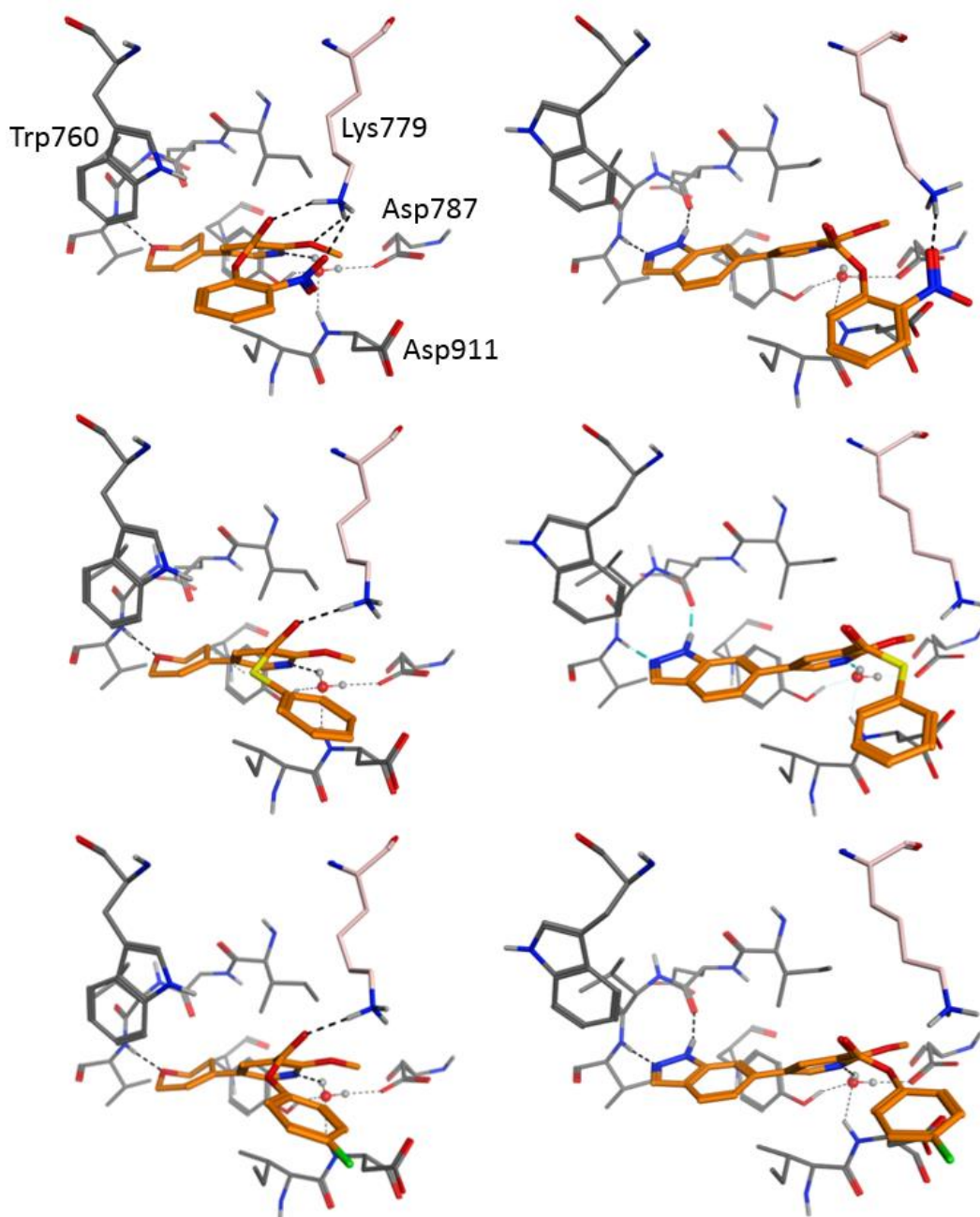


Figure 22 – Left hand side: Modelled non-covalently bound structures of DHP compounds **31 - 33**. Right hand side: Modelled non-covalently bound structures of indazole compounds **34 - 36**.

Entry	Ester	C=O towards Lys779 / kcal·mol ⁻¹	C=O away from Lys779 / kcal·mol ⁻¹
1	<i>o</i> -NO ₂ (31)	9.25	8.93
2	thioester (32)	8.51	8.68
3	<i>p</i> -F (33)	8.27	7.99

Table 3 – Comparison of the calculated affinities for the DHP series with the carbonyl of the ester group pointing towards Lys779 (as in **Figure 22**) and away from Lys779 (structures not shown).

Finally, both series were modelled as covalently bound structures. A bond was forced between Lys779 and the ligand, and the aromatic leaving group was deleted. Energy minimised structures are shown below (**Figure 23**). Calculated affinity values could not be obtained as the ligands are now covalently attached to the protein, therefore affinity could be considered as the strength of the newly formed C-N bond.

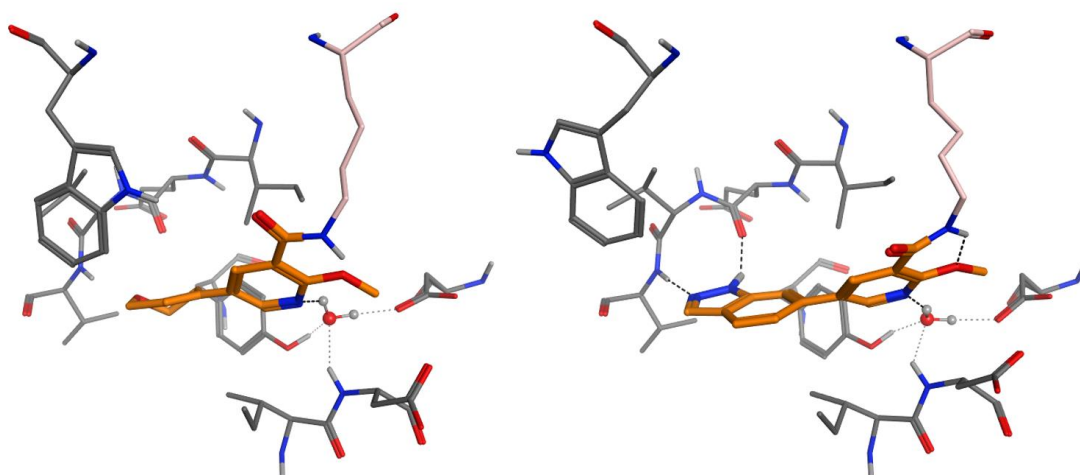


Figure 23 – Left: Modelled covalently bound DHP inhibitor. **Right:** Modelled covalently bound indazole inhibitor.

The models above indicated that both series have the potential to covalently bind to Lys779. They both showed the carbonyl to be pointing away from the lysine, as expected, and retention of the solvent bridge between the pyridyl nitrogen and Tyr813, that was evident in the non-covalently bound models. What differed significantly between the two was the hinge region. In the indazole series, there was little change here, however in the DHP series the ligand was pulled away from the hinge by 1.05 Å (**Figure 24**) to compensate for the larger distance between the electrophilic centre and the nucleophilic amine (**Figure 20**). As the hinge residues were excluded from the minimisation procedure in the modelling, this movement destroyed the hydrogen bond between the pyranyl oxygen and Val828. The flexibility of Lys779 was also evident again, as the side-chain had adopted slightly different conformations to accommodate the differently sized ligands.

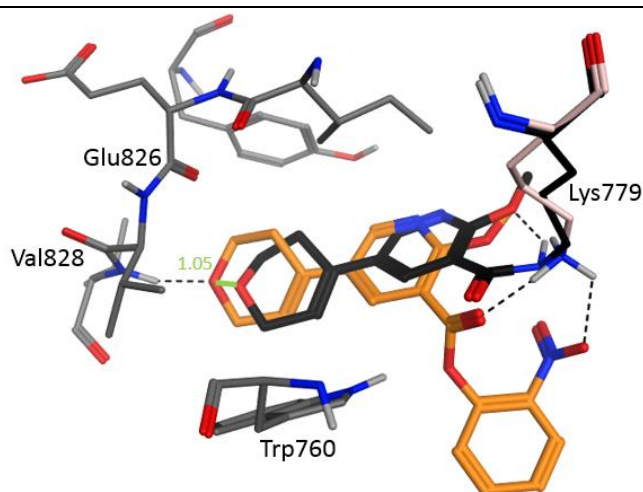
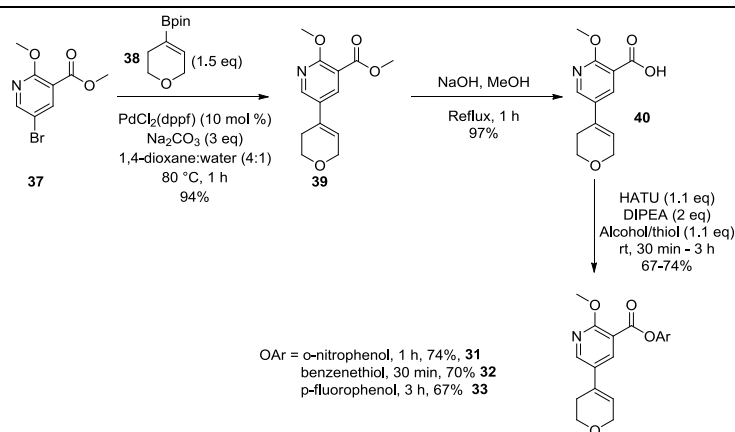


Figure 24 – Overlay of the modelled non-covalently bound (orange ligand, pink lysine) and the covalently bound (black ligand and lysine) DHP structures to show how the ligand is pulled away from the hinge upon formation of the covalent bond. Distance moved is shown in green, in Å.

In conclusion, computational modelling found that all six proposed compounds had reasonable calculated affinities for the PI3K δ ATP binding pocket, in a reversibly bound pose. Investigation of the minimum energy structures showed how conformations of the ligands could be obtained where the carbonyl was orientated such that the nucleophilic nitrogen of Lys779 can approach with a trajectory closer to the optimal Bürgi-Dunitz angle of $\sim 110^\circ$.¹⁹⁴ Forcing the covalent bond for both series produced plausible structures for a covalently bound inhibitor, indicating that these compounds may be suitable for covalent inhibition, and therefore all six were progressed to synthesis and *in vitro* assessment of activity.

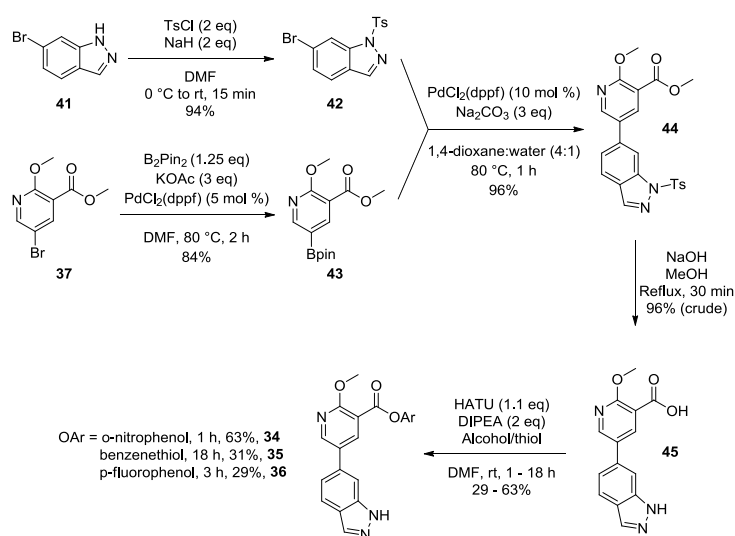
2.2.1.2 Synthesis of DHP and Indazole Hinge Binders

Synthesis of the DHP series proceeded via the route shown in **Scheme 2** from bromomethoxynicotinic acid **37**. After some exploration of Suzuki conditions, [1,1'-bis(diphenylphosphino)ferrocene] dichloropalladium(II) ($\text{PdCl}_2(\text{dppf})$) with sodium carbonate, in dioxane/water, heated thermally was found to give the greatest yield of coupled product **39**. Alternative conditions explored using different catalyst systems and microwave heated caused hydrolysis of the ester, which inhibited reaction progress, and was not straightforward to purify from the reaction mixture. Compound **39** was hydrolysed under typical basic conditions to afford acid **40**, which was then coupled to the desired phenols using 1-[bis(dimethylamino)methylene]-1*H*-1,2,3-triazolo[4,5-*b*]pyridinium 3-oxid hexafluorophosphate (HATU) as the coupling reagent.



Scheme 2 – Synthesis of DHP esters.

In a similar fashion, the indazole esters were also synthesised by HATU-mediated couplings from the parent carboxylic acid (compound **45**). Synthesis of this intermediate required protection of the indazole nitrogen with tosyl chloride and sodium hydride, in order to prevent suspected chelation of the indazole nitrogen to the palladium centre in the Suzuki step, which halted conversion. Borylation of compound **37** to compound **43** allowed a high yielding convergent route to the tosyl protected methyl ester **44**. This intermediate was deprotected and hydrolysed in tandem to afford the crude acid **45** in good yield (**Scheme 3**).



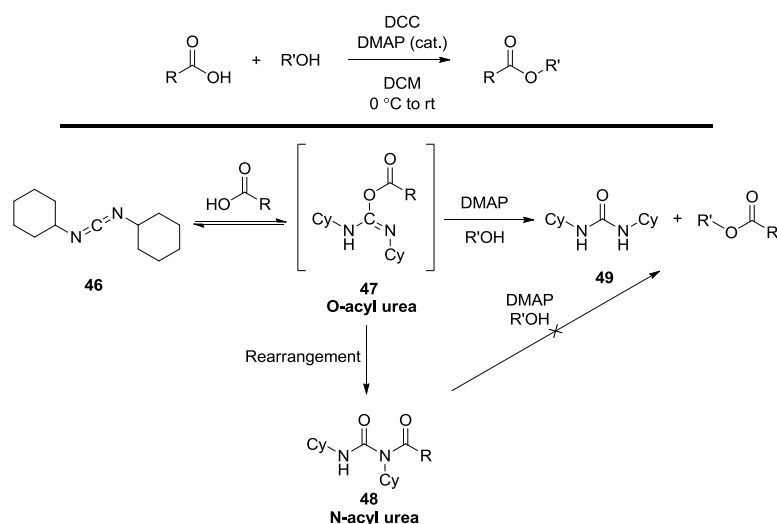
Scheme 3 – Synthesis of indazole esters.

The final esterification step was originally achieved through Steglich esterifications¹⁹⁵ utilising *N,N'*-dicyclohexylcarbodiimide (DCC, **46**) as the coupling agent. However, poor yields due to formation of a known side-product of this reaction (**Scheme 4**, observed by Liquid Chromatography-Mass Spectrometry (LCMS) in the reaction profile),¹⁹⁶ led to the use of

HATU as an alternative coupling reagent. One exception to this situation was the indazole thioester (compound **35**, Table 4 Entry 5), which proceeded in much greater 57% yield by DCC coupling than HATU coupling.

Entry	Hinge	Phenol	Product	DCC % Yield	HATU % Yield
1		<i>o</i> -nitrophenol	31	54	74
2	DHP	thiophenol	32	52	70
3		<i>p</i> -fluorophenol	33	56	67
4		<i>o</i> -nitrophenol	34	15 ^a	63
5	Indazole	thiophenol	35	57	31
6		<i>p</i> -fluorophenol	36	20 ^b	29

Table 4 – Yields from DCC and HATU couplings to the esters. a = Crude yield; b = Percentage conversion by LCMS, product not isolated.



Scheme 4 – Reactions of DCC **46**.¹⁹⁶ The top route shows the general reaction. In the mechanism below, the desired reaction proceeds via the *O*-acyl urea **47** intermediate to the ester. Rearrangement to the unreactive *N*-acyl urea **48** was observed by LCMS in all reactions, and led to the use of HATU as the coupling agent of choice to avoid this byproduct.

The scheme above shows the desired reaction of **46**, through the *O*-acyl urea intermediate **47**. This is not easily isolable¹⁹⁶ due the potential reversibility of its formation, and rearrangement to the unreactive *N*-acyl urea **48**. This side-product was observed (by LCMS) in all reactions, but most notably in the syntheses of compounds **31** and **33**, leading to the use of HATU as the preferred reagent for these couplings.

2.2.1.3 Biological Characterisation of the DHP and Indazole Hinge Binders

All six compounds, and the two corresponding carboxylic acids were assessed in the initial *in vitro* PI3K isolated enzyme assays (**Table 5**). It is important to reiterate at this stage that the activity may be time-dependent due to potential covalent binding of the inhibitors to the PI3K isoforms, and the pIC_{50} values reported may therefore alter with incubation time. However, these assays, and all PI3K isolated enzyme assays presented herein, were quenched at 1 h to provide contextualisation of the data. A description of the assay design is provided in Section 6.1.1 Biochemical TR-FRET Assay, along with the detailed experimental protocol in Section 6.2.1 Isolated Enzyme Assay.

Entry	Series	R	Number	pIC_{50}			
				δ	α	β	γ
1			40	<4.5	<4.5	<4.5	<4.5
2			33	5.0	<4.5	4.9 ^a	<4.5
3			32	5.0	4.7	4.9	<4.5 ^b
4			31	6.4	5.5	6.0	4.9
5			45	5.3	<4.5	<4.5	<4.5
6			36	5.4	<4.5	5.3	<4.5
7			35	6.8	5.8	6.6	<4.5
8			34	7.2	6.2	7.2	5.3

Table 5 – PI3K isolated enzyme data for the synthesised compounds. pIC_{50} values are given first for the acid intermediates, and then the esters in increasing order of PI3K δ potency within each series. ^a Results from N = 1, with one additional value <4.5. ^b Results from N = 3, with one additional value = 4.8.

Two patterns immediately emerged from this dataset. Firstly, the indazole hinge binder in every case was more potent at the δ isoform than the corresponding DHP ester. The carboxylic acid inhibitors **40** and **45** cannot covalently bind to the kinases, therefore their activity arose purely from non-covalent interactions. From these data, it was clear that the indazole motif represented a better hinge binder than the DHP unit, which was not predicted by the molecular modelling. This may have arisen from better alignment of the indazole group to the hinge Val and Glu residues, giving a stronger hydrogen bonding interaction

(Figure 20), as well as π interactions with the aromatic system of the indazole rings. This observation implied that the overall improved activity of the indazole series may be arising solely due to better non-covalent interactions.

The second pattern observed was that potency generally increased in the expected order based on calculated affinities obtained from the molecular modelling for each series (Table 2). The modelling predicted a roughly 3.5-fold (0.5 log unit) change in potency (see Section 6.2.13 Computational Modelling) between compounds 31 and 32, with 31 being the more potent. Clearly, the fold-change measured significantly greater, at ~20-fold. This change could be reflecting covalent binding of the nitro compound 31.

In the indazole series, the modelling predicted roughly a 2-fold change in potency (0.3 log units) across the three compounds (Table 2). Again, the measured potency increased significantly more than this (~63 fold), which may be due to covalent interaction with the kinase. This is supported by the observation that the activity of this series increases in order of the expected electrophilic reactivity of the esters, based on consideration of the pK_a values of the leaving groups (Table 6).^{197,198} However, such a trend was not observed in the study performed by Choi *et al.*,¹⁰⁸ where all three esters had similar activities *in vitro* (Table 6). The reported pIC_{50} values may not be reflecting the true covalent nature of their system, or reactivity of the ester does not affect potency in their systems.

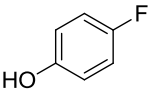
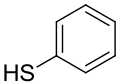
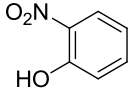
Leaving group			
	50	51	52
pK_a	9.89	7.78	7.23
pIC_{50} (Choi <i>et. al</i>) ¹⁰⁸	5.7	5.7	5.7

Table 6 – pK_a and pIC_{50} values of the phenols corresponding to Choi *et al.*'s leaving groups. For a covalent inhibitor, where potency is directly related to reactivity of the ester, potency (pIC_{50}) would be expected to increase as pK_a decreases.

Overall, the compounds were poorly selective for the δ isoform. Compounds 31, 34 and 35 were approximately 10-fold selective over the α and γ isoforms, but none of the inhibitors presented significant selectivity over PI3K β . This lack of selectivity was not a concern at this stage of the project as the compounds did not yet possess any groups in the selectivity region next to Trp 760.¹⁷⁵

One hypothesis for the potency of the *o*-nitrophenol esters was that the nitro group was interacting with Lys779, as indicated in the molecular modelling (**Figure 22**). To test this theory, *p*-nitrophenol-DHP ester **54** was modelled following the process discussed above. This revealed that the nitro group at the para position could not interact with Lys779, which resulted in a calculated affinity of 7.92 kcal·mol⁻¹, a value noticeably lower than that predicted for the other esters from that series (**Table 2**), which would predict an approximately 10-fold decrease in measured potency compared to the *o*-NO₂ compound. Compound **54** was synthesised via the DCC route, and tested in the *in vitro* assays (**Figure 25**).

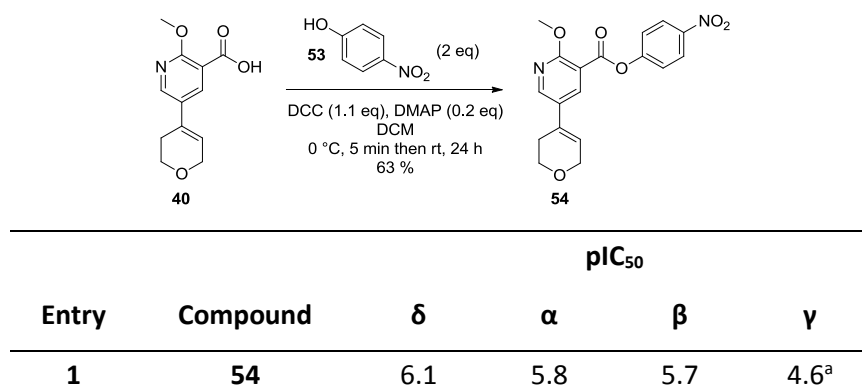


Figure 25 – Synthesis of *p*-nitrophenol-DHP ester **54** and its PI3K isolated enzyme data. ^a Results from N = 2 with one additional value <4.5.

This inhibitor was found to have a pIC₅₀ for PI3Kδ of 6.1, not significantly different from that obtained by the *o*-nitrophenol ester **31** (pIC₅₀ = 6.4). This indicated that the *o*-nitro group did not increase potency solely by forming a hydrogen bonding interaction with Lys779, as suggested by the molecular modelling. As the leaving group ability of *p*-nitrophenolate **53** was predicted to be similar to that of *o*-nitrophenolate **52** (pK_as of the phenols = 7.15 and 7.23, respectively),¹⁹⁸ this suggested that the superior affinity of nitrophenol esters for PI3Kδ was driven by either electron deficiency of the ring in the reversible binding step, or covalent reaction of the inhibitors with the kinase.

A reactivity assessment of the esters was then carried out under basic conditions. This test aimed to confirm that the compounds can react with the terminal amine of the lysine side-chain, and investigate whether the reactivity trend observed correlates with the activity measured in the biochemical assays. To simulate the entropic system of the active site, an excess of *N*_α-(*tert*-butoxycarbonyl)-L-lysine (*N*-Boc-Lys) was used to increase the probability of collision between the free amine and the electrophilic centre. In addition to this, a large

excess of non-nucleophilic base (*N,N*-diisopropylethylamine (DIPEA)) was used to ensure that the *N*-Boc-Lys does not exist in its zwitterionic form, liberating the free amine for nucleophilic attack. It is important to note that this may not be an accurate representation of the protonation state of the lysine in the active site, as an equilibrium between the free base and the protonated form is likely to exist. However, buried lysines have been shown to exhibit dramatically decreased pK_a values (from ~ 10 to ~ 5),⁵⁶ which would imply that Lys779 could be deprotonated, and therefore hyper-reactive in the active site of these enzymes. Reactions were analysed by LCMS at regular intervals to determine the percentage conversion from ester to amide (**Figure 26**).

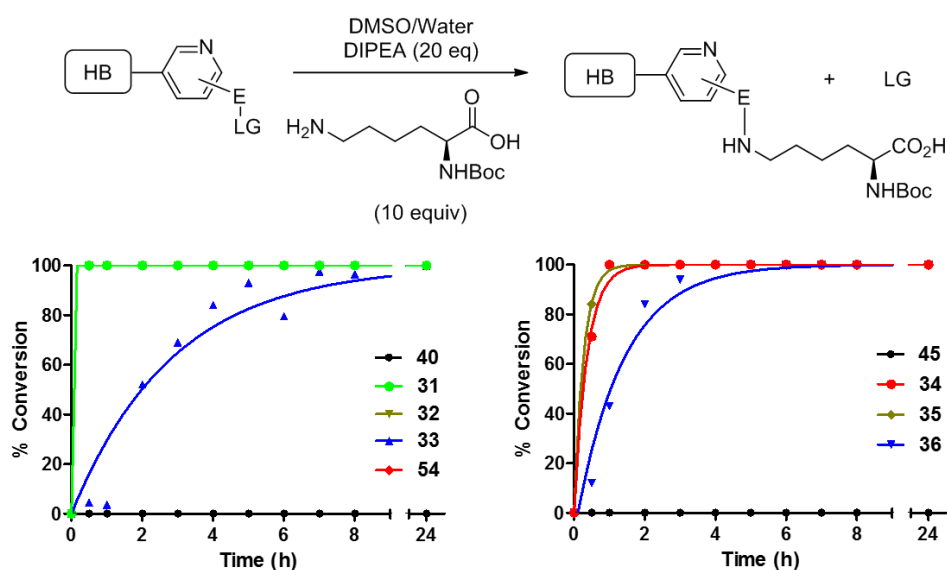


Figure 26 – Results of reactivity tests. Percentage conversion is measured at a specific time period by LCMS, calculated as $\%A/(\%A + \%I)$, where $\%$ = percentage of the total area of the UV trace obtained by LCMS, A = amide and I = inhibitor. For the DHP compounds on the left, the curves for both nitrophenol esters and the thioester are on top of each other.

These tests showed that all esters could efficiently undergo an amidation reaction, in a purely chemical setting, suggesting that they have the potential to covalently modify Lys779. As predicted, acids **40** and **45** did not show any potential for covalent inhibition, with the percentage conversion to the amide in both series remaining at zero after 24 h (black circles). This further supported the conclusion above that the indazole group was the better hinge binding moiety due to more efficient non-covalent interactions, as exhibited by the >4 -fold increase in pIC_{50} values when moving from the DHP hinge binder to the indazole hinge binder. Furthermore, in both series, the thioester and nitrophenol esters were equally reactive (up to the limits of the detection method), and significantly more reactive than the fluorophenol esters. This difference in reactivity of the fluorophenol ester was also more significant in the

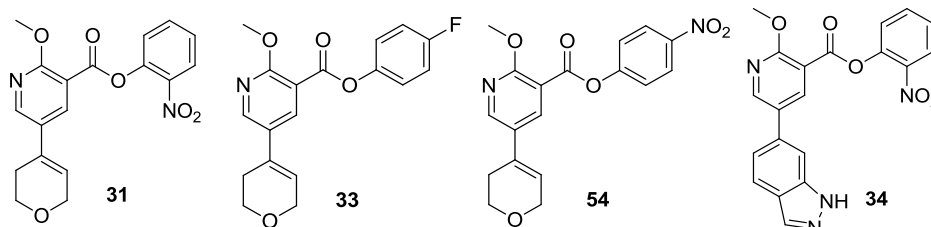
DHP series than the indazole series. This was inconsistent with the enzyme assay data, which would suggest that the fluorophenol and thiophenol DHP esters (**32** and **33**) were equally reactive if they were covalent binders, and if the $pI_{C_{50}}$ value observed was strongly influenced by the reactivity of the ester. This may be evidence for these two esters not being covalently bound, as there is no trend with the expected reactivity based on pK_a analysis.

Mechanistically, thiophenol esters have been found to undergo amidation reactions faster than the corresponding oxo-esters.^{199,200} This is proposed to be due to a smaller degree of conjugation from the sulfur atom into the carbonyl, relative to the bridging oxygen atom of an oxo-ester, rendering the thioester more reactive.²⁰¹ Indeed, the activation energy for reaction of ammonia with methyl acetate was found to be 4.6 kcal.mol⁻¹ greater than the activation energy for the analogous reaction with methyl thioacetate.²⁰⁰ This implies that, rather than leaving group ability (pK_a of the phenol) describing the reactivity of these esters, there may be a greater reliance on addition into the carbonyl. Indeed, amidation reactions primarily are two-step in nature, consisting of an addition to form a tetrahedral intermediate, and subsequent elimination with expulsion of a leaving group, either of which could be rate-determining.²⁰² The mechanistic implications of this reactivity, in an enzymatic setting, are discussed in greater detail in Section 4.1 Kinetic Analysis of Binding, and Mechanistic Implications.

At this stage, no conclusion can be drawn about the impact of this reactivity assessment on the biological profile of these inhibitors, other than the fact that these esters can react with a deprotonated lysine residue. Covalent inhibition is two-step in nature consisting of reversible binding and then covalent inactivation. It could be the case at this stage that all of the variation in $pI_{C_{50}}$ observed is purely due to non-covalent interactions. Perhaps the sulfur atom at this position is not tolerated by the enzyme due to its larger size and polarizability, or the presence of the nitro group has other favourable interactions in the back pocket not determined by the modelling. The interaction with Lys779 predicted for the *o*-nitrophenol esters **31** and **34** would support this theory, if the *p*-nitrophenol ester **54** did not show such a consistent potency.

In light of these results, it was determined that all compounds showed potential for covalent inhibition, and that their mode of inhibition had to be determined. Compounds **31**, **33**, **54** and **34** were therefore submitted for structural analysis by x-ray crystallography. The thioesters were discovered to decompose over time, possibly due to greater reactivity as

discussed above. The nitrophenol esters were found to be more potent, and easier to handle, therefore the thioesters were not pursued further. Compound **33** was submitted over **36** as the pIC₅₀ values differed by only two-fold, and **33** was available in sufficient amount for testing. Results of the crystallography investigations are given in **Table 7**, and are discussed below.



Covalent?	Yes	Unknown	Yes	Yes
------------------	-----	---------	-----	-----

Table 7 – Summary of x-ray crystallography investigations

The crystal structure of compound **31** in the PI3K δ active site was obtained, resolved to 2.8 Å (**Figure 27**). It showed the oxygen of the DHP ring engaging Val828 via a monodentate hydrogen bond. It also displayed Trp760 in the same configuration as the modelled structures, and the pyridyl ring occupying the back-pocket region, also in agreement with the modelling. The solvent bridge formed with the pyridyl nitrogen in the model was, however, no longer evident in the crystal structure. This could be due to rotation of the pyridyl ring out of the correct orientation for a favourable interaction, or due to inadequate resolution in the electron density. Most importantly, the crystal structure depicted clear, continuous electron density from the Lys779 side-chain onto the ligand. It also showed an absence of electron density for the nitrophenol leaving group, indicating that this compound was indeed covalently bound to the active site. Finally, overlay of the crystal and modelled structures shows that the hinge region (*i.e.* Val828) shifts towards the inhibitor when the ligand covalently binds to Lys779. This movement was partially predicted by the molecular modelling, as it anticipated that for the covalent bond to be formed, the ligand had to be pulled away from the hinge by 1.05 Å. However, in the computational modelling the hinge was fixed in its initial position, hence this movement destroyed the hydrogen bonding interaction between the pyranyl oxygen and Val828. In reality, the hinge amino acids possess the ability to move slightly to maintain the hydrogen bond, whilst the covalent bond is being formed. The crystal structure for compound **54**, bearing the *p*-nitrophenol leaving group was

also obtained. However, the structure was identical to that of **31**, and therefore is not discussed further.

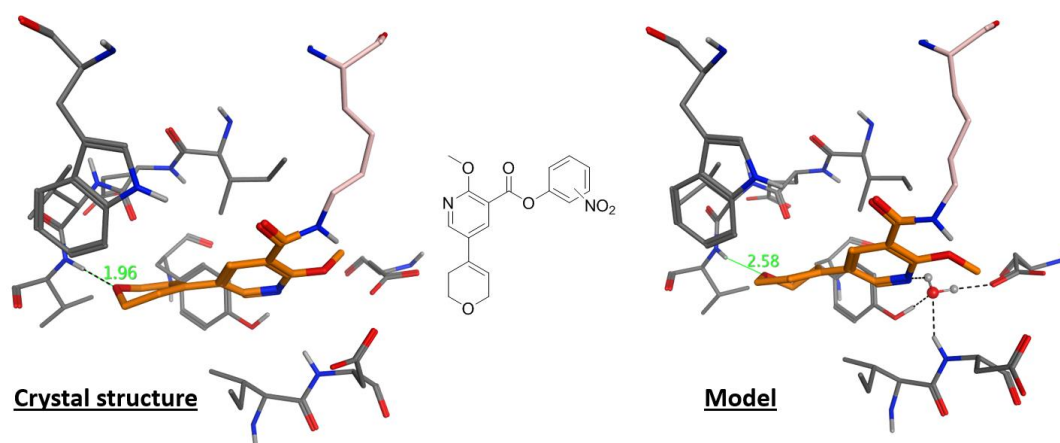


Figure 27 – Left: Crystal structure of **31** and **54** covalently bound to PI3K δ . Right: Modelled structure from **Figure 23**. Distances between the pyranyl oxygen and Val828 are given (in Å) in both structures to emphasise how the hinge shifts with the ligand to maintain this hydrogen bonding interaction.

The crystal structure of the corresponding *o*-nitrophenol indazole ester (**34**) was also obtained, resolved to 2.4 Å. Clear electron density from Lys779 onto the ligand was seen, with an absence of electron density for the leaving group, concluding that this compound was also a covalently bound inhibitor (**Figure 28**). Again, the model was in reasonable agreement with the determined structure. One obvious difference was that the pyridyl water was, again, no longer visible in the electron density. Also, there was a noticeable difference in the coplanarity of the indazole and pyridine rings. The crystal structure depicted much greater rotation of this bond, to bring the pyridyl ring out of the plane of the indazole rings, which may explain the absence of the pyridyl water molecule. This rotation brought the carbonyl group closer to the lysine residue, minimising the movement required by the protein to form the covalent bond.

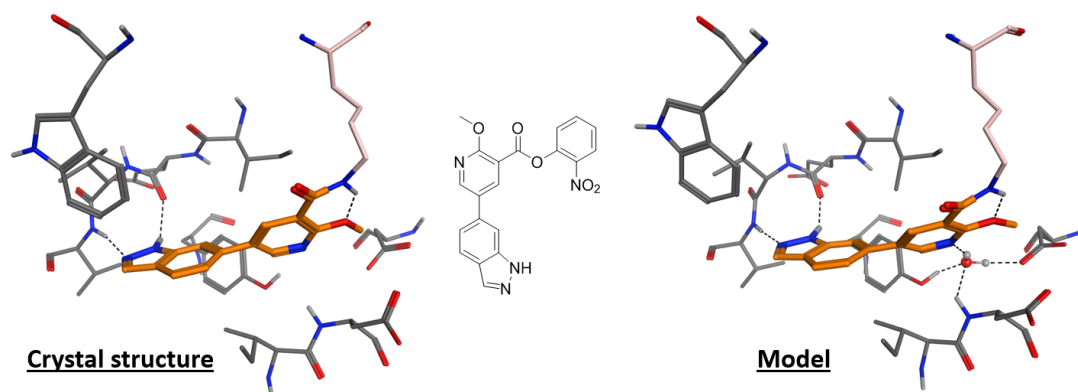


Figure 28 – Left: Crystal structure of **34** covalently bound to PI3K δ . Right: Modelled structure from **Figure 23**.

The *p*-fluorophenol DHP inhibitor (compound **33**) was not observed in the active site of PI3K δ , implying that the compound was not potent enough to efficiently occupy the active site, or was not sufficiently soluble at the high concentrations required for this experiment. Its binding mode was not determined, hence it could not be concluded at this stage whether the *p*-fluorophenol leaving group was also activated enough for covalent inhibition. In fact, it may be the case that the nitrophenol leaving group is too activated for selective inhibition, and that after maximising the non-covalent interactions, the *p*-fluorophenol group could be a better leaving group for selective inhibition, by being sufficiently unreactive until the inhibitor is residing in the active site for a longer period of time.

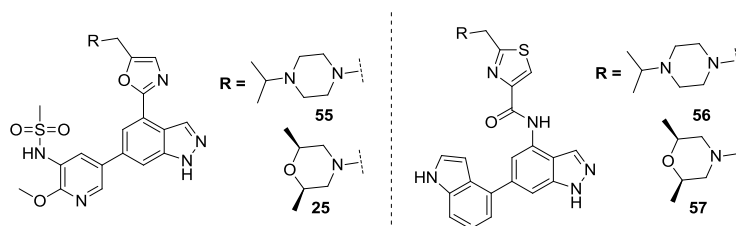
In conclusion, this section of work has shown that phenolic esters can efficiently form amides with a reactive lysine amine. Furthermore, it has been shown by crystallography that nitrophenol esters are able to undergo this transformation within the active site of PI3K δ , with the targeted amino acid. However, crystallography experiments could not conclude whether the less reactive fluorophenol ester was also susceptible to this reaction in the enzyme active site. This was likely due to poor non-covalent interactions with the inhibitor and protein, reflected in a low pIC₅₀ value and lack of occupancy in the crystal structure. Thiophenol esters were also explored, and found to be equally (if not more) reactive as the nitrophenol ester in a flask, despite pK_a predictions suggesting the relationship should be inverted. This highlighted how pK_a may not be a reliable parameter for predicting reactivity of these (thio)esters, due to the two-step nature of the reaction. The thioesters were also found to be particularly unstable and degraded as solids, so were not pursued further. It was also shown that the indazole hinge binder has better non-covalent interactions with the kinase, which may facilitate the use of less reactive electrophiles as the project progresses. Finally, none of these compounds showed a great level of selectivity; however this was not a concern due to the lack of any selectivity inducing group in either the induced fit pocket or the selectivity region of the kinase **Figure 16**.

With these proof-of-concept experiments completed, the next section aims to improve upon the potency and selectivity of these esters. Three areas are explored to achieve this – firstly by introducing a pendant amine arm on the indazole hinge-binder; secondly, variation of the electrophilic centre; and, thirdly, exploration of alternative back-pocket groups.

3. Optimisation of Irreversible Binders

3.1 Exploring the Selectivity Pocket with a Basic Amine

Section 2.1 PI3K δ Inhibitor Chemotypes discussed two ways of introducing selectivity and potency for PI3K δ by binding to one of two selectivity pockets. The first was the induced pocket exploited by propeller-shaped inhibitors such as Idelalisib,¹⁷² and the second was a solvent-exposed region next to Trp760,¹⁷⁵ exploited by the indazole structures developed in our laboratories.¹⁶³ As our compounds were closely related to the indazole structures, it was decided to employ a basic amine side-chain coming off this indazole hinge binder. Two options were identified as potent and selective side-chains in prior studies – isopropylpiperazine (compound **24**) or dimethylmorpholine (compound **25**) in **Figure 15**.¹⁶³ In the matched pairs **55** vs **25** and **56** vs **57** below, both show comparable potency and selectivity. However, the isopropylpiperazine group gives improved solubility measured by chemiluminescent nitrogen detection (CLND). This feature is likely to be beneficial with introduction of a lipophilic aromatic ester, therefore the isopropylpiperazine group was pursued.



Entry	Compound	δ (p <i>K_i</i>)	p <i>C</i> ₅₀			CLND (μ M)
			α	β	γ	
1	55	9.4 (10.1)	6.9 ^a	6.0	5.9	>402
2	25	9.1 ^b (10.1)	6.3	6.2	6.3	354
3	56	8.5	5.9	5.8	5.4	166
4	57	8.7	4.9	5.3	5.6	41

Table 8 – Biochemical p*C*₅₀ data and solubility (CLND) data for matched pairs **55** vs **25** and **56** vs **57**, showing a preference in solubility for the isopropylpiperazine side chain. ^a Data reported from N = 5, with one additional empty value. ^b Data reported from N = 17, with one additional empty value

It was envisaged that an increase in potency at PI3K δ may facilitate the use of a significantly less electrophilic centre (*i.e.* methyl ester), which would presumably be more stable than the

activated aromatic esters. Compounds **58** - **60** below were therefore proposed as initial targets to assess the effects of introduction of a basic amine in this region.

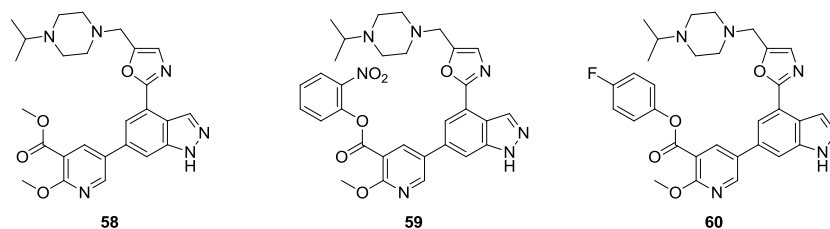


Figure 29 – Structures of esters **58** - **60** proposed for this investigation.

3.1.1 Molecular Modelling

Molecular modelling indicated that these compounds may (non-covalently) be more potent than compound **24**, which was used as the benchmark for ideal activity. The values obtained for the aryl esters would predict an approximately 200-fold (2.3 log unit change) in potency compared to the corresponding esters without the amine side chain, if covalent interactions did not contribute to potency. Results of the modelling are shown numerically in **Table 9**, and pictorially in **Figure 30** below.

Entry	Compound	Calculated affinity / kcal·mol ⁻¹
1	24	10.88
2	58 – methyl ester	11.19
3	59 – <i>o</i> -nitrophenol ester	11.87
4	60 – <i>p</i> -fluorophenol ester	11.65

Table 9 – Calculated affinity values for esters **58** - **60**

Overall the non-covalently bound structures looked very similar (**Figure 30**). The key interactions at the hinge were satisfied, and the interaction with the pyridyl water was maintained. As seen earlier, the nitro group of compound **59** interacted with Lys779, which may have generated the slight increase in calculated affinity over compounds **58** and **60**. There was a slight perturbation in the orientation of the carbonyl group relative to Lys779, and the orientation of the methoxy group adjacent to it between the compounds. However, these were very small changes, and as no observable interactions were made or disturbed, thus it was unlikely that they impacted greatly on the calculated affinities observed. As nitrophenol esters have already been shown to be successful covalent inhibitors, this

interaction likely has little effect on observed pIC_{50} , but may explain why the calculated affinity of the nitrophenol ester was greater than the fluorophenol ester.

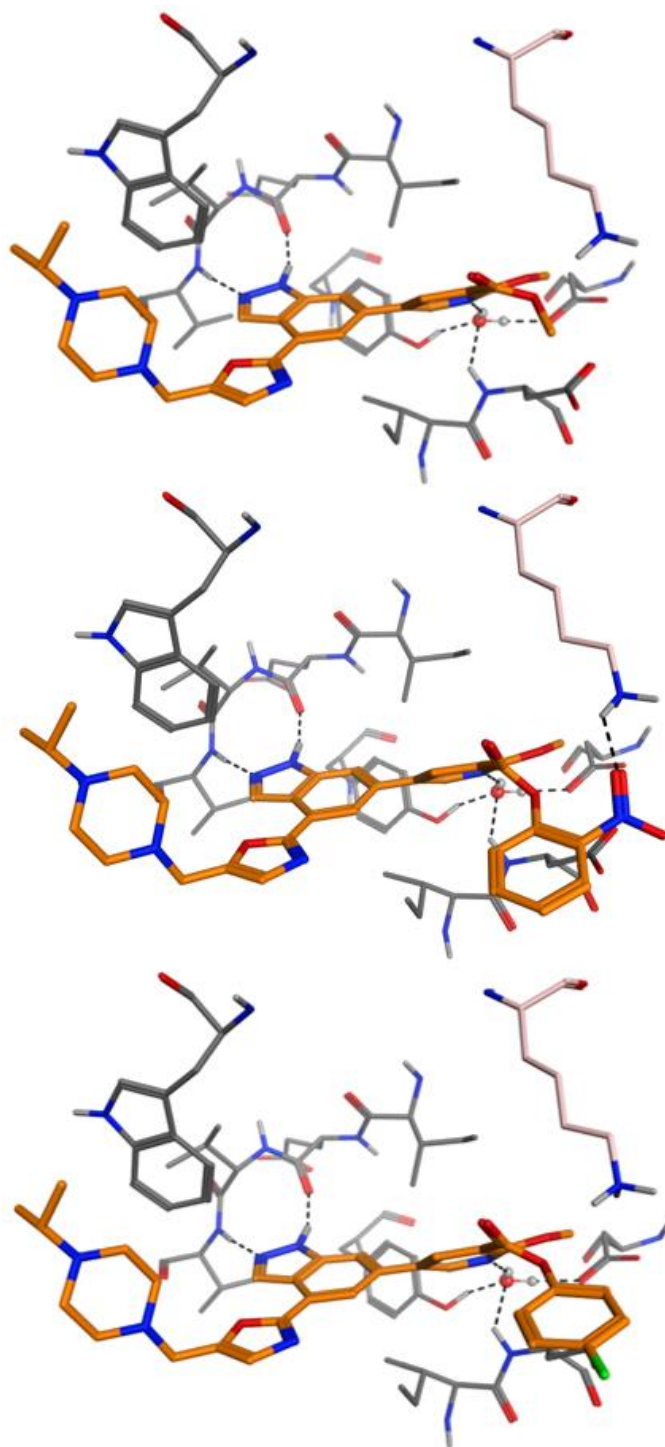


Figure 30 – Modelled non-covalently bound structures of compounds **58** (top), **59** (middle) and **60** (bottom).
Shown below in **Figure 31** is the covalently bound model for inhibitors **58** - **60**, which was identical for all three after loss of the leaving group. The structure was, as expected, nearly identical to that of the first set of inhibitors without the isopropylpiperazine arm (pink). One

observable difference was that the current inhibitors (orange) were bound more closely to the hinge by 0.3 Å. This is likely to be due to the isopropylpiperazine group preventing movement of the ligand by packing more effectively into the active site. This movement was very minor, especially when compared to the 1.05 Å shift predicted by the DHP series (**Figure 23**), and was therefore unlikely to greatly affect the potential covalent binding nature of these ligands.

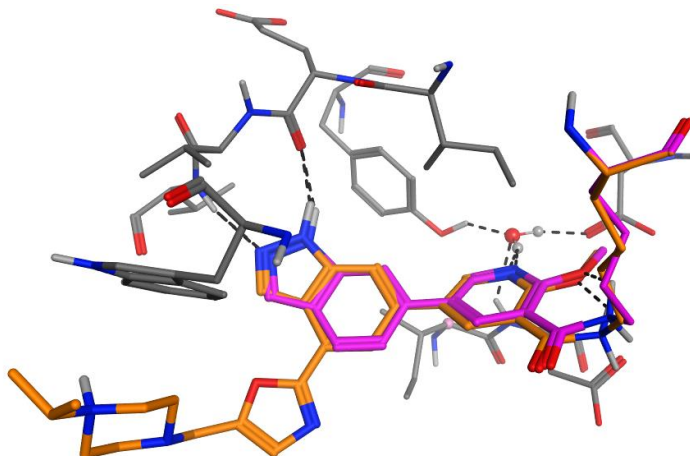


Figure 31 – Overlap of modelled indazole inhibitors with (orange) and without (pink) the pendant arm. Inhibitor **34** (already known as covalent inhibitor) is shown in pink, and the model for inhibitors **58 - 60** is shown in orange. Very close overlap is seen, with the isopropylpiperazine inhibitor moving 0.3 Å closer to the hinge.

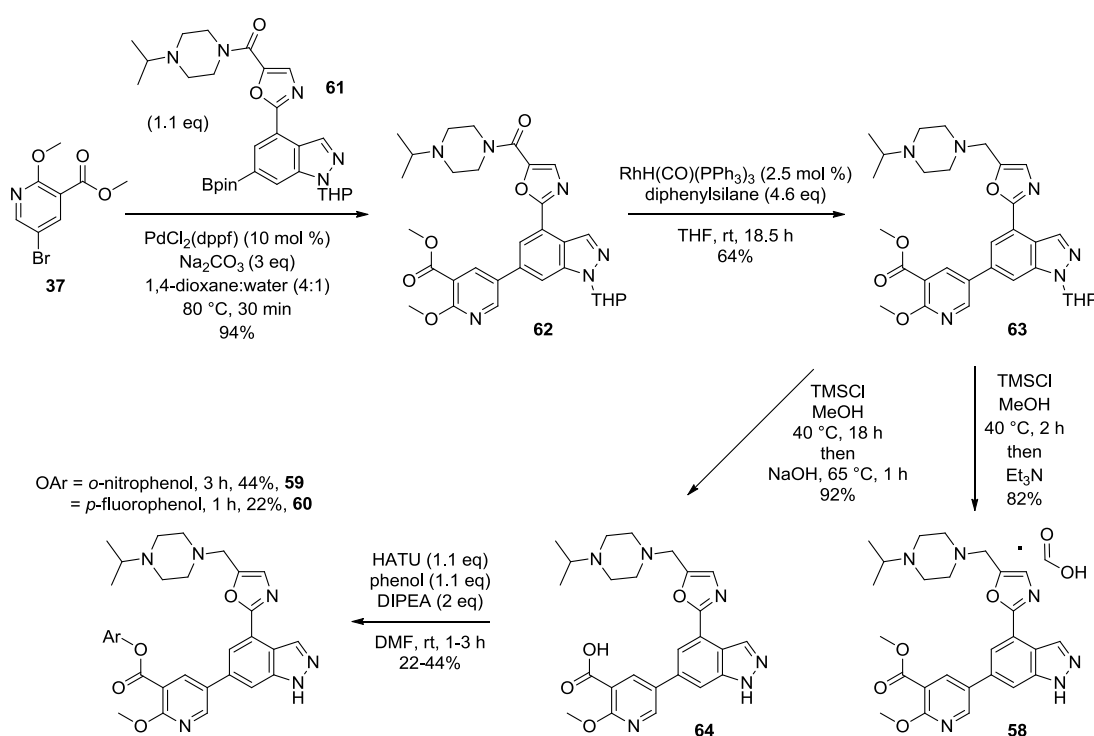
In conclusion, this section of modelling showed that the proposed compounds retain their potential for covalent inhibition upon incorporation of the isopropylpiperazine fragment. It also indicated that these compounds should be significantly more potent than the less elaborated indazoles from consideration of the binding energy differences. All three compounds were therefore taken forward to synthesis.

3.1.2 Synthesis

Compound **61** was already available in multigram quantities within our laboratories,²⁰³ significantly reducing the number of steps required to reach the desired esters. The final route used is shown below in **Scheme 5**.

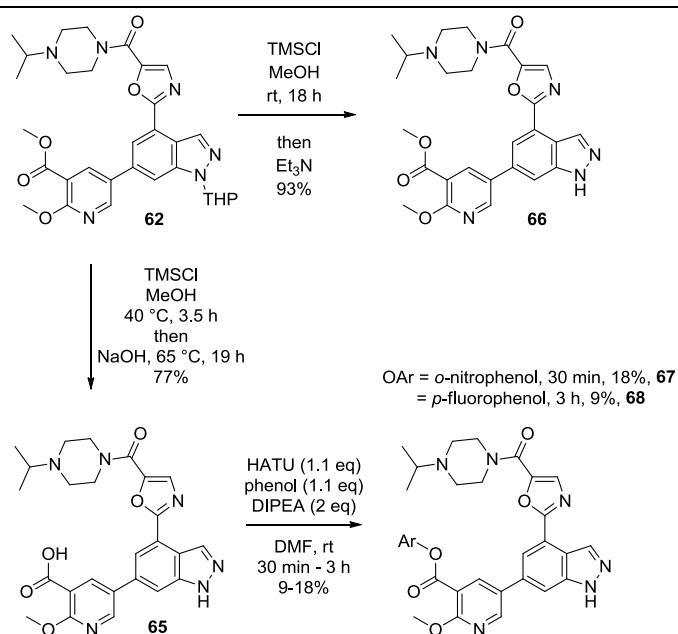
The first step invoked a Suzuki coupling using the conditions previously established to avoid hydrolysis of the ester group, affording intermediate **62** in excellent yield. Chemoselective reduction of the amide over the ester was the key step in this synthesis, and is discussed further below. Successful conditions utilised a rhodium-catalysed hydrosilylation, originally reported by Ito *et al.*²⁰⁴ in 1998. The reaction proceeded in moderate yield, with excellent

selectivity over the ester to afford intermediate **63**. This was then deprotected with anhydrous HCl in methanol, generated from chlorotrimethylsilane *in situ*, and careful selection of workup allowed isolation of either the acid **64** or the methyl ester **58** (as its formic acid salt) as desired, in high yields. The final step consisted of coupling **64** with the desired phenol to form the desired activated esters **59** and **60**. Observed instability of the nitrophenol ester to decomposition under the reaction conditions, and hydrolysis to the starting materials during purification is the likely cause of the lower yield observed. The coupling of *p*-fluorophenol was more facile, as the compound was much more stable to the reaction conditions. However multiple impurities were observed in the reaction profile. The product was isolated in 22% yield, providing enough compound for testing.



Scheme 5 – Synthesis of indazole esters **58** - **60** bearing the isopropylpiperazine arm.

Whilst the chemoselective reduction was being investigated, the synthesis was also carried through with the amides still in place. The amide-bearing equivalent of compound **24** has not been tested previously, therefore the effects of this carbonyl on potency were unknown. It may be the case that the amide has no effect on potency or selectivity, and thus these compounds would be of great interest for this project. The route to these molecules, from intermediate **62**, is shown in **Scheme 6**.

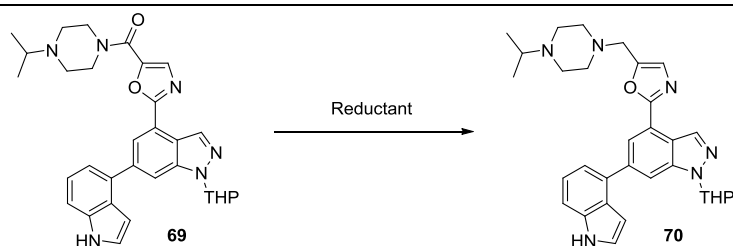


Scheme 6 – Synthesis of amide bearing compounds **66** - **68** to investigate the effects of this group on potency and selectivity, relative to the reduced species **58** - **60**.

From the coupled product, **62**, similar conditions to those used in **Scheme 5** were established to deprotect the THP group and hydrolyse the methyl ester. Isolation of zwitterionic acids **64** and **65** proved troublesome, and was investigated by liquid-liquid extraction, ion-exchange chromatography (both anionic and cationic), precipitation and reverse phase chromatography. This concluded that purification by reverse phase chromatography, without workup, was the best method of isolation. HATU coupling to afford the activated esters **67** and **68** proceeded in poor yield due to competitive amide formation by ammonia that remained after isolation of the acid by high *pH* reverse phase chromatography (product observed by LCMS).

3.1.2.1 Chemoselective Reduction of the Tertiary Amide

The key step, and major synthetic challenge, in the route presented in **Scheme 5** was to find reduction conditions that were chemoselective for the amide, and tolerated by either the boronic or methyl esters (**61** or **62**). In the route to compound **24**, where chemoselectivity was not an issue, the group explored an extensive array of reduction conditions summarised in **Figure 32** below.²⁰⁵



Failed conditions: 9-BBN; NaBH₄; LiBH₄; DIBALH; LiAlH₄, THF;
 NaBH₄, BF₃.DMS; NaBH₄, BF₃.THF; NaBH₄, BF₃.Et₃N;
 Zn(OAc)₂, (EtO)₃SiH; H₂PtCl₆, TMDS; NaBH₄, H₂SO₄
 Successful conditions: LiAlH₄, AlCl₃, THF

Figure 32 – Previously trialed reduction conditions for this amide in the route to compound **24**.

Three sets of conditions not considered in the above campaign were initially investigated, as well as the successful conditions reported above. The first utilised triirondodecacarbonyl (Fe₃(CO)₁₂) with polymethylhydrosiloxane (PMHS),²⁰⁶ while the second used methyldiethoxysilane and zinc acetate at elevated temperature.²⁰⁷ Similar conditions to the latter were explored in the above campaign (zinc acetate and triethoxysilane at room temperature);²⁰⁸ however Beller *et al.* published a second paper using methyldiethoxysilane at elevated temperature, which was explored here.²⁰⁷ A third set of hydrosilylation conditions developed by Ito *et al.*²⁰⁴ were also investigated, utilising a rhodium hydride complex in combination with diphenylsilane, A summary of these reactions using examples from each publication is given below in **Figure 33**.

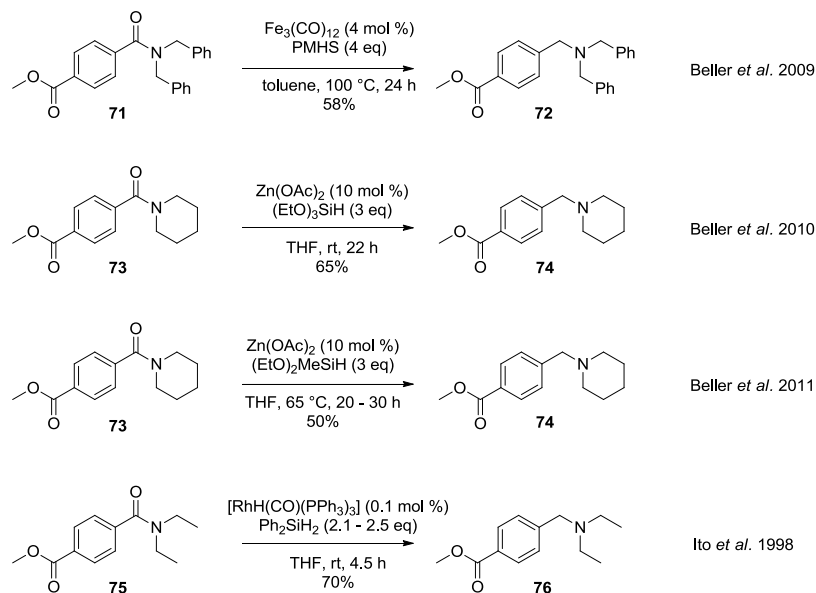
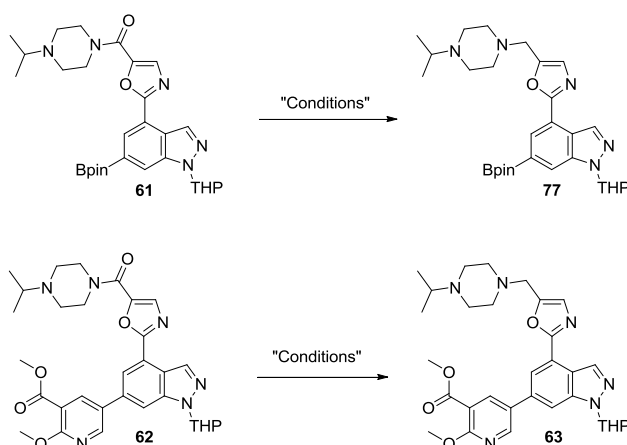


Figure 33 – Literature examples of chemoselective amide reduction conditions investigated.^{204,206–208}

The reductions were first investigated with the boronic ester **61**, in an attempt to bring the reduction step in as early in the synthesis as possible. Full conversion was observed by LCMS

with zinc acetate and (EtO)₂MeSiH; however isolation was unsuccessful, with 5% being the greatest isolated yield achieved (**Table 10 Entry 2**). This reaction was then investigated with the methyl ester **62** and the conditions proved to be successful, by LCMS, on test scale; however upon scale-up these conditions failed to give good conversion to product, which was therefore not isolated. The iron-catalysed reduction, and the original LiAlH₄ conditions both failed to give conversion with the boronic ester, and were therefore not tested on the methyl ester derivative (**Table 10 Entries 1 and 4**).



Entry	Conditions	Time, % conversion, (isolated yield %)	
		Boronic ester 61	Methyl Ester 62
1	[Fe ₃ (CO) ₁₂], PMHS 100 °C	24 h, 0	NT
2	Zn(OAc) ₂ , (EtO) ₂ MeSiH 65 °C	60 h, 100, (5)	39 h, 100
3	[RhH(CO)(PPh ₃) ₃], Ph ₂ SiH ₂ rt	17 h ^a , 100, (57)	18.5 h ^b , 100, (64)
4	LiAlH ₄ , AlCl ₃	2 h, 0	NT

Table 10 – Results of initial reduction experiments. NT = not tested. ^a90% conversion seen after 1.5 h. ^b50% conversion was observed after 1.5 h, further equivalents of silane and catalyst added at 17 h to force completion.

The Rh-catalysed reaction proceeded successfully for both compounds, with yields comparable to the literature presented above for these transformations. A higher catalyst loading was used (1.2 mol%) in order to facilitate accurate weighing on the small scale used, with 2.3 equivalents of silane. Compound **61** underwent the reduction much more quickly than compound **62**, with 90% conversion observed after 1.5 h, compared to 50% for **62**. In fact, the methyl ester required another equivalent of catalyst and silane to be added to force the reaction to completion. Both compounds were purified and isolated in moderate to good yields (**Table 10 Entry 3**), with some loss of the reduced boronic ester **77** to the aqueous layer

as the boronic acid. Whilst reduction of compound **61** was achieved more quickly, the risk of partial hydrolysis of the boronic ester during workup forced selection of the slightly slower, yet higher yielding reduction of the methyl ester **62** as the preferred reaction to produce the final compounds.

3.1.3 Biological Characterisation

pIC₅₀ data are presented below, in **Table 11**, for the amides (**65 - 68**) and their corresponding amines (**58 - 60** and **64**). Immediately evident from the presented data was that reduction of the amide gave an, approximately, 10-fold increase in potency at PI3K δ . With the exception of the nitrophenol esters, all compounds also showed good selectivity over the other three isoforms. Finally, in all cases, potency had increased from the analogous truncated indazole, consistent with the ~200-fold increase predicted by the computational modelling due to incorporation of the isopropylpiperazine arm.

Entry	Series	R	Number	pIC ₅₀			
				δ	α	β	γ
1			65	7.0	<4.5	4.6	5.1 ^d
2			66	6.5	<4.5 ^b	<4.5 ^c	4.8 ^e
3			67	8.8 (8.1) ^a	6.8 (6.2) ^a	7.8 (7.0) ^a	6.8 (6.1) ^a
4			68	7.3	5.2	5.2	<4.5
5			64	7.9	4.9	4.7	4.8
6			58	7.4	5.0	<4.5	<4.5
7			59	8.3 (7.6) ^a	7.1 (5.6) ^a	6.7 (5.3) ^a	5.5 (4.9) ^a
8			60	8.1	5.5	5.3	4.8

Table 11 – Isolated PI3K enzyme data for the eight compounds synthesised. ^aData reported from N = 1, and from experiments 1 week apart to show effects of degradation. ^bData reported from N = 3, with one additional value = 4.6. ^cData reported from N = 3, with one additional value = 4.8. ^dData reported from N = 1 with one additional value <4.5. ^eData reported from N = 3 with one additional value <4.5.

Looking at the data in more detail, it was proposed that the acids formed a non-covalent interaction with Lys779 due to the decrease in potency found when comparing the acids to the methyl esters (entries **1** versus **2**, and **5** versus **6**). Adding the methyl group removed the potential for hydrogen bonding, or formation of a salt-bridge, to Lys779. It was therefore likely that the methyl esters were non-covalently bound, as no increase in potency, which could be attributed to covalent bond formation, was seen. Reactivity profiling of the targeted four amines (**Figure 34**) was concordant with that previously reported, and further supported this theory. The nitrophenol ester was cleaved most quickly, followed by the fluorophenol ester, with the methyl ester and acid remaining inert to amide bond formation. Only the targeted amines were subjected to this test, as it was believed that similar reactivity would be observed for the corresponding amides (**65 - 68**).

It was again evident from the reactivity profiling that the nitrophenol esters were very reactive, and this was reflected in the stability of these compounds. Esters **59** and **67** were found to hydrolyse to the parent acid when in solution and two pIC₅₀ values measured one week apart are shown in **Table 11** (entries **3** and **7**) to illustrate this. The values measured after one week in solution (reported in parentheses) can be seen to be approaching the profile of the carboxylic acids (entries **1** and **5**). The pIC₅₀ values for these two compounds must therefore be treated with caution. It was clear that these compounds were very reactive, and therefore very potent, however this came at the cost of selectivity. Assuming that compounds **59** and **67** were covalently bound, it was hypothesised that, as soon as they were present in the active site of the enzyme, the lysine residue displaced the nitrophenol group to afford the covalently bound complex (*i.e.* k_{inact} is very fast). As this lysine residue is conserved, each isoform would have become covalently inhibited as soon as the compound was in the active site. This is an excellent illustration of the equilibrium depicted in **Figure 4** where k_{inact} is too fast to allow any selectivity to be achieved by the non-covalent interactions (K_i).

Conversely, the fluorophenol esters (**60** and **68**) were shown in the reactivity profiling (**Figure 34**) to be less reactive, and they were also found to be stable in solution. This would allow equilibration of the inhibitor in the active site of the isoforms (K_i), prior to formation of the covalent bond, after the inhibitor has resided in the active site for a sufficient period of time. Assuming this was the case, and the fluorophenol esters were also covalently bound,

compound **60** would have been the most potent and selective inhibitor of the series. To test this hypothesis, compounds **58** - **60** were submitted to crystallography.

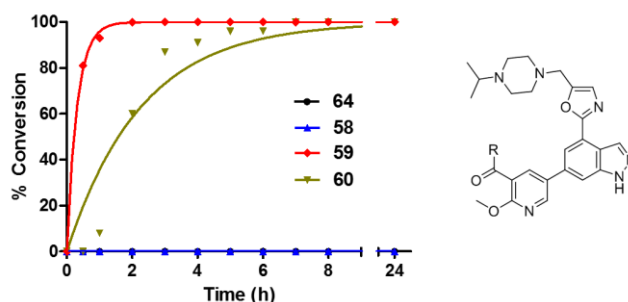


Figure 34 – Reactivity profiling of compounds **58** - **60** and **64** (shown in **Table 11**). The general structure of these compounds is shown on the right. The analogous amides (compounds **65** - **68**) were not profiled as they were not the target compounds, and it was believed that the amide carbonyl would not have any significant effect on the rate of covalent bond formation

As postulated, the activated esters **59** and **60** were covalently bound to PI3K δ , while the methyl ester **58** was not. The crystal structures are shown below in **Figure 35**, with continuous electron density and absence of the leaving group seen for compounds **59** and **60**. The structures for these compounds were identical and, again, in good agreement with the model (**Figure 31**). The pyridyl water interactions remained present, and rotation of the pyridyl ring out of the plane of the indazole rings to covalently interact with Lys779 was observed. The fact that the nitrophenol ester **59** was indeed covalently bound gave weight to the argument that the poorer selectivity seen for this compound might be due to its inherent reactivity, and that it was instantly trapped in the active site of all four isoforms.

The structure for compound **58** was noticeably different to the model (**Figure 30**) at the electrophilic centre. The methyl position was poorly resolved, however it seemed that the carbonyl engaged Lys779, akin to the interactions modelled for the DHP series. Therefore, in the absence of a sufficiently electrophilic site, the carbonyl may prefer to face Lys779, and engage in a hydrogen bonding interaction. This conformation was clearly an energy minimum in the active site of the protein, and could be reflected *in silico*. *Post-hoc* modelling confirmed this to be the case, however with a noticeably decreased calculated affinity value of 9.14 kcal·mol⁻¹ (vs. 11.19 kcal·mol⁻¹). Emphasis in the molecular modelling was placed on determining the calculated affinity for conformations which lend themselves, geometrically, to formation of a covalent bond. However, it is clear from these data that other conformations, not determined from molecular modelling, may be preferred in the system. Also, the restrictions placed on the system in this modelling exercise may have had subtle

effects that did not accommodate the conformation observed above as the preferred conformation.

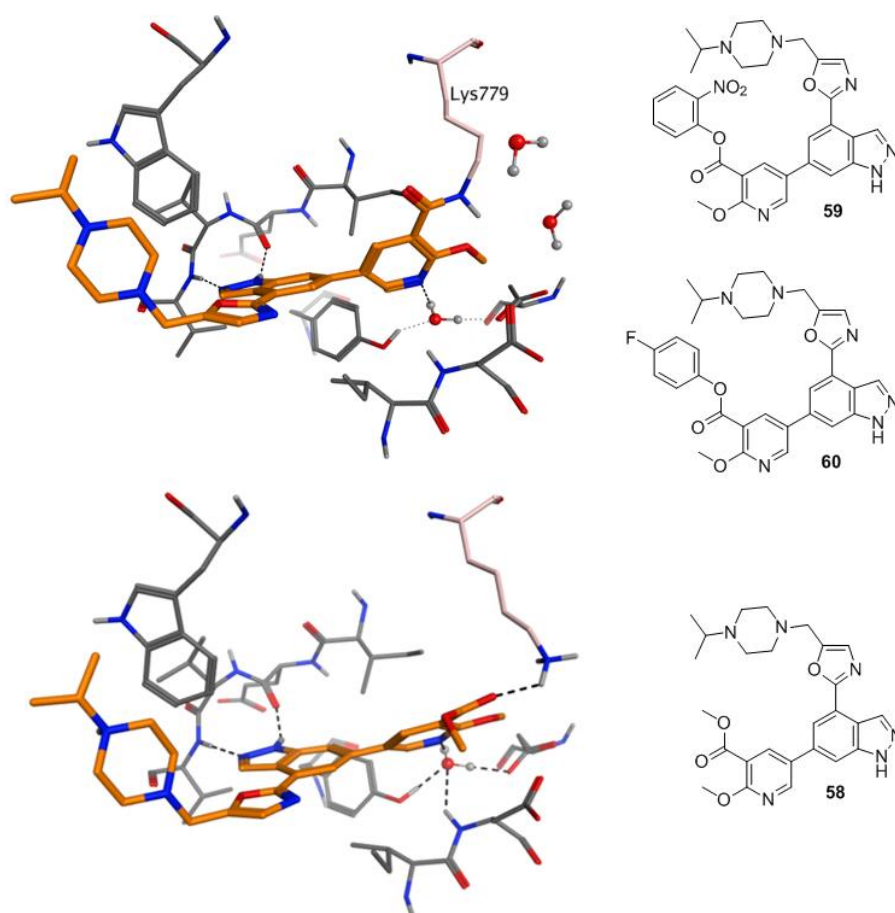


Figure 35 – Top: Crystal structure for compounds **59** and **60** covalently bound to PI3K δ , resolved to 2.2 Å (same structure for both inhibitors). **Bottom:** Crystal structure for compound **58**, resolved to 2.0 Å. The ligand is non-covalently bound to PI3K δ , characterised by a clear gap in electron density between Lys 779 and the ligand.

The stable amine compounds **58** and **60** were then assessed in a phenotypic human whole-blood (hWB) assay measuring secretion of the inflammatory marker interferon γ (IFN γ) after treatment with T-cell stimulated antibody CytoStim¹⁶³ (see Section 6.1.2 Human Whole-blood Assay for assay description). As this assay takes place in a cellular context, compounds typically show a decrease in potency (termed “drop off”), which can be attributed to a variety of parameters. Firstly, the added complexity of the cellular system can cause non-specific protein binding, reducing the amount of free inhibitor present. Secondly, the permeability of the compound is important. A compound that is potent in the isolated enzyme assay, but poorly permeable, will show a drop-off as it simply cannot cross the cell membrane to reach the target (assuming the target is intracellular, which is the case for PI3K δ). Furthermore, active efflux of the drug from the cell can decrease the active concentration of drug in the

cell. Finally, for ATP competitive inhibitors such as those discussed in this project, the higher levels of ATP in the cell (1-2 mM)^{209,210} compared to the biochemical assay run at K_M (80 μ M of ATP for PI3K δ)¹⁶³ causes a decrease in observed potency by out-competing the inhibitor.²¹¹

Compound **60** showed little drop off in this assay, whilst the acid **64** and the methyl ester **58** showed considerable differences in pIC_{50} . The magnitude of the drop-off in potency qualitatively correlated with the permeability of the compounds (*i.e.* the least permeable acid showed the greatest drop-off in potency between isolated enzyme and whole-blood assay). The more permeable compound **60** was therefore more able to access the target in the cell. By this logic, compound **25** should also show very little drop-off, however this was not the case, and a drop of 0.6 log units was observed. As this assay was incubated for a longer period of time, there was a much greater potential for maximising the amount of inhibitor covalently bound to the target. This may therefore have increased the observed whole-blood potency of compound **60**, relative to the potency seen in the isolated enzyme assay, thus decreasing the observed drop-off. The fact that potency is retained so well is promising for the presence of covalent interactions.

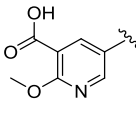
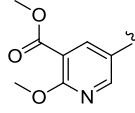
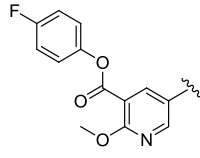
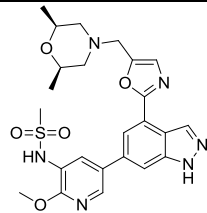
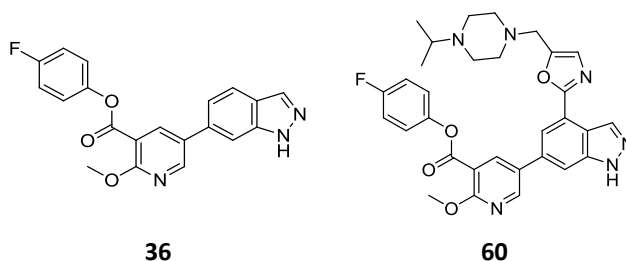
				
	64	58	60	25
PI3Kδ pIC_{50} (pK_i)	7.9	7.4	8.1	9.1 ^a (10.1)
hWB pIC_{50}	5.0	7.0	7.9	8.5
Perm. / nm\cdotsec⁻¹	<10	58	180 ^b	203

Table 12 – Isolated enzyme data, human whole-blood data, and artificial membrane permeability data for the stable compounds **64**, **58**, **60**, and the indazole clinical backup compound **25** possessing the methoxypyridyl back-pocket group. ^a Data reported from N = 17, with one additional empty value. ^b Data reported from N = 1, with one additional empty value.

The aim of this section was to improve upon the potency and selectivity seen for the truncated compounds in Section 2.2 Investigation of Hinge-Binding Groups, by incorporating a basic amine side-chain. Comparing the pIC_{50} data for truncated indazole *p*-fluorophenol ester **36** to compound **60**, it can be seen that this objective has been achieved. Potency at the target has increased 500-fold, with no large increase at any of the other three isoforms. As a direct consequence of this, selectivity has increased from a minimum of 1.3-fold for

compound **36**, to a minimum of ~400-fold for compound **60**. Compound **60** was confirmed to be covalent by crystallography, and retained its potency in the whole-blood assay, which is comparable to that obtained for clinical candidate **25**. In addition, the covalent mode of inhibition of these inhibitors may provide other beneficial properties, such as an increased duration of action, which is explored later in Section 4.3.4 Phenotypic Consequences of Covalent PI3K δ Inhibition.



Isoform	pIC ₅₀	x-fold	pIC ₅₀	x-fold
δ	5.4	-	8.1	-
α	<4.5	>7.9	5.5	398
β	5.3	1.3	5.3	630
γ	<4.5	>7.9	4.8	1995

Table 13 – Comparing isolated enzyme potencies and selectivities for the truncated and elaborated indazoles.

Building on this established chemotype, that suggested selective covalent inhibition was possible, exploration of the electrophilic warhead and the back-pocket binding group were explored.

3.2 Effects of Varying the Electrophilic Centre

Of the lysine-directing electrophiles known at the outset of this project, sulfonyl fluorides had shown considerable promise in the literature. FSBA has been used to covalently modify the conserved lysine of kinases,^{34,98,212,213} and indeed the p110 subunit of PI3K kinases²¹⁴ (although the specific residue was not stated in this report). In addition, sulfonyl fluorides have been reported recently to be very selective, and hydrolytically stable, covalent modifying groups by Sharpless^{99,215} and others.^{100,213,216} Sulfonyl fluorides have also found applications as covalent proteasome and protease inhibitors,^{217,218} and recently have been shown to covalently inhibit the same lysine residue that Choi *et al.* inhibited with the activated esters used so far.^{99,108} Furthermore, reactivity profiling similar to that discussed

above has shown that aliphatic sulfonyl fluorides are cleaved by nitrogen nucleophiles under physiologically relevant conditions.^{103,219}

In addition to sulfonyl fluoride, sulfonate esters have been identified as stable sulfonyl chloride alternatives for the preparation of sulfonamides in organic synthesis.^{220–223} Again, reactivity experiments on these compounds have shown that the phenolic group (pentafluorophenol (PFP), 2,4,6-trichlorophenol (TCP), or *p*-nitrophenol) is susceptible to displacement by amines.^{221,224,225} It was envisaged that these sulfonate esters could be more hydrolytically stable than the previous activated esters, and the inherently weaker electrophilicity of S=O compared to C=O electrophiles²²⁶ may provide insight into the reactivity required to covalently engage Lys779. The four proposed compounds for investigation are shown below (**Figure 36**). Included are the sulfonyl fluoride **78**, the PFP sulfonate ester **79**, the TCP sulfonate ester **80**, and finally the *p*-nitrophenol sulfonate ester **81**.

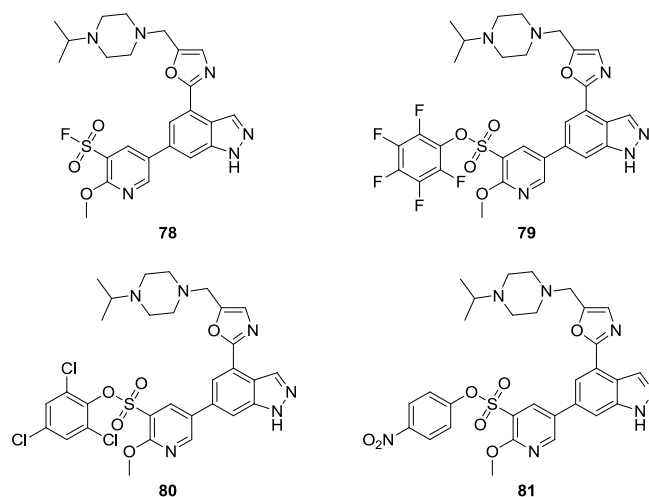
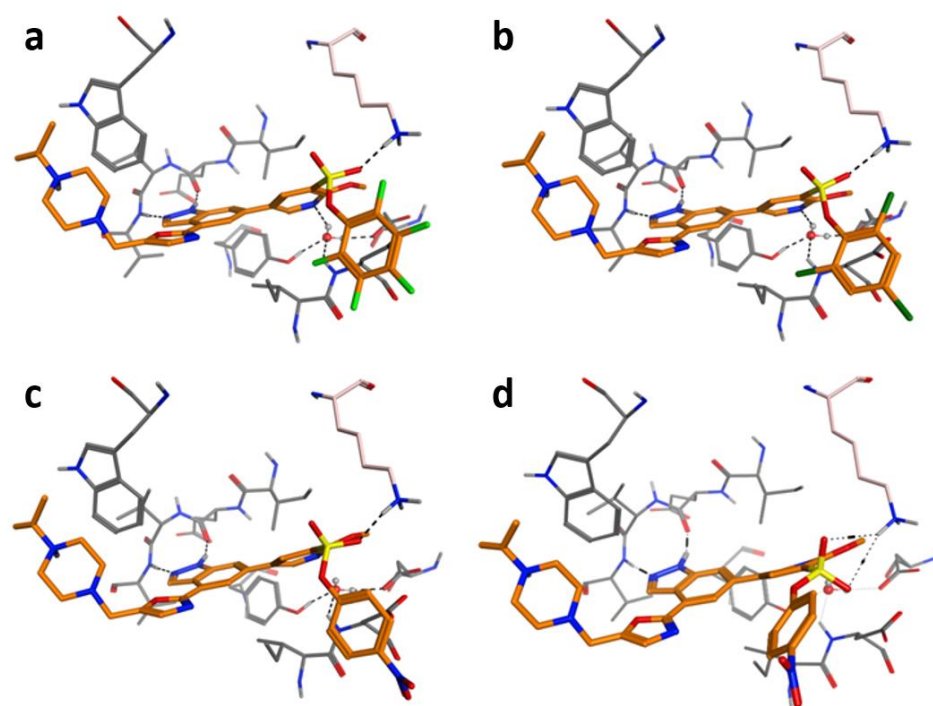


Figure 36 – Proposed electrophilic sulfur containing compounds **78** - **81**.

3.2.1 Molecular Modelling of Sulfur Electrophiles and Synthesis

Molecular modelling of compounds **78** - **81** predicted a high calculated affinity for the non-covalently bound structures (**Figure 37**). The covalently bound models were identical to the sulfonyl fluoride **78** (**Figure 38C**), and looked reasonable, with no abnormal bond length or angles. One area of concern was that of the angle of attack at the sulfur centre depicted in the energy minimised models (**Figure 37A-C**) may not be optimal, as the models placed an oxygen of the sulfonate ester towards Lys779. Rotation of the C-S bond to point the S-OAr

bond away from Lys779 gave a better angle of attack at the S-O σ^* orbital (**Figure 37D**). Unfortunately, this was identified as an energy maximum in all cases, and the structure could not be minimised around this conformation to generate a calculated affinity. In a similar way to what has been seen previously, it could be possible that, if the electrophilic centre is reactive enough, this reactive conformation would be trapped by the nucleophilic Lys779 if it forms in the active site. However, this was an early indicator that these bulky sulfur electrophiles may be poorly aligned for irreversible inhibition.



Entry	Compound	Calc. affinity / kcal·mol ⁻¹
1	PFP (79)	12.69
2	TCP (80)	12.42
3	<i>p</i> -nitrophenol (81)	12.30

Figure 37 – Non-covalently bound models of compounds **79** - **81** in the active site of PI3K δ . (a): Compound **79**, (b): Compound **80**, (c): Compound **81**, (d): Compound **81** with C-S bond rotated to expose the S-O σ^* orbital to Lys779. This structure is representative of similar structures attainable for **79** and **80**. **Table**: Calculated affinity data for compounds **79** - **81**. Calculated affinity values could not be obtained for structures of the form depicted in (D) as it was an energy maximum in all cases.

The sulfonyl fluoride group is rather special in its reactivity. It has been hypothesised in the literature that, in order for loss of fluoride in the active site, a water molecule or acidic side-chain in close proximity to the fluoride leaving group is required (**Figure 38D**).^{99,215} Fortunately, there is an intricate water network in the back pocket of PI3K δ , and an aspartic

acid residue (Asp911) close to Lys779 (**Figure 38**). The basic energy minimisation places the fluorine away from this residue (calc. affinity = 11.17 kcal·mol⁻¹), in order to maximise the interaction between the sulfonate oxygen and Lys779 (**Figure 38A**). However, again, alternative conformations were available, both with little loss in calculated affinity. Firstly, a conformation could be obtained that placed the fluorine within 5 Å of Asp911 (calc. affinity = 10.97 kcal·mol⁻¹) (**Figure 38B**), however the trajectory of attack at the S-F σ^* orbital was not optimal. Asp911 was fixed during the minimisation procedure, thus it is possible that this residue could rotate or move to bring it closer to the fluoride and facilitate the loss of the leaving group. Further rotation of the C-S bond, to place the S-F σ^* orbital towards Lys779, and expose the fluorine to solvent, generated a structure with a calculated affinity of 11.00 kcal·mol⁻¹ (structure not shown). Again, multiple conformations were evident, which may be trapped by Lys779 if electrophilic enough. The covalently bound model for compound **78** and the sulfonate esters **79 - 81** is shown in **Figure 38C**.

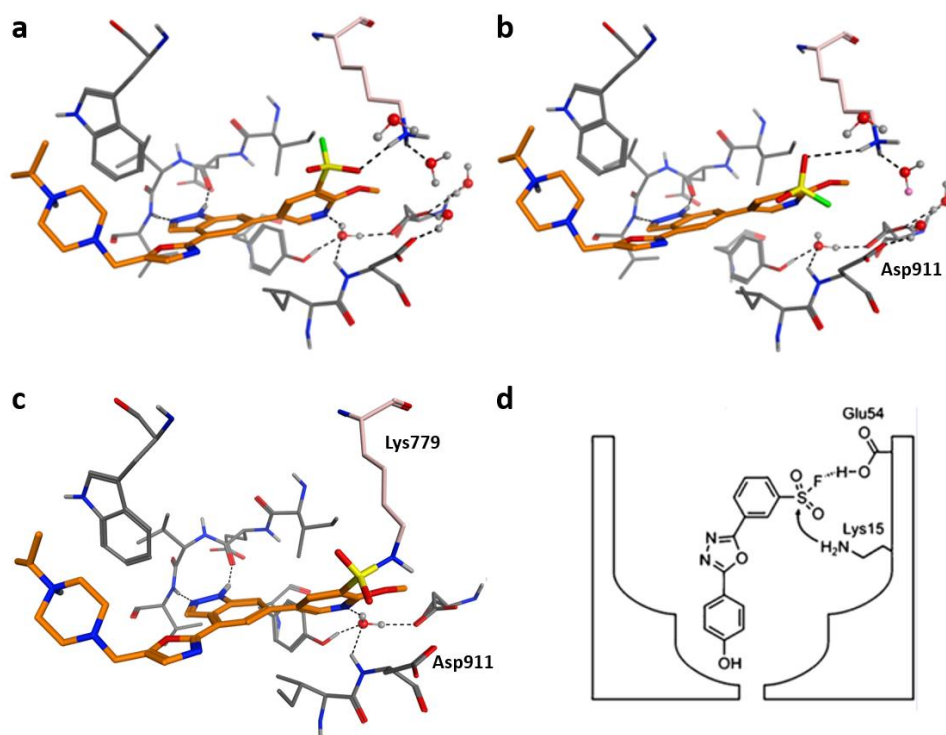


Figure 38 – (a): Non-covalently bound model of compound **78** in the active site of PI3K δ . (b): Alternative conformation of model (a) with the fluorine pointing towards Asp911. (c): Covalently bound model for compounds **78 - 81**. (d): Schematic diagram depicting the stabilisation of the fluoride leaving group by an acidic side-chain in transthyretin. Reused with permission from Grimster *et al.*⁹⁹ Copyright 2013 American Chemical Society.

Although the pK_a of aspartic acid (≈ 4)¹⁹⁸ would indicate that this residue is deprotonated at physiological pH, it is possible that the equilibrium in the back pocket may generate the

protonated acid at some point, allowing the covalent bond to form. Furthermore, in the lower dielectric constant environment (relative to water) observed in folded proteins, the pK_a values of all neutral side chains (-OH, -SH, -CO₂H) can *increase* significantly, whilst the pK_a of positively charged amine side-chains can *decrease*.⁵⁷ In a study by Grimsley *et al.*, the lowest pK_a values of protonated Asp residues (-CO₂H) was found to be 0.5, the highest 9.2, and the average 3.5. For protonated lysine residues (-NH₃⁺), the lowest pK_a value was found to be 5.7, the highest 12.1 and the average 10.5.⁵⁷ If the extreme limits of these measurements were found, it could indeed be that the Asp residue is protonated at physiological pH, and the lysine deprotonated, which could facilitate rapid displacement of the fluoride.

The compounds were accessed from sulfonyl chloride **87**, which was obtained by oxidation of benzylthioether **85** using 1,3-dichloro-5,5-dimethylhydantoin **86** (DCDMH),²²⁷ after similar Suzuki, reduction and deprotection steps to those used previously. Conversion to sulfonyl fluoride **78** was achieved by an on-water reaction of potassium bifluoride (KHF₂). The on-water nature of this reaction ensures that hydrofluoric acid generation is minimised, as the bifluoride anion [FHF]⁻ is thermodynamically stable, and highly solvated.²²⁸ At the aqueous-organic interface, bifluoride presents a nucleophilic F⁻ atom to attack the electrophilic sulfonyl chloride centre in the organic phase.²¹⁵ The sulfonate esters **79** - **81** were accessed by treating a stirred solution of phenol and base with **87**. This synthetic route is summarised in **Figure 39**.

Unfortunately, the compounds were found to be unstable with respect to hydrolysis in workup and purification by reverse-phase chromatography. Small amounts of compounds **78** - **80** could be isolated, however this instability impacted upon the medicinal chemistry of these compounds, as described below. Because of this, nitrophenol ester **81** was not pursued.

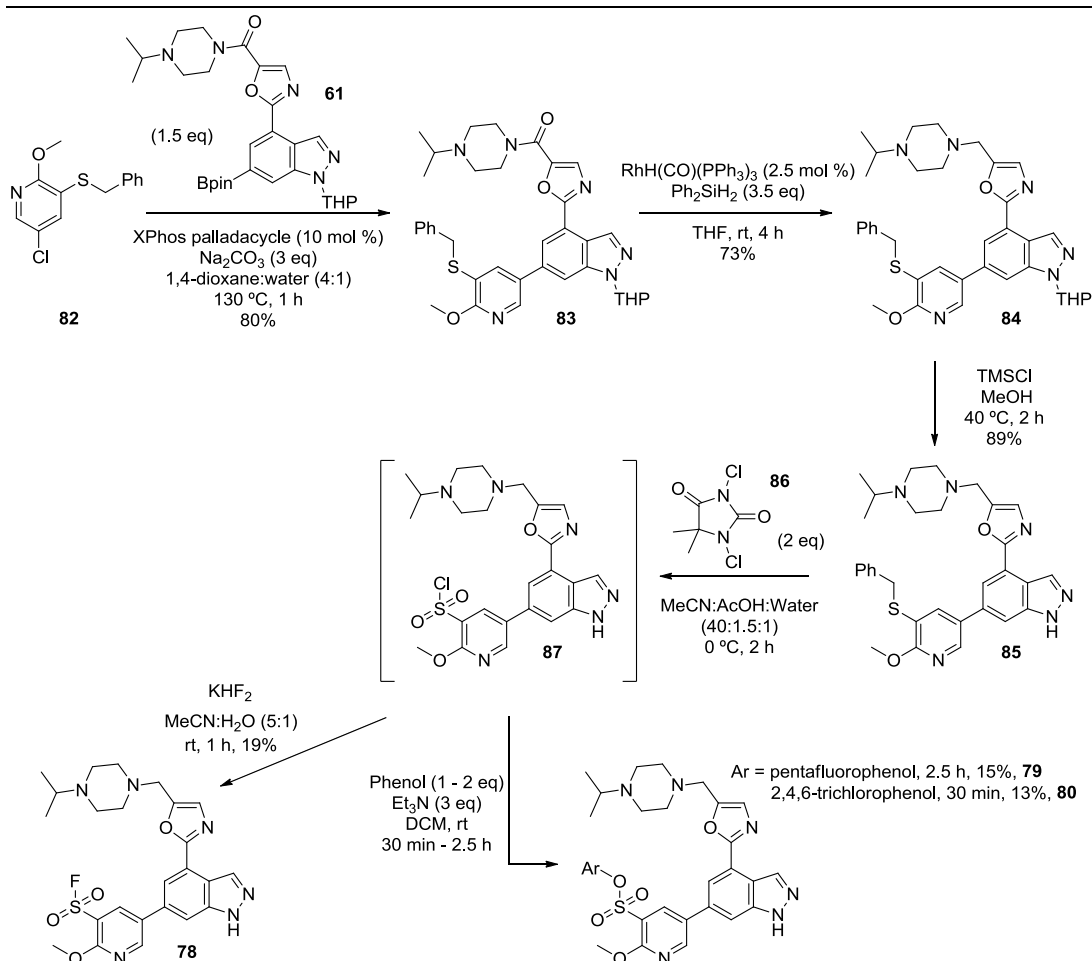


Figure 39 – Synthesis of sulfur-based compounds **78** - **80**.

3.2.2 Medicinal Chemistry of Sulfur-based Electrophiles

Despite their precedence for stability in the literature, these compounds were found to be unstable in DMSO stock solutions, and soak solutions for crystallography. The pIC_{50} values obtained from the isolated enzyme assays are given in **Table 14**.

Entry	Compound	pIC_{50}			
		δ	α	β	γ
1	78 - SO ₂ F	7.2	4.6	<4.5	<4.5
2	79 - PFP	6.9	5.2	4.9	4.9 ^a
3	80 - TCP	7.1	5.3	5.1	5.4

Table 14 – pIC_{50} data obtained for compounds **78** - **80**. ^a Data shown from N = 1, with one additional value <4.5.

The data showed little variation between the compounds, which may be explained by their instability. LCMS analysis of the sulfonyl fluoride **78** and PFP ester **79** stock compound

solutions in DMSO, and the crystallographic soak solutions after 3 weeks at <0 °C showed major decomposition to the sulfonic acid in both cases, as well as other products that could not be identified from their mass spectra. This instability could be due to the electron-deficient nature of the pyridine ring, which has been exploited in deoxyfluorination reactions using the reagent PyFluor.²²⁹ Indeed, the sulfonyl fluoride-based reagents that have been used for modification of active site lysine residues attach the reactive group to a standard phenyl ring,^{5,100,213} the electronics of which will be significantly different to the pyridine group employed here. Presumably the phenyl ring renders the sulfur centre less reactive, and therefore more amenable to a biological setting. It may therefore be the case that methoxypyridyl sulfur-based electrophiles are too reactive to be a successful warhead for targeting lysine residues.

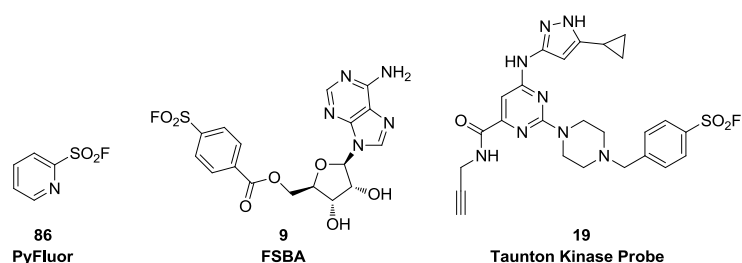


Figure 40 – Structures of PyFluor **88**, FSBA **9** and the Taunton Kinase Probe **19**.

Furthermore, the crystal structure of the PFP sulfonate ester **79** showed no density for the leaving group, however also an absence of electron density from Lys779 onto the ligand supporting degradation of this compound. The sulfonyl fluoride also showed no density from the lysine onto the ligand; however it could not be determined from the electron density whether the reactive centre was still intact, or whether it had been hydrolysed. The crystal structure for compound **78** is shown in **Figure 41**, with one of the groups arbitrarily modelled as a fluorine. The density for PFP ester **79** looked identical to this, suggesting that the same decomposition product had formed. TCP ester **80** was not analysed by crystallography.

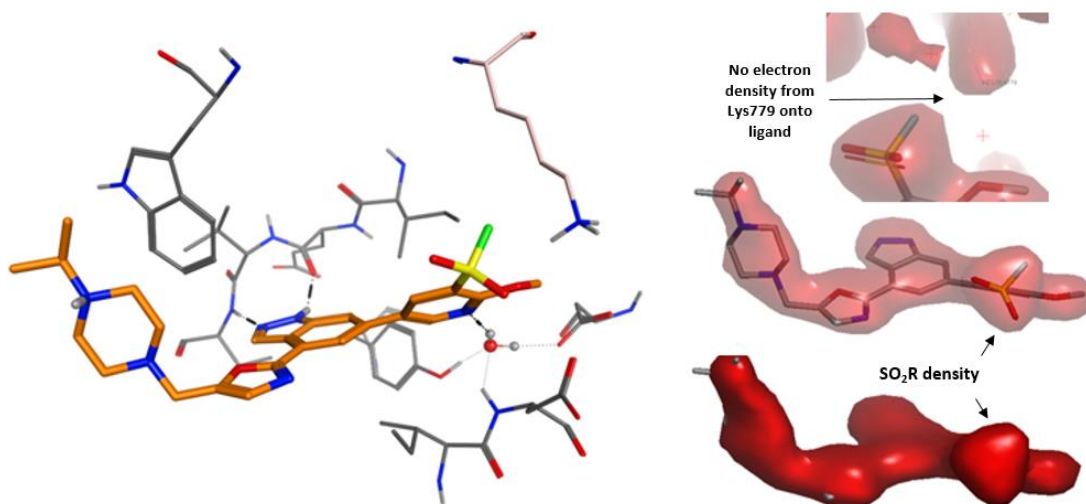


Figure 41 – Left: Crystal structure for sulfonyl fluoride **78**. Right: Electron density maps for this structure, to show the symmetry about the SO₂R centre. The presence of sulfonyl fluoride or sulfonic acid could not be determined from this density map. The electron density for the PFP ester **79** looked identical, indicating that hydrolysis of the PFP ester may have occurred.

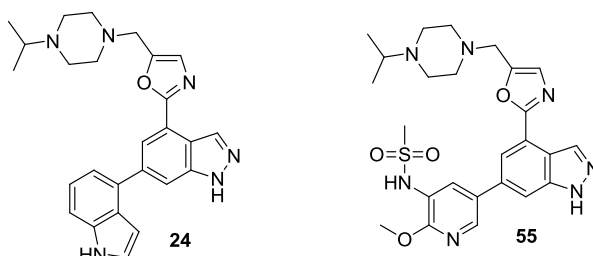
The electron density maps for the PFP ester **79** and sulfonyl fluoride **78** were reasonably symmetrical about the sulfur centre, indicating that instead of the SO₂R structure, this centre may in fact be the acid, -SO₃⁻, due to hydrolysis. This may then also be the case for the isolated enzyme assays, and the similar profiles seen may due to presence of the sulfonic acid in the assay. If the sulfonyl fluoride centre was still intact, however, the lack of covalency may have arisen due to poor angle of attack of Lys779 into the S-F σ* orbital, or lack of required protic environment surrounding the leaving group.²¹⁵ In order to investigate this further, the sulfonic acid was made by hydrolysis of the sulfonyl chloride. This compound, however, was insoluble in the enzymatic assay and could not be progressed further.

At this point, the decision was made to halt investigation into sulfur-based electrophiles, and focus on activated esters. These electrophiles provided potent compounds, with good selectivity in the biochemical assays, and clear data supporting covalent inactivation of PI3Kδ. This presented a good opportunity to further understand the reactivity of these centres, and the applicability of these electrophiles to selective covalent inactivation of PI3Kδ in native biological systems.

3.3 Variation of the Back-Pocket Binding Group

The back-pocket binding region of the general inhibitor scaffold stood out as a final modifiable area for developing a better inhibitor than compound **60** (p-F compound). In

particular, the indole back-pocket group has been identified in the literature as a privileged group for obtaining PI3K δ selectivity.¹⁷⁵ This is exemplified by its presence in clinical candidate **24**. Comparison of the biochemical potency data for compounds **24** and **55** highlights the preference for the indole containing compound **55** for obtaining selectivity for PI3K δ (**Table 15**).



	pIC_{50} (pK_i)	
δ	9.0 (9.9)	9.4 (10.1)
α	5.3	6.9 ^a
β	5.8	6.0
γ	5.2	5.9

Table 15 – Comparison of the biochemical data for compounds **24** and **55** showing how the indole back-pocket group is superior in terms of selectivity for PI3K δ . ^a Data from N = 5, with one additional empty value.

An overlay of the crystal structure for compound **24** with the non-covalent model for *p*-fluorophenol ester **60** developed so far indicated good alignment of the C-3 position of the pyridyl ring, with C-6 of the indole. This suggested that incorporation of an ester at this position should afford a covalent inhibitor, shown below in **Figure 42**. *o*-Nitrophenol and *p*-fluorophenol were targeted to provide matched pairs to the methoxypyridine esters **59** and **60**. Due to the similarity to the methoxypyridyl structure, and the success of these inhibitors in engaging covalent reactions with Lys779, these compounds were not subjected to the full computational modelling procedure, and progressed immediately to synthesis.

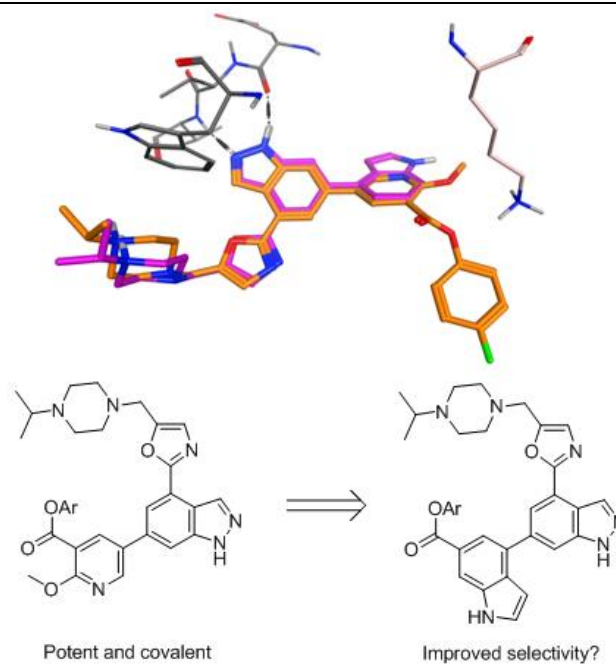
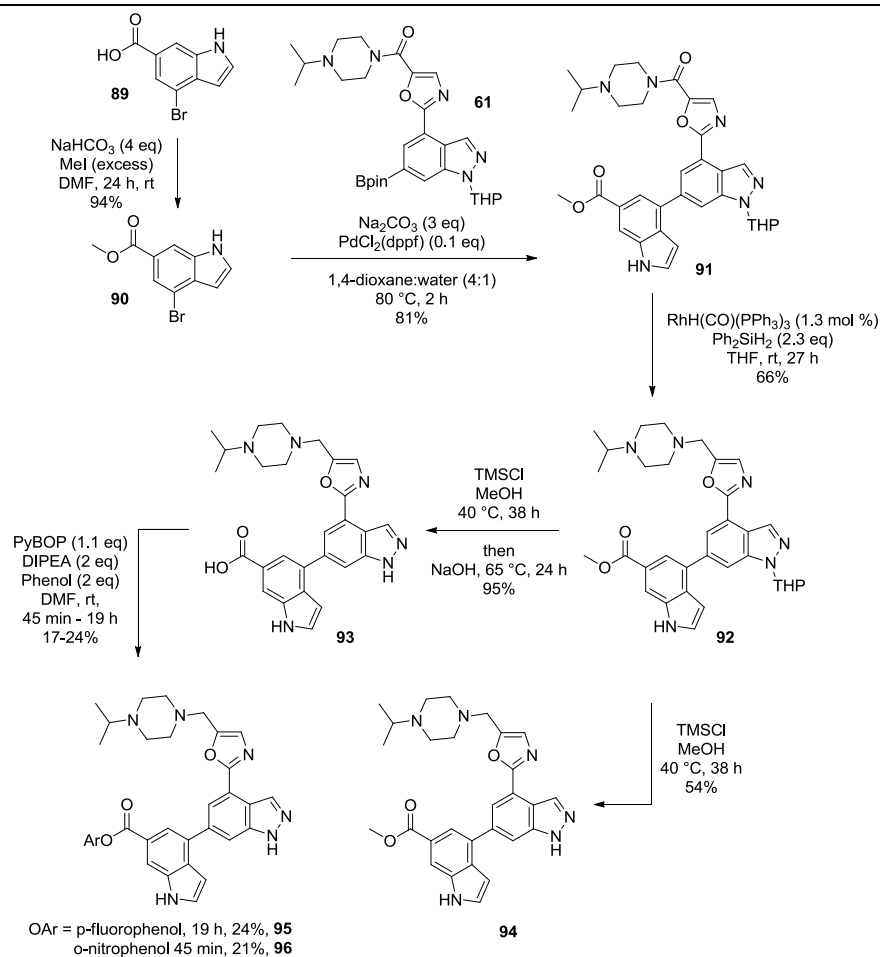


Figure 42 – Top: Overlay of crystal structure for compound **24** (blue) and the non-covalent model for *p*-fluorophenol ester **60** developed so far (orange). Good overlap between C-3 of the pyridyl ring and C-6 of the indole can be seen. **Bottom:** Rationale for this section of work.

3.3.1 Synthesis of Indole-containing Activated Esters

Syntheses of compounds **95** and **96** proceeded via a route analogous to the methoxypyridyl esters. After esterification of indole acid **89** to methyl ester **90**,²³⁰ this was coupled to boronic ester **61** via Suzuki reaction using the previously optimised conditions. Following the established reduction, deprotection, and hydrolysis steps, acid **93** was coupled using an alternative PyBOP coupling protocol, which was found to give improved reaction profiles to the HATU couplings described previously in this thesis. As previously, a sample of the reduction product **92** was only deprotected, to afford the methyl ester **94** for biological testing, with acid **93**.



Scheme 7 – Synthetic route to compounds **93** - **96**.

An empirical observation was made during these syntheses, that the indole esters appeared to be more stable than the methoxypyridyl esters encountered so far, potentially due to the more electron-rich nature of indole compared to pyridine.²²⁹ The reasons for this suspicion were that hydrolysis of indole methyl ester **94** took 24 h, whereas the corresponding methoxypyridyl methyl ester **58** took 1 h under identical conditions. Furthermore, the equivalent PyBOP coupling of *p*-fluorophenol was complete within 5 min for the methoxypyridyl ester **60**, but took 19 h for the indole ester **95**. Also, during this coupling, the activated hydroxybenzotriazole (HOBt) ester **97** could be observed, by LCMS, in reactions of the indole acid, however the analogous HOBt methoxypyridyl ester **98** was never observed. As discussed in the next section, this may have implications for the covalent binding nature of these compounds.

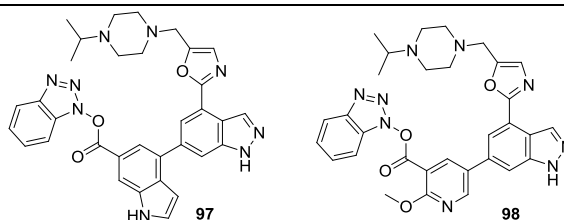
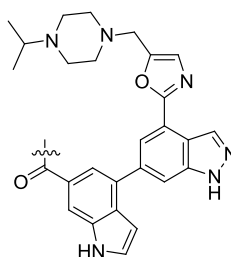


Figure 43 – HOBt activated intermediates in PyBOP couplings. Indole intermediate **97** can be observed by LCMS, whereas methoxyipyridyl intermediate **98** cannot, which indicated that esters on the indole scaffold may be more stable.

3.3.2 Medicinal Chemistry of the Indole Compounds

Data for the two esters synthesised, along with comparison to the methyl ester and acid are shown below in **Table 16**.



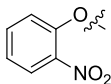
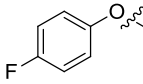
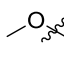
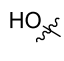
				
	96	95	94	93
δ	8.8	7.1	8.1	9.1
pIC₅₀	α	5.0	5.0	5.0
	β	6.1	5.0	4.7
	γ	5.1	5.3	<4.5
hWB pIC₅₀	7.8 ^a	7.2	6.6	6.8
Perm. / nm·s⁻¹	200	180	190	<3

Table 16 – Biological data for indole back-pocket compounds **93** - **96**. ^a Data from N = 4, with one additional empty value.

Acid **93** from this series showed exceptional potency ($\text{pIC}_{50} = 9.1$) and selectivity (>6000-fold), compared to the compounds synthesised so far. This could be due to the formation of a salt-bridge interaction between the acidic group and Lys779. However, the poor permeability of this compound (<3 nm·s⁻¹) caused a large drop-off in the whole-blood potency. Selectivity was maintained for methyl ester **94** (>2500-fold), however the potency at PI3K δ was

decreased 10-fold ($pIC_{50} = 8.1$), presumably due to removal of the salt bridge. *p*-Fluorophenol ester **95** showed another 10-fold drop in potency ($pIC_{50} = 7.1$), however its whole-blood potency increased ($pIC_{50} = 7.4$), potentially due to covalent interaction with the kinase. This resulted in the compound becoming more potent than methyl ester **94** in the whole-blood assay ($pIC_{50} = 7.4$ and 6.6 , respectively), despite similar permeability for these compounds (180 and $190 \text{ nm}\cdot\text{s}^{-1}$, respectively). *o*-Nitrophenyl ester **96** showed the highest biochemical potency ($pIC_{50} = 8.8$), but a 10-fold drop-off in whole-blood potency ($pIC_{50} = 7.8$).

As noted above, *p*-fluorophenol ester **95** showed a lower potency than expected. Indeed, its activity in the PI3K δ biochemical assay was significantly lower (>10-fold) than the analogous methoxy pyridine compound **60** (Table 11, Entry 8). This suggests that either the bulky aromatic group in combination with the bigger indole back-pocket group is not a favourable pairing, or that the greater stability observed for the indole esters prevents covalent bond formation which would serve to increase the pIC_{50} . Supporting the hypothesis of reactivity being essential are the data for the *o*-nitrophenol ester **96**. The potency at the target for this compound was found to be 40-fold greater than the fluorophenol analogue **95**, and the selectivity observed was greater than the comparable methoxy pyridine compound **59** (500-fold vs 15-fold, Table 11 Entry 7). These results combined supported the hypothesis that the reactivity of the electrophile is key to activity and selectivity. Too reactive, and poor selectivity is observed (compound **59**), but subtle electronic effects from varying either the leaving group, or the scaffold upon which the electrophile is built can affect the selectivity profile observed.

The whole-blood pIC_{50} for compound **96** was also increased relative to the *p*-fluorophenol indole ester **95**. However, the whole-blood potency was no greater than the best fluorophenol methoxy pyridyl ester **60**, despite the greater biochemical potency of compound **96**, supporting compound **60** as the best compound so far, based on pIC_{50} analysis. This could, again, be due to hydrolysis of this more reactive ester over the longer assay time used for to determine hWB potency. In addition, the known toxicity risk of aromatic nitro groups²³¹ would cause the fluorine containing compound to be favoured for progression in a drug discovery campaign.

Crystallography confirmed the covalent binding mode of the *p*-fluorophenol ester **95**. As previously, continuous electron density was observed from Lys779 onto the ligand, and an absence of electron density for the *p*-fluorophenol group of the ligand was observed. The key

hydrogen bond from the indole N-H to Asp787 that is hypothesised to induce the selectivity for the indole back-pocket can also be seen.¹⁷⁵ The nitrophenol ester was not tested, as this electrophile was found to covalently modify previously, and is more reactive than the fluorophenol ester therefore would be expected to also covalently modify PI3K δ .

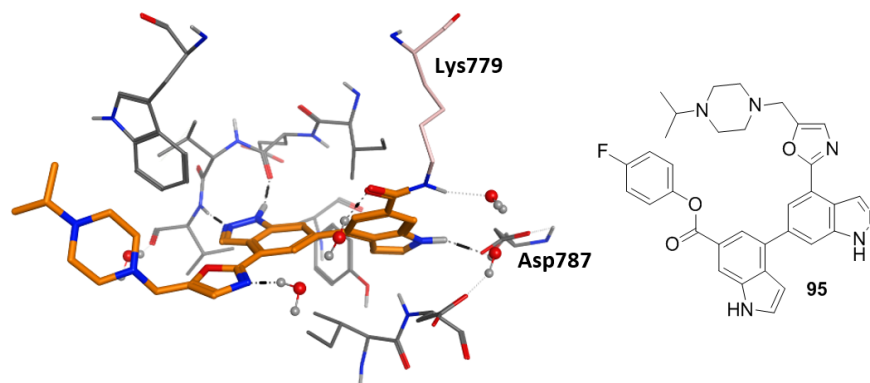


Figure 44 – Crystal structure for compound **95** resolved to 2.05 Å. Clear electron density from Lys779 onto the ligand, and an absence of electron density for the leaving group could be observed.

Clearly, subtle effects are present between the leaving groups, thus the next investigation sought to understand these effects on potency and covalency of these esters, by investigating the effect of varying the electronics of the phenyl ring of the leaving group.

3.4 Variation of the Electronics of the Phenyl Leaving Group

To this stage, this work has shown that covalent inhibition of PI3K δ is possible using activated esters attached to known scaffolds that are selective for PI3K δ inhibition. It has also been shown how the nature of the leaving group can affect the potency and selectivity of these compounds. It is not currently understood whether this is due to reversible binding, or the rate of covalent inactivation with the kinase, which is explored later (Section 4.1 Kinetic Analysis of Binding, and Mechanistic Implications). In addition, the nature of the back-pocket group can also seemingly affect the stability of the electrophilic centre, which was noted by observation of an intermediate in the esterification reaction, and the general stability upon handling of these compounds. This section now seeks to further probe these observations, by determining the effect of varying the leaving group on inhibitor potency. This investigation was focussed solely on the methoxypyridine series, as these compounds were superior to the indole-based inhibitors.

As an estimate of electrophilicity, a range of leaving groups were selected based on pK_a of the alcohol. It was assumed that, in accordance with Hammett parameters, lower pK_a leaving groups would imply a more electron-withdrawing phenol, which could impact upon the addition or elimination rate of aminolysis. Using pK_a also allowed aliphatic leaving groups to also be considered in this analysis. To simplify the analysis, *para*-substituted phenolic groups were chosen over *ortho*-substituted isomers, to remove the added complexity of steric influences on the reactivity of the electrophile, and indeed on reversible recognition of the inhibitor in the active site of the enzyme. One *ortho*-substituted phenol (compound **104**) was included to investigate this hypothesis. The leaving groups investigated are shown below (**Figure 45**), arranged by pK_a and Hammett substituent constant²³² (for aromatic groups). The structures were not subjected to any molecular modelling due the experimental evidence already obtained in this thesis that esters in this position afford covalent inhibitors.

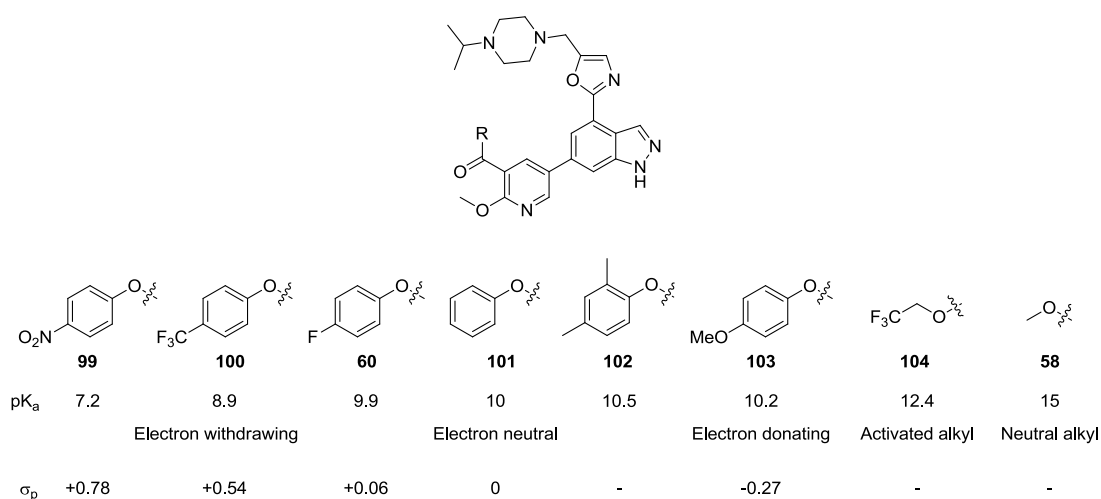
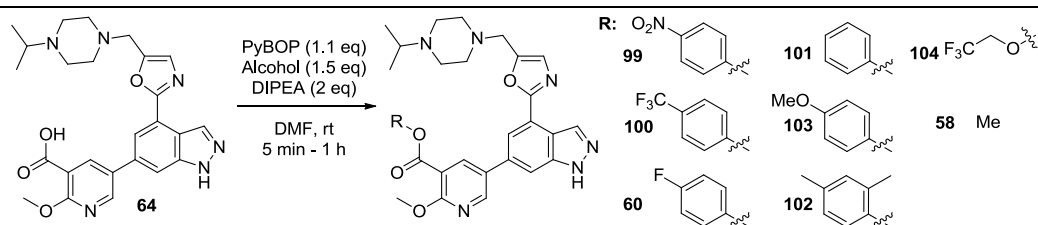


Figure 45 – Leaving groups to be investigated, ranked according to pK_a value and Hammett substituent value.²³²

3.4.1 Medicinal Chemistry Data for Varying of the Leaving Group

The esters were synthesised from the parent carboxylic acids using a PyBOP coupling reagent. This was found to afford marginally improved yield (22% for **60** with HATU vs 46% with PyBOP) of the desired esters. The synthetic yields for this last step, isolated enzyme and hWB $pI_{C_{50}}$ data for the esters are given in **Table 17**.



Entry	Cpd	% Yield	δ	α	pIC ₅₀		hWB	Covalent ^b ?
					β	γ		
1	99	14%	9.2 ^a	8.2 ^a	7.2 ^a	5.8 ^a	N.T.	N.D.
2	100	39%	8.3	5.6	5.1	4.6	8.1	N.D.
3	60	46%	8.1	5.5	5.3	4.8	7.9	Yes
4	101	25%	8.2	5.6	5.4	4.9	7.9	Yes
5	103	18%	7.3	4.8	4.9	5.0	7.4	Yes
6	102	12%	6.4	4.8	4.8	5.0	6.9	Yes
7	104	19%	6.5	4.8	<4.5	4.7 ^c	5.5 ^d	Inconclusive
8	58	-	7.4	5.0	<4.5	<4.5	7.0	No

Table 17 – Synthesis, Biochemical potency at the four PI3K isoforms, hWB potency, and crystallography summary of compounds **58**, **60**, and **99** - **104**. ^a Compound found to be unstable in DMSO, data from N=2 only. ^b Covalency was determined by crystallography, and supported by binding kinetics (Section 4.1 Kinetic Analysis of Binding, and Mechanistic Implications). ^c Data reported from N = 2 with one additional value <4.5. ^d Data reported from N = 3, with two additional empty values. N.T. = Compound not tested due to instability. N.D. = Not determined. Y = yes; N = no.

Synthetically, the yields of these compounds were still low, due to issues mainly around isolation or stability of the compounds. At elevated pH, these compounds were susceptible to cleavage of the ester bond, and this was indeed problematic in their isolation by reverse-phase chromatography. In acidic modifiers, the compounds often coeluted with the phosphine oxide by-product of PyBOP, whereas basic modifiers afforded excellent separation, but partial hydrolysis upon solvent removal. The yields shown are the best obtained after significant attempts to improve this isolation procedure - using alternative stationary phases (basic alumina, cyano-capped silica, strong cation exchange), precipitation and conventional silica chromatography with acidic and basic modifiers. In particular, compound **99** was very unstable, and a fresh DMSO stock solution was required prior to any biological experiments. It was also unstable as a solid stored at -20 °C, and significant decomposition was observed after *ca.* 1 week under these conditions. The remaining esters

did not exhibit such a significant instability, and indeed they were found to be stable as solids at -20 °C for over a year (measured by LCMS). In DMSO solution, compound **60** was extensively studied, with <10% decomposition observed after stirring a 10 mM solution at room temperature for 3 days. Furthermore, the 10 mM DMSO stock was repeatedly freeze-thawed over a period of three months, with no significant degradation observed.

In this methoxypyridyl series, there existed a clear trend between reactivity of the leaving group, and potency. It was also evident that a very reactive ester (*e.g.* **99**) afforded exquisite sub-nanomolar potency in the biochemical assay, however at the cost of selectivity. One exception to this trend was the CF₃ ester **100**, as its significantly higher σ_p , and therefore lower pK_a , which may be expected to translate to a greater potency. This compound was marginally more potent than the less reactive esters, however still within the statistical error of the assay (two-fold, 0.3 log units). The penalty of having *ortho*-functionalised phenols in this series was evident with the dimethyl ester **102**, which showed an approximately 10-fold decrease in potency from the *p*-OMe ester **108**, which would not be predicted based on pK_a where these esters should be equipotent. In addition, the *p*-NO₂ ester **105** further emphasised this point by increasing the target potency ~10-fold over the *ortho*-substituted isomer **59** (pIC_{50} = 9.2 vs 8.3 in **Table 11**).

The aryl esters all maintained their potency in the hWB assay, a common trait for covalent inhibitors due to the increased incubation time and time-dependent nature of the reaction. Indeed, the dimethyl ester **102** improved in potency in the cellular assay, suggesting that the covalent reaction may be slow, and incomplete after the 1 h incubation time in the biochemical assay. A significant drop-off was observed for the activated alkyl ester **104**, suggesting that this ester may not be covalently bound. The activity was also significantly lower than methyl ester **58** in this experiment, indicating that larger esters may not be as well tolerated in this region in the initial reversibly bound enzyme-inhibitor complex. There was still an increase in potency for the aromatic esters, over the methyl ester **58**, which could be attributed to the extent of covalent binding for these compounds. However, there is clearly still a difference in pIC_{50} , which appears to be correlated with electron deficiency of the ester. This could also be due to favourable interactions with electron-deficient phenols in formation of the reversible complex, or due to differences in the rate of inactivation of the kinase, which is explored in a later section.

The aromatic esters **101-103**, expected to possess a lower reactivity than **60** were submitted for crystal structure determination, and found to be covalently bound (x-ray structures were the same as compound **60**, **Figure 35**). The two esters (**99** and **100**), which were expected to be above **60** in reactivity were assumed to also covalently bind to the kinase, based on the previous observation that *p*-NO₂ esters can covalently bind (**Figure 27**). These data suggested that aromatic esters have the potential to covalently inactivate the kinase, and could not distinguish any reactivity differences of these esters. However, this may not be surprising as the kinase and the inhibitors are incubated overnight in this experiment, with an excess of inhibitor. This should cause saturation of the binding site and therefore facile covalent bond formation. To further investigate these reactivity differences in the protein, a thorough kinetic analysis is required (see Section 4.1 Kinetic Analysis of Binding, and Mechanistic Implications).

Interestingly the activated alkyl ester **104** showed inconclusive evidence for covalent bond formation. Incomplete electron density was observed for the leaving group, (in two repeat experiments at 2.26 and 2.45 Å resolution) indicating either displacement by a nucleophilic moiety or disorder in this region (**Figure 46**). LCMS analysis of the crystallography stock solutions showed no evidence of compound degradation, suggesting disorder.

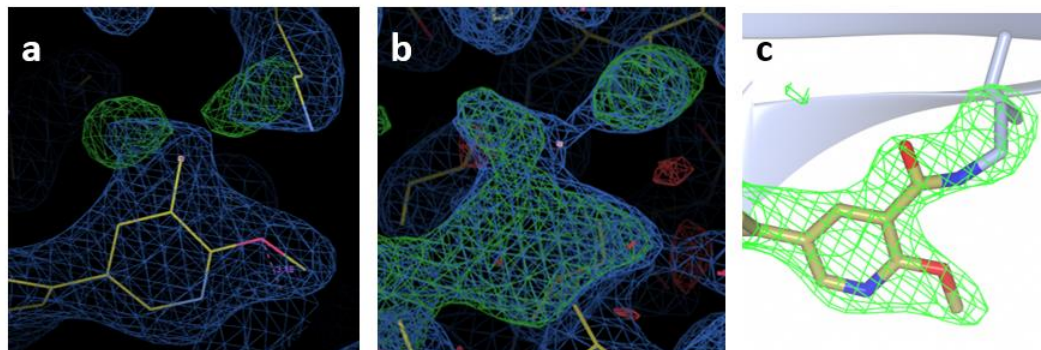


Figure 46 – Electron density maps for compound **104**. (a): Crystal 1. $2F_{\text{obs}}-F_{\text{calc}}$ map at 1.0 rmsd (blue) and $F_{\text{obs}}-F_{\text{calc}}$ map at 3.0 rmsd (green) for model with ligand and full lysine residue. A clear break between the ligand and Lys779 can be observed in the $2F_{\text{obs}}-F_{\text{calc}}$ density. (b): Crystal 2. $2F_{\text{obs}}-F_{\text{calc}}$ map at 1.0 rmsd (blue) and $F_{\text{obs}}-F_{\text{calc}}$ map at 3.0 rmsd (green) for model without the ligand, and lysine truncated to alanine. A thin bridge can be seen from the ligand onto Lys779 in the $2F_{\text{obs}}-F_{\text{calc}}$ map. The absence of ligand or Lys779 side-chain in the model are identified by the green $F_{\text{obs}}-F_{\text{calc}}$ map. (c): Regular model and $F_{\text{obs}}-F_{\text{calc}}$ density for covalently bound inhibitor **60**, with Lys779 truncated to alanine. Clear continuous electron density from Lys779 onto the ligand can be seen. All structures are shown in the same pose, for comparison.

The $2F_{\text{obs}}-F_{\text{calc}}$ density for one crystal showed a clear break in density (**Figure 46A**, blue map) indicating no covalent adduct, and for the other a clear thinning of continuous density onto the ligand (**Figure 46B**, blue map), suggesting a poorly resolved covalent linkage.

Furthermore, the $F_{\text{obs}}-F_{\text{calc}}$ density (**Figure 46A**, green map) showed a small amount of density not accounted for by the model, which could be the C=O of the ester, with the amide link to Lys779. (In **Figure 46A**, the molecule is truncated at the carbonyl C to give the two lobes of $F_{\text{obs}}-F_{\text{calc}}$ density not accounted for in the model. In **Figure 46B**, the structure is modelled with an absence of ligand, and the lysine truncated to alanine, hence the large proportion of $F_{\text{obs}}-F_{\text{calc}}$ density observed.) Also, the pyridyl ring was rotated to place the electrophilic centre towards Lys779, consistent with what was observed for the covalently bound inhibitors (**Figure 46C**). This experiment suggested that the covalent bond was partially forming with this inhibitor, however it was not as conclusive as the other covalent inhibitors synthesised so far (**Figure 46C**). In the biochemical assay, it was equipotent to the covalent dimethyl ester **102**, despite pK_a analysis predicting that it should be less susceptible to covalent bond formation. This, again, suggests that bulky aromatic esters may not be as well tolerated as originally thought in this region of the kinase during formation of the reversible enzyme-inhibitor complex. No further efforts were made into characterising the binding mode of this inhibitor, as the crystallography is conducted with an excess of inhibitor, and an overnight incubation. These are forcing conditions, so covalent bond formation would be expected to occur in this experiment.

This section showed that aromatic esters, regardless of electronics, and steric obstruction, possess the requisite reactivity to covalently bind to the target by formation of an amide bond to Lys779. In order to establish the origin of the differences in potency observed, a thorough kinetic analysis was required to determine the magnitude of both the reversible, and reactivity contributions to potency.¹ This analysis is included in the next section, which aims to further characterise the biology of these methoxypyridine-based compounds by kinetic analysis, mass-spectrometry, cellular washout studies and chemoproteomics.

4. Further Biological Characterisation

4.1 Kinetic Analysis of Binding, and Mechanistic Implications

The biochemical and hWB assays detailed so far, together with crystallography, established an idea of potency, relative reactivity of each of the inhibitors, and strong evidence of whether the compounds covalently modified PI3K δ or not. However, this does not give a full characterisation of a covalent inhibitor that is suitable for SAR analysis. The need to gain an understanding of the different binding parameters that contribute to the potency of covalent inhibitors (**Figure 4**) has been well documented in the literature.^{1,8,53,96} For example, the compounds detailed in the previous section bear different leaving groups on the same scaffold and show different potencies in the enzyme and hWB assays. It could be rationalised that the observed changes in enzyme potency arose due to the differing reactivities of the electrophilic centres. Whilst this may indeed be the case, this assumption neglects the non-covalent contribution to inhibitor potency. In order to separate these kinetic and thermodynamic parameters, the use of a time-course assay that monitors inhibition with time was employed.

The commercially available ADP Quest™ kit from DiscoverX²³³ was adapted for this purpose. The principle behind this assay is to monitor the production of adenosine diphosphate (ADP) from the kinase reaction, by converting it through coupled-enzyme reactions to a fluorescent molecule, resorufin (See Section 6.1.3 Kinetic Assay for detailed description of the assay principle). In this experiment, compounds are assayed against a fixed concentration of PI3K δ in a dose-dependent manner, and the effects of inhibition are measured by a fluorescent readout, in a time-dependent manner. The no-inhibitor control produces a linear progress curve over the course of the assay, and addition of a rapidly equilibrating reversible inhibitor causes a decrease in the gradient of this progression curve. Importantly, this progression plot is linear at all concentrations for reversible inhibitors as equilibrium is achieved quickly on the timescale of the experiment. From the gradients of the straight lines fitted to these points, an IC₅₀ can be determined (**Figure 47 Left**). For covalent inhibitors, the second covalent binding step is slow, and does not achieve equilibrium. This causes a shift away from linearity as the assay progresses, and eventually results in a gradient close to zero (*i.e.* the enzyme is fully inhibited). As the concentration of inhibitor increases, the time to achieve full

inactivation decreases, until the active site is saturated with reversibly bound inhibitor, and the assay is then measuring the maximal rate of covalent inactivation of the kinase. The raw data are fitted to a rate equation to derive an observed rate constant (k_{obs}), which is replotted against concentration of inhibitor to generate a characteristic hyperbolic curve. From this curve, k_{inact} can be read from the asymptote of the curve as the maximal rate of inactivation, and K_i can be defined as the concentration of inhibitor that achieves half of the maximal rate of inactivation (**Figure 47 Right**).

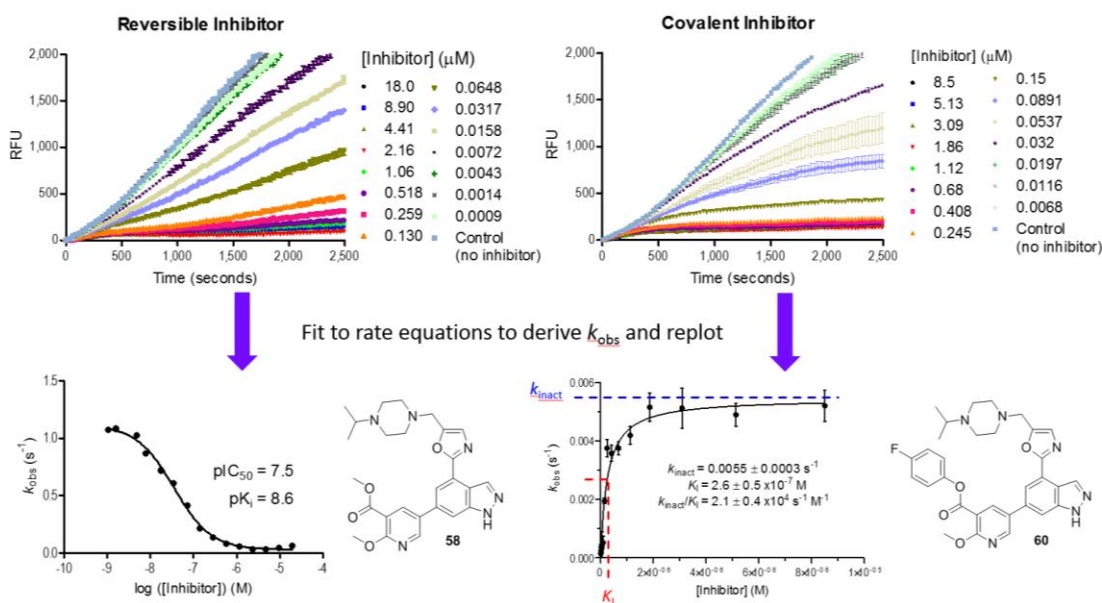


Figure 47 – General representation of the raw and replotted data from the kinetic assay for a reversible (left) and covalent (right) inhibitor. Methyl ester **58** was used as the reversible inhibitor control, and fluorophenyl ester **60** is exemplified. See Section 4.1 Kinetic Binding Assay at PI3K δ for detailed analysis method including equations used, and plots for all activated esters.

The activated esters synthesised in the previous section were all subjected to this experiment, with saturating concentrations of competing ATP (1 mM). As these inhibitors compete with ATP for binding to the active site of the kinase, increasing the concentration of ATP slows down the kinetics of covalent inactivation to a measurable rate. It is important to note that the kinetic binding parameter (k_{inact}) is concentration-independent, as it is measured upon saturation of the active site with reversibly bound inhibitor; therefore it is not affected by the high concentrations of ATP used. If a rapid equilibrium is assumed in the first step, K_i can be considered comparable to the apparent thermodynamic dissociation constant for reversible binding (K_i^{app}), which is concentration-dependent, and can be corrected for the saturating concentrations of ATP used to afford the absolute value (K_i) using the Cheng-Prusoff relationship.^{193,234,235} In this investigation, the values of k_{on} and k_{off} (**Figure 4**) were not explicitly determined, and thus this assumption cannot be made confidently. This

value is therefore reported as K_i , which describes the concentration of inhibitor required to achieve the half-maximal rate of covalent inactivation under these conditions. This is an empirical constant for this system, and is not corrected for the saturating concentrations of ATP used. The data for the derived K_i and k_{inact} values are shown below in tabular form and a graphical form adapted from a study of covalent EGFR inhibitors by Schwartz *et al.*⁵³ In this plot, k_{inact} is plotted as a function of K_i , both on a logarithmic scale. The second order rate constant (k_{inact}/K_i) was also derived, which can be used instead of an IC_{50} to more accurately compare the potency of covalent inhibitors. Consideration of the individual parameters allows determination of the origins of differing potency between two covalent inhibitors.

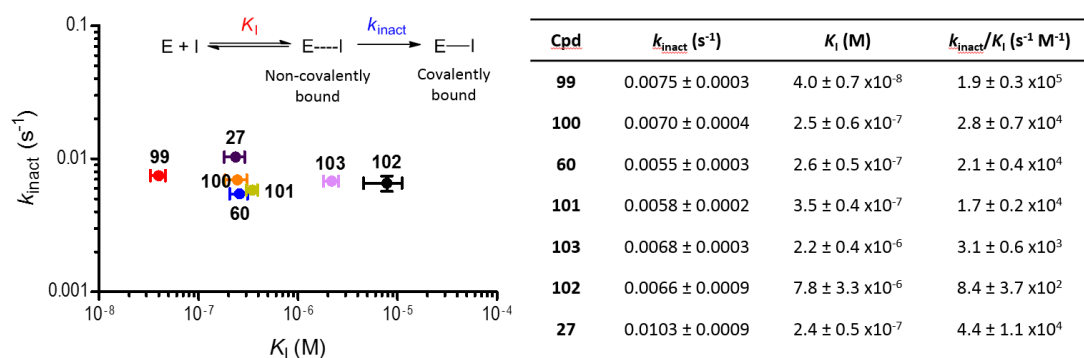


Figure 48 – Derived k_{inact} , K_i and k_{inact}/K_i values for the methoxy-pyridyl activated esters, and Wortmannin. The graph depicts k_{inact} as a function of K_i , as used by Schwartz *et al.*⁵³ There is a significant difference in K_i across the series, which correlates with the expected chemical reactivity of the ester, yet the rate constant for inactivation (k_{inact}) varies <2-fold across the series. Implications of this are discussed in the text. The table shows the numerical data in this graph, and the derived k_{inact}/K_i ratio. Kinetic measurements were carried out in triplicate, and results are shown as the mean \pm s.e.m. The general two-step binding model considered is shown above the k_{inact} vs K_i graph.

The raw fluorescence data for the methyl ester **58** showed linear progression curves over the entire time-course of the assay, and at all tested concentrations, supporting this compound as a reversibly bound inhibitor. The derived $\text{p}K_i$ value was ~ 10 -fold higher than the biochemical TR-FRET assay reported earlier. Further investigation with other reversible inhibitors showed this to be a constant difference, arising due to the different analysis methods used (FRET vs. coupled enzyme fluorescence, kinetic vs. end-point etc.). All aryl esters showed non-linear progression curves, consistent with the covalent inactivation, and the desired thermodynamic and kinetic parameters were successfully derived after fitting to a two-step binding model using the replot method for all 6 esters. Wortmannin was also processed through this analysis, as a positive control for covalent inactivation. It exhibited non-linear progression curves consistent with the activated esters, and valid binding parameters were also derived.

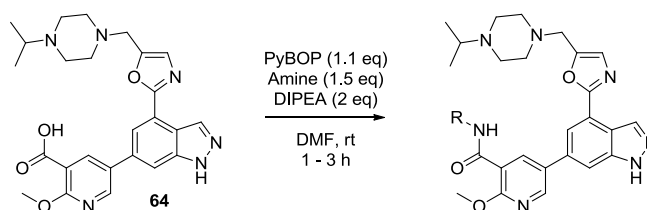
The surprising result from this analysis was that the reactivity of these esters with the protein (k_{inact}) varied only 1.4-fold across the series, and not in accordance with the expected reactivity of these esters from pK_a and Hammett analysis (**Figure 45**). In other words, the *p*-OMe and *p*-NO₂ substituted esters (**99** and **103**) were equally reactive with the protein, and indeed the sterically hindered dimethyl ester **102** also showed equal reactivity. In contrast, the K_i values obtained for these esters spanned two orders of magnitude, from 40 nM (compound **99**) to 7.8 μ M (compound **102**) (195-fold difference). This indicated that the electronic nature of the phenolate leaving group (*i.e.* pK_a value), and therefore expected chemical reactivity/leaving group ability, did not correlate with the rate of the covalent inactivation in this system. Rather, there is a correlation with K_i , suggesting that either the electronic nature of this group significantly affects an interaction with the kinase in this region during the reversible binding step, or that a more complex mechanism is involved than the traditional two-step scheme depicted.

To investigate this observation further, the corresponding amides were synthesised from the parent carboxylic acid. These would be expected not to covalently bind to the kinase, thus providing a close analogue to the esters to investigate the reversible binding contribution of the aryl ring. Of course, the N-H of the amide may now affect the interactions in this region, so this is only an approximation of the reversible binding. These data are summarised in **Table 18** below.

In synthetic terms, these reactions proceeded with decreasing yields from the aliphatic trifluoroethylamine, through to the highly electron-deficient anilines. Indeed, the most electron-deficient nitroaniline showed no evidence of coupling in this reaction, presumably because it was too unreactive to displace the activated PyBOP ester.

Gratifyingly, the methyl amide **112** showed potency at PI3K δ comparable to the methyl ester **58** (pIC_{50} = 7.2 vs 7.4 for the ester), suggesting that the substitution of an oxygen linker for the N-H moiety was tolerated by the enzyme for reversible binding. Additionally, trifluoroethyl amide **111** was tolerated in this region of the protein, with no significant loss in potency. However, upon addition of the bulkier aromatic group, an approximately 10-fold loss in potency at PI3K δ was observed, suggesting that these groups are not actually well tolerated in this region of the kinase. X-ray crystal structure analysis, and kinetics analysis both supported a reversible binding mode for amide **107** (**Figure 49**). The crystal structure showed poor density for the aromatic group of the amide, which is believed to be due to

disorder in this region, so is modelled in the crystal structure as a methyl group. The 2F₀-F_c electron density map is shown in **Figure 49A** at 0.8 rmsd, where extra density beyond the modelled methyl group is clearly visible, which is presumed to be from the aryl ring.



Entry	Amine	Cpd	Yield	δ	pIC_{50}		
					α	β	γ
1		105			Did not couple		
2		106	10%	5.3	5.0	5.0	4.9
3		107	27%	5.9	<4.5	<4.5	4.7
4		108	29%	6.0	4.7 ^a	4.8 ^a	4.9
5		109	36%	5.7	4.8	5.0	5.1
6		110	62%	5.8	4.8 ^a	4.7	4.9 ^a
7		111	67%	7.1	4.6	<4.5	<4.5
8		112	25% ^b	7.2	<4.5	<4.5	<4.5

Table 18 – Summary of synthetic data and biochemical enzyme data for the corresponding amides **105** - **112**. ^a Data from N = 2 with one additional value <4.5.

Furthermore, the aromatic amides all showed a $pIC_{50} \approx 6$ (6-fold difference between the most and least potent compounds, which do not correlate with electron deficiency), suggesting that electronic effects of the phenyl ring do not have a significant effect upon reversible binding affinity. When compared to their corresponding esters, this suggests that the

increase in potency must be associated with the covalent contribution to $pI_{C_{50}}$. However, the k_{inact} values determined for these esters were roughly constant across the series (1.4-fold difference), whereas the reversible contribution exhibited by K_I varied 195-fold. To explain these conflicting results, an alternative multistep mechanism for the covalent reaction with the kinase is discussed below.

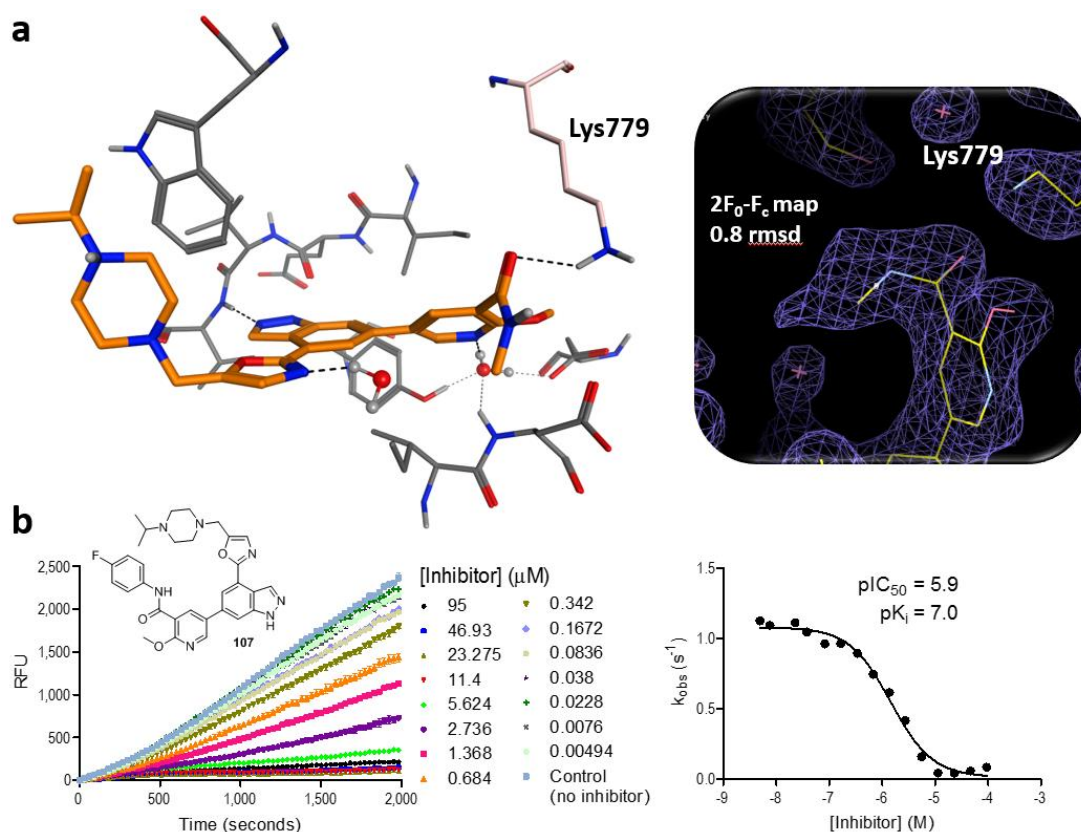
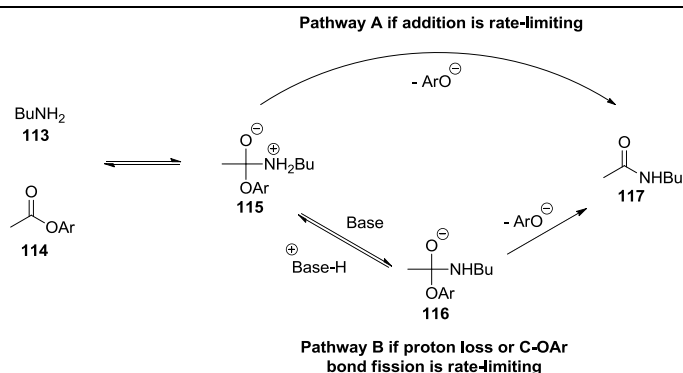


Figure 49 – (a) Crystal structure and kinetic binding profile for amide **107**. The crystal structure shows a clear break in electron density between Lys779 and the C=O of the amide, indicating that this ester is a non-covalent binder. There is an absence of density for the *p*-F phenyl group, which is reflected in the final model. This is believed to be due to disorder in this region, due to free rotation of this solvent-exposed group. $2F_0-F_c$ electron density map is viewed at 0.8 rmsd in Coot. (b) Binding kinetics show linear traces, again supporting reversibility at the concentrations tested (up to 100 μM). Kinetic experiments were carried out in triplicate, with results plotted as the mean \pm s.e.m.

A study by Maude *et al.* on the butaminolysis of phenyl esters deduced that, in solution, amide bond formation proceeds via a non-concerted mechanism consisting of formation, and subsequent collapse, of a tetrahedral intermediate **115**.²⁰² These studies showed that the reaction can proceed via two pathways, after formation of intermediate **115**. In pathway **A**, the rate-determining step involves addition into the carbonyl to form **115**, whereas pathway **B** has two potential scenarios. The rate-determining step here involves either proton loss from **115** to **116**, or fission of the C-OAr bond of **116** to expel the leaving group (**Scheme 8**).²⁰²

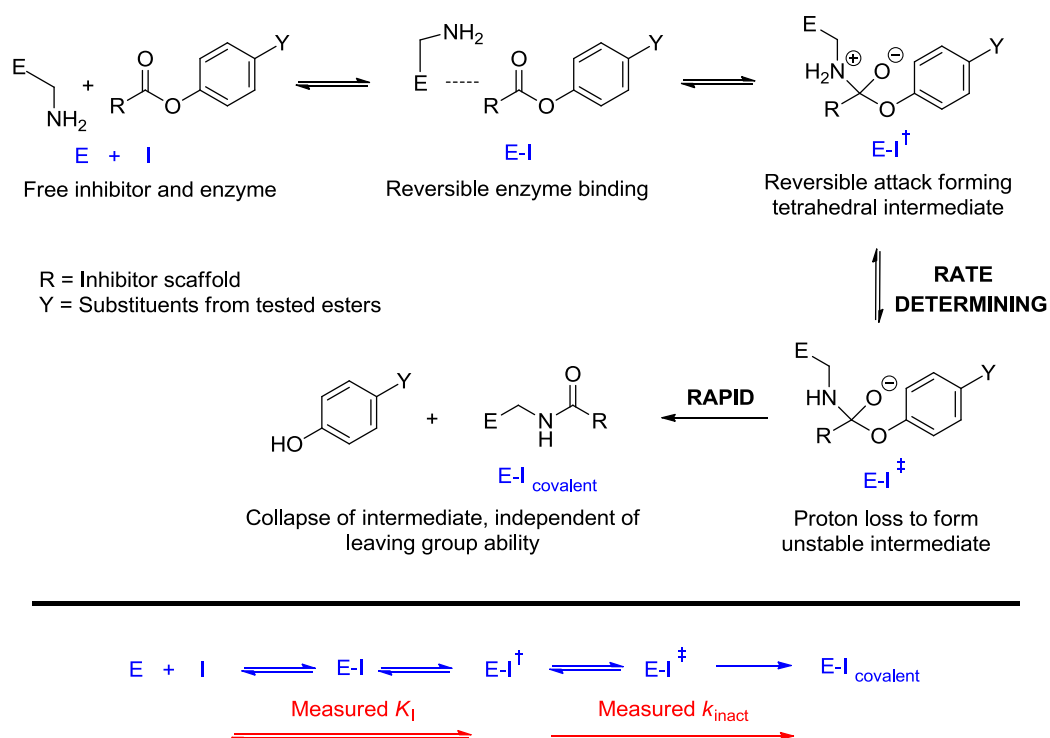


Scheme 8 – Summary of mechanistic observations by Maude *et al.*²⁰² Amidation reactions of phenols, in solution, proceeds via a non-concerted mechanism of addition to form the tetrahedral intermediate **115**, and subsequent collapse with expulsion of phenolate leaving group.

The rate of inactivation (k_{inact}) is measured upon saturation of the binding site with inhibitor, therefore is separated from the reversible binding step (K_i). The observation that k_{inact} is constant across the chemical series implies that the rate-determining chemical step in the covalent bond-forming reaction with the enzyme (k_{inact}) is independent of the structure of the ester. This excludes pathway **A** and pathway **B** with C-OAr fission as the rate-limiting step, as both of these pathways would be expected to correlate with the $\text{p}K_a$ of the leaving group and Hammett constants. Pathway **B** with proton loss as the rate-determining step therefore remains as a potential mechanism to explain these kinetic observations. This could be expected, as kinases do not possess the catalytic machinery that is observed in hydrolase enzymes to efficiently deprotonate the active site nucleophile^{54,55} (**Figure 5**). For K_i to show a dependence on reactivity of the ester, this implies that the addition step into the carbonyl is also reversible, and manifests in this parameter. Taking these two arguments together, the mechanism shown below in **Scheme 9** is proposed.

First, the inhibitor binds into the kinase active site through typical reversible interactions to form E-I. From the corresponding amides, it is assumed that this affinity is roughly in the micromolar range. Attack from Lys779 then forms the first tetrahedral intermediate (E-I⁺); this step will also be reversible and will be affected by the nature of the phenol due to inductive effects on the reactivity of the carbonyl group. The measured K_i values above are therefore proposed to encompass these two steps, explaining the observed correlation with electron-deficiency of the phenol. The remaining two steps form k_{inact} , where proton transfer to form E-I⁺ is rate limiting, in accordance with Williams' observations.¹⁵ Collapse of this intermediate will be rapid, and irreversible, and thus the absolute value for k_{inact} is independent of the $\text{p}K_a$ of the leaving group, consistent with the kinetic data presented. The

methyl ester is inherently unreactive, and the equilibrium for formation of E-I[‡] from E-I is therefore far to the left, thus covalent adduct formation is not observed.



Scheme 9 – Proposed multi-step sequence to enzyme inactivation by amide bond formation to the conserved lysine residue of PI3K δ .

4.2 Specificity of the Covalent Interaction

To further assess and quantify the reactivity of the lead compound **60**, an automated HPLC assay was developed to accurately quantify the reactivity of this compound under various conditions. This assay was based on the reactivity assays reported earlier in this thesis, but certain parameters were assessed to improve reproducibility. Firstly, the DMSO/water system at room temperature previously used was found to produce an emulsion in some cases, which may have contributed to erroneous values, and was not fully representative of a biological system. A study by Dahal *et al.*⁹⁷ assessing the reactivity of a series of electrophiles with lysine residues showed that, at pH 7.4, reactivity with lysine was almost non-existent due to protonation of the reactive amine. To simulate reactivity in an aqueous environment, they employed a borate buffer at pH 10.2, however compound **60** was found to be insoluble in this system. Thus, a solvent system of acetonitrile/water/DMSO was developed, which gave full dissolution of the compound and lysine mimetic. To simulate a deprotonated, reactive lysine, two equivalents of base (relative to lysine) were added to

initiate the reaction. This experiment was also carried out with methyl ester **58** as an inactive control. To simulate reactivity with surface lysine residues, the same reaction was carried out using a potassium phosphate buffer at pH 7.4 with 10% DMSO. In addition, this reaction was investigated without any lysine, in order to establish the hydrolytic stability of the ester. These latter two reactions were carried out at a physiologically relevant temperature of 37 °C. All reactions were performed using liquid handling of stock solutions (see Experimental for further details) to facilitate greater reproducibility and minimise the quantity of compound required. End of assay HPLC traces are shown in **Figure 50**.

Consistent with the reactivity analyses conducted previously, ester **60** showed good reactivity with a deprotonated lysine mimetic **118**. The reaction profiles for this looked very good, and excellent reproducibility was seen across three replicates. Using pseudo-first order kinetic analysis (see Section 6.2.3 HPLC Reactivity Assays for details), a half life of 1.32 h was determined from these experiments. Also, consistent with Dahal *et al.*,⁹⁷ minimal conversion was observed at physiological pH. This suggests that reactivity of this electrophile is specific in nature towards activated lysines, and that it is unlikely to non-specifically react with surface lysine residues. Furthermore, the methyl ester **58** remained inert to conversion under the forcing conditions. Finally, the activated ester showed excellent hydrolytic stability, with <5% decomposition observed after 24 h, giving confidence that the biochemical potency and selectivity data obtained for this ester are accurately reporting the activity of the intact ester.

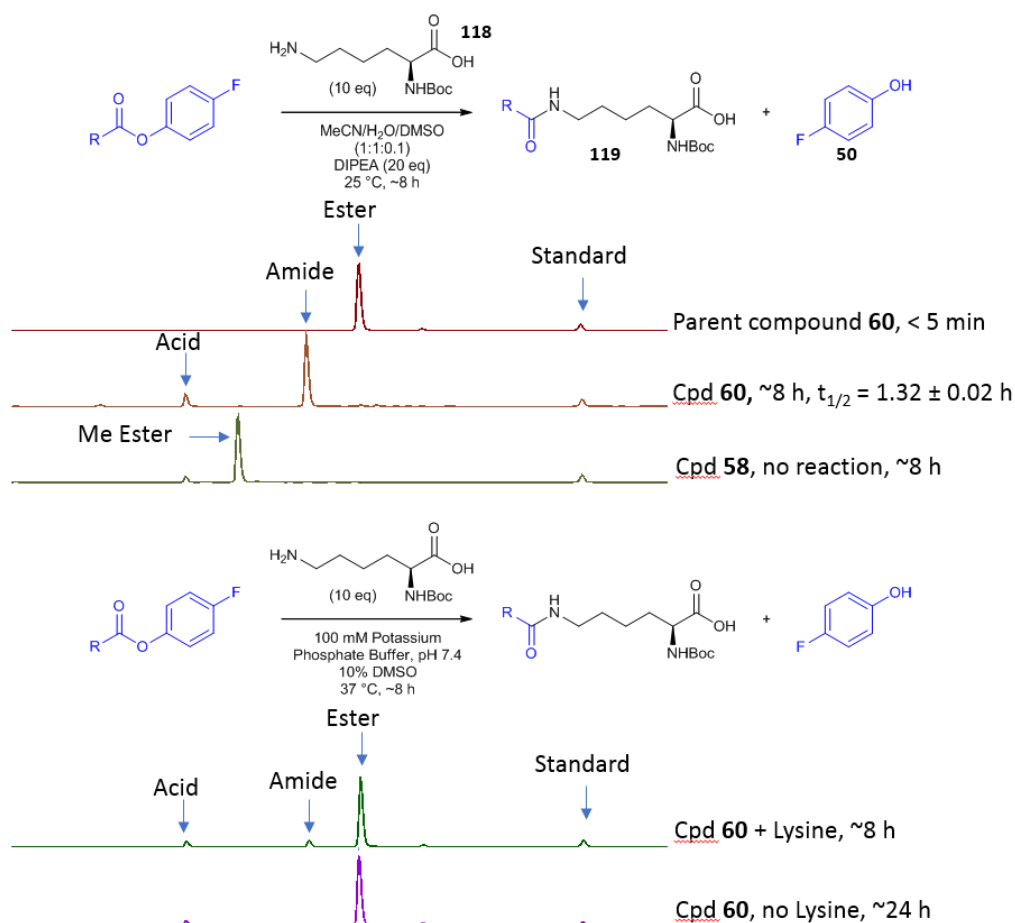


Figure 50 – End of assay HPLC traces investigating the reactivity of compound 60. Top panel, from top to bottom: Parent ester 60 for internal marker; Representative trace for compound 60 under the forcing conditions shown, after *ca.* 8 h of reaction showing clean conversion to the expected amide (derived half life is shown as mean of three replicates \pm s.d., two replicates were only run for 6 h); No reaction was seen for methyl ester 58 under the same conditions, after 8 h. **Bottom panel:** End of assay HPLC trace for ester 60 under physiological conditions showed little conversion to amide, and a small amount of hydrolysis to carboxylic acid 64; <math>< 5\%</math> decomposition to carboxylic acid 64 was observed after 24 h under these conditions, without nucleophile.

For an accurate assessment of physiological stability, an assessment should be carried out in human whole-blood, or blood plasma due to an abundance of esterase proteins.²³⁶ However, technical difficulties were experienced in this assay, so robust and reliable data were not obtained. A recent study by Zaro *et al.*²³⁶ identified how incorporating metabolically labile esters can in fact increase the selectivity of a covalent inhibitor (**Figure 51**). Working with ibrutinib 6, they incorporated a metabolically labile fumarate ester motif into the covalent warhead (compound 120). This modification maintained potency and covalent binding to the target enzyme, BTK, yet showed rapid esterase-dependent degradation in mouse plasma ($t_{1/2}$ <math>< 2\text{ min}</math> for tested compounds vs >2 h for control compound without this group) to an unreactive carboxylic acid analogue 121. This suppresses off-target reactivity, and improves

the selectivity profile of the parent inhibitor. Using this method, the researchers showed *in situ* and *in vivo* that this afforded greater covalent labelling selectivity over the proteome. Extending this concept to this system with activated esters, it is hypothesised that a kinetic selectivity advantage may be observed here if the compound exhibited a short plasma half-life. Providing it is stable enough to reach the target, hydrolysis of excess unbound inhibitor will afford the unreactive carboxylic acid **64**, thus removing any issues from off-target covalent inactivation.

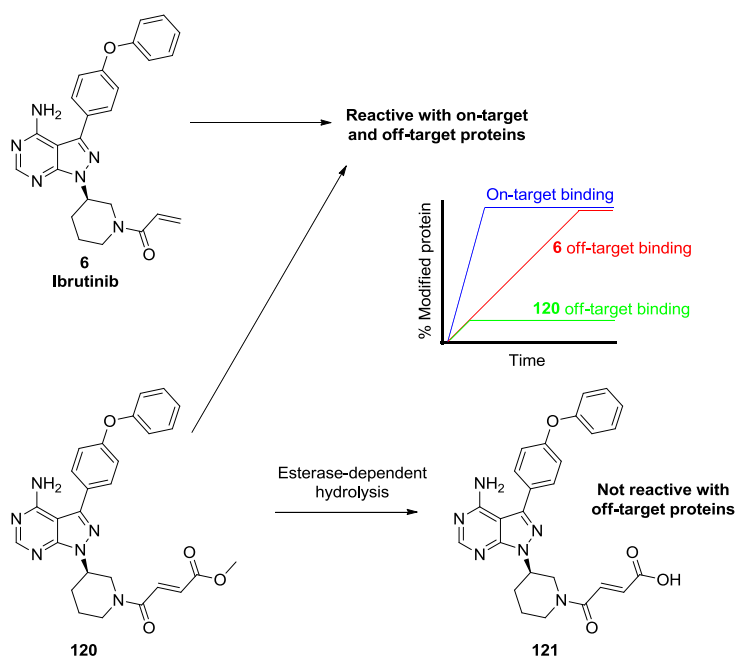


Figure 51 – Summary of a study by Zaro *et al.*²³⁶ showing how metabolically labile esters impart kinetic selectivity to covalent drugs. Derivatised ibrutinib probe **120** is susceptible to hydrolysis by esterases present in the blood, generating an unreactive carboxylic acid. The study showed how this feature could be exploited to improve the selectivity profile of ibrutinib **6** *in vitro* and *in vivo*.

To support the conclusion that compound **60** does not modify surface-exposed lysines, isolated protein mass spectrometry was investigated (**Figure 52**). In a simple experimental set-up, the inhibitor was added in a two-fold excess to full-length recombinant human PI3K δ enzyme. Analysis of the mixture after 5 minutes by LCMS showed full modification of the enzyme, with a mass change consistent with addition of the ester and loss of fluorophenol. Only one modification was observed, and indeed pushing this system further with 10 equivalents of **60** and an overnight incubation did not modify the protein further. It was concluded that the single modification observed was due to modification of Lys779 observed in the crystal structure. To support this, the enzyme was preincubated with the potent and reversibly binding inhibitor **122**, which was known to bind to the ATP binding site.¹⁶³ This completely abrogated covalent binding in the time-frame where full modification had

previously been observed, supporting this modification to be in the ATP binding site of the enzyme. Further studies such as trypsinolysis and LC-MS/MS identification of the resulting peptides, or site-directed mutagenesis, would be expected to confirm the modified residue as Lys779.^{62,96} However, these methods were not pursued due to strong evidence obtained from the crystal structure. Additionally, as an inactive control, carboxylic acid **64** did not covalently modify the protein when incubated in a large excess. These data, taken together with the HPLC reactivity analysis support ester **60** as a stable, and specifically lysine-reactive PI3K δ inhibitor.

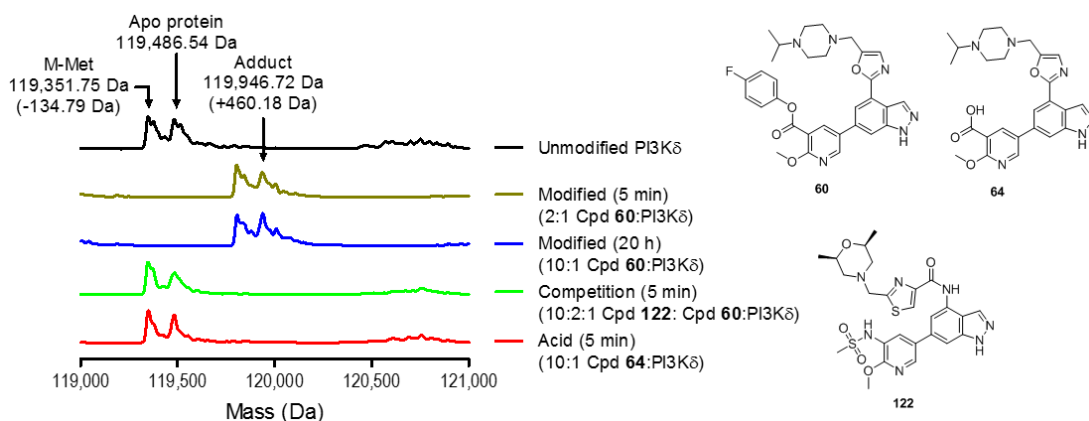


Figure 52 – Intact protein mass spectrometry analysis. Top to bottom – apo protein, the lefthand peak may correspond to a loss of N-terminal methionine (M-134.79 Da observed, calculated M-131 Da); protein treated with two equivalents of **60**, analysed at 5 min; protein treated with 10 equivalents of **60** overnight; protein pretreated with 10 equivalents of **122** for 15 min, prior to addition of two equivalents of **60**, and analysed at 5 min; protein incubated with 10 equivalents of **64** and analysed at 5 min.

4.3 Selectivity Profile of Ester **60**

Having now extensively profiled the kinetics of binding, the chemical reactivity and stability, and the non-specific binding potential of compound **60**, the next stage was to thoroughly assess the selectivity of this compound. This was carried out in a stepwise manner, by firstly investigating the binding kinetics at two closely related PI3K isoforms, then investigating the biochemical selectivity of the compound over a series of lipid and protein kinases, and finally by invoking a proteome-wide analysis of binding selectivity in a native biological system. This analysis builds up a full picture of the selectivity of this compound, which will be invaluable when using this compound as a probe or a drug for targeting PI3K δ .

4.3.1 Kinetic Selectivity Analysis at Closely Related Isoforms

Closely related kinases pose the greatest risk of off-target interactions due to their structural similarity to the target protein. In this case, the key enzymes identified as off-targets are the

remaining Class I PI3K proteins, PI3K α , β , and γ . Using the ADP Quest assay detailed above, the binding of compound **60** was investigated at these enzymes. Unfortunately, PI3K γ was not amenable to this assay due a very low K_M for ATP (15 μ M), which produced poor quality data in this kinetic format. In a cellular environment, this low K_M should translate to a greater selectivity in the reversible binding step, therefore this enzyme was not pursued further in kinetic analysis. PI3K α and β performed well in control experiments in this format, and were investigated further.

Initially, jump dilution assays were investigated to establish the potential for irreversibility at high concentrations of inhibitor, in the absence of a competing ligand. Similar to the mass spectrometry and crystallography investigations, this experiment should force covalent inactivation to occur, if possible. Initially, the enzyme is incubated at 100x the final concentration required for the kinetic readout, with a concentration of inhibitor equal to the IC₉₀ value (or the concentration of protein for the most potent inhibitors). The IC₉₀ was estimated as 10x the TR-FRET IC₅₀ for PI3K α and β , and 10x the IC₅₀ determined at 1500 s in the ADP Quest kinetic experiment detailed above for PI3K δ . (Each 30 s time point in this assay format provides a 16-point dose-response curve, which is replotted as an IC₅₀ - see Section 6.2.8 Kinetic Binding Assay at PI3K α and PI3K β for further details.) The mixture is then diluted 100-fold, to a final concentration of enzyme suitable for kinetic analysis, and a concentration of inhibitor roughly equal to IC₁₀. In this experiment, reversible inhibitors will rapidly re-equilibrate to allow the enzyme reaction to proceed, whereas slow tight-binding inhibitors (which would exhibit the same kinetic inhibitory behaviour as covalent inhibitors) will slowly dissociate, and irreversible inactivators will not.

This analysis was carried out at PI3K δ , α , and β with the lead compound **60**, Wortmannin **27**, and reversibly binding controls **58** and **64**. The raw data are shown below in **Figure 53**. Consistent with the data obtained to date, the reversible controls showed rapid equilibration, and regeneration of kinase activity after the dilution, supporting a non-covalent binding mode. In addition, consistent with the literature, Wortmannin showed sustained inactivation of all three isoforms, supporting its known promiscuous covalent binding nature. The compound of interest, **60**, also covalently inactivated all three kinases. These data suggest that the inhibitor is capable of inhibiting closely related kinases covalently, at high concentrations in an absence of any competing ligand.

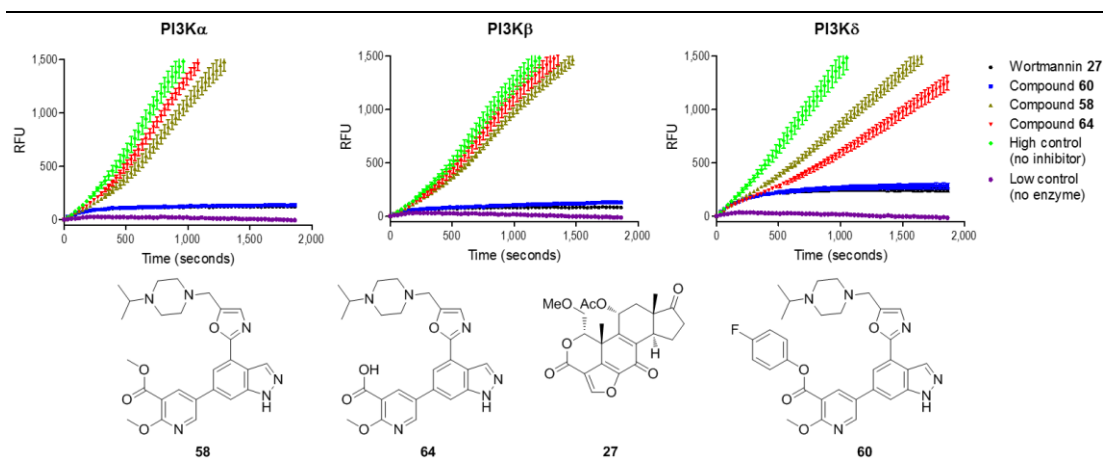


Figure 53 – Jump dilutions conducted at PI3K α (left), PI3K β (middle) and PI3K δ (right) in the absence of competing ATP. Covalent inactivation of all three kinases was observed under these conditions by **60**. Inhibitor assays were conducted in triplicate and controls in duplicate. Results are plotted as mean \pm s.e.m

This result is not surprising, due to the conservation of the targeted lysine residue, and that the incubation concentrations were calculated based on the IC₅₀ for each individual enzyme. In reality, if this compound were to be used as a chemical probe or drug for PI3K δ , it will be dosed into a cellular environment. In this environment, there are competing ligands present, which would decrease the apparent binding affinity of the inhibitor. Furthermore, the dose applied would likely be optimised around the PI3K δ IC₅₀ value, not the off-target enzyme IC₅₀. For the jump dilution experiment above, compound **60** was incubated at 32-fold and 24-fold higher concentrations at PI3K α and β , respectively, compared to PI3K δ , reflecting the large differences in IC₅₀ values at these kinases. To more accurately investigate the covalent off-binding to these targets in a more physiologically relevant setting, the full kinetic assay was carried out with a dose-range tailored to PI3K δ inhibition for each inhibitor, with saturating concentrations of competing ATP (1 mM). Data from this experiment are shown in **Figure 54**.

Starting with reversibly bound methyl ester **58**, linear progress plots were observed at all tested concentrations, at all three enzymes, consistent with rapid onset of inhibition. Furthermore, the absence of a non-linear, slow phase at PI3K δ was reproduced with PI3K α and β consistent with the established reversible binding mode for this inhibitor. The concentrations shown in **Figure 54** are the PI3K δ IC₉₀ calculated from the IC₅₀ measured in this experiment, and the corresponding IC₉₉ values calculated from this value. The gradient of the plots at the off-target enzymes is decreased relative to the no-inhibitor control (black), showing that this enzyme is still inhibited in this experiment by these concentrations of inhibitor. Conversely, and using the same analysis, Wortmannin **27** showed non-linear reaction progression curves at the same concentrations dosed at all three kinases. These

curves were consistent with slow-binding, which was known to be irreversible from the jump-dilution experiment in **Figure 53**. Again, this is consistent with the biochemical TR-FRET data obtained earlier, and literature data stating Wortmannin as a pan-PI3K covalent inhibitor. Finally, applying this analysis to the lead ester **60**, showed that, up to concentrations equal to 5x the PI3K δ IC₉₉ calculated in this assay, this inhibitor does not covalently inactivate these two off-target enzymes. Again, the gradient of these plots was decreased relative to the no-inhibitor control, suggesting that the catalytic function of the enzyme is still inhibited by this inhibitor, however not by covalent binding over the time-frame of this assay (25 minutes). This assay was not carried out longer than this, as non-linearity was observed in the PI3K α control curve.

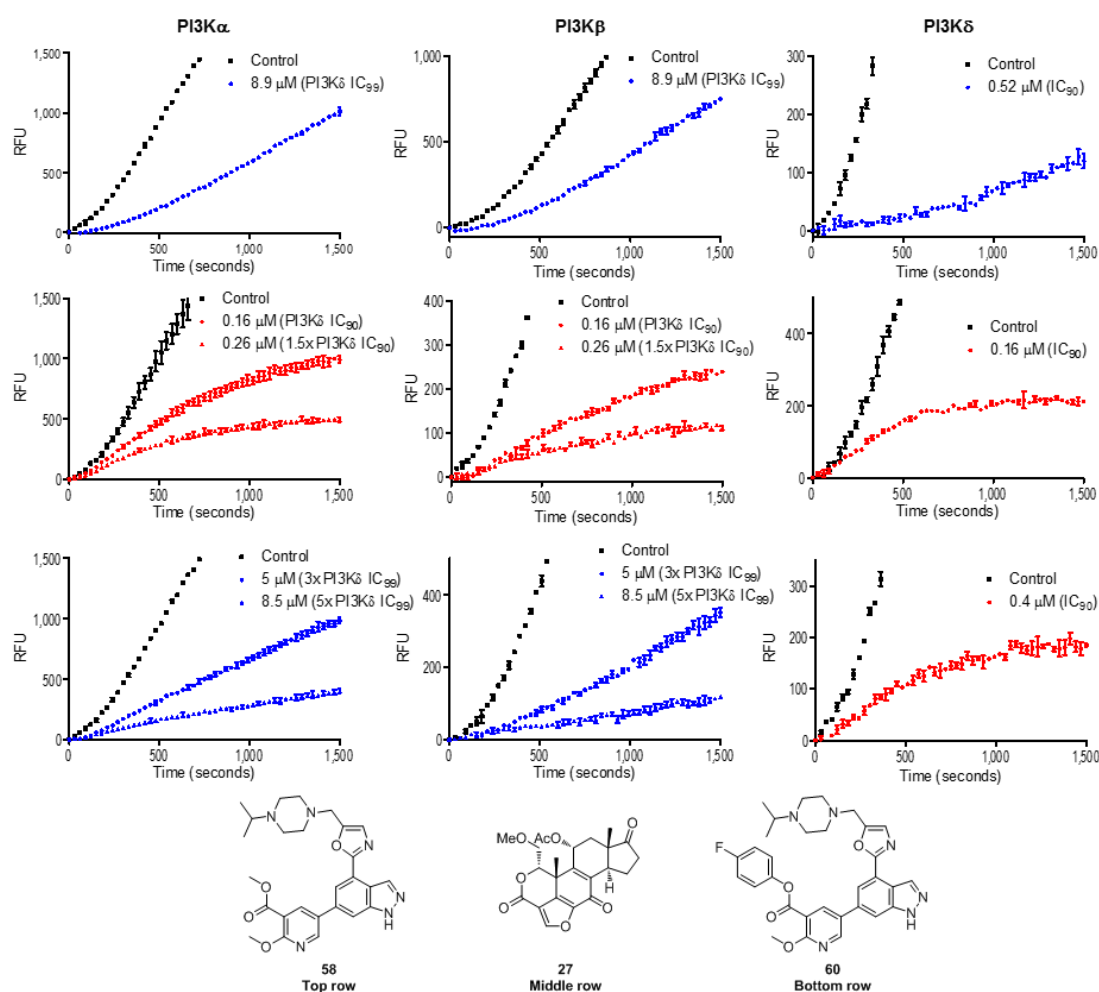


Figure 54 – Kinetic plots of the inhibition over time under saturating ATP conditions (1 mM). Linear plots (blue) relative to no-inhibitor controls (black) are typical of reversible inhibitors. Non-linear plots (red) relative to no-inhibitor controls (black) are typical of slow-binding inhibitors (confirmed to be irreversible by jump dilution experiments above). The top row depicts reversible ester **58**, showing linear progress at IC₉₀ at PI3K δ , and at PI3K α and β at the PI3K δ IC₉₉. Middle row depicts irreversible inactivation of all three kinases by Wortmannin **27** at IC₉₀ for PI3K δ (1.5x PI3K δ IC₉₀ curves are also shown). Bottom row shows selective ester **60**, exhibiting covalent inhibition at PI3K δ at IC₉₀, and reversible inhibition at PI3K α and β at 3x and 5x PI3K δ IC₉₉. Assays were conducted in duplicate, and results are shown as mean \pm s.e.m.

Additionally, these kinetic data can be processed along the time axis as a series of 16-point dose-response curves, to derive IC_{50} values every 30 seconds. As covalent inhibition is a time-dependent process, IC_{50} values decreasing with time is a common way to assess whether there may be covalent interactions in an enzyme-inhibitor system.¹⁰⁴ This analysis was carried out on these kinetic data (**Figure 55**), and showed that the IC_{50} value at PI3K δ does become more potent with time for ester **60**, however not at the two off-target enzymes. Conversely, Wortmannin **27** does show a time-dependent decrease in IC_{50} consistent with covalent inactivation of all three enzymes. The control reversible compound **58** does not show this behaviour, consistent with reversible binding, and giving confidence to the conclusions drawn for the activated ester at the off-target enzymes.

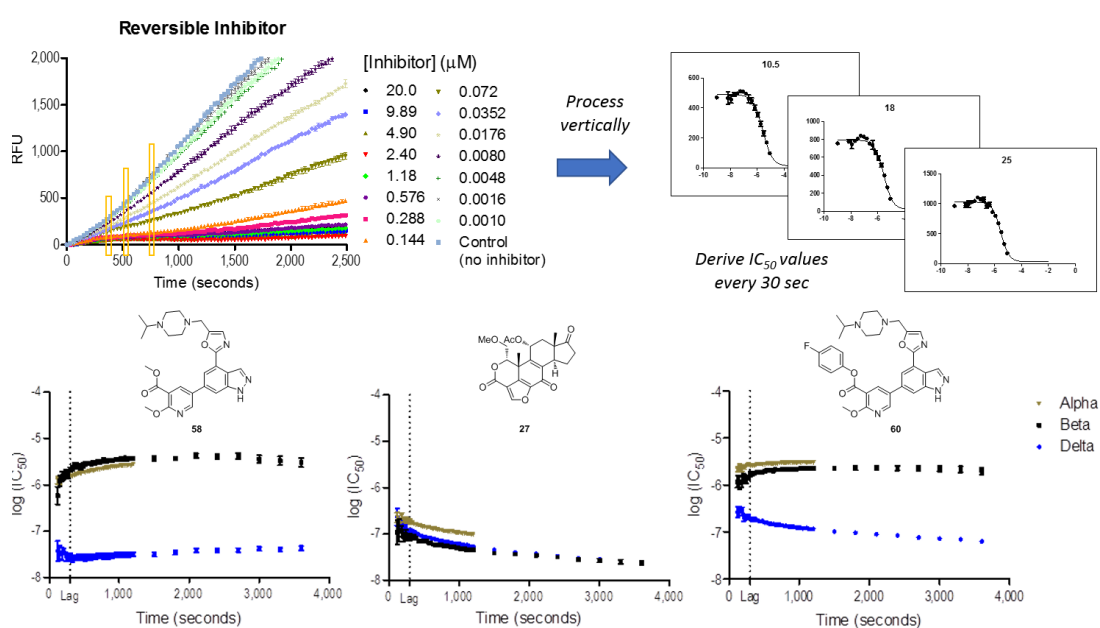


Figure 55 – Time dependent decrease in $\log IC_{50}$ for compound **60 at PI3K δ only supports selective covalent inhibition.** **Top:** Summary of data processing method. Each 30 sec set of data constitutes a 16-point dose-response curve, from which IC_{50} values can be derived every 30 sec over the time-course. **Bottom:** Change in $\log IC_{50}$ with time for reversible control compound **58**. No change in IC_{50} , consistent with reversible inhibition at all three isoforms is observed. Change in $\log IC_{50}$ with time for pan-PI3K irreversible control compound **27**. A time-dependent decrease is observed at all three isoforms. Change in $\log IC_{50}$ with time for selective compound **60**. Time-dependent decrease is only observed at PI3K δ , supporting selective covalent inhibition.

The kinetic data, taken together with the jump dilution data, strongly suggest that in physiologically relevant systems there exists a concentration window where selective covalent inactivation of PI3K δ can be achieved. Furthermore, this must reside in the initial reversible interactions of the inhibitor with the kinase, rather than reactivity as the reactive residue is conserved between these enzymes. To assess this accurately, derivation of the individual K_i and k_{inact} values at the two off-target enzymes would be required. This was

attempted, however at the high concentrations of inhibitor used, the assay produced unreliable data and so was not pursued further.

4.3.2 Wider Kinome Selectivity Analysis Under Biochemical Conditions

Having established that the lead inhibitor showed excellent selectivity over the closely-related PI3K family members, it was now desired to investigate the selectivity of compound **60** over the wider kinome. To do this, the inhibitor was submitted to the University of Dundee MRC PPU International Centre for Kinase Profiling.

Two experiments were carried out, against a selection of lipid kinases, and then a selection of protein and atypical kinases. In the lipid kinase analysis, the compound was tested in dose-response against 10 enzymes, in duplicate. Nine of these kinases showed no inhibition, up to the highest tested concentration of inhibitor (10 μM , $\text{pIC}_{50} < 5.0$) implying high levels of selectivity over these kinases. One kinase, diacylglycerol kinase β returned a pIC_{50} of 5.1, which still provided high levels of selectivity towards PI3K δ . In the second analysis, the compound was tested at 1 μM single-concentration, in duplicate, against 150 enzymes (**Figure 56**). Of these enzymes, only Tropomyosin receptor kinase A (TrkA) showed statistically significant inhibition of 35%, and was followed-up in dose-response format. The assay was conducted at 20 μM ATP, for a measured $K_{\text{M}}(\text{ATP})$ of 28 μM , deriving a pIC_{50} of 6.55 ($N = 2$). Assuming competitive inhibition, in a cellular environment (2 mM ATP) this gives an estimated cellular selectivity of 115-fold towards PI3K δ .

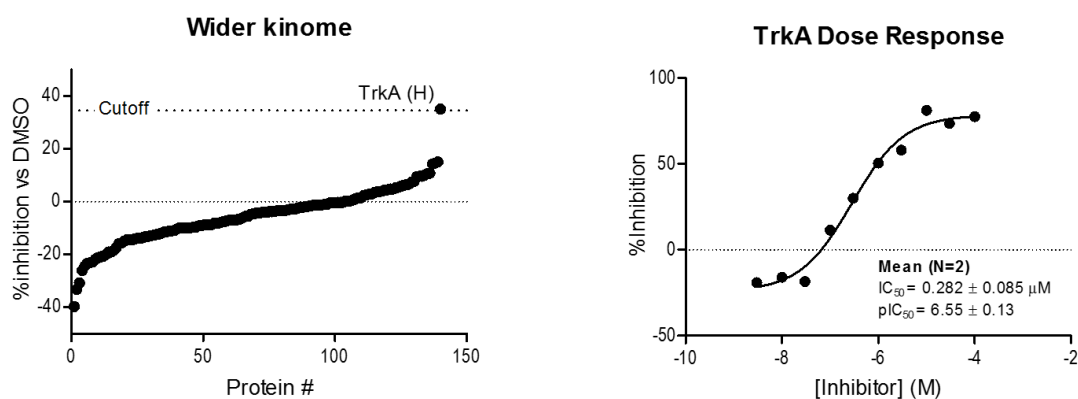


Figure 56 – Waterfall plot of % inhibition vs DMSO of compound **60** against 150 kinases carried out at the University of Dundee MRC PPU International Centre for Kinase Profiling. TrkA was the only protein that returned a statistically significant inhibition value ($>$ mean of all values + 3x s.d.). This kinase was followed up in full curve dose-response, deriving a pIC_{50} of 6.55. Data in both plots are shown as the mean of two replicates, without error bars for clarity.

A key limitation of these biochemical assays when investigating covalent inhibitor selectivity is the incubation time. The assays reported above are incubated between 15 min and 45 min, with the biochemical TR-FRET assays incubated for 60 minutes (See Section 6.2.9 Wider-kinome Selectivity Screening). Given the time-dependent nature of the covalent binding reaction, the pIC_{50} values reported should therefore be treated with some caution, as they may be prone to variation with incubation time. Furthermore, to facilitate the high-throughput nature required from this third-party service, the enzymes are also grouped into assay bundles arranged by their $K_M(ATP)$. This results in some kinases being assayed above their $K_M(ATP)$, and some (for example TrkA) assayed below. Assuming the inhibitor is competitive with ATP, as is the case for the target kinase, this may also produce non-realistic pIC_{50} values. Nonetheless, use of screens such as this one, and other commercial sources, is an industry-wide method of quickly generating selectivity data against a large number of targets for a desired compound.

The data obtained from this investigation were promising for the selectivity of this compound against a wide range of kinases within the lipid kinome, and outside of the lipid kinome. However, these experiments were carried out in a relatively simple biological context and therefore may not truly represent the off-target profile of this compound in physiologically relevant environment. To address this issue, a mass spectrometry based experiment in live cells was designed, which assessed the global off-target profile of the compound **60** in native biological systems using quantitative chemoproteomics.

4.3.3 Proteome-wide Determination of Off-Targets of Compound 60

4.3.3.1 Chemoproteomic Platforms for Assessing Target Engagement

Chemoproteomic platforms have been widely used as methods to assess target profiles of compounds in cellular, and even *in vivo* systems.^{52,90} Due to technological advances in chromatography systems, mass-spectrometry and computational power, routine proteomic experiments can easily identify thousands of proteins with high confidence from a complex biological mixture.^{237,238} Furthermore, changes in the relative levels of these proteins after treatment with small molecules can be used as a method to evaluate target engagement. One of the forefront methods in this field is Activity-Based Protein Profiling (ABPP), developed by the Cravatt Laboratory.⁵² The general concept behind these experiments is to involve a reactive probe that can modify a subset of cellular proteins via covalent bond formation. In addition, this probe is modified with a reporter tag to enable click chemistry to

attach fluorogenic groups or biotin handles. These handles then allow an in-gel fluorescence-based readout, or direct enrichment from the cellular mixture (termed “pull-down” experiment) for mass spectrometry (MS)-based identification of proteins. This platform can then be used to interrogate changes in protein levels between different systems. For example, comparative ABPP can be used to differentiate expression profiles between different cell lines and disease states to identify protein targets in disease,^{44,52} or the binding profile of inhibitors and fragments can be assessed by competition-based experiments with the ABPP probe (Figure 57).^{41,42,47}

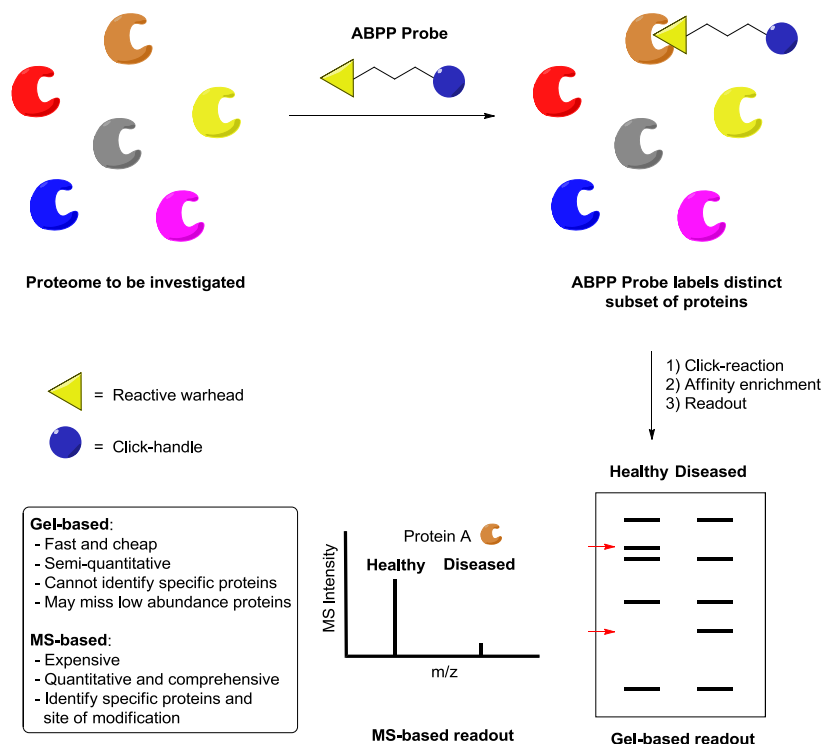


Figure 57 – General principles of Activity-Based Protein Profiling (ABPP). An ABPP probe possessing a reactive warhead is added to a proteome, where it labels a specific subset of proteins. The ABPP probe also possesses a click handle (commonly an alkyne) that can be conjugated onto either a fluorogenic dye, or biotin handle. The fluorophore will facilitate a gel-based readout by in-gel fluorescence, whilst the biotin handle will facilitate affinity enrichment and identification of protein targets by mass spectrometry-based methods.

Commonly, non-selective binders are used to interrogate binding to particular protein classes, or specific residues across the proteome. Examples of this include fatty-acid based probes for assessing lipid-protein interactions,⁴⁶ Kinobead and KiNativ technologies to assess inhibitor binding profiles against kinases and other ATP binding proteins in cell lysates,^{37,239,240} iodoacetamide probes for reactive cysteines,^{44,58} activated ester probes for reactive lysine residues,^{42,109} and novel chemotypes for selectively engaging methionine⁴³ and glutamic acid⁹⁵ residues (Figure 3).

An alternative way of investigating the targets of a covalent compound is to generate a “clickable” analogue of the parent inhibitor. Initially, this clickable analogue is used to identify a preliminary list of target binders from a physiologically relevant system (*e.g.* live cells or cell lysates). Then, by competing the binding of the enriched proteins to this probe, by preincubating with the parent inhibitor, targets of the parent inhibitor can be identified.^{60,130} The first documentation of this approach in the covalent kinase inhibitor field was in 2014, where Lanning *et al.* utilised an alkyne-tagged derivative of ibrutinib (probe **123**) to identify covalent off-target proteins in live cancer cells (**Figure 57**). To do this, they first added the alkyne to cancer cells, and carried out a pull-down experiment to identify 14 specific binders of this probe. Next, by competing the binding of this probe to the target proteins by preincubation with ibrutinib **6**, the team identified 10 off-target proteins. Furthermore, they identified these off-target proteins as proteins possessing a conserved cysteine residue. However, some structurally distinct off-targets (such as sterile alpha motif- and leucine zipper-containing kinase, ZAK) were also identified. Despite structural differences in the active sites, the covalent reaction still engaged an active site-proximal cysteine.⁶⁰

This general method has been used to identify off-targets of key clinical compounds such as ibrutinib and afatinib,⁶⁰ next generation BTK inhibitors,¹³⁰ as well as high-profile clinical failures such as the fatty acid amide hydrolase (FAAH) inhibitor BIA 10-2474 that led to a fatality of one volunteer and hospitalisation of four others in a first-in-human study.²⁴¹ This last example, in particular, highlights the need to accurately assess off-target profiles of covalent inhibitors in physiological and medically relevant settings, for which chemoproteomic methods provide an excellent tool to do so.

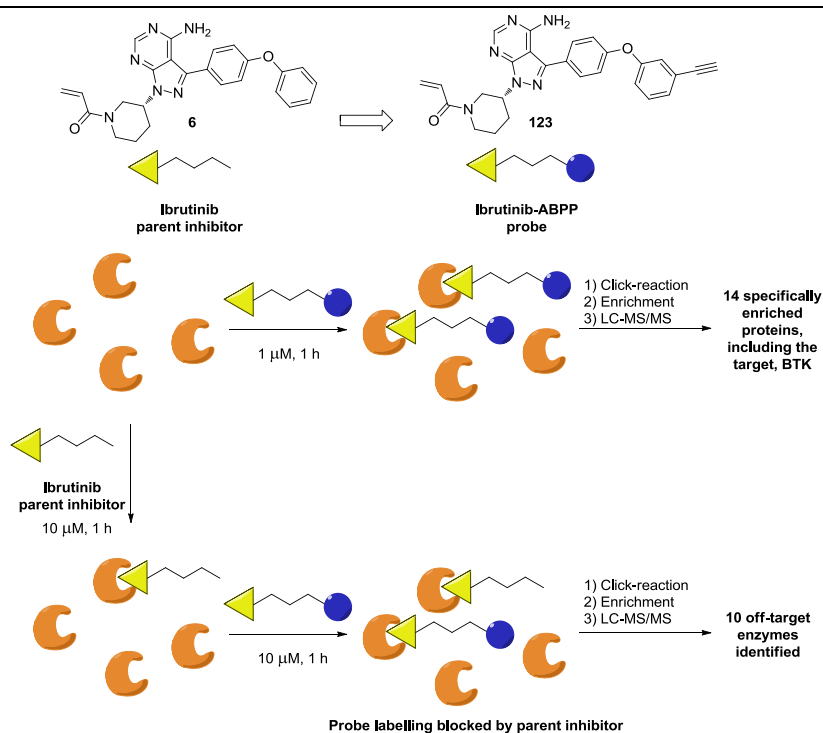


Figure 58 – Example of a competitive ABPP experiment used to identify off-target binders of ibrutinib **6**, in live cancer cells.⁶⁰

4.3.3.2 Design of Clickable Probe for Investigation of Covalent PI3K δ Inhibitor Off-targets

For this particular investigation, a work-flow was designed based on the ABPP method used for identifying targets of ibrutinib **6**, and related analogues, by incorporating a clickable tag into compound **60**.^{60,130} The reactions used to carry out these transformations are called bioorthogonal click reactions. Initially coined in 2001 by Sharpless, “click reactions” refer to those which are high yielding, broad in scope, fast, reliable, air-stable, form benign products and are purified easily.²⁴² These include energetically favourable reactions such as cycloadditions, ring opening reactions of strained electrophiles, non-aldol carbonyl reactions (*e.g.* condensations, acylation etc.), and additions into C=C bond.^{242,243} The “bioorthogonal” parameter was introduced in 2005 by Bertozzi²⁴⁴ to describe reactions that exhibit fast kinetics in water, are inert to biological nucleophiles, and avoid the use of cytotoxic metals. Common reactions used for these experiments are copper-catalysed azide-alkyne cycloaddition (CuAAC),^{245,246} strain-promoted azide-alkyne cycloaddition (SPAAC),²⁴⁷ and inverse electron-demand Diels-Alder reactions (IEDDA).²⁴⁸ A summary of these reactive partners, and the relative rates of these reactions is shown below.²⁴⁸

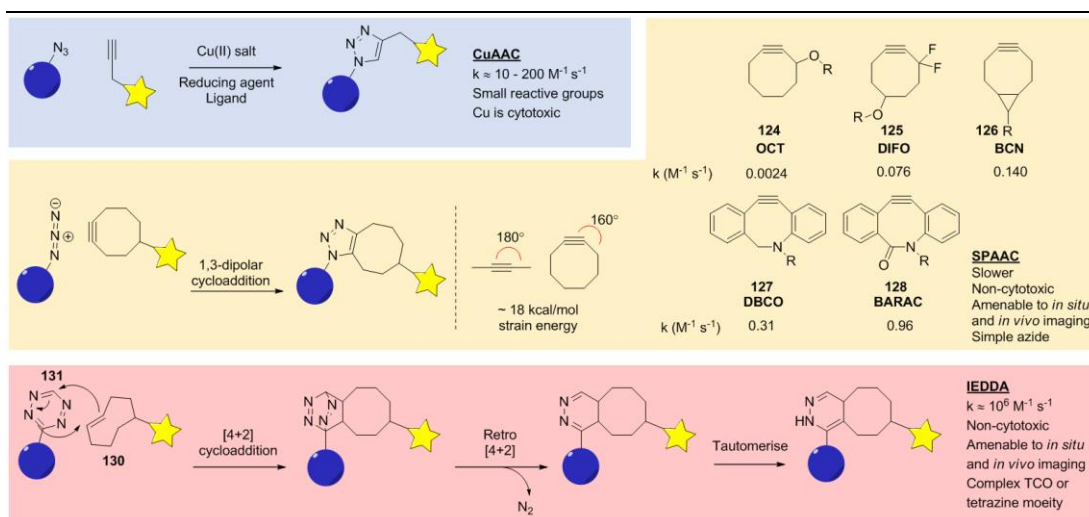


Figure 59 – Comparison of three commonly used bioorthogonal click reactions. Blue spheres and yellow stars represent the two coupling partners. These can be biological macromolecules, tagged small molecules, fluorophores, biotin handles etc.

CuAAC reactions are the archetypal click reaction,²⁴⁵ invoking an alkyne on the probe, and an azide into the click handle (either a fluorophore or biotin). The use of copper(I) salts formed by the *in situ* reduction of copper(II) salts with biological reducing agents such as ascorbic acid or tris-(2-carboxyethyl)phosphine (TCEP), and mediated by ligands such as tris[(1-benzyl-1H-1,2,3-triazol-4-yl)methyl]amine (TBTA) facilitates a highly efficient reaction.^{243,245,246} Experiments have shown that inverting these reactive partners generates a considerably higher background signal.²⁴⁹ Unfortunately, Cu(I) is cytotoxic, which has prevented this reaction from use in live-cell systems.²⁴³ To circumvent this issue, researchers have developed alternative reactions such as SPAAC and IEDDA.

SPAAC reactions utilise an azide group on the probe, and a strained alkyne group in the click handle.²⁴⁷ Many different options of alkyne group exist (e.g. **124** - **128**), with the hypothesis being that introducing strain into the ring provides sufficient energy to remove the need for a copper catalyst.^{243,250} These reactions are not as efficient as CuAAC, and the lipophilic phenyl moieties used for some of the click groups (e.g. DBCO, BARAC) can cause accumulation of the dye in membranes and proteins. However, the removal of toxic Cu salts facilitates the use of this technique in living systems.^{244,251} Furthermore, with the small azide tag required on the probe, this coupling reaction is very popular.

Finally IEDDA is a relatively new bioorthogonal coupling reaction, between a *trans*-cyclooctene (TCO) group **130** and a tetrazine moiety **131**.²⁵² These reactions are exceptionally fast and selective, which provides the ability to label low-abundance proteins, and are

therefore deemed the current gold-standard in the field.^{248,251} However, in our hands, the tetrazine and TCO coupling partners exhibit poor chemical stability, are not particularly synthetically tractable, and can severely affect binding to the target and the physicochemical properties of the molecule due to the large steric bulk imparted to the probe. Additionally, CuAAC reactions have proven poorly reproducible in our laboratories.²⁵¹ Therefore, in this particular investigation, SPAAC was chosen as the method of choice due to greater reliability than CuAAC in our laboratories, and a more straightforward synthetic route to the azide-bearing probe.

For a successful probe, the reactive partner should be included into a position that does not significantly affect the binding to the target. Typically, this will require incorporation into a solvent-exposed region of the inhibitor. In the case of covalent ester **60**, the crystal structure showed that the isopropyl group was solvent-exposed (**Figure 60**), thus compound **131** was synthesised with an azide tag in this position.

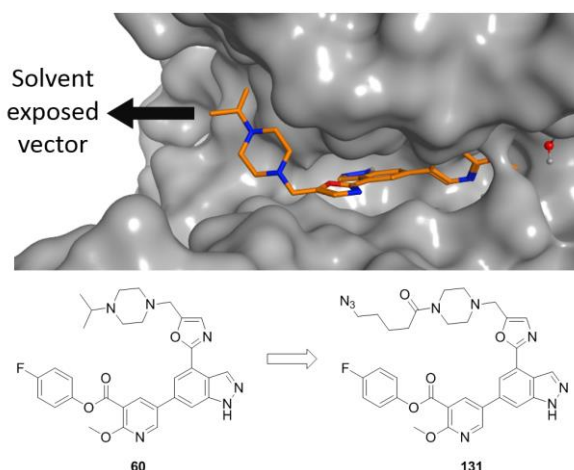


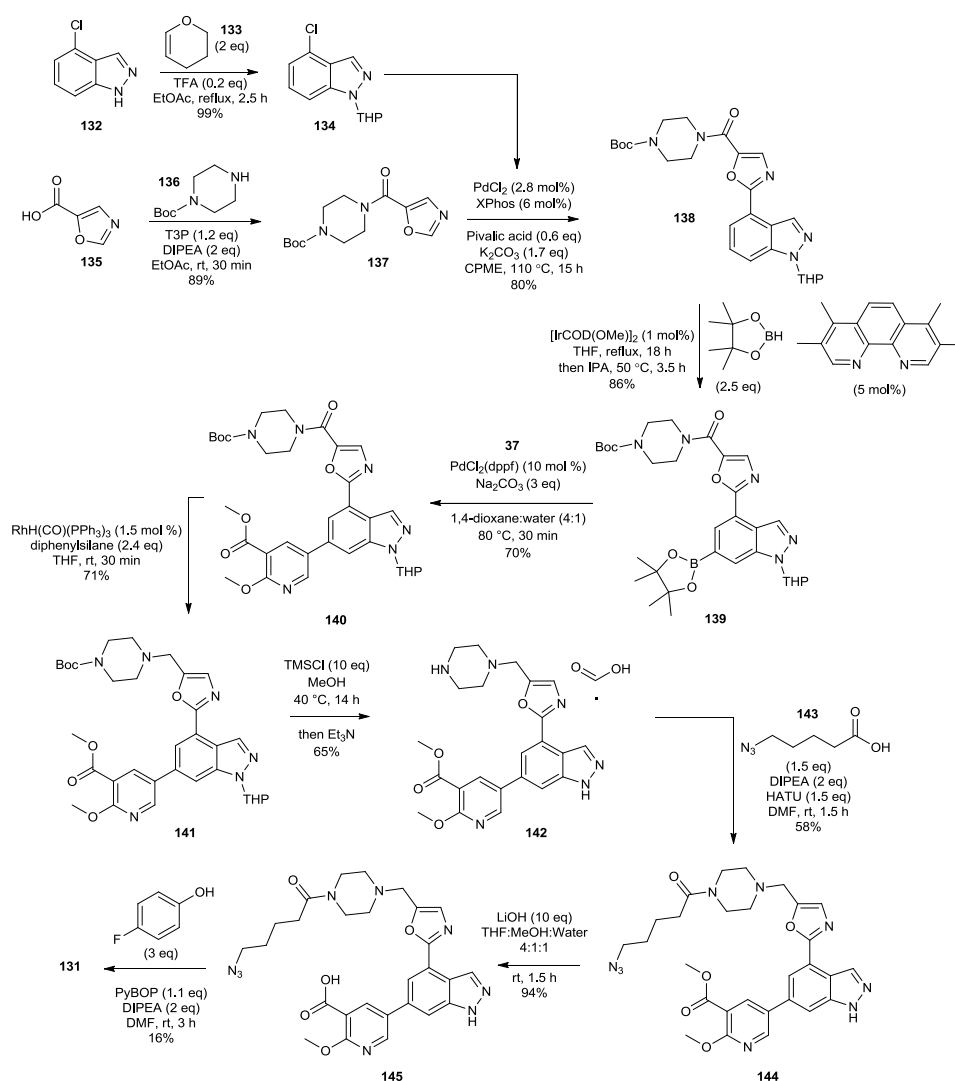
Figure 60 – Design considerations for development of a clickable analogue of covalent inhibitor **60**. The isopropyl group is exposed to solvent when covalently bound, thus presenting an ideal vector to incorporate a small bioorthogonal reactive group.

4.3.3.3 Synthesis and Biochemical Activity of Azide Probe **131**

Due to lack of availability of the boronic ester fragment **139** with a protected amine, the synthesis of azide **131** began from commercially available materials (**Scheme 10**). The chemistry used was based upon the methodology used to synthesise boronic ester fragment **61**.²⁰³ Chloroindazole **132** was first THP protected by treatment with strong acid at reflux. The second building block was synthesised from commercially available oxazole-carboxylic acid **135** and Boc-protected piperazine **136**, by an amide coupling mediated by propylphosphonic anhydride (T3P®). These two fragments **134** and **137** were then coupled together using C-H

activation methodology, on gram scale in excellent yield to afford intermediate **138**. A subsequent iridium-mediated C-H activation²⁵³ was then invoked, again on gram scale, to afford the desired Bpin fragment **139** in excellent yield.

The remainder of the synthesis proceeded via steps analogous to those used previously in this thesis. Notably, the amide reduction step to form compound **141** was performed on 0.75 g scale, with excellent selectivity over the ester and carbamate groups also present on the molecule. Furthermore, the product was isolated by crystallisation from boiling isopropanol, removing a time-consuming workup previously used.²⁰⁴ The azide functionality was incorporated by amide coupling to azidopentanoic acid **143**, and was stable to base-mediated hydrolysis and the final PyBOP coupling to afford azide probe **131**.



Scheme 10 – Synthesis of azido probe **131** from commercially available materials.

The probe was submitted to the biochemical PI3K δ assay, and showed a small reduction in potency compared to the parent inhibitor **60** (pIC₅₀ = 7.6 vs. 8.1). However, this decrease may be expected due to the increased steric bulk, and the presence of an amide rather than a basic amine which may affect the binding interaction with Trp760 that is known to increase PI3K δ potency (**Figure 16**).¹⁷⁵ These decreases were not so significant as to cause concern for the selectivity profiling, and thus this compound was progressed to cell lysate-based target engagement studies, and full proteomic analysis.

4.3.3.4 Cell Lysate-based Target Engagement Analysis

To obtain information around the suitability of probe **131** for assessing binding interactions of its parent compound **60**, it was subjected to a target engagement analysis in THP-1 cell lysates. These cells are an immortalised monocyte-like cell line, originally obtained from the peripheral blood of a child with acute monocytic leukaemia.²⁵⁴ Furthermore, these cells are commonly used as a model for primary human peripheral blood monocytes (PBMCs) obtained from healthy volunteers,²⁵⁵ and monocytes and macrophages in the cardiovascular system.²⁵⁶ As this project has been based on a drug discovery programme optimised for inhaled delivery, these cells therefore represent an ideal surrogate system for primary cells.

Probe **131** (1 μ M) was added to a solution of lysate, and then conjugated to a fluorogenic handle using SPAAC reaction with dibenzocyclooctyne-Cy5 dye (DBCO-Cy5). This showed strong probe-dependent labelling of a roughly 110 kDa protein when viewed by in-gel fluorescence, consistent with the mass of the catalytic p110 δ subunit. Unfortunately, considerable non-specific background labelling of the proteome was observed by the DBCO-Cy5 dye, in the absence of probe, at lower molecular weights, making it difficult to assess the selectivity of the probe in this region. Immunostaining with rabbit anti-p110 δ antibody, and then goat anti-rabbit fluorescent secondary antibody showed coelution with the Cy5 signal, supporting this specifically labelled band to be the p110 δ subunit of PI3K δ . Furthermore, this labelling by probe **131** was competed in a dose-dependent manner by pretreatment of the lysates with increasing concentrations of the parent compound **60**. This afforded a pIC₅₀ of 7.5, supporting potent and competitive engagement of PI3K δ by the probe and the parent compound (**Figure 61**).

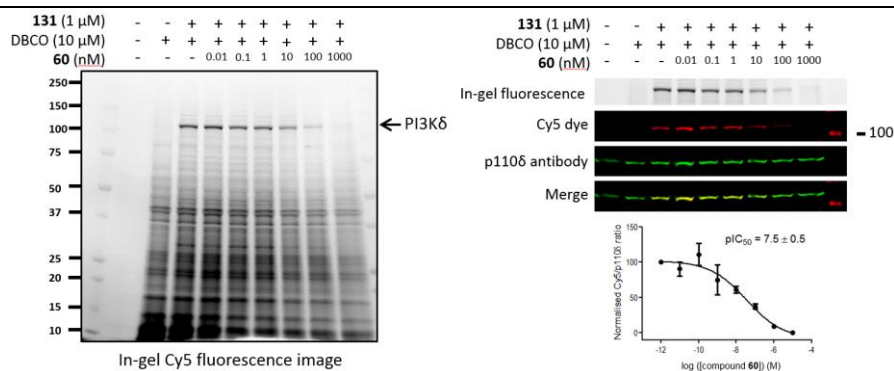


Figure 61 – Probe **131** labels a protein with molecular weight consistent with p110 δ . Immunostaining with anti-p110 δ antibody supports engagement of this protein by the probe. Labelling was competing in a dose-dependent manner by pretreatment with increasing concentrations of the parent inhibitor **60** to derive an in-lysate pIC₅₀.

4.3.3.5 Proteomic Characterisation of Probe **131** and Compound **60**

An introduction to proteomic techniques, and discussion of the design considerations of this experiment are given in Section 6.1.4 Proteomics. This section will briefly summarise the experiment, and discuss only the results of this investigation.

To accurately assess covalent and non-covalent targets of **60**, an experiment was designed using Tandem Mass Tag (TMT) labelling to investigate, firstly, what proteins were specifically enriched by probe **131** over DMSO, and subsequently the dose-dependent binding of the parent inhibitor **60** at each of the probe-enriched proteins by competition. Use of an irreversibly binding probe significantly reduces sample complexity by facilitating the use of harsher enrichment conditions to remove background proteome labelling.

In this experiment, a two-step enrichment procedure was designed to identify covalent and non-covalent targets of the probe. Firstly, treatment of the enriched protein beads with detergent (sodium dodecyl sulfate, SDS) causes denaturation, and therefore elution of non-covalently bound proteins and proteins in complexes with covalently and non-covalently bound targets. The second step utilises on-bead proteolysis to access covalently bound targets of the probe. Due to the structural similarities of probe **131** and inhibitor **60**, it is assumed that targets competed in a specific fraction by treatment with **60** are bound in the same manner as the probe (*i.e.* covalent or non-covalent). Using TMT labelling, these experiments were multiplexed to facilitate determination of probe-enriched targets, and dose-dependent competition of probe binding to these targets by **60** in a single MS experiment. A schematic representation of this experiment is given below in **Figure 62**.

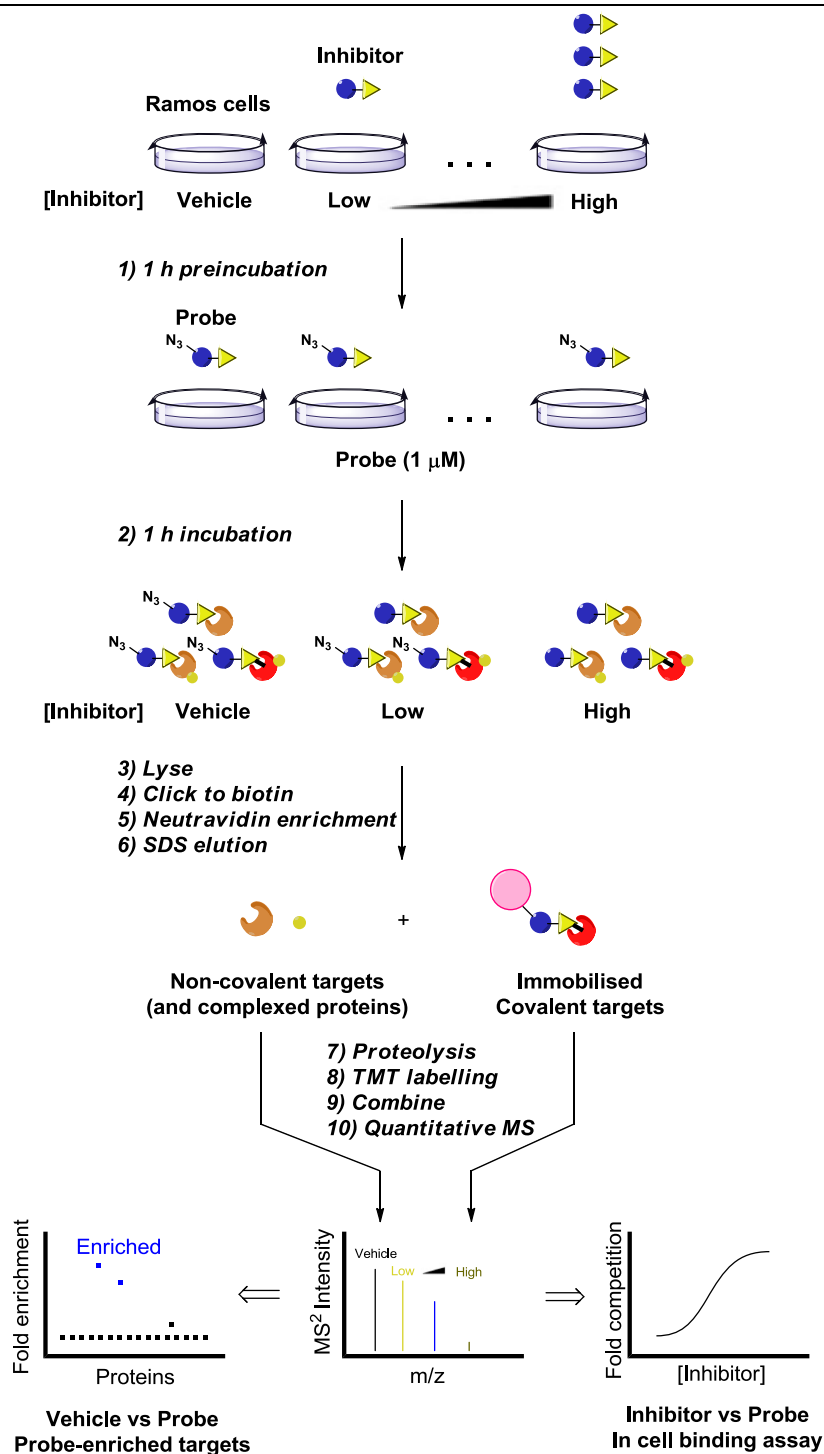


Figure 62 – Schematic representation of the proteomic experiment carried out to identify covalent and non-covalent targets of inhibitor **60**. Cells are initially treated with DMSO or inhibitor **60** in a dose-dependent manner for 1 h, and then a fixed concentration of azido probe **131** for a further 1 h. The cells are then lysed, and a SPAAC click reaction carried out to add a biotin handle for affinity enrichment with neutravidin beads. SDS denaturation of enriched proteins and washing steps separates non-covalently bound proteins, and proteins in complexes with covalent and non-covalent targets from the covalently bound targets that remain immobilised on the bead. Separate proteolysis of these two fractions, TMT labelling, combination, and quantitative MS then identifies covalent and non-covalent targets of **60** by comparison of MS² intensities for the TMT reporter ions.

For this assay to be as physiologically relevant as possible, live Ramos cells were treated *in situ* with the two compounds. This cell line is derived from Burkitt Lymphoma B-cell lymphocytes,²⁵⁷ so is also biologically relevant for the study of these compounds. The first stage of this experiment identified proteins that were specifically enriched in a probe-dependent manner. Comparison to vehicle-treated cells identified 22 out of ~1000 identified proteins that were specifically enriched >2-fold by *in situ* treatment with **131** (Figure 63).

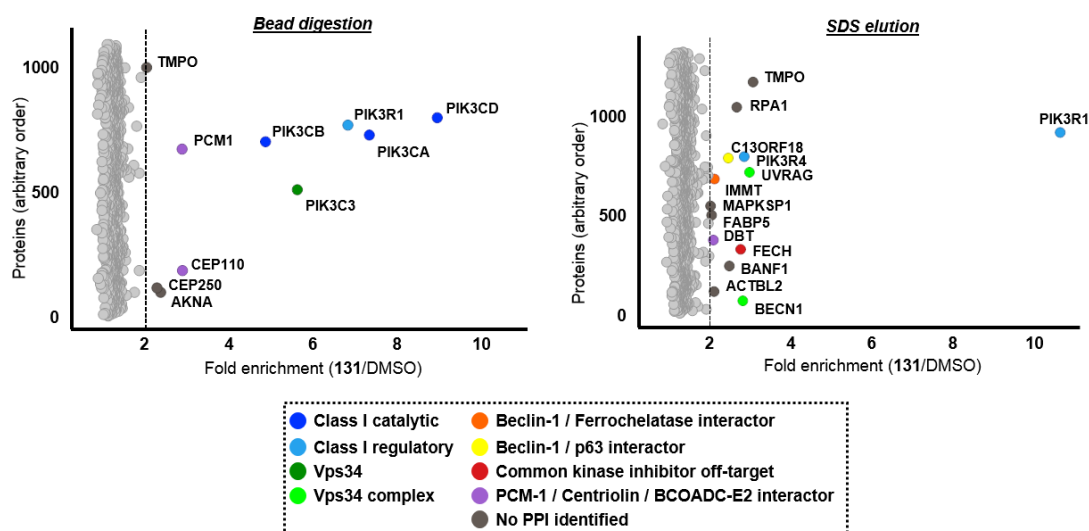


Figure 63 – Identification of proteins that are specifically enriched by *in situ* treatment with probe **131** (1 μ M, 1 h), and subsequent SPAAC conjugation to biotin and neutravidin enrichment, relative to DMSO control. Proteins were accessed by enzymatic bead digestion or SDS elution from the bead. The dotted lines represent 2-fold enrichment (**131**/DMSO) and proteins with >2-fold enrichment are deemed specific targets of **131**, and are labelled by their entrez gene ID. Data were filtered with the criteria that quantified unique peptide matches > 1 and quantified unique peptide to spectra matches >2. Proteins were required to be identified and quantified in both replicates to be included in the analysis, and data are plotted as the mean of the TMT label ratios (MS^2) for the three most abundant peptides (MS^1) per protein.

Of those 22 proteins, eight were exclusively identified after direct proteolysis, including the class I catalytic subunits of PI3K δ (gene ID PIK3CD), PI3K α (gene ID PIK3CA), PI3K β (gene ID PIK3CB), and the class III PI3K protein Vps34 (gene ID PIK3C3), suggesting these proteins as covalent targets of **131**. In contrast, the Vps34 regulatory subunits,²⁵⁸ PI3K regulatory subunit 4 (gene ID PIK3R4), Beclin-1 (gene ID BECN1), p63 (gene ID UVRAG), mitofilin (gene ID IMMT), and protein RUBCNL-like (gene ID C13ORF18) as well as the common kinase inhibitor off-target ferrochelatase²⁵⁹ (gene ID FECH), were only found in the SDS eluates. This result, that those proteins can be eluted from the capturing matrix with SDS buffer, implicates those proteins as reversible binders of **131**, or proteins in complexes with enriched targets. The PI3K regulatory subunit α (gene ID PIK3R1) was identified in the bead digest fraction as well as in the SDS eluates. Signal abundances of detected tryptic peptides (MS^1 intensities)

indicated a 3 to 4-fold higher abundance in the SDS fraction than in the bead digests. This suggests major, but incomplete, elution of this known interactor of class I catalytic PI3K subunits¹⁴¹ with the applied conditions.

The second stage of this experiment was to assess the binding of compound **60** to these specifically enriched targets, in a dose-dependent manner. Prior studies using this ABPP technique have used Stable Isotope Labelling in Culture (SILAC) methodology to derive heavy/light competition ratios at specifically enriched targets, with a fixed concentration of competing ligand.^{60,130} Whilst this does well to identify off-targets at high competing concentrations (often 10x excess of competitor), it does not take into account the dose-response behaviour of small molecule inhibitors due to the limit of two experimental conditions per MS run. For example, in the jump dilution and kinetic investigations above, it was shown that at high concentrations of inhibitor, off-target PI3K isoforms are covalently inactivated. Yet, at lower concentrations this was not observed, implying that there is a concentration window where efficient covalent inactivation of the target is possible. To take these factors into account, competition at the probe-enriched targets was carried out with a wide dose range (10 μ M to 3.2 nM) of competing inhibitor **60**. Due to the multiplexing capability of TMT labelling (10 samples in one MS experiment vs 2 for typical SILAC experiments), this was accurately carried out in a single MS experiment, which significantly reduces experimental error and sampling time.

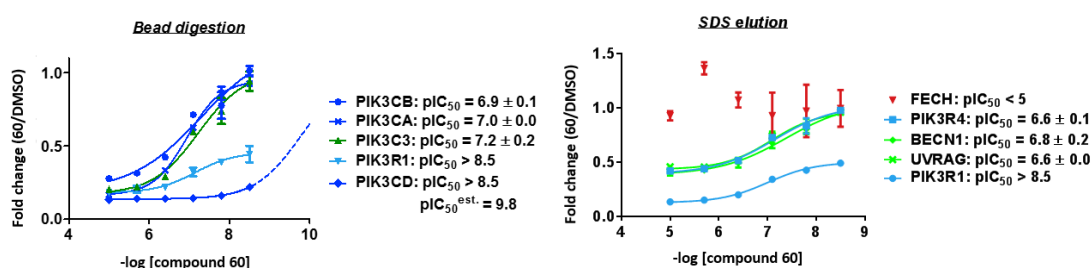


Figure 64 – Dose-response curves for competition of **131** binding to specifically enriched targets after pretreatment of cells for 1 h with **60**. Binding curves and resulting pIC_{50} values are shown for proteins enriched >2-fold. With the exception of FECH, values are not plotted if no binding curve could be fitted using GraphPad Prism 7.03. The values represented are the average \pm s.e.m. from two biological replicates. Data were filtered with the criteria that quantified unique peptide matches >1 and quantified unique peptide to spectra matches >2. Proteins were required to be identified and quantified in both replicates to be included in the analysis, and data are plotted as the mean of the TMT label ratios (MS^2) for the three most abundant peptides (MS^1) per protein.

For the specifically enriched proteins exclusively found in the bead digests, calculated pIC_{50} values for PI3K δ , PI3K α , PI3K β , and Vps34 were >8.5, 7.0, 6.9 and 7.2, respectively. This indicated that irreversible binding of PI3K δ to **131** can be competed by **60** with >20-fold

selectivity at the used incubation conditions. Furthermore, extrapolation of the PI3K δ IC₅₀ curve (dotted curve) estimated an exceptionally potent pIC₅₀ of 9.8, which would translate to *ca.* 350-fold selectivity window. It is worth reiterating that the targeted residue is conserved not only in the identified off-targets, but throughout the entire kinome of ~500 proteins. Thus, this high level of selectivity with an activated ester, in live cells at 37 °C, is a very promising validation of this approach to generate selective covalent kinase inhibitors.

For the proteins identified exclusively in the SDS fraction, reasonable binding curves were determined for Beclin-1, p63, and PI3K regulatory subunit 4. All resulted in very similar pIC₅₀ values (pIC_{50,BECLN1} = 6.8; pIC_{50,UVRAG} = 6.6; pIC_{50,PIK3R4} = 6.6). Binding curves were incomplete for those proteins (maximal competition by 10 μ M compound *ca.* 50%), suggesting they were interacting with a known complex partner,²⁵⁸ rather than being true targets of the compound. A similar effect might be observed for PI3K regulatory subunit α for which a pIC₅₀ value >8.5 was determined. As a complex partner of PI3K α , PI3K β , and PI3K δ ,¹⁴¹ the determined apparent dose-dependent competition may result from a combination of competitive binding to any of these PI3K proteins. Within the tested concentration range, mitofilin, ferrochelatase, and protein RUBCNL-like, (as well as the remaining proteins that were specifically enriched with **131**) did not show strong competition of binding by **60**, suggesting low affinity binding.

Taken together with the kinetic data described above, these data support **60** as a potent and selective, irreversible PI3K δ inhibitor. Consistent with these kinetic data, covalent binding to off-target enzymes was observed at high concentrations of inhibitor. However, the key point to observe is that there still exists a dose range where selective covalent inhibition of a highly conserved residue can be achieved. Furthermore, if this ester motif does exhibit metabolic instability, this selectivity could be driven even higher by kinetic selectivity effects.²³⁶

4.3.4 Phenotypic Consequences of Covalent PI3K δ Inhibition

Having established that compound **60** covalently, and selectively, inhibits the target enzyme at sub-nanomolar concentrations in live cells, the consequences of this *in vitro* were investigated. One of the major advantages of covalent inhibition is the ability to decouple pharmacokinetics and pharmacodynamics.¹ The consequence of this is that the duration of action of a covalent inhibitor can be maintained after the compound has been cleared from the system. For treatment of the chronic diseases that PI3K δ overactivation is implicated in, this could be highly beneficial for patients by decreasing their dosing frequency significantly.

It also has the potential to reduce toxicity due to systemic exposure, as much lower concentrations of the active drug will be present.^{1,8}

To assess the duration of action of this covalent inhibitor in a physiologically relevant setting, a cellular washout study in primary immune cells (CD4+ T cells) isolated from venous human blood was designed. The hypothesis was that covalent inhibition of PI3K δ will produce a phenotypic response that is maintained after drug removal by washing of the cells. The control hypothesis is that a reversible inhibitor will not show a sustained duration of action. Again, production of IFN γ after stimulation was used as the readout for PI3K δ activity. Cell viability was also measured after 48 h using a CellTiter-Glo assay to ensure that any observed inhibition was not a result of general cytotoxicity. The design of this experiment, and results are shown below (**Figure 65**). Reversible compound **122**, that was previously used in the intact protein MS experiments, was employed as the reversible control compound. This compound showed comparable activity to the covalent compound in the phenotypic hWB assay ($pIC_{50} = 7.9$), and was therefore deemed a suitable reversibly binding control compound.

Under the non-washed conditions, both compounds showed very potent, picomolar-level inhibition of IFN γ response (**Figure 65B**, blue points), which is believed to be indicative of PI3K δ inhibition.¹⁶³ Reversible binder **122** returned a pIC_{50} of 9.9, and covalent binder **60** returned a pIC_{50} of 10.4, roughly consistent with the estimated pIC_{50} in the chemoproteomic competition experiment ($pIC_{50}^{est} = 9.8$). Furthermore, the dose range employed for the covalent compound (up to 100 nM), was below that at which significant reduction (>2-fold) in off-target binding of probe **131** was competed by **60** in the chemoproteomic experiment. This gives confidence that the effects are due to covalent inactivation of the target, not off-target enzymes that may also contribute to IFN γ secretion. Cell viability studies also showed that, at the highest concentrations of inhibitor, there was no evidence of cytotoxicity (**Figure 65C**). Therefore, the effects on IFN γ secretion observed are not due to cell death, supporting PI3K δ engagement by these compounds.

In the washed condition, the reversibly binding compound showed a clear loss of inhibitory activity at all tested concentrations (**Figure 65B**, black points). In contrast, the covalent compound maintained its potent inhibitory effect ($pIC_{50} = 10.5$), with no evidence of cytotoxicity. These data are highly supportive of this approach for generating long-lasting inhibitors of PI3K δ , which could have applications in the clinic for the treatment of chronic

inflammatory disease. However, it should also be noted that covalent compound **60** possesses a dibasic piperazine group, whereas reversible binding compound **131** does not. Protonation of the piperazine inside the cell affords a cationic compound which is impermeable and cannot pass out of the cell. As a result of this, dibasic piperazine-containing compounds are known to accumulate in cells,^{260,261} which could also be a contributing factor to the sustained duration of action for the covalent compound. Nonetheless, given the strong evidence presented supporting covalent inactivation of PI3K δ , it is believed that this will be the main contributing effect to duration of action of this compound.

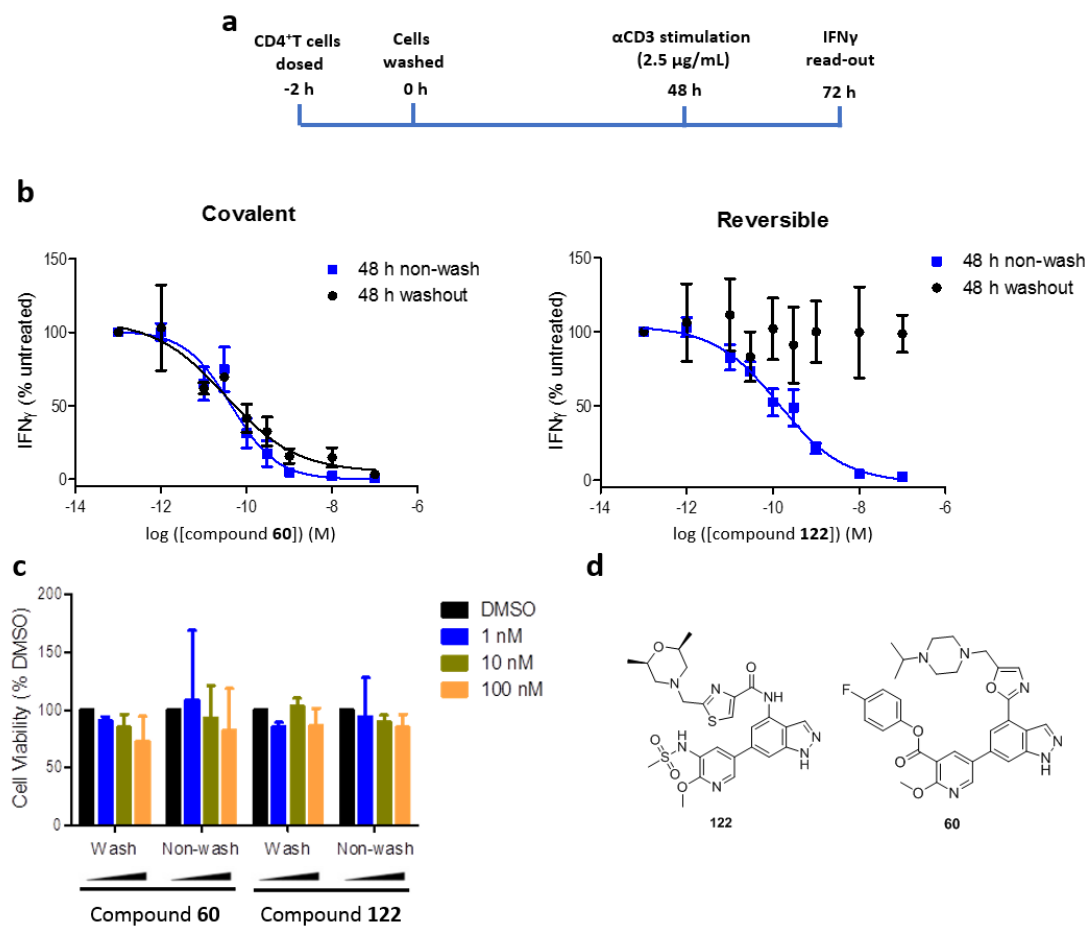


Figure 65 – (a) Design of the cellular washout experiment. Freshly isolated CD4⁺ T cells from human whole-blood were treated for 2 h with compounds **60** or **122**, in dose-response, washed, incubated for 48 h and then stimulated with α CD3 prior to readout of IFN γ levels after a further 24 h. (b) Dose-response curves for each compound tested. The experiment was repeated using 5 donors (for each donor: N = 3 replicates for washout, and N = 2 replicates for non-wash condition), and results are depicted as mean \pm s.e.m. Non-washed curves showing the dose-response after 48 h are shown in blue. (c) Cell viability measurements from CellTiter-Glo assay for both compounds under washed and non-washed conditions, relative to vehicle treated cells. Data are presented as the mean of two donors \pm S.D. For each donor, N = 3 replicates for washout and N = 2 for non-wash bars. (d) Structures of the inhibitors used in this experiment.

In conclusion to this section, a series of biochemical and biological experiments have been employed to further interrogate these covalent inhibitors. Kinetic binding assays have shown an unexpected trend in the dependence on reversibility vs inactivation rate for these compounds, and also derived a selectivity window for covalent inactivation of the target enzyme in a biochemical setting by the lead inhibitor **60**. Mass spectrometry and chemical-based HPLC have then been employed to characterise the chemical reactivity and stability of this compound, and also the specificity of the covalent binding reaction for the active site lysine residue over surface lysines and other potential nucleophilic residues on the protein. Furthermore, mass spectrometry has also been used to characterise the proteome-wide reactivity of **60**. A clickable analogue, probe **131**, was synthesised and used as an activity-based probe to facilitate these experiments. ABPP then identified 3 off-target covalent enzymes, which the parent inhibitor showed an estimated 350-fold selectivity window against for covalent inactivation. Finally, in primary immune cells, a washout experiment was conducted to validate the extended duration of action of the covalent compound, which could have implications in the design of long-lasting therapeutics for kinase-mediated pathways.

5. Conclusions and Future Directions

5.1 Conclusion

The overall aim of this project was to develop a selective, irreversible inhibitor of PI3K δ that targets the catalytic lysine in the ATP binding pocket. This thesis reports the development of compound **60** as a compound that achieves this goal. In Section 1.3 – Aims, the ideal profile for this inhibitor was stated as fit for purpose as a chemical probe.¹⁶² Specific criteria included nanomolar potency in biochemical assays, selectivity >100-fold over off-target enzymes under biochemical conditions, <1 μ M potency in a cell-based assay, and evidence of covalent selectivity in a cell-based system. Through efficient use of structure-based design, chemical synthesis, biochemical and cellular assays, kinetic investigations, and chemoproteomics, this lead compound has satisfied these criteria.

Initially this project used internal knowledge to identify two potential series that could be modified for the development of covalent inhibitors. These were the indazole and DHP series, possessing either an indazole or dihydropyran group as the hinge binding motif. Both of these series possessed a basic amine side-chain that occupied a selectivity region next to Trp760,¹⁷⁵ which served to boost potency and selectivity for the target. By truncating these compounds back to their simple hinge binder and back-pocket groups, installation of covalent warhead showed that both were amenable to covalent inhibitor development by interrogation of the crystal structure with PI3K δ . The indazole hinge binder showed better potency for the reversibly binding control compound, and so was progressed further to increase potency and selectivity.

By incorporation of a basic amine side-chain into the inhibitor, potency and selectivity at the target were significantly increased. Furthermore, this increase in reversible binding (shown by comparison of the carboxylic acids between the truncated and fully elaborated series) facilitated the incorporation of less chemically reactive esters to increase selectivity. From here, the alternative indole back-pocket binding group was explored, along with alternative sulfur-based electrophiles. Unfortunately, neither of these series produced inhibitors with better profiles than the methoxypyridine series, in particular compound **60**. Variation of the chemical reactivity of the electrophilic centre in this series was then explored, however any improvements in potency over **60** were met with either poorer selectivity, poor stability, or

poor solubility, highlighting this compound as the lead to progress to further biological studies.

A thorough kinetic analysis of the binding of the methoxypyridine esters was then carried out at PI3K δ , with the aim to separate the contributions to potency from reversible binding and reactivity. Perplexingly, the k_{inact} for this series of inhibitors was found to be almost constant across the series, yet K_i varied dramatically with the expected chemical reactivity of the ester. To attempt to rationalise this, the corresponding amides were synthesised and confirmed to be reversible binders by crystallography and binding kinetics. Furthermore, their pIC₅₀ values derived from the biochemical assay were found to be relatively constant with electron deficiency of the phenyl ring, suggesting the variation in potency of the esters had not arisen from a simple preference for electron-deficient groups in this region of the kinase during the initial collisional event. To rationalise this, a multi-step mechanism was proposed that placed reactivity of the ester as a contributor to K_i , and not k_{inact} .

From here, further analysis of the chemical reactivity and binding of **60** showed that it is hydrolytically stable, and unreactive with lysine residues until they become pK_a perturbed. Furthermore, it appears to be selective for a single modification on PI3K δ by intact protein MS, over surface lysine residues and other potentially nucleophilic residues in the protein. The selectivity of this inhibitor was then assessed using a biochemical kinetic assay against closely related off-targets PI3K α and β , which revealed a concentration window where efficient covalent inactivation of the target was observed over the off-target enzymes. The compound is capable of covalently modifying off-target kinases, however only at high concentrations in this experiment. To further support this conclusion, a clickable analogue of the parent inhibitor was synthesised and shown to modify PI3K family proteins in lysates and live cells by gel-based and MS-based readouts. Binding of this compound to its targets was depleted in dose-response by the parent inhibitor **60**. Indeed, this competition was found to be exquisitely potent for the target, and highly selective with an estimated window of 350-fold. This result is remarkable given the presence of other reactive moieties in cellular systems that may be expected to react with an activated ester.

The final experiment used to characterise this inhibitor was a cellular washout. This was conceived to investigate the potential increase in duration of action attainable for covalent inhibitors. Indeed, covalent compound **60** was found to exhibit an extended duration of action relative to a reversible inhibitor with a similar potency in biochemical and hWB assays.

The pIC₅₀ measured for this compound was, again, exquisitely potent returning a picomolar pIC₅₀ (~10.5) at 48 h after compound removal.

Together, these data are highly supportive of a covalent method of engagement of PI3K δ , and that this interaction can be highly selective in a native biological system despite high conservation of the targeted residue. Given the importance of PI3K δ in the treatment of inflammatory disease, this compound could have applications in the development of clinical compounds to treat these conditions. Indeed, the potency and selectivity of this lead compound in biochemical and hWB assays are comparable to the clinically approved PI3K δ inhibitor Zydelig, and superior to Wortmannin (**Table 19**). Selectivity in this case was obtained from the inherent selectivity in the reversible scaffold onto which the electrophile was incorporated.

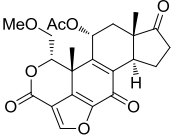
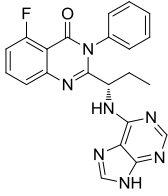
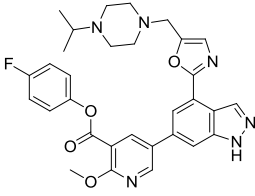
			
PI3Kδ pIC₅₀	8.3	8.1	8.1
PI3Kα pIC₅₀	8.1	5.0	5.5
PI3Kβ pIC₅₀	8.0	5.8	5.3
PI3Kγ pIC₅₀	8.2	6.6	4.8
hWB pIC₅₀	6.7	6.7	7.9

Table 19 - Summary of biochemical and hWB data for covalent PI3K inhibitor Wortmannin **27**, clinically approved PI3K δ drug Zydelig **21**, and the lead covalent inhibitor from this investigation **60**.

With this knowledge in-hand, and the high conservation of the targeted lysine, it is envisaged that this general approach could be used as a method to generate selective covalent inhibitors of kinases. In particular, kinases not possessing an activated cysteine residue that is amenable to covalent inactivation. Using this as an orthogonal method to cysteine targeting, researchers may be able to generate selective, irreversible inhibitors of any chosen kinase. This could have significant impact on the development of chemical probes and approved drugs for understanding and treating kinase-mediated diseases.

5.2 Future Work

Five key pieces of future work are evident for this project, which have applications in chemical biology and drug development using this approach. These are summarised below:

- **Biological Validation:** The work presented in this thesis has been primarily biochemical and *in vitro* in nature. Some *in situ* experiments have been carried out for phenotypic screens (hWB, cellular washout), and chemoproteomics; however the applicability of this approach to an *in vivo* system has not been demonstrated. Key questions around toxicity, and whether this compound will also demonstrate a functional, prolonged response in animal models remain unanswered.
- **Applicability:** The most outstanding piece of future work is to show that this approach truly is a general approach, and applicable to any chosen kinase. Work is already underway within our laboratories to investigate the applicability of this approach to the development of a covalent inhibitor for an alternative lipid kinase. However, to be truly applicable, this approach should be validated with kinases outside of the lipid kinome, and potentially other proteins possessing active site lysine residues.
- **Mechanism:** The observation that covalent inactivation of the kinase is seemingly independent of chemical reactivity, yet the reversible binding affinity of these compounds is strongly influenced by electronics of the leaving group is another key area for investigation. Ultra-fast methods to investigate the rates of the initial collision with the enzyme are currently under investigation to attempt to delineate the proposed mechanistic steps in **Scheme 9**. For example, the use of intrinsic tryptophan fluorescence in stopped flow, quenched-flow studies, or ligand-FRET assays to measure changes on the millisecond scale.
- **Reactivity and optimisation for drug discovery:** Whilst the aromatic esters presented here have proven highly successful as a proof of concept, and to produce chemical biology tools, they may not be applicable in a drug discovery setting. For example, the increased lipophilicity of these molecules is likely to significantly affect the physicochemical properties, and therefore potential *in vivo* readouts for these compounds. Furthermore, the phenolic leaving group may have toxic effects, however at the low concentrations likely to be employed this may be tolerable (aspirin, for example, releases a phenol²). Potentially, variation of this electrophilic centre to a different moiety may provide more beneficial physicochemical properties, that may be

more amenable to drug development. Indeed, the ideal system would be one that does not possess a leaving group, such as an α,β -unsaturated system, epoxide, or alternative cyclic electrophile. Furthermore, reversible covalent inhibitors pose another field of electrophiles, and benefits that may be preferred for drug discovery.⁵ The slow off-rates attainable with reversible covalent inhibitors will prevent complete knock-down of the protein (which may not be beneficial), and also will minimise off-target covalent toxicity, as this reaction can now reverse.⁵ A series of alternative electrophiles exist for this purpose, with one in particular standing out from the recent literature. Scientists from AstraZeneca recently demonstrated reversible covalent binders of the anti-apoptotic protein Myeloid cell leukaemia 1 (Mcl-1) by formation of a stabilised iminoboronate **147** with a lysine residue.¹⁰⁷ Incorporation of this motif into the inhibitor scaffolds used in this thesis may furnish a highly efficient reversible covalent inhibitor **148** (Figure 66). However, this structure may suffer from the known instability of ortho-pyridylboronates.²⁵³

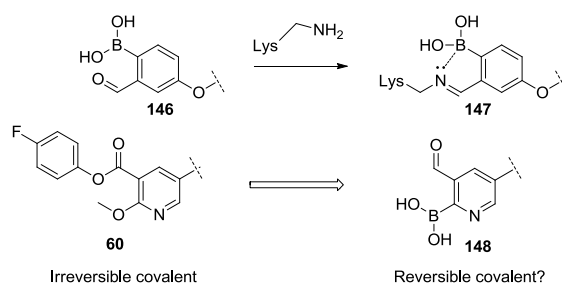


Figure 66 – Proposal for incorporation of a lysine-selective reversible covalent warhead to tune residence time

- **Generation of Activity-Based Probes:** Now in the knowledge that the conserved lysine of PI3K isoforms, and related family members can be engaged by this reactive warhead, the possibility of covalently engaging significantly more kinases (both lipid and protein) by a similar mechanism is proposed. Activity-based probes based on ATP (compound **10**) and ADP (compound **11**), and the Kinobead platform, give excellent coverage of the kinome, however are only applicable to use in cell lysates.^{37,39,262} The recent cell-permeable unselective lysine-reactive kinase probe (probe **19** in **Figure 40**)⁹⁸ modified 133 endogenous kinases. This probe was used to identify off-targets of a known reversible kinase inhibitor, including new targets not found with Kinobeads or ATP/ADP-based probes. However, the lipid kinome was poorly represented in the 133 kinases identified in this report. Wortmannin-based activity probes have been disclosed in the literature for monitoring a subset of lipid kinases, however the synthetic steps to make

these molecules have prevented their use, and they also exhibited poor cell permeability.^{263,264} As the sulfonyl fluoride group was not stable on the methoxypyridine scaffold used here, this alternative activated ester moiety may provide access to a cell permeable pan-lipid kinome covalent probe, which could be used to interrogate the selectivity of lipid kinase inhibitors. Furthermore, through SAR analyses, this activated ester motif could be designed to inhibit a greater proportion of the human kinome.

6. Experimental

6.1 Summary of Biological Assays Used

A series of biological assays are used to assess the inhibitors synthesised in this project. These include the routine biochemical enzyme assay to determine a pIC_{50} at the four PI3K isoforms, a reactivity assay with a lysine mimic, intact protein MS, a kinetic assay to establish that the compounds bind to PI3K δ and monitor the time-dependent inhibition of the compounds to derive K_i and k_{inact} ,^{1,62} a jump-dilution assay to confirm the irreversible nature of slow-binding inhibitors in the kinetic assay, cellular wash-out studies to confirm irreversibility in a cellular context, and chemoproteomic investigation of off-targets. This section provides brief introductions to, and details of, the concepts behind the more biochemically and biologically-oriented assays described in this thesis.

6.1.1 Biochemical TR-FRET Assay

Förster Resonance Energy Transfer (FRET) depicts the transfer of energy from an excited donor molecule, to an acceptor molecule in close proximity.²⁶⁹ This donation causes an increase in fluorescence of the acceptor partner, which can be measured and quantified relative to a reference.²⁷⁰ The FRET interaction is strongly dependent on distance between the FRET partners ($1/r^6$),²⁷¹ and is therefore used routinely to study biological systems.^{272–274}

Figure 67 depicts the Time-resolved FRET system (TR-FRET) used to study the PI3-kinases.²⁷⁵

The intact FRET complex (**Figure 67**, bottom right) consists of a europium labelled anti-glutathione S-transferase (GST) antibody, bound to a GST antibody on a pleckstrin homology (PH) domain. This PH domain very specifically binds to PtdIns(3,4,5)P₃, the product of PI3K reaction with ATP, PtdIns(4,5)P₂, and Mg²⁺. For a FRET signal to be observed, a biotinylated PtdIns(3,4,5)P₃ compound must bind into the PH domain. The very high affinity of a streptavidin-allophycocyanin conjugate (Strep-APC) for biotin ensures tight binding of the biotinylated PtdIns(3,4,5)P₃ to Strep-APC which, when bound into the PH domain, causes FRET transfer between the Eu and the APC chromophores. When Eu is excited at 330 nm, FRET transfer to APC causes emission at 665 nm. It is the change in this signal at 665 nm that is monitored in the FRET assay.²⁷⁵

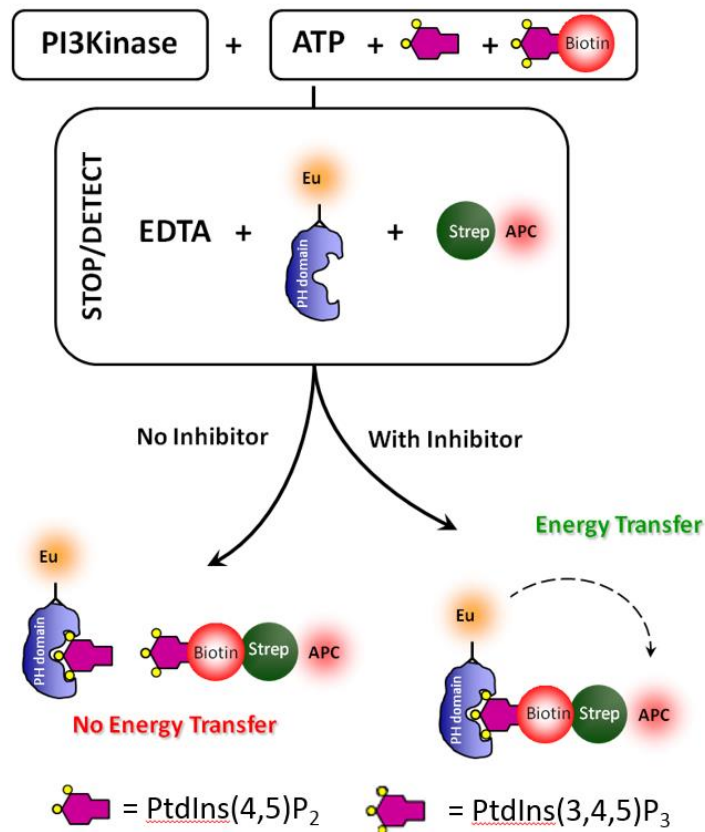


Figure 67 – FRET system used to study the biochemical activity of PI3K enzymes.²⁷⁵

When a PI3K enzyme produces PtdIns(3,4,5)P₃, this competes with the biotinylated-PtdIns(3,4,5)P₃ binding into the PH domain, disrupting the FRET complex, therefore reducing the observed fluorescence signal from APC. Inhibitors are preincubated with the enzyme for 15 minutes, and then with substrate solution (PtdIns(4,5)P₂, ATP, biotinylated-PtdIns(3,4,5)P₃ and Mg²⁺) for 1 h prior to the addition of a stop/detect solution. The stop/detect solution contains ethylenediaminetetraacetic acid (EDTA) to sequester Mg²⁺ (thus halting the phosphate transfer reaction catalysed by PI3K), the Eu-GST tagged PH domain, and the Strep-APC conjugate. After equilibration of the PtdIns(3,4,5)P₃ and biotinylated PtdIns(3,4,5)P₃ in the mixture with the FRET components, the assay is subjected to 330 nm light, and the emission at 665 nm read. Comparison of this signal to two blank reactions (one with fully inhibited PI3K using Wortmannin, and one without inhibitor) allows determination of percentage inhibition, and therefore a pIC₅₀. Full inhibition produces no PtdIns(3,4,5)P₃, therefore no competition with the biotinylated PtdIns(3,4,5)P₃ for binding to the PH domain, and a full fluorescence signal at 665 nm, whilst no inhibition causes an absence of emission due to competition with natural PtdIns(3,4,5)P₃ for the PH domain.²⁷⁵

6.1.2 Human Whole-blood Assay

To probe the phenotypic response of PI3K δ inhibition in a cellular environment, T-cell stimulating antibody, CytoStim, was used to stimulate cytokine production.¹⁶³ Production of IFN γ in these samples was measured by immunoassay techniques. IFN γ is a 20 kDa cytokine that can be reliably stimulated by CytoStim, and is highly sensitive to PI3K δ inhibition.^{163,265} The V-PLEX Human IFN γ kit from Mesoscale Discovery (MSD) is highly sensitive with a detection limit for IFN γ of 0.9 pg mL⁻¹, and was therefore used to measure the levels of IFN γ produced at different concentrations of inhibitor.²⁶⁶

This assay is based on well-established enzyme-linked immunosorbent assay techniques, and relies on the binding affinity of anti-IFN γ antibodies that are tagged with an electrochemiluminescent SULFO-TAGTM developed by MSD, to IFN γ . Firstly, the compounds are incubated with human whole-blood (hWB) at the desired concentrations for 1 h. At this point, CytoStim is added to stimulate production of cytokines, and the compounds incubated for a further 20 h. An aliquot of this mixture is then dispensed onto MSD assay plates containing a capture antibody, specific for IFN γ , attached to the bottom of a conductive well. The wells are then washed to remove any unbound cytokines, and the MSD detection solution containing MSD SULFO-TAGTM antibodies is added. The sample is washed again to remove unbound SULFO-TAGTM and, after equilibration of this mixture, a detection buffer is added. A voltage is then applied to the plate, which causes the captured SULFO-TAGTM antibodies to emit light from electron transfer between ruthenium complexes. The intensity of this light is then measured by an automated plate reader to give a quantitative measure of the concentration of IFN γ in the sample.²⁶⁷ Plotted relative to calibration curve of known cytokine concentrations, this allows determination of an IC₅₀ curve.²⁶⁸ **Figure 68** depicts the general assay steps described above. This general method was also used in the analysis step of the cellular washout experiment.

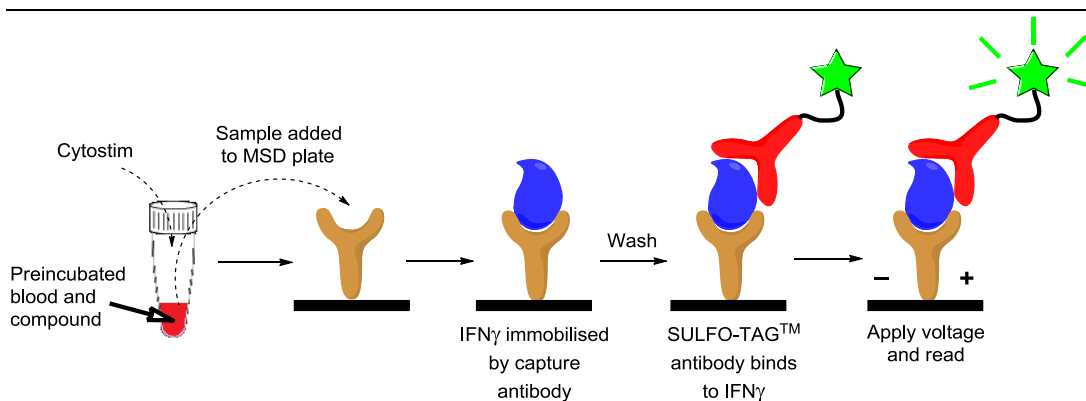


Figure 68 – Cartoon depiction of the enzyme-linked immunosorbent assay (ELISA) hWB assay to determine IFN γ release following PI3K δ activation. A preincubated sample of blood and compound is stimulated to release IFN γ with CytoStim, and added to a custom plate with immobilised capture antibody (available from MSD). Addition of MSD SULFO-TAG™ to bind to the immobilised IFN γ , and application of a voltage causes electrochemiluminescence from the ruthenium complexes in the SULFO-TAG™, which is indicative of the concentration of IFN γ in the well. Comparison to calibration curves of known IFN γ concentration allows determination of percentage inhibition, therefore producing an IC₅₀ curve.

6.1.3 Kinetic Assay

To accurately assess the contributions of reversible binding and reactivity to the observed pIC₅₀ of these inhibitors (**Figure 4**), a kinetic time-course assay was employed. The assay used here was the commercially available ADP Quest™ kit from DiscoverX.²³³ The principle behind this assay is to monitor the production of ADP from the kinase reaction, by converting it through a series of coupled-enzyme reactions to a fluorescent molecule, resorufin. The scheme of reactions used to achieve this is shown below in **Figure 69**.²³³

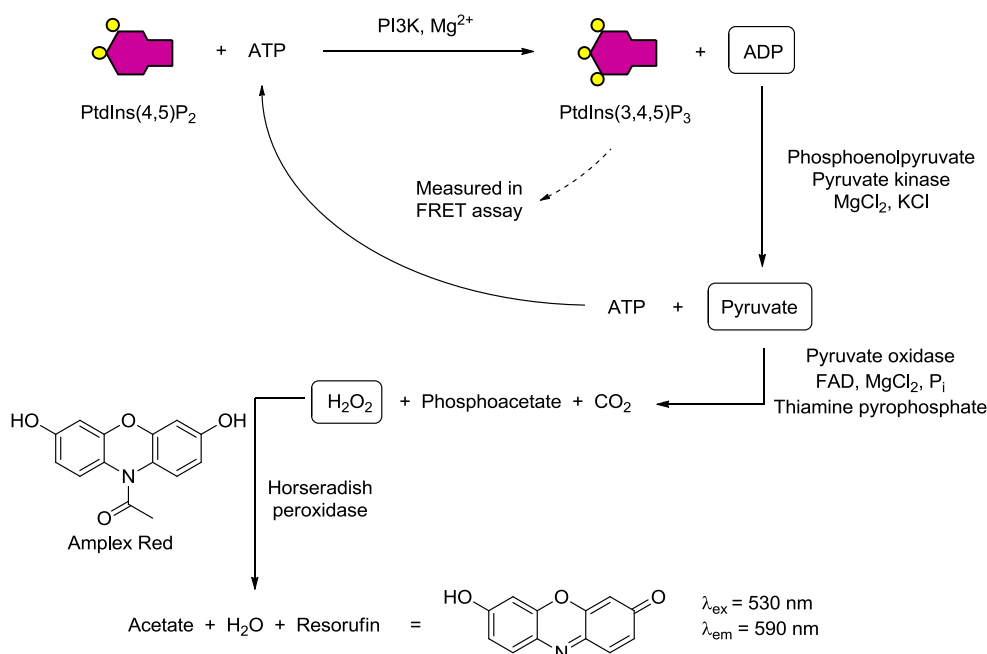


Figure 69 – Coupled enzyme reactions used to convert ADP into the fluorescent signal from resorufin.²³³

First, a molecule of ADP produced from the PI3K reaction is converted back to ATP and pyruvate, using pyruvate kinase and its cofactor, phosphoenolpyruvate. This maintains a constant level of ATP within the reaction, ensuring that a depletion in signal does not occur from a lack of ATP. Pyruvate is then converted into phosphoacetate, CO₂, and hydrogen peroxide using pyruvate oxidase. Finally, horseradish peroxidase utilises the hydrogen peroxide produced to oxidise amplex red to resorufin. Resorufin fluoresces at 590 nm, when excited at 530 nm, and can be easily monitored at regular intervals by an automated plate-reader. The fluorescence signal from resorufin therefore increases with time as more ADP is produced, and provides a direct measure of the current activity of the kinase. Inhibition of PI3K affects the relative fluorescence of resorufin, when compared to a control without inhibitor.²³³ The data are then fitted as described in Section 6.2.5 Kinetic Binding Assay at PI3K δ . This assay procedure was also used to measure the activity of the kinase following jump-dilution experiments.

6.1.4 Proteomics

Proteomics refers to an MS-based method used to characterise a cell's complete protein make up (the proteome) collectively.⁷⁹ The common workflow to achieve this is to obtain a proteome (with or without an experimental treatment), enrich the proteome to allow analysis of specific proteins (often with an ABPP-based molecule), digest the proteins into smaller peptides by a process known as proteolysis using specific hydrolase enzymes such as trypsin, subject these peptides to a sequence of chromatography and MS steps to identify the peptides (and therefore parent proteins) by matching their characteristic fragmentation patterns (MS² spectra) to databases (**Figure 70**).²³⁷ Typically, this is achieved using Multidimensional Protein Identification Technology (MudPIT) methods.²⁷⁶ Here, two orthogonal methods of chromatography are used to maximise separation of peptides (termed LC/LC) using strong cation-exchange chromatography (SCX) and reverse phase chromatography on C18 silica gel. This chromatography step feeds directly into a mass-spectrometer for two successive MS steps (termed MS¹ to identify the mass of the parent peptide, and MS² to generate a specific fragmentation pattern for that peptide which is matched to a database for identification).^{237,276}

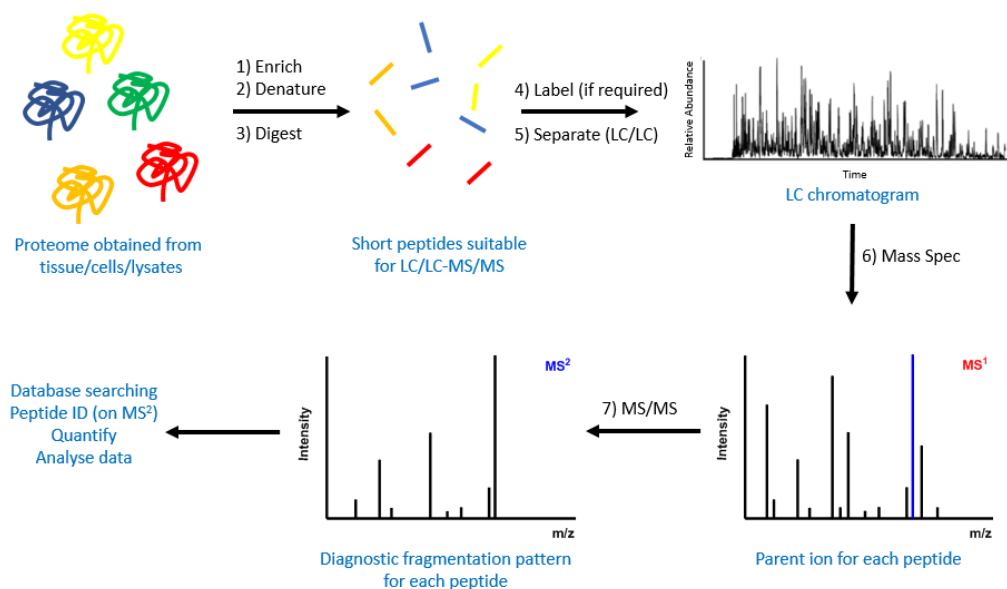


Figure 70 – Basic workflow steps of a proteomics experiment.

Identification of the proteins in a complex mixture is highly information rich, however the real power of proteomics comes from the ability to quantify the relative levels of peptides between two experimentally different proteomes (*i.e.* with and without pretreatment with an inhibitor).⁵² Label-free methods to do this exist, but they are laborious and error-prone due to the need to process all samples separately through the work flow, including the data analysis.²⁷⁷ To overcome this limitation, and provide accurate relative quantification in a significantly reduced analysis time, multiplexed methods such as TMT labelling with isobaric tags have been developed.^{278–281}

For this type of experiment, the treatment/enrichment/proteolysis steps are carried out separately, and each sample is labelled with an amine-reactive isobaric tag. Hydrolase enzymes such as Trypsin and LysC are used to specifically cleave at the carboxyl end of lysine and arginine residues.^{282,283} This exposes at least one reactive amine on each product peptide which can react with the TMT reagent. Due to the isobaric nature of the mass tags, peptides elute with the same MS¹ readout and fragmentation patterns for identification. Each TMT reagent is isotopically enriched in a specific pattern which, upon fragmentation, affords a unique low molecular weight group that is used for quantitation.²⁸⁴ Quantitation is therefore carried on the MS² level, by comparing the intensities of each TMT reporter ion.²⁷⁸ Originally, TMT quantitation was limited to six unique samples that were separated by 1 Da in the MS² spectrum (TMT126, TMT127, TMT128, TMT129, TMT130 and TMT131).²⁸¹ However, the discovery that the mass difference arising from simultaneously exchanging ¹³C to ¹²C, and ¹⁴N

to ^{15}N afforded tags that are 6 mDa lighter (e.g. TMT127L vs TMT127H, **Figure 71**) facilitated multiplexing of up to 10 unique samples.^{279,280} In this multiplexed format, MS time is significantly reduced, and proteomic methodologies can now be used to investigate dose-dependent relationships.^{280,285}

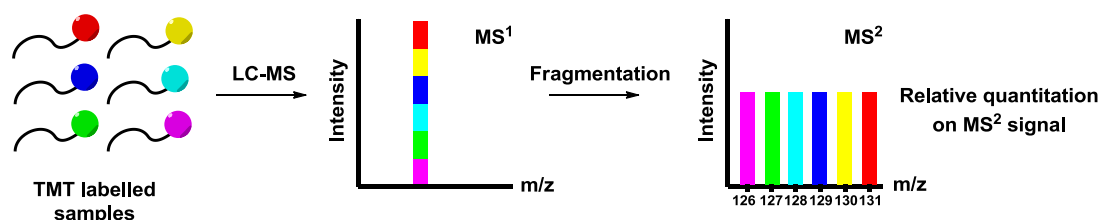
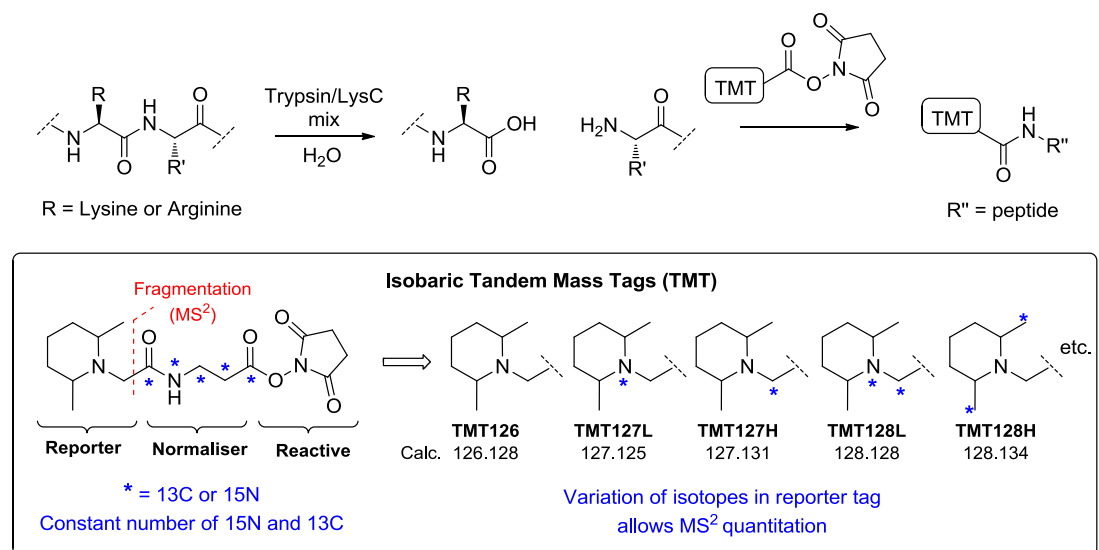


Figure 71 – TMT labelling principles. Digested peptides are labeled with amine-reactive TMT tags. Each tag possesses the same number of isotopically enriched ^{13}C or ^{15}N atoms, which are distributed amongst the reporter region to generate isotopically encoded fragments, which are quantified in the tandem MS/MS spectrum.^{279,280}

TMT 8-plex technology has been used in this thesis to identify specifically enriched targets of probe **131**, and dose-response curves for competition of this binding by compound **60** in live cells. One channel of the TMT mixture represented a DMSO treated condition, another the probe-only treated condition to identify specifically enriched targets, and the remaining six channels formed the dose-response curve for pretreatment with compound **60** prior to a fixed concentration of probe **131**. The workflow and results are summarised in Section 4.3.3.5 Proteomic Characterisation of Probe **131** and Compound **60**, and further technical experimental details are given in Section 6.2.11 Proteomic In-cell Selectivity Analysis of Compound **60**.

6.2 Biology and Computational

6.2.1 Isolated Enzyme Assay

The PI3K enzyme assays were carried out as part of a routine assay for the in-house PI3K δ program by Mr James Rowedder (GSK).

Inhibition of PI3K enzymatic activity was determined using an TR-FRET assay kit based on the method described by Gray *et al.*²⁷⁵ Briefly, reactions were performed in assay buffer containing 50 mM HEPES, pH 7.0, 150 mM NaCl, 10 mM MgCl₂, 2.3 mM sodium cholate, 10 μ M CHAPS, and 1 mM DTT. Enzymes were preincubated with compound, serially diluted 4-fold in 100% DMSO, for 15 min prior to reaction initiation upon addition of substrate solution containing ATP at K_M for the specific isoform tested (α at 250 μ M, β at 400 μ M, δ at 80 μ M, and γ at 15 μ M), PtdIns(4,5)P₂ at either 5 μ M (PI3K δ) or 8 μ M (PI3K α , β , and γ) and 10 nM biotin-PtdIns(3,4,5)P₃. Assays were quenched after 60 min by addition of a quench/detection solution prepared in 50 mM HEPES, pH 7.0, 150 mM NaCl, 2.3 mM sodium cholate, 10 μ M CHAPS, 30 mM EDTA, 40 mM potassium fluoride, and 1 mM DTT containing 16.5 nM GRP-1 PH domain, 8.3 nM streptavidin-APC, and 2 nM europium-anti-GST and were left for a further 60 min in the dark to equilibrate prior to reading using a Perkin Elmer EnVision plate reader. Ratio data were normalized to high (DMSO) and low (no enzyme or enzyme in the presence of 8.3 μ M Wortmannin) controls prior to fitting using a logistical four-parameter equation (Equation 1) to determine IC₅₀, where y is the response; Bottom is the lowest plateau of the curve; Top is the highest plateau of the curve; x is the molar concentration of inhibitor; and S is the Hill Slope.

$$y = \text{Bottom} + \frac{\text{Top} - \text{Bottom}}{1 + \left(\frac{x}{\text{IC}_{50}}\right)^S} \quad (1)$$

Taking the negative natural log ($-\log_{10}$) of this figure affords the pIC₅₀. IC₅₀ can be converted to K_i , and therefore p K_i , using the Cheng-Prusoff Equation (Equation 2).¹⁹³ IC₅₀ is in molar units, S is the concentration of substrate used, and K_M is the substrate concentration at which 50% of the maximal enzyme turnover rate is achieved.

$$K_i = \frac{\text{IC}_{50}}{1 + \left(\frac{[S]}{K_M}\right)} \quad (2)$$

Therefore, for assays carried out at $K_M(\text{ATP})$, the K_i is approximately 2-fold more potent than the measured value, which corresponds to roughly 0.3 log unit increase in pIC_{50} .

6.2.2 Human Whole-blood Assay

The PI3K enzyme assays were carried out as part of a routine assay for the in-house PI3K δ program by Mrs Collette Chitty (GSK).

V-PLEX Human IFN γ kit was purchased from Mesoscale Discovery (MSD, K151QOD-4). 100 μL of heparinised human blood sourced from healthy volunteers (1% v/v heparin sodium 1000 U $\cdot\text{mL}^{-1}$ endotoxin free, Fannin UK) was transferred into wells containing 0.5 μL of compound at the desired concentration in DMSO and incubated at 37 $^\circ\text{C}$, 5% CO_2 for 1 h. 25 μL of stimuli solution (CytoStim stock solution diluted 1:300 in low endotoxin RPMI 1640 medium supplemented with 1% GlutaMAX and 1% penicillin/streptomycin) was added to each well and briefly shaken. The plates were sealed and incubated at 37 $^\circ\text{C}$, 5% CO_2 for 20 h. 70 μL of MSD Diluent 2 was then added to each well and shaken for 15 minutes at room temperature. The plates were then centrifuged at 1300 rpm for 10 min. The MSD IFN γ plates were prepared and analysed according to the manufacturer's instructions, using 50 μL of supernatant from the centrifuged plate. Data were normalised to high (DMSO) and low (10 μM ZSTK474 inhibitor) controls prior to fitting using a logistical four-parameter equation to derive the IC_{50} . The human biological samples were sourced ethically and their research use was in accord with the terms of the informed consents.

6.2.3 HPLC Reactivity Assays

Method for Sections 2 to 3 (initial method)

To separate LCMS vials were added the inhibitors (8.3 μmol) and DMSO (500 μL). To each of these vials was added N_α -(tert-butoxycarbonyl)-L-lysine (N -Boc-Lys) (21 mg, 83 μmol) in water (400 μL) and N,N -diisopropylethylamine (DIPEA) (29 μL , 170 μmol). Reaction initiation was deemed at the point of DIPEA addition. Reactions were analysed by LCMS at 30 min, 1 h, and then every hour for 7 h, and finally at 24 h. Percentage conversion was calculated by Equation 3, where % = percentage of total area of the UV trace measured by LCMS, FI = free inhibitor, BI = bound inhibitor.

$$\% \text{ conversion} = \frac{\%BI}{(\%FI + \%BI)} \quad (3)$$

Optimised method for compound 60

Assay Protocol

25 μL of a 20 mM stock of inhibitor in DMSO was added to a stirred solution of internal standard (fluorene, 25 μL of 2 mM stock in DMSO), 450 μL of 11.1 mM *N*-Boc-lysine stock in 100 mM potassium phosphate buffer at pH 7.4, or 450 μL of 11.1 mM *N*-Boc-lysine stock in 50:50 acetonitrile:water plus 1.7 μL of DIPEA. Reactions were then analysed immediately by HPLC. Two reactions were run simultaneously for 23 samplings each (*ca.* 8 h reaction time). Inhibitor for the second reaction was only added in the last 2 min of the HPLC run for reaction 1, to achieve as early sampling as possible in the reaction time-course. Reactions >8 h were then sampled at *ca.* 24, 48 and 72 h. LCMS was used after sampling completion to confirm peak identity by mass. Data and kinetic analyses are given below.

HPLC Method

The liquid chromatography (LC) analysis was conducted on an Phenomenex Kinetex[®] XB-C18 column (50 mm x 3.0 mm internal diameter, 2.6 μm packing diameter) at 40 °C using a 0.5 μL injection volume.

The solvents employed were A = 0.05% v/v solution of trifluoroacetic acid in water, and B = 0.05% v/v solution of trifluoroacetic acid in acetonitrile.

The gradient employed was:

Time / min	Flow Rate / mL·min ⁻¹	% A	% B
0.00	1	100	0
8.00	1	5	95
8.01	1	100	0
10.00	1	100	0

The UV detection was conducted at 260 nm.

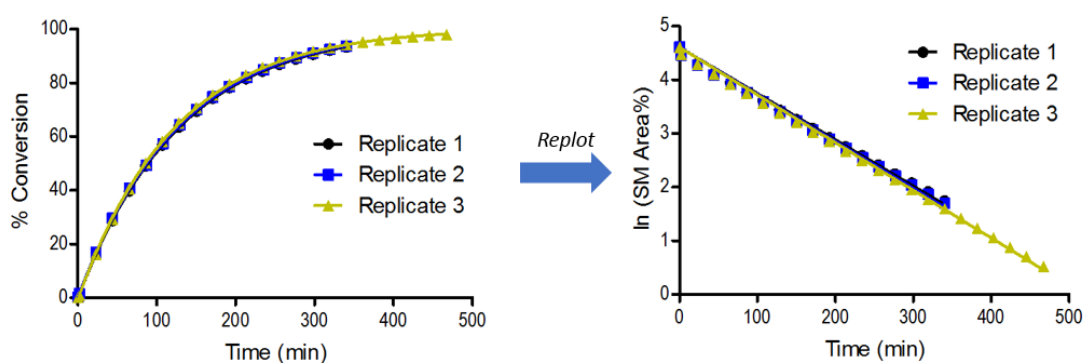
Percentage conversion was calculated by comparison of the total area percentage of starting material (SM) and product (P). Half-lives (where reported) were derived from the linear fit of \ln [SM Area %] vs time. The experimental results, and kinetic analysis of compound 4 is shown in below.

Kinetic analysis of ester 4 under reactive conditions

Pseudo-first order kinetic analysis was employed (as documented in the literature for similar assays),⁶⁹ according to equations 4 and 5 below. SM Area % denotes the % of the total area of the HPLC trace occupied by starting material peak, and $k_{\text{pseudo 1st}}$ denotes the pseudo first order rate constant for this process.

$$\ln(\text{SM Area } \%)_t = -k_{\text{pseudo 1st}}t + \ln(\text{SM Area } \%)_0 \quad (4)$$

$$t_{1/2} = \frac{\ln(2)}{k_{\text{pseudo 1st}}} \quad (5)$$



	k / min^{-1}	$t_{1/2} / \text{min}$	$t_{1/2} / \text{h}$
Replicate 1	0.0086	80.5	1.34
Replicate 2	0.0088	79.1	1.32
Replicate 3	0.0089	78.0	1.30
Average	0.0088	79.2	1.32
St Dev	0.0001	1.2	0.02

Figure 72 – Half life derivation for ester 60 under reactive conditions. Top: Percentage conversion vs time plot for each replicate. Bottom: Plot of ln (Starting Material Area %) vs time for each replicate showed linear progress, consistent with pseudo-first order kinetics. The gradient of each linear fit corresponds to the rate constant (k / min^{-1}), and using standard manipulations, this can be converted to a half life in h⁶⁹

6.2.4 X-Ray Crystallography

X-ray crystallography experiments and data processing was carried out by Dr Máire A Convery (GSK).

Crystallography methods

The protein was expressed and purified as described previously.¹⁶³ Crystals were grown by co-crystallisation of PI3K δ with an inhibitor previously seen to give reproducible high quality crystals using a modified version of the protocol described previously.¹⁶³ A 50 mM compound stock solution in DMSO was prepared from which 3.5 μL was mixed with 28 μL of 5% w/v *N*-

dodecyl- β -D-maltoside (DDM) prior to addition to 280 μ L of protein solution at 5 mg·mL (in 20 mM Tris/HCl pH 7.2, 50 mM ammonium sulphate, 5 mM dithiothreitol, 1% ethylene glycol, 1% betaine, 0.02% CHAPS). The mixture was incubated at room temperature for 60 min and then spun at 4 °C for 15 min. A crystal seeding solution was made by transferring an existing PI3K delta crystal into 5 μ L of Morpheus screen (Molecular Dimensions Ltd) condition G2 (0.1 M buffer system 1 pH 6.5, 0.1 M carboxylic acids, 30% ethylene glycol/PEG 8000). The crystal was crushed and added to 1 mL of Morpheus screen condition G2 and vortexed vigorously. The seed stock was typically thawed and then diluted by a factor of 20 to 40 with Morpheus screen condition G2 and then vortexed before use in the crystallisation protocol. The crystallisation was carried out by sitting drop vapour diffusion using plates prepared with a Mosquito liquid handling robot with crystallisation drops consisting of 200 nL protein, 200 nL well solution and 100 nL seeding solution, using Morpheus screen condition G2 for the wells. Crystals were transferred for soaking to drops containing Morpheus screen condition G2 with 10% glycerol and 5% compound solution (200 mM compound stock solution in DMSO) added. The crystals were soaked for 18 h prior to flash freezing direct from the soaking drop in liquid nitrogen ready for data collection. X-ray diffraction data were collected at 100 K using Pilatus-6M detectors at the Diamond Light Source, or the European Synchrotron Radiation Facility. The data were processed and scaled utilising XDS,²⁸⁶ AIMLESS²⁸⁷ and the CCP4 suite of programs.²⁸⁸ The structure was determined using the coordinates of an isomorphous unliganded protein model (unpublished). Coot²⁸⁹ was used for model building and refinement was carried out with autoBUSTER.²⁹⁰

Electron Density Map in Figure 46C

The co-ordinates for the side chain of Lys779 and the ligand were removed from the final model and a cycle of refinement carried out using BUSTER. The resulting $F_o - F_c$ omit map is shown in green at 2.7 rmsd visualised in CCP4MG.

6.2.5 Kinetic Binding Assay at PI3K δ

Kinetic assays were carried out with assistance from Dr Daniel A Thomas (GSK). Data processing was assisted by Dr John P Evans (GSK).

Assay Protocol

The PI3K δ kinetic assay was performed in 384-well plate format using the ADP QuestTM assay according to manufacturer's instructions.²³³ ADP QuestTM reagents A and B were added to

buffer containing 50 mM HEPES, pH 7.0, 150 mM NaCl, 10 mM MgCl₂, 2.3 mM cholate, 10 μM CHAPS (w/v) together with 1.25 mM ATP and 50 μM PtdIns(4,5)P₂. Compounds were dissolved as 10 mM stocks in DMSO-*d*₆, (accurate concentrations determined by quantitative NMR, with data adjusted during analysis), and titrated using a HP D300e Digital Dispenser, with DMSO concentration normalised to 1% (v/v) (**Table 20**). Wortmannin, as a standard inhibitor, was titrated from 2 to 0.02 μM, and no-inhibitor controls were also included. Briefly, substrate solution was added to compound titrations and reactions initiated upon the addition of 50 nM PI3Kδ enzyme. Fluorescence intensity was measured every 30 s for 60 min using a Tecan Infinite M1000 Plate Reader ($\lambda_{\text{ex}} = 544 \text{ nm}$, $\lambda_{\text{em}} = 590 \text{ nm}$). Assays were conducted in triplicate.

Compound dilutions

Bespoke dilutions were made for each compound as detailed below in **Table 20** and **Table 21**, from 10 mM nominal stocks. Accurate concentrations of stock solutions were determined by quantitative NMR,²⁹¹ and corrected in data analysis.

Table 20 – Dilutions for covalent compounds 27, 60, and 99-103 used in kinetic assay at PI3Kδ. All concentrations are shown in μM.

Well	Cpd 99 p-NO2	Cpd 100 p-CF3	Cpd 60 p-F	Cpd 101 H	Cpd 103 p-OMe	Cpd 102 2,4-Dimethyl	Cpd 27 Wm
A	2	10	10	10	100	100	2
B	1.2064	6.032	6.032	6.032	66.72	66.72	1.21
C	0.7264	3.632	3.632	3.632	44.48	44.48	0.726
D	0.4384	2.192	2.192	2.192	29.6	29.6	0.438
E	0.2624	1.312	1.312	1.312	19.68	19.68	0.262
F	0.16	0.8	0.8	0.8	13.12	13.12	0.16
G	0.096	0.48	0.48	0.48	8.8	8.8	0.096
H	0.0576	0.288	0.288	0.288	5.92	5.92	0.0576
I	0.0352	0.176	0.176	0.176	3.84	3.84	0.0352
J	0.02096	0.1048	0.1048	0.1048	2.56	2.56	0.021
K	0.01264	0.0632	0.0632	0.0632	1.76	1.76	0.0126
L	0.00752	0.0376	0.0376	0.0376	1.16	1.16	0.00752
M	0.00464	0.0232	0.0232	0.0232	0.768	0.768	0.00464
N	0.00272	0.0136	0.0136	0.0136	0.512	0.512	0.00272
O	0.0016	0.008	0.008	0.008	0.344	0.344	0.0016
P	Blank	Blank	Blank	Blank	Blank	Blank	Blank
Fold Corrected stock (mM)	1.66	1.66	1.66	1.66	1.50	1.50	1.65
	5.5	8.5	8.5	8.5	8.0	7.6	10

Table 21 - Dilutions for reversible compounds 58 and 107 in kinetic format at PI3Kδ. All concentrations are shown in μM .

Well	Cpd 58 Me ester	Cpd 107 p-F amide
A	20	100
B	9.89	49.4
C	4.9	24.5
D	2.4	12
E	1.18	5.92
F	0.576	2.88
G	0.288	1.44
H	0.144	0.72
I	0.072	0.36
J	0.0352	0.176
K	0.0176	0.088
L	0.008	0.04
M	0.0048	0.024
N	0.0016	0.008
O	0.00104	0.0052
P	Blank	Blank
Fold Corrected stock (mM)	Varying 9.0	Varying 9.5

Data Analysis

Covalent compounds

Briefly, raw fluorescence data were zero-corrected by subtracting the fluorescence value at $t = 0$ from all data points. They were then fitted by the local progress curves analysis and replot method, using a modified progress curve, equation 6 (where [P] is the response in relative fluorescence units (RFU), v_i is the initial state velocity, t is the time in s, v_s is the steady state rate, and k_{obs} is the observed rate constant in units of s^{-1}), to derive k_{obs} values^{49,292}. Equation 6 was modified to include a conditional term to offset t_0 to better accommodate the lag phase of the coupled enzyme assays. The notation for use of this equation in Graphpad Prism 5 is given also. For data points where background ADP oxidation caused an obvious increase in signal after loss of kinase activity (characterised by a rapid increase in fluorescence after inactivation), these data were excluded from the fit. Data from three replicates were fitted and averaged to derive k_{obs} as the mean \pm s.e.m. These k_{obs} values were

then replotted against concentration of inhibitor, and fitted to equation 7 (where k_{inact} denotes the rate constant for inactivation of the kinase in units of s^{-1} , $[I]$ is the molar concentration of inhibitor, and K_i is the concentration at which the half maximal rate of inactivation is achieved, in molar units) to derive the k_{inact} and K_i values (\pm s.e.m.).¹ Finally, the k_{inact}/K_i ratios derived, and the errors derived from standard error propagation theory. The raw data plots, processed plots, $k_{\text{inact}} \pm$ s.e.m., and $K_i \pm$ s.e.m. for each inhibitor are given below.

If $t < t_0$, $[P] = \text{background}$

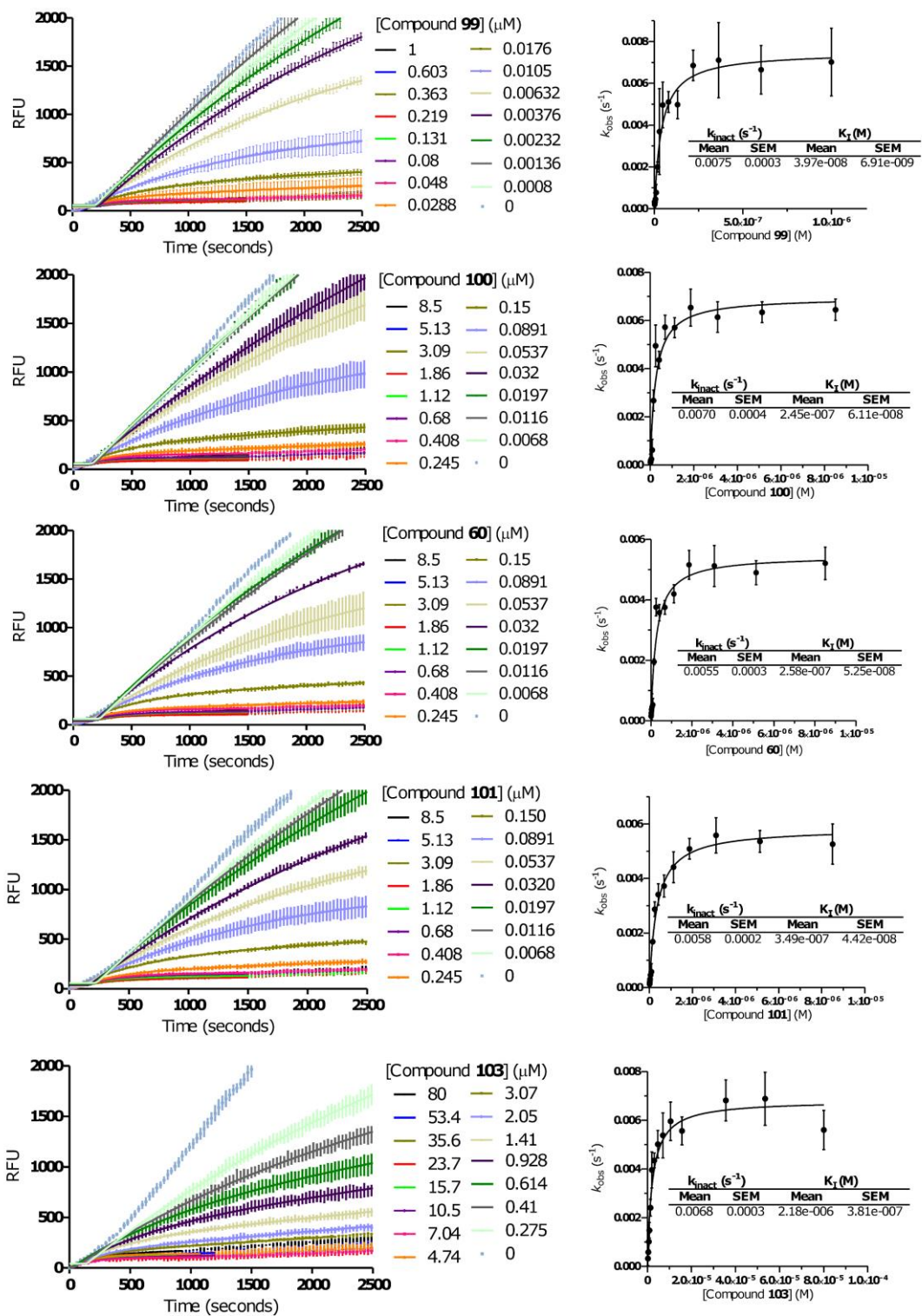
$$\text{If } t > t_0, [P] = \text{background} + v_s(t - t_0) + \frac{v_i - v_s}{k_{\text{obs}}} [1 - e^{-k_{\text{obs}}(t-t_0)}] \quad (6)$$

Graphpad notation: $Y = \text{If}(X < X_0, Y_0, Y_0 + v_f * (X - X_0) + ((v_i - v_f) / k_{\text{obs}}) * (1 - \exp(-k_{\text{obs}} * (X - X_0))))$

$$k_{\text{obs}} = \frac{k_{\text{inact}} [I]}{K_i + [I]} \quad (7)$$

Reversible compounds

Briefly, raw fluorescence data were zero-corrected by subtracting the fluorescence value at $t = 0$ from all data points. Linear fits were then applied to each progress plot, excluding the first 300 sec due to the lag phase of coupled enzyme assays, to determine k_{obs} . These values were replotted against the log of the corrected inhibitor concentration, and fitted to equation 1 to determine IC_{50} , which was converted to K_i using equation 2.



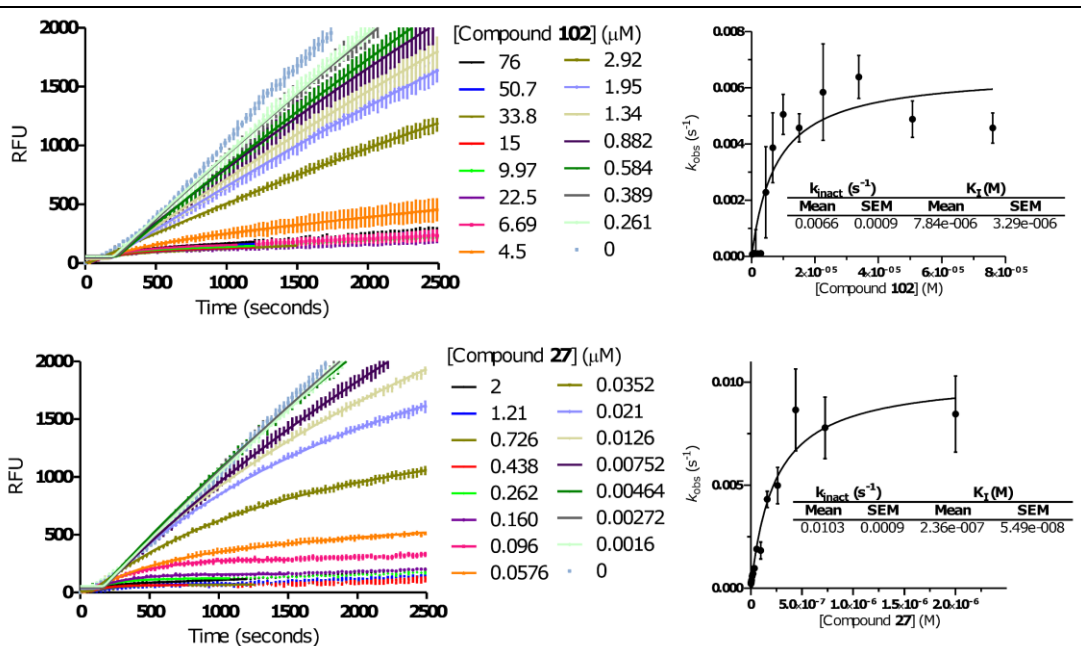


Figure 73 – Kinetic analysis for compounds 27, 60, and 99-103. Left: Raw fluorescence data plotted against time, after time zero-correction, fitted as described in the text. Concentrations are in accordance with **Table 20** after correction for 10 mM stock concentration. Right: Plot of derived k_{obs} against inhibitor concentration. The tables show the k_{inact} and K_I values derived from fitting these points to equation 7.

6.2.6 Intact Protein Mass Spectrometry

Assay Protocols

Covalent Adduct Assessment

Compounds **60** or **64** were incubated with 1 μ M of PI3K δ protein in a 10:1 inhibitor:protein ratio in buffer containing 50 mM HEPES, pH 7.0 (NaOH), 150 mM NaCl, 10 mM MgCl₂, 2.3 mM cholate, and 10 μ M CHAPS. After the desired time, the assays were quenched with a 10% (v/v) formic acid solution, and analysed by LCMS.

Competition Experiment

Compound **122** was incubated with 1 μ M protein in a 10:1 inhibitor:protein ratio in buffer containing 50 mM HEPES, pH 7.0 (NaOH), 150 mM NaCl, 10 mM MgCl₂, 2.3 mM cholate, 10 μ M CHAPS at room temperature. After 15 min, compound **60** was added in a 2:1 inhibitor:protein ratio and the samples incubated at room temperature. The assay was quenched at 5 min and analysed using the procedure detailed above.

LCMS Protocol

Protein LCMS was conducted on an Agilent 6224 TOF LC/MS equipped with Agilent 1200 Series autosampler. Analytes were separated on a Polymer Labs (Agilent) PLRP-S column (50 mm x 1 mm internal diameter, 5 μ m particle size). LC conditions were 0.5 mL·min⁻¹ flow rate, 70 °C, 10 μ L injection volume. Gradient elution with (A) water containing 0.2% (v/v) formic acid and (B) acetonitrile containing 0.2% (v/v) formic acid. Gradient conditions were initially 10% B, increasing to 30% after 0.5 min, and then linearly to 80% B over 4.5 min, prior to a 1.2 min flush with 100% B and then a 1.9 minute equilibration with 10% B prior to the next injection. Mass spectra were then deconvoluted using Agilent MassHunter Qualitative Analysis version B.06.00 over the mass range 70 – 170 kDa to obtain the intact protein mass.

6.2.7 Jump Dilution Experiment

Jump dilution experiments were carried out with assistance from Dr Daniel A Thomas (GSK).

Assay Protocol

5 mM stock of compounds **27**, **58**, **60**, and **64** in DMSO-*d*₆ were dispensed at an incubation concentration equal to 10x IC₅₀, or the concentration of PI3K isoform included in the preincubation, with a normalised DMSO concentration of 1% (v/v) (**Table 22**). Assays were carried out in triplicate. PI3K enzymes were diluted to 100x assay concentration (final assay concentration PI3K α = 7.5 nM, PI3K β = 20 nM, PI3K δ = 6 nM) in buffer solution (contains 50 mM HEPES pH 7.0 (NaOH), 150 mM NaCl, 10 mM MgCl₂, 2.3 mM sodium cholate, 10 μ M CHAPS). 100x enzyme solution was added to compound wells, and incubated for 15 min before diluting 100-fold with ADP Quest™ detection reagents (DiscoverX, catalog number: 90-0071) containing 1 mM ATP and 40 μ M PtdIns(4,5)P₂. Enzyme activity, characterised by an increase in fluorescence intensity, was monitored continuously using a Tecan Safire II plate reader at 30 s intervals for 30 min (λ_{ex} = 544 nm, λ_{em} = 590 nm). Data were fitted using a standard linear regression model (**Table 23**) to determine the proportion of activity recovered relative to high (no inhibitor) and low (no protein) controls, and expressed as a percentage.

Compounds Dilutions

Compounds **27**, **58**, **60**, and **64** were dispensed as shown below for preincubation with 100x protein stock solution (final assay concentration PI3K α = 7.5 nM, PI3K β = 20 nM, PI3K δ = 6 nM).

Table 22 – Preincubation concentrations of compounds 27, 58, 60, and 64. All concentrations are shown in μM .

Well	Compound	PI3K α	PI3K β	PI3K δ
A		1	2	0.6
B	Compound 27	1	2	0.6
C		1	2	0.6
D		32	24	1
E	Compound 60	32	24	1
F		32	24	1
G		28	39	0.6
H	Compound 58	28	39	0.6
I		28	39	0.6
J		30	32	0.6
K	Compound 64	30	32	0.6
L		30	32	0.6
M	High (no compound) controls			
N	High (no compound) controls			
O	Low (no protein) controls			
P	Low (no protein) controls			

Data were analysed using standard linear regression to determine the proportion of enzyme activity recovered, as a percentage, relative to uninhibited controls. Calculated maximum % recovery, and measured % recovery are shown below. Note for compounds **58**, **64** and **27**, due to their potency at PI3K δ (and PI3K β for compound **27**), the initial incubation concentration of compound required to have a concentration equal to the concentration of protein to effect 100% inhibition, caused the maximum potential % recovery to be less than the desired 90%.

Table 23 – Calculated maximum % recovery, and measured % recovery for compounds 27, 58, 60, and 64.

	<u>Calculated maximum % recovery</u>			<u>Measured % recovery</u>		
	PI3K α	PI3K β	PI3K δ	PI3K α	PI3K β	PI3K δ
Compound 27	90	48	87	2	2	5
Compound 60	92	92	92	3	4	7
Compound 58	92	92	84	79	85	66
Compound 64	98	99	65	92	93	47

6.2.8 Kinetic Binding Assay at PI3K α and PI3K β

Kinetic assays were carried out with assistance from Dr Daniel A Thomas (GSK).

Assay Protocol

Compounds titrations used were identical to those used for the PI3K δ -only kinetic assay (**Table 24**) with a normalised DMSO concentration of 1% (v/v). Briefly, substrate solution (prepared as for the PI3K δ -only kinetic assay) was added to compound titrations, and reactions initiated upon the addition of PI3K enzyme (PI3K δ = 50 nM stock, PI3K α = 75 nM stock, PI3K β = 100 nM stock). Fluorescence intensity was measured every 30 s for 60 min using a Tecan Infinite M1000 Plate Reader (λ_{ex} = 544 nm, λ_{em} = 590 nm). Assays were conducted in duplicate. Results were analysed qualitatively for linearity; those demonstrating curvature (consistent with covalent inhibition) or linearity (consistent with reversible inhibition).

Compound Dilutions

Compounds **27**, **58**, and **60** were titrated as shown below from 10 mM nominal stocks. Accurate concentrations of stock solutions were determined by quantitative NMR,²⁹¹ and corrected in data analysis.

Table 24 – Compound dilutions for PI3K isoform kinetic assay. All concentrations are shown in μM .

Well	Cpd 60	Cpd 58	Cpd 27
A	10	20	2
B	6.032	9.888	1.2064
C	3.632	4.896	0.7264
D	2.192	2.4	0.4384
E	1.312	1.184	0.2624
F	0.8	0.576	0.16
G	0.48	0.288	0.096
H	0.288	0.144	0.0576
I	0.176	0.072	0.0352
J	0.1048	0.0352	0.02096
K	0.0632	0.0176	0.01264
L	0.0376	0.008	0.00752
M	0.0232	0.0048	0.00464
N	0.0136	0.0016	0.00272
O	0.008	0.00104	0.0016
P	blank	blank	blank

Change in IC₅₀ with time

The raw kinetic data were read along the x-axis (time), with each 30 s set of time points forming a 16-point IC₅₀ curve. We carried out this analysis every 30 s up to 20 min, and then every 300 s (5 min) until the end point at 3600 s. PI3K α analyses were stopped at 1200 s due to non-linearity in the control curve at 1500 s. Fittings for compounds **58** and **60** where the IC₅₀ curve was incomplete (>50% coverage of the curve was observed in all cases) used the signal for 2 μ M Wortmannin at that enzyme at that time point as the lower limit for the Hill curve to converge to. The natural log of the IC₅₀ derived from this analysis was then replotted against time to derive the plots below. Note: There was an inherent lag in this assay until *ca.* 300 s, causing variation in this region.

6.2.9 Wider-kinome Selectivity Screening

Lipid and protein kinase selectivity analyses for compound **60** were conducted at the University of Dundee MRC PPU International Centre for Kinase Profiling. Results are given below.

Table 25 – Lipid kinase selectivity data. Data reported as the mean from two full-curve dose-response assays.

Lipid Kinase	pIC ₅₀	Notes	Incubation Time (min)
PI3K δ	8.1	Data from in-house TR-FRET assay (Fig 1)	60
PI3K α	5.5	Data from in-house TR-FRET assay (Fig 1)	60
PI3K β	5.3	Data from in-house TR-FRET assay (Fig 1)	60
PI3K γ	4.8	Data from in-house TR-FRET assay (Fig 1)	60
PI4K2a	<5.0	Data from Dundee Panel	45
PIP4K2A	<5.0	Data from Dundee Panel	15
PIK4B	<5.0	Data from Dundee Panel	45
DAG Kinase β	5.1	Data from Dundee Panel	40
DAG Kinase γ	<5.0	Data from Dundee Panel	40
DAG Kinase ζ	<5.0	Data from Dundee Panel	40
Choline Kinase α	<5.0	Data from Dundee Panel	40
CHKB	<5.0	Data from Dundee Panel	40
SPHK1	<5.0	Data from Dundee Panel	40
SPHK2	<5.0	Data from Dundee Panel	30

Premier Kinase Screen

Percentage inhibition is shown as the mean of two tests, with compound **60** dosed at 1 μ M. A value of zero or negative indicates no inhibition observed.

Table 26 – Wider kinome selectivity screen. Data reported from two assays, reporting mean percentage inhibition at 1 μ M, at K_M (ATP), or below.

Target	Mean (N = 2)	St Dev	Incubation time (min)
JNK1(H)	-0.94	9.77	30
p38a MAPK (H)	-7.56	14.75	30
p38b MAPK (H)	-11.93	18.07	30
p38d MAPK (H)	-13.14	14.20	30
p38g MAPK (H)	-9.19	3.82	30
MAPKAP-K2 (H)	-4.38	8.68	30
MSK1 (H)	-0.33	24.80	30
PRAK (H)	-21.84	15.99	30
PDK1 (H)	-21.17	5.75	30
PKBa (H)	-14.88	2.17	30
SGK1 (H)	-0.26	11.14	30
S6K1 (H)	-9.69	2.88	30
GSK3b (H)	4.52	1.29	30
ROCK 2 (R)	14.32	9.33	30
CHK1 (H)	-8.01	25.65	30
CSK (H)	-1.25	3.01	30
NEK6 (H)	-3.13	8.85	30
NEK2a (H)	-11.47	0.82	30
Lck (H)	1.51	20.25	15
PKA (H)	0.40	2.24	30
PHK (H)	-33.21	9.84	15
TBK1 (H)	-4.15	6.34	30
IKKb (H)	-1.03	2.54	30
RSK2 (H)	9.49	12.76	30
JNK2 (H)	-9.95	21.69	30
IKKe (H)	7.69	13.73	30
DYRK2 (H)	-22.75	3.89	30
SmMLCK (H)	-8.24	6.79	30
PRK2 (H)	-8.22	2.13	30
MNK2 (H)	-30.74	37.73	30
Aurora B (H)	-7.17	6.22	30
CAMK1 (H)	14.64	12.54	30
CAMKKb (H)	-9.70	11.34	30
CHK2 (H)	0.27	1.15	30
PIM2 (H)	-6.75	12.79	30
JNK3 (H)	-8.74	3.16	30
MAPKAP-K3 (H)	-19.06	5.49	30
ERK8 (H)	-2.72	22.85	30
MNK1 (H)	-12.70	10.36	30
SRPK1 (H)	1.34	3.13	30
PKBb (H)	-3.43	17.48	30

EF2K (H)	-2.85	6.36	30
MARK3 (H)	-4.81	11.79	30
MST2 (H)	2.98	5.65	30
PKD1 (H)	1.20	15.10	30
HIPK2 (H)	-17.29	19.07	30
HIPK3 (H)	-20.01	8.99	30
PAK4 (H)	-5.51	10.88	30
PAK5 (H)	-12.98	8.93	30
PAK6 (H)	-14.41	11.63	30
PIM1 (H)	0.17	11.98	30
PIM3 (H)	2.56	12.47	30
PLK1 (H)	-20.86	20.79	30
BRSK2 (H)	-9.88	15.03	30
MELK (H)	-1.18	1.62	30
PKCz (H)	-13.21	12.93	30
ERK1 (H)	-3.79	6.64	30
DYRK3 (H)	-3.46	16.73	30
FGF-R1 (H)	2.85	11.66	30
IRR (H)	-9.08	0.68	30
EPH-A2 (H)	-2.34	13.47	30
MST4 (H)	-1.85	0.45	30
SYK (H)	-4.24	9.66	30
YES1 (H)	-0.37	6.15	30
IGF-1R (H)	-0.29	21.00	30
VEG-FR (H)	9.61	14.36	30
BTK (H)	-1.54	13.33	30
IR (H)	7.35	4.36	30
EPH-B3 (H)	-7.71	26.14	30
PKCa (H)	-6.93	2.29	30
GCK (H)	-6.54	12.59	30
IRAK4 (H)	-9.85	6.07	30
NUAK1 (H)	-26.02	29.62	30
MLK1 (H)	-11.03	5.91	30
MINK1 (H)	4.05	10.48	30
MLK3 (H)	6.37	14.17	30
LKB1 (H)	-23.33	0.96	30
HER4 (H)	5.32	5.36	30
TTK (H)	-0.43	14.10	30
DYRK1A (H)	-3.70	6.86	30
Src (H)	2.36	3.14	30
RIPK2 (H)	0.68	5.17	30
Aurora A (H)	10.77	5.00	30
PAK2 (H)	-24.37	10.28	30
BRSK1 (H)	-2.72	5.03	30

HIPK1 (H)	-11.54	16.97	30
MARK2 (H)	-12.44	8.29	30
MARK4 (H)	-14.37	6.10	30
EPH-B4 (H)	-4.03	16.54	30
JAK3 (H)	10.08	10.29	30
EPH-A4 (H)	-8.87	13.36	30
TAK1 (H)	-13.77	0.98	30
TrkA (H)	35.04	0.03	30
MEKK1 (H)	5.89	2.14	30
MARK1 (H)	-3.43	3.22	30
CK1δ (H)	3.88	13.48	30
CLK2 (H)	3.46	13.69	30
DAPK1 (H)	5.44	2.10	30
EPH-B2 (H)	6.65	6.22	30
EPH-B1 (H)	-13.84	13.49	30
TAO1 (H)	-19.05	39.08	30
ASK1 (H)	-39.75	10.75	30
MKK6 (H)	-14.47	26.41	30
MKK2 (H)	-3.26	11.49	30
ERK2 (H)	-13.59	1.45	30
RSK1 (H)	-2.00	2.53	40
CK2 (H)	-6.02	2.11	30
ABL (H)	-2.02	2.99	30
BRK (H)	9.64	3.46	30
PKCg (H)	-10.38	2.33	30
MPSK1 (H)	-1.71	4.68	30
STK33 (H)	-15.66	18.46	30
TIE2 (H)	-11.17	7.29	30
ZAP70 (H)	-1.22	9.20	30
CDK2-Cyclin A (H)	-20.62	11.85	30
MKK1 (H)	4.78	4.86	30
EIF2AK3 (H)	-4.53	1.03	30
IRAK1 (H)	-9.93	14.94	30
TLK1 (H)	-6.86	1.11	30
TSSK1 (H)	-18.46	3.21	30
TESK1 (H)	-4.02	9.75	30
TTBK1 (H)	3.79	7.91	30
MST3 (H)	-8.81	9.70	30
CK1γ2 (H)	-8.68	18.95	30
SIK2 (H)	-23.11	4.86	30
SIK3 (H)	-10.86	4.93	30
WNK1 (H)	15.03	0.91	30
CDK9-Cyclin T1 (H)	4.78	8.87	30
DDR2 (H)	-5.56	6.94	30

OSR1 (H)	6.12	1.87	30
ULK1 (H)	-15.90	1.63	30
ULK2 (H)	4.46	4.35	30
TTBK2 (H)	-14.14	3.67	30
MAP4K3 (H)	-12.31	3.46	30
MAP4K5 (H)	-6.91	3.00	30
AMPK (H)	-9.85	4.43	30
PDGFRA (H)	10.56	5.17	30
TGFBR1 (H)	-0.21	10.66	30
ERK5 (H)	-3.78	4.52	30
PNK (H)	-1.30	1.02	30

6.2.10 In-lysate Binding Assay for Probe 131

THP-1 lysates were supplied by Lars Dittus (Cellzome) and diluted to a working concentration of $2 \text{ mg}\cdot\text{mL}^{-1}$ in HEPES buffer (50 mM HEPES pH 7.4, 5% glycerol, 1.5 mM MgCl_2 , 150 mM NaCl, 1 mM Na_3VO_4 , 1 mM DTT), and distributed across reaction wells of a black greiner 384-well plate. Probe **60** at 100x the desired concentration in DMSO, was then added to desired wells, and incubated on ice in the dark for 1 h. Probe **131** at 100x the desired concentration in DMSO was then added and the plate incubated for a further 1 h on ice in the dark. Iodoacetamide (270 mM in water, $1.67 \mu\text{L}$, $15 \mu\text{M}$ final concentration) was then added to all wells, and the plate incubated at room temperature in the dark for 30 min. DBCO-Cy5 dye ($250 \mu\text{M}$ in DMSO, $1.27 \mu\text{L}$, $10 \mu\text{M}$ final concentration) was then added, and the plate incubated for 10 min at room temperature in the dark. Reactions were quenched by the addition of 1:1 4x NuPage LDS sample buffer (invitrogen, NP0007):50 mM DTT in water, and heating to $95 \text{ }^\circ\text{C}$ for 5 min. Samples were then separated by SDS-PAGE on 4-20% Tris-Glycine Novex gels with Laemmli running buffer, and visualised by in-gel fluorescence on an Odyssey fluorescence imager. Proteins were then transferred to PVDF membranes using iBlot gel transfer kit (Life Technologies, IB401002), and blocked with LiCor Odyssey Blocking Buffer (LiCor, 927-40000) for 1 h. Membranes were then incubated with rabbit p110 δ primary antibody (1 in 1000 dilution, Cell Signaling Technology, #34050S) overnight at $4 \text{ }^\circ\text{C}$, and then goat anti-rabbit IRDye 800CW (1 in 10,000 dilution, LiCor, #926-32211) for 1 h at room temperature. Membranes were visualised using an Odyssey fluorescence imager. Images were processed using LiCor Image Studio Lite version 5.2. Cy5 signal intensities were normalised to total p110 δ signal intensity in the corresponding lane, and then normalised to high (no inhibitor **60**) and low (no probe **131**) controls. These values were plotted against concentration of **60** and fitted to a standard four-parameter logistic equation to derive IC_{50} .

6.2.11 Proteomic In-cell Selectivity Analysis of Compound 60

This experiment was designed in collaboration with Mr Lars Dittus (Cellzome), and carried out by Lars. Data analysis and interpretation was done in collaboration.

Cell treatment and lysis

For one replicate, Ramos cells were grown in RPMI-1640 medium (Gibco #21875-034) supplemented with 10% FBS (Gibco #10270) to get 5×10^8 cells (passage 8, 98% viability). Cells were harvested by centrifugation and were re-suspended in 90 mL medium containing 0.1% FBS to get a cell concentration of 5.56×10^6 cells/mL. 9 mL of this suspension was transferred to 8x T25-flasks. 0.5 mL of a dilution of compound **60** (prepared as 20X concentration in RPMI, 0.1% FBS) was added to the flasks to have final concentrations of 0 μ M – 10 μ M – 2 μ M – 0.4 μ M – 0.08 μ M – 0.016 μ M – 0.0032 μ M – 0 μ M, all at a final DMSO concentration of 0.25%. The cells were incubated for 1 h at 37 °C, 5% CO₂, 50 rpm shaking. To sample 1, DMSO was added to have a final DMSO concentration of 0.5%. To the other samples, compound **131** was added to have a final concentration of 1 μ M of compound **131** at 0.5% DMSO. The cells were incubated for 1 h at 37 °C, 5% CO₂, 50 rpm shaking. The cells were harvested and the pellets were lysed in two cell pellet volumes of lysis buffer (50 mM HEPES pH 7.4, 1% glycerol, 1.5 mM MgCl₂, 150 mM NaCl, 1 mM Na₃VO₄, 25 mM NaF, 0.8% IGEPAL CA-630, protease inhibitor (Roche 11873580001)). After 30 min of incubation at 4 °C, the lysates were ultracentrifuged for 30 min at 4 °C and protein concentrations were determined using the Bradford assay.

SPAAC reaction of azide with DBCO-biotin conjugate

Protein concentrations were adjusted to get 210 μ L lysate at a concentration of 2 mg/mL total protein using dilution buffer (50 mM HEPES pH 7.4, 1% glycerol, 1.5 mM MgCl₂, 150 mM NaCl, 1 mM Na₃VO₄). The maximal amount of compound **131** added to the cells was calculated to be 10 nmol. To saturate all potentially available azide, 2.1 μ L of a 5 mM DBCO-biotin (Sigma #760749-5MG) solution (50% DMSO in dilution buffer) was added to all lysate samples. Subsequently, the lysates were incubated in a sealed 96-well plate for 2 h, 4 °C, overhead rotating. After clicking, the excess of DBCO-biotin was removed using size-exclusion chromatography with the Zeba Spin Desalting plates (Thermo #89807) equilibrated with dilution buffer according to the manufacturer's protocol. The cleaned lysates were added to 7.5 μ L neutravidin beads contained in a 0.22 μ m filter plate and enrichment was performed for 2 h, 4 °C, overhead rotating. After enrichment, beads were washed 7x with 200 μ L dilution

buffer/0.4% IGEPAL CA-630 and subsequently 7x with 100 μ L dilution buffer/0.2% IGEPAL CA-630. Reversibly captured targets were eluted in 50 μ L 2X LDS sample buffer (Thermo #NP0007) after incubating for 45 min at room temperature (rt).

Bead digestion

After SDS elution, beads were washed 8 x with 200 μ L 20 mM Tris/400 mM NaCl/0.4% SDS, 5x with 200 μ L 20 mM Tris/400 mM NaCl, 4x with 200 μ L 50mM TEAB/2 M urea, and 3x with 200 μ L 50mM HEPES Buffer pH 8.5. 50 μ L digestion solution (25 mM HEPES pH 8.5, 2.5 mM tris(2-carboxyethyl)phosphine, 7.5 mM chloroacetamide, 0.001 μ g/ μ L trypsin, 0.001 μ g/ μ L LysC) was added to all samples. After overnight digestion (rt, 600 rpm) and collection of the digestion solution, peptide elution was completed by washing with 2x 50 μ L 50 mM HEPES. The recovered peptides dried *in vacuo* and labeled with TMT reagent as described below.

SDS elution

The eluted proteins were captured by magnetic carboxylate modified particles (50% GE Healthcare Sera-Mag #45152105050250/50% GE Healthcare Sera-Mag #65152105050250) for 15 min, 600 rpm, rt. After washing the beads 4x with 200 μ L 70% ethanol, digestion solution was added to the beads. Enzymatic digestion was performed as above. The digested peptides were collected and elution was completed by washing once with 10 μ L 2%DMSO in H₂O. The eluates were dried *in vacuo* and labeled with TMT labeling reagent as described below.

TMT Labelling

Lyophilized peptides were re-suspended in 10 μ L ultrapure water before 10 μ L TMT reagent (Thermo; 5 mg dissolved in 580 μ L 100% acetonitrile) was added. Labeling was done for 1 h, shaking at rt. Non-reacted TMT reagent was quenched for 15 min with 5 μ L 2.5% NH₂OH in 100 mM HEPES pH 8.5 at rt before pooling samples corresponding to one experiment. After lyophilization, sample clean-up was done using a C18SCX approach. For this, the lyophilized samples were re-suspended in 100 μ L 4% TFA and loaded to a layer of C18 material. After washing with 100 μ L 0.5% TFA/2% acetonitrile, peptides were eluted to SCX material using 100 μ L 0.5% TFA/60% acetonitrile. After washing with 200 μ L 0.5% TFA/60% acetonitrile, cleaned samples were eluted in 100 μ L 5% NH₃, 80% acetonitrile. Samples were dried *in vacuo*.

Mass spectrometry analysis

Mass spectrometry measurements of associated bead digests and SDS eluates were acquired directly after each other before running a BSA sample to avoid carry-over of contaminant proteins from a previous sample set.

Samples were resuspended in 0.05% trifluoroacetic acid in water. 30% of the sample was injected into an Ultimate3000 nanoRLSC (Thermo Fisher Scientific) coupled to a Orbitrap Fusion Lumos (Thermo Fisher Scientific). Peptides were separated on custom-made 35 cm x 100 μm (ID) C18 reversed-phase columns (Reprosil) at 55 °C. Gradient elution was performed from 3.5% acetonitrile to 35% acetonitrile in 0.1% formic acid over 2 h. Samples were online injected into the mass spectrometer operating with a data-dependent top speed method with a 3 sec cycle time. MS spectra were acquired by using 60,000 resolution and an ion target of 4E5 for MS1 scans. Higher energy collisional dissociation (HCD) scans were performed with 38% NCE at 30,000 resolution (at m/z 100) and the ion target settings was set to 1×10^5 so as to avoid coalescence.²⁸⁴ The instruments were operated with Tune 2.1 and Xcalibur 4.0.27.10. For peptide and protein identification, Mascot (Matrix Science) was used and peptide and protein quantification was done as previously described.²⁵¹

Data analysis

For analyzing the data, identified proteins were filtered for identifications with more than 1 quantified unique peptide matches and more than 2 quantified unique peptide to spectra matches in each replicate. To be included in the analysis, proteins were required to be identified and quantified in both replicates. Fold enrichment for the 3 most abundant peptides per protein was calculated by dividing MS^2 ion signals achieved for proteins after treating cells with **131** or DMSO without competition by **60** (fold enrichment = $MS^2_{1 \mu\text{M } 131 \text{ (TMT130L)}} / MS^2_{\text{vehicle (TMT126)}}$). From both replicates, the mean and standard errors of the mean were calculated. Selected binding curves and resulting pIC_{50} values were derived from fold competition (MS^2 ion signals of protein binding competed by **60** relative to vehicle control for the 3 most abundant peptides per protein) using GraphPad Prism v7.03 and built in analysis algorithms [non-linear regression, log(inhibitor) vs. response – Variable slope (four parameters)].

6.2.12 Cellular Washout Experiment

Cellular washout experiments were carried out in collaboration with Dr Joao Nunes (GSK).

General

Growth media consisted of RPMI 1640 + glutamax + HEPES (Gibco), 10% heat inactivated foetal bovine serum (Gibco), 1x minimum essential medium (MEM) non-essential amino acids (Gibco), 50 U·mL⁻¹ penicillin and 50 µg·mL⁻¹ streptomycin (Gibco)). All incubations were performed at 37 °C and 5% CO₂. The human biological samples were sourced ethically and their research use was in accord with the terms of the informed consents

Assay Protocol

CD4+ T cells were isolated from leukodepletion filter samples taken from healthy volunteers using Histopaque 1077 (Sigma Aldrich). Briefly, blood was allowed to drip into a 50 mL falcon tube and mixed with PBS (40 mL). 20 mL of diluted blood was then slowly layered onto 15 mL of Histopaque in a 50 mL falcon tube, which was then centrifuged at 800 rcf for 20 min at room temperature. The PBMC layer was then collected with a pasteur pipette into a new 50 mL falcon tube, and up to 50 mL of PBS was added. Cells were centrifuged at 300-400 rcf for 10 min at room temperature, supernatant was discarded and a second washing step was performed with PBS. Cells were then resuspended in 40 mL PBS + 0.5% Bovine Serum Albumin (BSA). Isolation of CD4+ T cells was performed according to manufacturer's protocol (Miltenyi Biotec, 130-096-533). 1x10⁶ CD4+ T cells were dispensed into a 24 well plate with a final volume of 1 mL per well. Compounds at 1000x the final assay concentration, or DMSO, were then added to wells and cells were incubated for 2 h. 2x10⁵ cells and media was transferred to a 96-well plate (in duplicate) and classified as no-wash. For the washout, the remaining cells and supernatant were transferred to a 1 mL eppendorf and centrifuged at 1500 rcf for 1 min. Supernatant was removed, cells were resuspended in 1 mL PBS and the mixture transferred to a new 1.5 mL eppendorf and incubated for 10 min. Cells were then centrifuged at 1500 rcf for 1 min, PBS aspirated, and the cells resuspended in 0.6 mL growth media. The suspensions were split into 3 x 200 µL aliquots and added to a 96-well plate. Cells were incubated for 10 min followed by centrifugation at 800 rcf for 5 min. Media was removed, cells were resuspended in 200 µL of media and transferred into a new 96 well plate and incubated for further 10 min. For the last washing step, cells were incubated for 20 min prior to centrifugation at 800 rcf for 1 min and aspiration of growth media. Cells were then resuspended in 200 µL of growth media incubated for 48 h (96 well plate). Cells were

transferred to a new U-bottom 96-well plate pre-coated with α CD3 stimulant ($2.5 \mu\text{g}\cdot\text{mL}^{-1}$) and further incubated for 24 h. Supernatant and cells were centrifuged at 800 rcf for 5 min and 120 μL of supernatant was collected and analysed using MSD IFN γ kit as detailed above for the human whole-blood assay.

Cellular Viability

Cellular viability was measured after 48 h in washed and non-washed using the commercially available CellTiter-Glo assay (Promega) according to the manufacturer's instruction.

6.2.13 Computational Modelling

Structures were modelled using Molecular Operating Environment (MOE) 2013 (2013.0802 release). Known crystal structure for compound **26** (DHP compounds, unpublished), **25** (Indazole compounds with methoxypyridine back-pocket group, PDB accession code: 5AE9),¹⁶³ or compound **24** (Indole back-pocket compounds, PDB accession code: 5AE8)¹⁶³ was prepared for simulation using the inbuilt structure preparation tool to balance charges, cap free protein residues, and simulate proton locations throughout the structure. For non-covalently bound models, the ligands were then modified using the building tool to represent the desired compound. The potential of the system was then fixed (excluded from simulation) with the exception of Lys779 and the ligand. The energy of the structure was then minimised using the Amber10:EHT force field to obtain a calculated affinity for the structure. Comparison of calculated affinity between the covalent inhibitors and **24** provided an estimate for their reversible binding affinity. For the covalently bound model, the covalent bond was drawn between the ligand and Lys779, and the leaving group deleted. The potentials for the side-chain, ligand and protein were set as before and the energy minimised. The structure was then investigated qualitatively for any abnormal bond angles or bond lengths that would indicate that this structure may not form.

The calculated affinity can be converted to a predicted fold-change in IC_{50} using the following derivations:

The calculated affinity is an expression of the Gibbs free energy (ΔG) for the system. Typically, more negative values of ΔG translate to more thermodynamically stable systems, however in this thesis, the calculated affinities shown throughout are actually shown as $-\Delta G$. Therefore, the more positive the value, the more stable the system. In this description, the typical equation for ΔG becomes:

$$\Delta G = RT \ln(K) \quad (8)$$

Where R is the ideal gas constant (0.00199 kcal·mol⁻¹), and T is the temperature of the system (assumed to be 298 K).

Therefore, the change in ΔG between two states can be expressed as:

$$\begin{aligned} \Delta\Delta G &= RT \ln(K_2) - RT \ln(K_1) \quad (9) \\ &= RT [\ln(K_2) - \ln(K_1)] \\ &= RT \ln\left(\frac{K_2}{K_1}\right) \end{aligned}$$

K_i values are an expression of an IC₅₀ value as described by the Cheng-Prusoff relationship,¹⁹³ therefore K_2/K_1 depicts the fold change between two K_i values. To estimate the expected change in binding energy (or ΔG) between two states from IC₅₀ values, **Equation 9** above can be used. To do the opposite, and estimate the fold-change expected between two computationally derived affinity values, **Equation 10** below can be used:

$$\frac{K_2}{K_1} = \exp\left(\frac{\Delta\Delta G}{RT}\right) \quad (10)$$

For example, if two inhibitors have a 10-fold difference in binding affinity, $K_2/K_1 = 10$. From **Equation 9**, $\Delta\Delta G = RT \ln(10) = 1.37$ kcal·mol⁻¹. Thus, if a difference in calculated affinity between two inhibitors in this thesis is roughly 1.4 kcal·mol⁻¹, this is expected to translate to a roughly 10-fold change in *reversible* binding affinity. Note that for a covalent inhibitor, where covalent inactivation will affect potency, the determined IC₅₀ values may differ considerably. Also note that this treatment *does not* derive an IC₅₀ from a calculated affinity, rather it estimates the fold change in IC₅₀ between two computationally derived calculated affinity values.

6.3 Synthetic Chemistry

General

All reagents were used as received from commercial sources (Sigma Aldrich, Alfa Aesar, Apollo Scientific etc.), unless otherwise stated. In all syntheses, anhydrous solvents were used, and commercially available HPLC grade solvents were used for work-up and isolation procedures, unless otherwise stated. Automated column chromatography was conducted on a Teledyne Isco Combiflash Rf system using RediSep Rf Silica cartridges (for normal phase), or Biotage KP-C18-HS cartridges (for reverse phase). Elution utilised standard HPLC grade solvents provided by Sigma Aldrich, with the desired modifier (for reverse phase) added in-house, unless otherwise stated.

Liquid Chromatography Mass Spectrometry (LCMS) methods used for reaction monitoring, and final purity analysis are referred to as Method A, B, or C in the synthetic procedures below. Mass Directed Automated Preparative HPLC (MDAP) purifications were conducted on a Waters FractionLynx system comprising of a Waters 600 pump with extended pump heads, Waters 2700 autosampler, Waters 996 diode array and Gilson 202 fraction collector. The high performance liquid chromatography (HPLC) separation was conducted on a Sunfire or Xselect C18 column (150 mm x 30 mm internal diameter, 5 μ m packing diameter) at ambient temperature, utilising an appropriate solvent system and elution gradient as determined by analytical LCMS (*i.e.* formic acid, ammonium bicarbonate, or trifluoroacetic acid modifier). The software used was MassLynx 3.5 with FractionLynx 4.1.

NMR spectra were recorded using a Bruker AV-400 (^1H = 400 MHz, ^{13}C = 101 MHz, ^{19}F = 376 MHz), AV-500 (^1H = 500 MHz, ^{13}C = 126 MHz) or AV-600 (^1H = 600 MHz, ^{13}C = 151 MHz). Chemical shifts (δ) are reported in parts per million (ppm) relative to residual non-deuterated solvent signals (CHLOROFORM- d ^1H = 7.27 ppm, ^{13}C = 77.0 ppm; DMSO- d_6 ^1H = 2.50 ppm, ^{13}C = 39.5 ppm; MeOD ^1H = 3.31 ppm, ^{13}C = 49.2 ppm) and coupling constants (J) in Hz. The following abbreviations are used for multiplicities: s = singlet; br. s = broad singlet; d = doublet; t = triplet; q = quartet; m = multiplet; dd = doublet of doublets; dt = doublet of triplets; spt = septet. If not specifically stated, the NMR experiments were run at 30 $^\circ\text{C}$.

High Resolution Mass Spectrometry (HRMS) spectra were recorded by one of two methods. Method A: On a Micromass Q-ToF Ultima hybrid quadrupole time-of-flight mass spectrometer, with analytes separated on an Agilent 1100 Liquid Chromatography equipped

with a Phenomenex Luna C18 (2) reversed phase column (100 mm x 2.1 mm, 3 μm packing diameter). LC conditions were 0.5 $\text{mL}\cdot\text{min}^{-1}$ flow rate, 35 $^{\circ}\text{C}$, injection volume 2–5 μL . Gradient elution with (A) water containing 0.1% (v/v) formic acid and (B) acetonitrile containing 0.1% (v/v) formic acid. Gradient conditions were initially 5% B, increasing linearly to 100% B over 6 min, remaining at 100% B for 2.5 min then decreasing linearly to 5% B over 1 min followed by an equilibration period of 2.5 min prior to the next injection. Method B: On a Waters XEVO G2-XS quadrupole time-of flight mass spectrometer using positive electrospray ionisation, with analytes separated on an Acquity UPLC CSH C18 column (100 mm x 2.1 mm, 1.7 μm packing diameter). LC conditions were 0.5 $\text{mL}\cdot\text{min}^{-1}$ flow rate, 50 $^{\circ}\text{C}$, injection volume 0.2 μL . Gradient elution with (A) water containing 0.1% (v/v) formic acid and (B) acetonitrile containing 0.1% (v/v) formic acid. Gradient conditions were initially 3% B, increasing linearly to 100% B over 8.5 min, remaining at 100% B for 0.5 min then decreasing linearly to 3% B over 0.5 min followed by an equilibration period of 0.5 min prior to the next injection. Mass to charge ratios (m/z) are reported in Daltons.

Infrared spectra were recorded using a Perkin Elmer Spectrum One spectrometer. Absorption frequencies (ν_{max}) are reported in wavenumbers (cm^{-1}).

Melting points were recorded on a Stuart SMP40 or SMP10 apparatus.

LCMS Methods:

LCMS Method A:

The liquid chromatography (LC) analysis was conducted on an Acquity UPLC CSH C18 column (50 mm x 2.1 mm internal diameter, 1.7 μm packing diameter) at 40 $^{\circ}\text{C}$ using a 0.5 μL injection volume.

The solvents employed were A = 0.1% v/v solution of formic acid in water, and B = 0.1% v/v solution of formic acid in acetonitrile.

The gradient employed was:

Time / min	Flow Rate / $\text{mL}\cdot\text{min}^{-1}$	% A	% B
0.00	1	97	3
1.50	1	5	95
1.90	1	5	95
2.00	1	97	3

The UV detection was a summed signal from a wavelength of 210 nm to 350 nm. Mass spectra were recorded on a Waters ZQ mass spectrometer using alternate-scan positive and negative electrospray ionisation (ES⁺ and ES⁻) with a scan range of 100 to 1000 amu, scan time of 0.27 s and an inter-scan delay of 0.10 s.

LCMS Method B:

The liquid chromatography (LC) analysis was conducted on an Acquity UPLC CSH C18 column (50 mm x 2.1 mm internal diameter, 1.7 µm packing diameter) at 40 °C using a 0.3 µL injection volume.

The solvents employed were A = 10 mM ammonium bicarbonate in water adjusted to pH 10 with ammonia solution, and B = Acetonitrile.

The gradient employed was:

Time / min	Flow Rate / mL·min ⁻¹	% A	% B
0.00	1	97	3
0.05	1	97	3
1.50	1	5	95
1.90	1	5	95
2.00	1	97	3

The UV detection was a summed signal from a wavelength of 210 nm to 350 nm. Mass spectra were recorded on a Waters ZQ mass spectrometer using alternate-scan positive and negative electrospray ionisation (ES⁺ and ES⁻) with a scan range of 100 to 1000 amu, scan time of 0.27 s and an inter-scan delay of 0.10 s.

LCMS Method C:

The liquid chromatography (LC) analysis was conducted on an Acquity UPLC CSH C18 column (50 mm x 2.1 mm internal diameter, 1.7 µm packing diameter) at 40 °C using a 0.5 µL injection volume.

The solvents employed were A = 0.1% v/v solution of trifluoroacetic acid in water, and B = 0.1% v/v solution of trifluoroacetic acid in acetonitrile.

The gradient employed was:

Time / min	Flow Rate / mL·min ⁻¹	% A	% B
0.00	1	95	3
1.50	1	5	95
1.90	1	5	95
2.00	1	95	3

The UV detection was a summed signal from a wavelength of 210 nm to 350 nm. Mass spectra were recorded on a Waters ZQ mass spectrometer using positive electrospray ionisation (ES⁺) with a scan range of 100 to 1000 amu, scan time of 0.27 s and an inter-scan delay of 0.05 s.

MDAP Methods

Method A

Column: Xselect CSH C18 column (150 mm x 30 mm i.d. 5 µm packing diameter) at ambient temperature.

The solvents employed were:

A = 10 mM ammonium bicarbonate adjusted to pH 10 with ammonia in water.

B = MeCN.

Injection Volume : 1 mL

The DAD detection was 210 nm to 350 nm.

MS Conditions

MS : Waters ZQ

Ionisation mode : Alternate scan positive/negative Electrospray

Scan Range : 100 to 1000 AMU

Scan Time : 0.50 s

Inter scan Delay : 0.2 s

Method B

Column: Xselect CSH C18 column (150 mm x 30 mm i.d. 5 µm packing diameter) at ambient temperature.

The solvents employed were:

A = 0.1% v/v solution of formic acid in water

B = 0.1% v/v solution of formic acid in MeCN.

Injection Volume : 1 mL

The DAD detection was 210 nm to 350 nm.

MS Conditions

MS : Waters ZQ

Ionisation mode : Alternate scan positive/negative Electrospray

Scan Range : 100 to 1000 AMU

Scan Time : 0.50 s

Inter scan Delay : 0.2 s

Method C

Column: Xselect CSH C18 column (150 mm x 30 mm i.d. 5 µm packing diameter) at ambient temperature.

The solvents employed were:

A = 10 mM ammonium bicarbonate in water adjusted to pH 10 with ammonia.

B = MeCN.

Injection Volume : 3 mL

The UV detection was for a signal wavelength at 254nm.

MS Conditions

MS : Waters ZQ

Ionisation mode : Alternate scan positive/negative Electrospray

Scan Range : 100 to 1000 AMU

Scan Time : 0.50 s

Inter scan Delay : 0.2 s

Method D

Column: Xselect CSH C18 column (150 mm x 30 mm i.d. 5 µm packing diameter) at ambient temperature.

The solvents employed were:

A = 0.1% v/v solution of TFA in water

B = 0.1% v/v solution of TFA in MeCN.

Injection Volume : 3 mL

The UV detection was for a signal wavelength at 254nm.

MS Conditions

MS : Waters ZQ

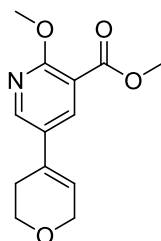
Ionisation mode : Alternate scan positive/negative Electrospray

Scan Range : 100 to 1000 AMU

Scan Time : 0.50 s

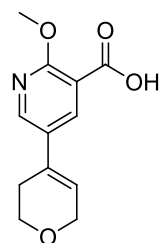
Inter scan Delay : 0.2 s

Methyl 5-(3,6-dihydro-2H-pyran-4-yl)-2-methoxynicotinate (39)



A round-bottomed flask was charged with methyl 5-bromo-2-methoxynicotinate **37** (0.505 g, 2.05 mmol), 2-(3,6-dihydro-2H-pyran-4-yl)-4,4,5,5-tetramethyl-1,3,2-dioxaborolane **38** (0.645 g, 3.07 mmol), (PdCl₂(dppf)) (0.150 g, 0.205 mmol), and sodium carbonate (0.655 g, 6.18 mmol) in 1,4-dioxane (10 mL) and water (2.5 mL). The vessel was purged with nitrogen and heated at 80 °C for 1 h. The mixture was then filtered through celite, washed with methanol and concentrated *in vacuo*. The residue was taken up in ethyl acetate (EtOAc) and washed with distilled water (3 x 15 mL) and brine (1 x 15 mL). The organic layer was dried through a hydrophobic frit and the solvent removed *in vacuo*. The residue was purified by automated column chromatography on silica gel (0-100% EtOAc:cyclohexane, DCM). The appropriate fractions were combined and the solvent removed *in vacuo* to afford the title product as an off-white solid (483 mg, 1.94 mmol, 94%). M.pt.: 106-108 °C. ν_{max} (neat): 2954, 1728, 1482, 1216, 1085 cm⁻¹. ¹H NMR (400 MHz, METHANOL-d₄) δ = 8.37 (1H, d, *J* = 2.4 Hz), 8.20 (1H, d, *J* = 2.7 Hz), 6.20 (1H, tt, *J* = 2.7, 1.6 Hz), 4.29 (2H, app. q, *J* = 2.9 Hz), 3.99 (3H, s), 3.92 (2H, t, *J* = 5.5 Hz), 3.89 (3H, s), 2.56 - 2.46 (2H, m). ¹³C NMR (101 MHz, METHANOL-d₄) δ = 167.4, 162.9, 148.2, 138.6, 131.8, 130.4, 124.4, 114.8, 66.8, 65.5, 54.6, 52.9, 28.0. LCMS (Method A): *t*_R = 0.87 min, [M+H⁺] 250.0, (100% purity). HRMS: (C₁₃H₁₆NO₄) [M+H⁺] requires 250.1074, found [M+H⁺] 250.1067.

5-(3,6-Dihydro-2H-pyran-4-yl)-2-methoxynicotinic acid (40)



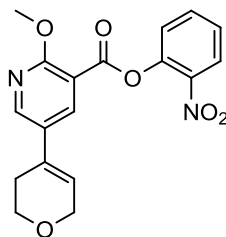
To a stirred solution of methyl 5-(3,6-dihydro-2H-pyran-4-yl)-2-methoxynicotinate **39** (450 mg, 1.81 mmol) in methanol (18 mL) was added aqueous NaOH (5 M, 0.9 mL, 4.5 mmol). The reaction was heated at reflux for 1 h and then cooled to room temperature and concentrated *in vacuo*. The residue was partitioned between EtOAc (25 mL) and aqueous NaOH (2 M, 25 mL). The layers were separated and the organic extracted with more NaOH (2 M, 2 x 25 mL). The organic layer was put aside, and the aqueous layer was acidified to pH 4 by the addition of aqueous HCl (25% w/w) and washed with EtOAc (3 x 25 mL). The aqueous layer was further acidified to pH 2 by the addition of aqueous HCl (25% w/w) and washed again with EtOAc (5 x 25 mL). The organics were dried through a hydrophobic frit concentrated *in vacuo* to afford the crude product as a brown suspension. Addition and then removal of methanol (15 mL) *in vacuo* afforded the product as an off-white powder (410 mg, 1.74 mmol, 97%). M.pt.: 180-183 °C (decomp). ν_{\max} (neat): 2940, 1678, 1602, 1563, 1485 cm^{-1} . ^1H NMR (400 MHz, DMSO- d_6) δ = 8.39 (1H, d, J = 2.4 Hz), 8.08 (1H, d, J = 2.4 Hz), 6.28 (1H, tt, J = 2.4, 1.5 Hz), 4.21 (2H, app. q, J = 2.4 Hz), 3.91 (3H, s), 3.82 (2H, t, J = 5.4 Hz), 2.48 - 2.42 (2H, m) (carboxylic acid proton not observed). ^{13}C NMR (151 MHz, DMSO- d_6) δ = 166.2, 160.4, 145.5, 136.2, 129.7, 128.4, 123.0, 115.5, 65.0, 63.4, 53.6, 26.1. LCMS (Method A): t_{R} = 0.71 min, $[\text{M}+\text{H}^+]$ 236.3, (100% purity). HRMS: ($\text{C}_{12}\text{H}_{14}\text{NO}_4$) $[\text{M}+\text{H}^+]$ requires 236.0917, found $[\text{M}+\text{H}^+]$ 236.0922.

General procedure for HATU couplings of 40 to afford esters 31-33

To a stirred solution of 5-(3,6-dihydro-2H-pyran-4-yl)-2-methoxynicotinic acid **40** (1 eq) in *N,N*-dimethylformamide (DMF) was added HATU (1.1 eq) and DIPEA (2 eq). The reaction was stirred for 10 min at room temperature, before phenol/thiol (1.1 eq) was added. The reaction was left to stir at room temperature and monitored by LCMS. Upon completion of the reaction, the mixture was diluted with diethyl ether or DCM and washed with aqueous LiCl solution (5%). The organics were dried through a hydrophobic frit, concentrated *in vacuo* and purified by either MDAP or automated column chromatography on silica gel.

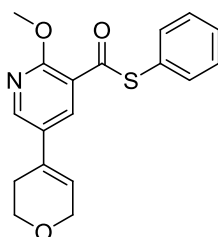
Following this general procedure, data for compounds **31-33** are presented as (a) amount of compound **40**; (b) amount of HATU; (c) volume of DIPEA; (d) amount of phenol/thiol; (e) volume of DMF; (f) reaction time; (g) purification system.

2-Nitrophenyl 5-(3,6-dihydro-2H-pyran-4-yl)-2-methoxypyridine-3-carboxylate (31)



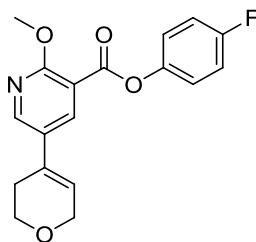
(a) 75 mg, 0.32 mmol; (b) 133 mg, 0.351 mmol; (c) 0.11 mL, 0.64 mmol; (d) *o*-nitrophenol **52** (49 mg, 0.35 mmol); (e) 2 mL; (f) 1 h; (g) MDAP (formic acid modifier). Off-white solid (84 mg, 0.24 mmol, 74%). M.pt.: 127-130 °C. ν_{\max} (neat): 3096, 2943, 1756, 1526, 1350 cm^{-1} . ^1H NMR (400 MHz, CHLOROFORM-*d*) δ = 8.45 (1H, d, J = 2.7 Hz), 8.44 (1H, d, J = 2.7 Hz), 8.16 (1H, dd, J = 8.3, 1.5 Hz), 7.72 (1H, td, J = 7.8, 1.7 Hz), 7.46 (1H, td, J = 7.8, 1.7 Hz), 7.41 (1H, dd, J = 8.1, 1.2 Hz), 6.19 (1H, tt, J = 2.9, 1.5 Hz), 4.35 (2H, app. q, J = 2.9 Hz), 4.10 (3H, s), 3.97 (2H, t, J = 5.5 Hz), 2.57 - 2.51 (2H, m). ^{13}C NMR (101 MHz, CHLOROFORM-*d*) δ = 162.2, 162.1, 148.1, 144.1, 141.8, 138.5, 134.7, 130.2, 129.3, 126.7, 125.9, 125.5, 123.5, 111.6, 65.7, 64.2, 54.5, 26.9. LCMS (Method A): t_{R} = 1.12 min, $[\text{M}+\text{H}^+]$ 357.4, (100% purity). HRMS: ($\text{C}_{18}\text{H}_{17}\text{N}_2\text{O}_6$) $[\text{M}+\text{H}^+]$ requires 357.1081, found $[\text{M}+\text{H}^+]$ 357.1097.

***S*-Phenyl 5-(3,6-dihydro-2H-pyran-4-yl)-2-methoxypyridine-3-carbothioate (32)**



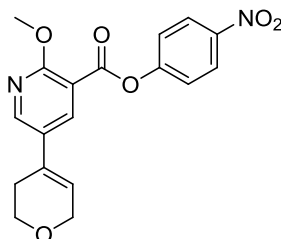
(a) 75 mg, 0.32 mmol; (b) 133 mg, 0.351 mmol; (c) 0.11 mL, 0.64 mmol; (d) thiophenol **51** (36 μL , 0.35 mmol); (e) 2 mL; (f) 30 min; (g) MDAP (formic acid modifier). Colourless gum (73 mg, 0.22 mmol, 70%). ν_{\max} (neat): 3053, 2926, 2851, 1650, 1475 cm^{-1} . ^1H NMR (400 MHz, CHLOROFORM-*d*) δ = 8.37 (1H, d, J = 2.4 Hz), 8.18 (1H, d, J = 2.4 Hz), 7.55 - 7.43 (5H, m), 6.15 (1H, tt, J = 2.9, 1.5 Hz), 4.33 (2H, app. q, J = 2.9 Hz), 4.13 (3H, s), 3.95 (2H, t, J = 5.5 Hz), 2.54 - 2.47 (2H, m). ^{13}C NMR (101 MHz, CHLOROFORM-*d*) δ = 188.4, 160.5, 147.1, 135.4, 134.9, 130.4, 129.5, 129.5, 129.2, 128.1, 123.3, 119.6, 65.7, 64.2, 54.2, 26.9. LCMS (Method A): t_{R} = 1.31 min, $[\text{M}+\text{H}^+]$ 328.1, (100% purity). HRMS: ($\text{C}_{18}\text{H}_{18}\text{NO}_3\text{S}$) $[\text{M}+\text{H}^+]$ requires 328.1002, found $[\text{M}+\text{H}^+]$ 328.1011.

4-Fluorophenyl 5-(3,6-dihydro-2H-pyran-4-yl)-2-methoxynicotinate (33)



(a) 50 mg, 0.21 mmol; (b) 90 mg, 0.24 mmol; (c) 74 μ L, 0.43 mmol; (d) *p*-fluorophenol **50** (26 mg, 0.23 mmol); (e) 1 mL; (f) 3 h; (g) automated column chromatography on silica gel (0-100% EtOAc:cyclohexane). Off-white solid (47 mg, 0.14 mmol, 67%). M.pt.: 146-149 °C. ν_{\max} (neat): 2929, 2836, 1725, 1606, 1561, 1510, 1480 cm^{-1} . ^1H NMR (400 MHz, CHLOROFORM-*d*) δ = 8.42 (1H, d, J = 2.7 Hz), 8.34 (1H, d, J = 2.7 Hz), 7.22 - 7.09 (4H, m), 6.17 (1H, tt, J = 2.9, 1.5 Hz), 4.35 (2H, app. q, J = 2.9 Hz), 4.09 (3H, s), 3.97 (2H, t, J = 5.5 Hz), 2.56 - 2.51 (2H, m). ^{13}C NMR (101 MHz, CHLOROFORM-*d*) δ = 163.4, 162.1, 160.4 (1C, d, J = 244.3 Hz), 147.7, 146.6 (1C, d, J = 2.9 Hz), 138.0, 130.4, 129.2, 123.3 (2C, d, J = 15.4 Hz), 123.1, 116.1 (2C, d, J = 23.5 Hz), 112.4, 65.7, 64.2, 54.4, 27.0. ^{19}F NMR (376 MHz, CHLOROFORM-*d*) δ = -116.8 (1F, s). LCMS (Method A): t_{R} = 1.19 min, $[\text{M}+\text{H}^+]$ 330.4, (100% purity). HRMS: ($\text{C}_{18}\text{H}_{17}\text{FNO}_4$) $[\text{M}+\text{H}^+]$ requires 330.1136, found $[\text{M}+\text{H}^+]$ 330.1131.

4-Nitrophenyl 5-(3,6-dihydro-2H-pyran-4-yl)-2-methoxynicotinate (54)

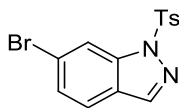


To a solution of 5-(3,6-dihydro-2H-pyran-4-yl)-2-methoxynicotinic acid **40** (50 mg, 0.21 mmol), in DCM (2 mL) stirred under nitrogen at 0 °C was added solid *p*-nitrophenol **53** (60 mg, 0.43 mmol) and 4-dimethylaminopyridine (DMAP) (5 mg, 0.04 mmol). *N,N'*-dicyclohexylcarbodiimide (DCC) (50 mg, 0.24 mmol) was then added and the reaction mixture was stirred at 0 °C for 5 min, then at room temperature. Further DMAP (2 mg, 0.02 mmol), *p*-nitrophenol (30 mg, 0.22 mmol) and DCC (25 mg, 0.12 mmol) were added after 22 h to force the reaction to completion. After 2 further hours of reaction, the precipitated urea was filtered off, washed with DCM and the filtrate concentrated *in vacuo*. The residue was dissolved in DCM and filtered to remove any precipitate before being washed twice with

aqueous HCl (0.5 M) and twice with saturated NaHCO₃ solution. The organic layer was dried through a hydrophobic frit, and the solvent removed *in vacuo*. The sample was dissolved in DMSO (6 mL) and filtered to remove insoluble material. The filtrate was purified by MDAP (formic acid modifier), the desired fractions combined and the solvent evaporated by nitrogen blow-down to afford the title product as a white solid. The remaining solid from filtration was found to also correspond to the required product. This was washed off the filter with DCM, and dried by nitrogen blow-down to afford the title product as a white solid (total yield 48 mg, 0.13 mmol, 63%). M.pt.: 171-172 °C. ν_{\max} (neat): 2931, 1758, 1601, 1562, 1517, 1488, 1345 cm⁻¹. ¹H NMR (400 MHz, CHLOROFORM-d) δ = 8.45 (1H, d, J = 2.4 Hz), 8.36 (1H, d, J = 2.4 Hz), 8.33 (2H, dd, J = 7.1, 2.0), 7.43 (2H, dd, J = 7.1, 2.0), 6.22 - 6.17 (1H, m), 4.35 (2H, app. q, J = 2.7 Hz), 4.11 (3H, s), 3.97 (2H, t, J = 5.5 Hz), 2.58 - 2.51 (2H, m). ¹³C NMR (101 MHz, CHLOROFORM-d) δ = 162.4, 162.2, 155.5, 148.4, 145.5, 138.1, 130.2, 129.3, 125.2, 123.6, 122.7, 111.6, 65.7, 64.2, 54.5, 27.0. LCMS (Method A): t_R = 1.18 min, [M+H⁺] = 357.4, (96% purity). HRMS: (C₁₈H₁₇N₂O₆) [M+H⁺] requires 357.1081, found [M+H⁺] 357.1083.

Synthesis of the Truncated Indazole Series

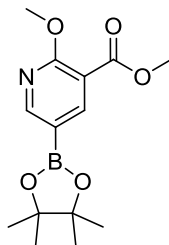
6-Bromo-1-tosyl-1H-indazole (42)²⁹³



To a solution of 6-bromo-1H-indazole **41** (3.00 g, 15.2 mmol, 75% pure by LCMS) in DMF (45 ml) stirred under nitrogen at 0 °C was added sodium hydride (60% w/w in oil) (1.25 g, 31.3 mmol) portionwise. The reaction was left to stir in ice for 10 min and then tosyl chloride (5.80 g, 30.4 mmol) was added portionwise. The reaction was left to warm to room temperature and, after 15 min, LCMS showed full conversion to product. The reaction was poured into iced water (100 mL) and the product extracted with EtOAc (3 x 75 mL). Solids formed in the organic washings, which were then concentrated *in vacuo*. Iced water (50 mL) was added to the flask, and the suspension isolated by filtration. The flask was rinsed with further iced water (2 x 50 mL), the cake sucked dry, and then dried in a vacuum oven at 40 °C to give the crude product. The solid was purified by automated column chromatography on silica gel (0-50% EtOAc:cyclohexane) to afford the title product as a yellow solid (3.75 g, 10.7 mmol, 94%). M.pt.: 148-150 °C. ν_{\max} (neat): 3110, 2920, 2330, 1739, 1604, 1375, 1172 cm⁻¹. ¹H NMR (400 MHz, CHLOROFORM-d) δ = 8.46 - 8.40 (1H, m), 8.14 (1H, d, J = 1.0 Hz), 7.92 - 7.87 (2H, m),

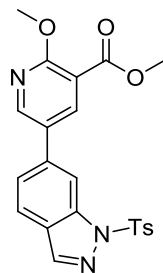
7.55 (1H, dd, $J = 8.6, 0.5$ Hz), 7.45 (1H, dd, $J = 8.4, 1.6$ Hz), 7.28 (2H, d, $J = 8.1$ Hz), 2.39 (3H, s). ^{13}C NMR (101 MHz, CHLOROFORM- d) $\delta = 145.7, 140.9, 140.8, 134.4, 130.0, 127.8, 127.7, 124.5, 123.9, 122.2, 116.3, 21.7$. LCMS (Method A): $t_{\text{R}} = 1.32$ min, $[\text{M}+\text{H}^+]$ 351.2 (94% purity). HRMS: ($\text{C}_{14}\text{H}_{12}^{79}\text{BrN}_2\text{O}_2\text{S}$) $[\text{M}+\text{H}^+]$ requires 350.9797, found $[\text{M}+\text{H}^+]$ 350.9810.

Methyl 2-methoxy-5-(4,4,5,5-tetramethyl-1,3,2-dioxaborolan-2-yl)nicotinate (43)²⁹⁴



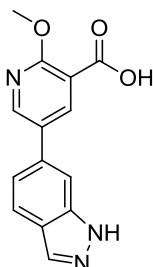
A flask was charged with methyl 5-bromo-2-methoxynicotinate **37** (1.55 g, 6.30 mmol), 4,4,4',4',5,5,5',5'-octamethyl-2,2'-bi(1,3,2-dioxaborolane) (2.00 g, 8.00 mmol), $\text{PdCl}_2(\text{dppf})$ (0.234 g, 0.320 mmol) and potassium acetate (1.855 g, 18.90 mmol). The vessel was evacuated and purged with nitrogen three times, then anhydrous DMF (30 mL) was added. The reaction was heated at 80 °C for 2 h, and then cooled to room temperature. The reaction was then filtered through celite and diluted with EtOAc (50 mL) before being washed with aqueous LiCl solution (5%, 8 x 10 mL). The organics were dried through a hydrophobic frit, concentrated *in vacuo* and purified by automated column chromatography on silica gel (0-100% EtOAc:cyclohexane, DCM). Desired fractions were collected and the solvent removed *in vacuo* to afford the title product as a white powder (1.55 g, 5.28 mmol, 84% yield). M.pt.: 127-129 °C. v_{max} (neat): 2977, 1738, 1600, 1561 cm^{-1} . ^1H NMR (400 MHz, CHLOROFORM- d) $\delta = 8.65$ (1H, d, $J = 2.0$ Hz), 8.50 (1H, d, $J = 2.0$ Hz), 4.08 (3H, s), 3.90 (3H, s), 1.35 (12H, s). ^{13}C NMR (101 MHz, CHLOROFORM- d) $\delta = 165.4, 164.2, 157.4, 147.2, 113.5, 84.1, 54.3, 52.1, 24.8$ (C attached to B not observed due to B quadrupole). LCMS (Method A): $t_{\text{R}} = 1.20$ min, $[\text{M}+\text{H}^+]$ 294.2, (95% purity). HRMS: (Calc. for hydrolysed boronic ester $\text{C}_8\text{H}_{11}\text{O}_5\text{N}^{11}\text{B}$) $[\text{M}+\text{H}^+]$ requires 212.0725, found $[\text{M}+\text{H}^+]$ 212.0722.

Methyl 2-methoxy-5-(1-tosyl-1H-indazol-6-yl)nicotinate (44)



A round-bottomed flask was charged with methyl 2-methoxy-5-(4,4,5,5-tetramethyl-1,3,2-dioxaborolan-2-yl)nicotinate **43** (1.25 g, 4.26 mmol), 6-bromo-1-tosyl-1H-indazole **42** (1 g, 3 mmol), PdCl₂(dppf) (0.21 g, 0.29 mmol), and sodium carbonate (0.905 g, 8.54 mmol) in 1,4-dioxane (20 mL) and water (5 mL). The vessel was purged with nitrogen and heated at 80 °C for 1 h. The reaction was cooled to room temperature, filtered through celite, washed with methanol and concentrated *in vacuo*. The residue was taken up in EtOAc (75 mL) and water (15 mL). The layers were separated and the organic washed with water (2 x 20 mL) and brine (1 x 20 mL). The organics were dried through a hydrophobic frit and concentrated *in vacuo*. The residue was purified by automated column chromatography on silica gel (0-100% EtOAc:cyclohexane, DCM) to afford the title product as a brown solid (1.19 g, 2.72 mmol, 96% yield). M.pt.: 140-145 °C (decomp) and 161-164 °C (decomp) (sample impure). ν_{\max} (neat) 2954, 1731, 1375, 1172 cm⁻¹. ¹H NMR (400 MHz, CHLOROFORM-d) δ = 8.64 (1H, d, *J* = 2.9 Hz), 8.47 - 8.45 (1H, m), 8.39 - 8.36 (1H, m), 8.21 (1H, s), 7.90 (2H, d, *J* = 8.3 Hz), 7.77 (1H, dd, *J* = 8.3, 1.0 Hz), 7.52 (1H, dd, *J* = 8.3, 1.5 Hz), 7.27 (2H, d, *J* = 8.3 Hz), 4.14 (3H, s), 3.98 (3H, s), 2.37 (3H, s). ¹³C NMR (101 MHz, CHLOROFORM-d) δ = 165.3, 162.2, 149.3, 148.2, 145.5, 141.0, 140.2, 138.3, 134.6, 129.9, 129.3, 127.6, 125.2, 123.6, 122.0, 114.0, 111.0, 54.5, 52.5, 21.6. LCMS (Method A): *t*_R = 1.27 min, [M+H⁺] 438.4, (91% purity). HRMS: (C₂₂H₂₀N₃O₅S) [M+H⁺] requires 438.1118, found [M+H⁺] 438.1123.

5-(1H-Indazol-6-yl)-2-methoxynicotinic acid (45)



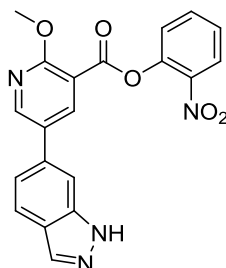
To a stirred solution of methyl 2-methoxy-5-(1-tosyl-1H-indazol-6-yl)nicotinate **44** (1.1 g, 2.5 mmol) in methanol (35 mL) was added sodium hydroxide (5 M, 2.50 mL, 12.5 mmol). The reaction was heated at reflux for 30 min, then cooled to room temperature and concentrated *in vacuo*, before EtOAc (15 mL) and water (15 mL) were added. The residue did not dissolve, and the solid was collected by buchner filtration, washed with EtOAc and water then dried in a vacuum oven at 40 °C for 1 h to afford the crude acid (440 mg). Further filtration of the filtrate afforded more solid (212 mg). Both solids were combined to provide the crude product (652 mg, 2.42 mmol, 96%) which was used without further purification. M.pt.: 210-212 °C (decomp.). ν_{\max} (neat): 3236, 2961, 1619, 1583, 1562, 1405, 1382 cm^{-1} . ^1H NMR (600 MHz, DMSO- d_6) δ = 13.38 (1H, br. s), 8.34 (1H, s), 8.06 (1H, s), 8.00 (1H, d, J = 5.5 Hz), 7.81 (1H, d, J = 8.4 Hz), 7.66 (1H, s), 7.35 (1H, d, J = 8.4 Hz), 3.86 (3H, s) (carboxylic acid proton not observed). ^{13}C NMR (151 MHz, DMSO- d_6) δ = 168.8, 159.8, 142.7, 140.7, 135.9, 135.4, 133.3, 129.2, 126.5, 122.0, 121.1, 119.6, 107.2, 53.1. LCMS (Method A): t_R = 0.77 min, $[\text{M}+\text{H}^+]$ 270.0 (93% purity). HRMS: ($\text{C}_{14}\text{H}_{12}\text{N}_3\text{O}_3$) $[\text{M}+\text{H}^+]$ requires 270.0873, found $[\text{M}+\text{H}^+]$ 270.0886.

General procedure for HATU couplings of 45 to afford esters 34-36

To a stirred solution of 5-(1H-indazol-6-yl)-2-methoxynicotinic acid **45** (1 eq) in DMF was added HATU (1.1 eq) and base (DIPEA or triethylamine) (2 eq). The reaction was stirred for 10 min at room temperature, before phenol/thiol (1.1 eq) was added. The reaction was left to stir at room temperature and monitored by LCMS. Upon completion of the reaction, the mixture was diluted with ether or DCM and washed with aqueous LiCl solution (5%). The organics were dried through a hydrophobic frit, concentrated *in vacuo* and purified by MDAP.

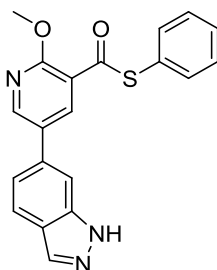
Following this general procedure, data for compounds **34-36** are presented as (a) amount of compound **45**; (b) amount of HATU; (c) base, and volume used; (d) amount of phenol/thiol; (e) volume of DMF; (f) reaction time; (g) purification system.

2-Nitrophenyl 5-(1H-indazol-6-yl)-2-methoxynicotinate (34)



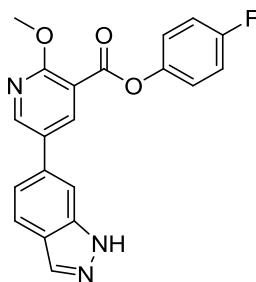
(a) 25 mg, 0.093 mmol; (b) 39 mg, 0.10 mmol; (c) triethylamine (26 μ L, 0.19 mmol); (d) *o*-nitrophenol **52** (14 mg, 0.10 mmol); (e) 1 mL; (f) 1 h; (g) MDAP (formic acid modifier, no workup). White solid (23 mg, 0.06 mmol, 63%). M.pt.: 189-190 $^{\circ}$ C. ν_{\max} (neat): 3231, 1760, 1606, 1527, 1342 cm^{-1} . ^1H NMR (400 MHz, DMSO- d_6) δ = 13.20 (1H, br. s), 8.91 (1H, d, J = 2.7 Hz), 8.73 (1H, d, J = 2.4 Hz), 8.23 (1H, dd, J = 8.2, 1.3 Hz), 8.13 (1H, s), 7.95 - 7.87 (2H, m), 7.85 (1H, s), 7.68 (1H, dd, J = 8.1, 0.9 Hz), 7.62 (1H, td, J = 7.8, 1.2 Hz), 7.48 (1H, dd, J = 8.6, 1.2 Hz), 4.06 (3H, s). ^{13}C NMR (101 MHz, DMSO- d_6) δ = 161.56, 161.29, 150.50, 143.09, 141.55, 140.34, 135.58, 133.51, 129.80, 127.47, 125.71, 125.56, 122.39, 121.36, 119.59, 119.14, 119.10, 111.26, 107.85, 54.27 (two decimal places are required to differentiate signals). LCMS (Method A): t_R = 1.12 min, $[\text{M}+\text{H}^+]$ 391.4, (99% purity). HRMS: ($\text{C}_{20}\text{H}_{15}\text{N}_4\text{O}_5$) $[\text{M}+\text{H}^+]$ requires 391.1037, found $[\text{M}+\text{H}^+]$ 391.1036.

S-Phenyl 5-(1*H*-indazol-6-yl)-2-methoxypyridine-3-carbothioate (**35**)



(a) 85 mg, 0.32 mmol; (b) 133 mg, 0.350 mmol; (c) DIPEA, (110 μ L, 0.631 mmol); (d) thiophenol **51** (36 μ L, 0.35 mmol); (e) 3 mL; (f) 18 h, another equivalent of HATU, DIPEA and thiophenol were added after 2 h to force reaction to completion; (g) MDAP (formic acid modifier, no workup). Off-white solid (35 mg, 0.01 mmol, 31%). M.pt.: 176-179 $^{\circ}$ C (decomp). ν_{\max} (neat): 3184, 2957, 1650, 1477 cm^{-1} . ^1H NMR (400 MHz, DMSO- d_6) δ = 8.81 (1H, d, J = 2.7 Hz), 8.43 (1H, d, J = 2.4 Hz), 8.12 (1H, s), 7.88 (1H, d, J = 8.3 Hz), 7.82 (1H, s), 7.59 - 7.49 (5H, m), 7.45 (1H, dd, J = 8.6, 1.5 Hz), 4.08 (3H, s) (indazole N-H not observed). ^{13}C NMR (101 MHz, DMSO- d_6) δ = 187.54, 159.50, 149.28, 140.44, 137.17, 134.75, 133.65, 133.38, 133.35, 130.00, 129.72, 129.33, 127.43, 122.36, 121.30, 119.60, 107.86, 54.18 (2 decimal places required to distinguish signals). LCMS (Method A): t_R = 1.26 min, $[\text{M}+\text{H}^+]$ 362.4, (100% purity). HRMS: ($\text{C}_{20}\text{H}_{16}\text{N}_3\text{O}_2\text{S}$) $[\text{M}+\text{H}^+]$ requires 362.0958, found $[\text{M}+\text{H}^+]$ 362.0975.

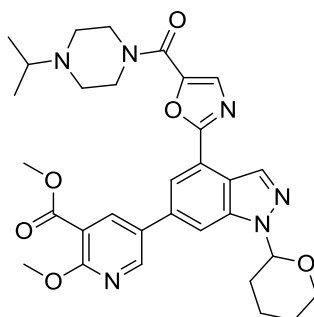
4-Fluorophenyl 5-(1H-indazol-6-yl)-2-methoxynicotinate (36)



(a) 20 mg, 0.07 mmol; (b) 31 mg, 0.08 mmol; (c) triethylamine (21 μ L, 0.15 mmol); (d) *p*-fluorophenol **50** (9 mg, 0.08 mmol); (e) 1 mL; (f) 3 h; (g) MDAP (formic acid modifier, no workup). White solid (8 mg, 0.02 mmol, 29%). M.pt.: 179-182 $^{\circ}$ C. ν_{\max} (neat): 3352, 1737, 1604, 1503, 1474 cm^{-1} . ^1H NMR (400 MHz, METHANOL- d_4) δ = 8.72 (1H, d, J = 2.4 Hz), 8.64 (1H, d, J = 2.7 Hz), 8.08 (1H, s), 7.88 (1H, d, J = 8.6 Hz), 7.77 (1H, s), 7.44 (1H, d, J = 8.6 Hz), 7.33 - 7.23 (2H, m), 7.22 - 7.14 (2H, m), 4.10 (3H, s) (indazole N-H not observed). ^{13}C NMR (151 MHz, DMSO- d_6) δ = 161.9 (1C, d, J = 244.0 Hz), 160.5, 158.9, 149.6, 146.5 (1C, d, J = 3.0 Hz), 140.2, 140.0, 133.7, 133.4, 129.6, 123.7 (2C, d, J = 8.8 Hz), 122.3, 121.3, 119.6, 116.1 (2C, d, J = 23.2 Hz), 112.7, 107.7, 54.1. ^{19}F NMR (376 MHz, METHANOL- d_4) δ = -119.1 (1F, s). LCMS (Method A): t_{R} = 1.15 min, $[\text{M}]^{-}$ 362.3, (100% purity). HRMS: ($\text{C}_{20}\text{H}_{15}\text{FN}_3\text{O}_3$) $[\text{M}+\text{H}^+]$ requires 364.1092, found $[\text{M}+\text{H}^+]$ 364.1093.

Synthesis of Elaborated Indazole Compounds Possessing Amide Side-Chain

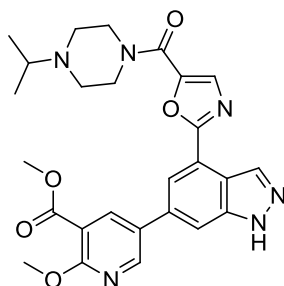
Methyl 5-(4-(5-(4-isopropylpiperazine-1-carbonyl)oxazol-2-yl)-1-(tetrahydro-2H-pyran-2-yl)-1H-indazol-6-yl)-2-methoxynicotinate (62)



A flask was charged with (4-isopropylpiperazin-1-yl)(2-(1-(tetrahydro-2H-pyran-2-yl)-6-(4,4,5,5-tetramethyl-1,3,2-dioxaborolan-2-yl)-1H-indazol-4-yl)oxazol-5-yl)methanone **61** (4.91 g, 8.94 mmol), methyl 5-bromo-2-methoxynicotinate **37** (2.00 g, 8.13 mmol), $\text{PdCl}_2(\text{dppf})$ (0.595 g, 0.813 mmol), and Na_2CO_3 (2.58 g, 24.4 mmol). 1,4-Dioxane (100 mL)

and water (25 mL) were then added and the reaction stirred. The vessel was degassed and purged with nitrogen three times and then heated at 80 °C for 30 min. The reaction was cooled to room temperature, filtered through celite and concentrated *in vacuo*. The residue was taken up in EtOAc (100 mL) and water (20 mL). The layers were separated and the organic phase washed with water (3 x 20 mL) and brine (3 x 20 mL). The organic layer was dried using a hydrophobic frit and concentrated *in vacuo*. The residue was purified by automated column chromatography on silica gel (0-30% EtOH:EtOAc). Desired fractions were combined and the solvent removed *in vacuo* to afford the product as a brown foam (4.5 g, 7.6 mmol, 94%). M.pt.: 160-161 °C (decomp). ν_{\max} (neat): 2947, 1733, 1713, 1627, 1420 cm^{-1} . ^1H NMR (400 MHz, CHLOROFORM-*d*) δ = 8.69 (1H, s), 8.66 (1H, d, J = 2.4 Hz), 8.50 (1H, d, J = 2.4 Hz), 8.15 (1H, d, J = 1.0 Hz), 7.89 - 7.86 (1H, m), 7.76 (1H, s), 5.86 (1H, dd, J = 9.0, 2.4 Hz), 4.14 (3H, s), 4.09-4.02 (1H, m), 3.97 (3H, s), 3.88 (4H, br. s), 3.84 - 3.76 (1H, m), 2.78 (1H, spt, J = 6.5 Hz) 2.69 - 2.60 (4H, m), 2.26 - 2.12 (2H, m), 1.90 - 1.57 (4H, m), 1.08 (6H, d, J = 6.6 Hz). ^{13}C NMR (126 MHz, CHLOROFORM-*d*) δ = 165.35, 162.09, 161.20, 157.39, 149.20, 144.87, 140.64, 140.18, 135.63, 134.12, 133.41, 129.23, 120.86, 120.56, 119.94, 113.90, 110.98, 85.62, 67.48, 54.54, 54.48, 52.46, 48.70 (2C, br. s), 47.06 (1C, br. s), 43.10 (1C, br. s), 29.44, 25.07, 22.38, 18.38 (two decimal places required to distinguish signals). LCMS (Method A): t_{R} = 0.79 min, $[\text{M}+\text{H}^+]$ 589.2 (96% purity). HRMS: ($\text{C}_{31}\text{H}_{37}\text{N}_6\text{O}_6$) $[\text{M}+\text{H}^+]$ requires 589.2769, found $[\text{M}+\text{H}^+]$ 589.2764.

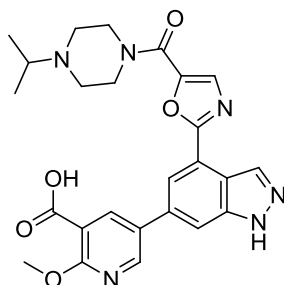
Methyl 5-(4-(5-(4-isopropylpiperazine-1-carbonyl)oxazol-2-yl)-1H-indazol-6-yl)-2-methoxynicotinate (66)



To a flask containing methyl 5-(4-(5-(4-isopropylpiperazine-1-carbonyl)oxazol-2-yl)-1-(tetrahydro-2H-pyran-2-yl)-1H-indazol-6-yl)-2-methoxynicotinate **62** (50 mg, 0.085 mmol) in anhydrous methanol (1 mL) under nitrogen was added chlorotrimethylsilane (TMSCl) (0.10 mL, 0.78 mmol). The reaction was stirred at room temperature for 18 h. Triethylamine (0.118 mL, 0.849 mmol) and methanol (1 mL) were added and the reaction heated to 60 °C to

dissolve the remaining solid. The reaction was then allowed to cool slowly. Poor precipitation was observed, and the solvent was removed *in vacuo*. The residue was purified by automated column chromatography on silica gel (0-35% EtOH:EtOAc). Desired fractions were combined and the solvent removed *in vacuo* to afford the product as an off-white solid (40 mg, 0.079 mmol, 93%). M.pt.: 154-160 °C. ν_{\max} (neat): 3208, 2954, 1736, 1705, 1606, 1564, 1479 cm^{-1} . ^1H NMR (400 MHz, CHLOROFORM-*d*) δ = 8.76 (1H, d, J = 1.0 Hz), 8.62 (1H, d, J = 2.7 Hz), 8.47 (1H, d, J = 2.7 Hz), 8.13 (1H, d, J = 1.2 Hz), 7.80 - 7.77 (1H, m), 7.75 (1H, s), 4.13 (3H, s), 3.96 (3H, s), 3.90 (4H, br. s), 2.79 (1H, spt, J = 6.6 Hz), 2.72 - 2.57 (4H, m), 1.09 (6H, d, J = 6.6 Hz) (indazole N-H not observed). ^{13}C NMR (151 MHz, CHLOROFORM-*d*) δ = 165.3, 162.1, 161.3, 157.5, 149.0, 144.8, 141.4, 140.1, 135.9, 135.4, 133.2, 129.0, 120.3, 119.9, 119.5, 113.9, 110.4, 54.6, 54.5, 52.5, 48.6 (2C, br. s), 47.1 (br. s), 43.1 (br. s), 18.4. LCMS (Method A): t_{R} = 0.58 min, $[\text{M}+\text{H}^+]$ 505.3 (95% purity). HRMS: ($\text{C}_{26}\text{H}_{29}\text{N}_6\text{O}_5$) $[\text{M}+\text{H}^+]$ requires 505.2194, found $[\text{M}+\text{H}^+]$ 505.2205.

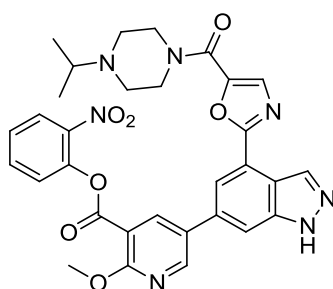
5-(4-(5-(4-isopropylpiperazine-1-carbonyl)oxazol-2-yl)-1H-indazol-6-yl)-2-methoxynicotinic acid (65)



To a flask containing methyl 5-(4-(5-(4-isopropylpiperazine-1-carbonyl)oxazol-2-yl)-1-(tetrahydro-2H-pyran-2-yl)-1H-indazol-6-yl)-2-methoxynicotinate **62** (800 mg, 1.36 mmol) in anhydrous methanol (30 mL) under nitrogen was added TMSCl (1.75 mL, 13.7 mmol). The reaction was stirred at 40 °C for 2 h, before aqueous NaOH (2 M, 6.80 mL, 13.6 mmol) was added slowly to neutralise the reaction, and the *pH* adjusted to 11 by the addition of more aqueous NaOH (2 M). The reaction was heated to 65 °C for 19 h then cooled to room temperature and the solvent removed *in vacuo*. The residue was purified by automated reverse phase column chromatography on C18 silica gel (5-95% acetonitrile:10 mM ammonium bicarbonate in water adjusted to *pH* 10 with ammonia, 1:1 water:DMSO slurry). Desired fractions were combined and the solvent removed *in vacuo* to afford the product as a brown solid (511 mg, 1.04 mmol, 77%). M.pt.: 202-205 °C (decomp). ν_{\max} (neat): 2961, 2856, 1737, 1713, 1622, 1604, 1472 cm^{-1} . ^1H NMR (400 MHz, DMSO-*d*₆) δ = 13.65 (1H, br. s), 8.64

(1H, d, $J = 2.7$ Hz), 8.53 (1H, s), 8.26 (1H, d, $J = 2.4$ Hz), 8.02 (1H, d, $J = 1.2$ Hz), 7.97 (1H, s), 7.94 (1H, s), 3.95 (3H, s), 3.73 (4H, br. s), 2.72 (1H, spt, $J = 6.4$ Hz), 2.54 (4H, s), 0.99 (6H, d, $J = 6.6$ Hz) (carboxylic acid proton not seen). ^{13}C NMR (126 MHz, DMSO- d_6) $\delta = 167.30, 161.11, 161.08, 157.08, 146.54, 144.83, 141.77, 138.26, 135.26, 133.62, 133.09, 128.82, 119.43, 119.12, 118.88, 111.47, 109.99, 54.21, 54.04, 48.85$ (2C, br. s), 47.16 (br. s), 43.08 (br. s), 18.54 (two decimal places required to distinguish signals). LCMS (Method A): $t_R = 0.50$ min, $[\text{M}+\text{H}^+]$ 491.5, (93% purity). HRMS: ($\text{C}_{25}\text{H}_{27}\text{N}_6\text{O}_5$) $[\text{M}+\text{H}^+]$ requires 491.2037, found $[\text{M}+\text{H}^+]$ 491.2025.

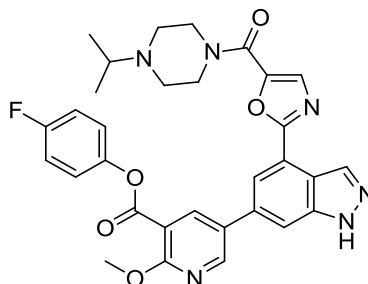
2-Nitrophenyl *5-(4-(5-(4-isopropylpiperazine-1-carbonyl)oxazol-2-yl)-1H-indazol-6-yl)-2-methoxynicotinate (67)*



To a stirred solution of 5-(4-(5-(4-isopropylpiperazine-1-carbonyl)oxazol-2-yl)-1H-indazol-6-yl)-2-methoxynicotinic acid **65** (50 mg, 0.10 mmol) in DMF (1 mL) was added HATU (43 mg, 0.11 mmol) and DIPEA (0.036 mL, 0.20 mmol). The mixture was stirred for 10 min at room temperature, before *o*-nitrophenol **52** (16 mg, 0.12 mmol) was added, and the reaction left to stir at room temperature for 30 min. The reaction was diluted with DCM and washed with aqueous LiCl solution (5%, 3 x 5 mL). The organics were dried through a hydrophobic frit, concentrated *in vacuo* and the residue purified by automated column chromatography on silica gel (0-50% EtOH:EtOAc, EtOAc). Desired fractions were combined, and the solvent removed *in vacuo* to give the product as an off-white solid (11 mg, 0.02 mmol, 18%). M.pt.: 135-138 °C (decomp). ν_{max} (neat): 2965, 1759, 1630, 1605, 1530, 1477, 1346 cm^{-1} . ^1H NMR (400 MHz, CHLOROFORM- d) $\delta = 8.77 - 8.75$ (1H, m), 8.70 (2H, s), 8.16 (1H, dd, $J = 8.1, 1.5$ Hz), 8.14 (1H, d, $J = 1.2$ Hz), 7.83 - 7.80 (1H, m), 7.76 (1H, s), 7.75 - 7.70 (1H, m), 7.49 - 7.42 (2H, m), 4.14 (3H, s), 3.90 (4H, br. s), 2.77 (1H, spt, $J = 6.4$ Hz), 2.69 - 2.61 (4H, m), 1.07 (6H, d, $J = 6.6$ Hz) (indazole N-H not observed). ^{13}C NMR (126 MHz, CHLOROFORM- d) $\delta = 162.8, 162.0, 161.2, 157.4, 150.5, 144.9, 144.1, 141.8, 141.3, 141.0, 135.6, 135.4, 134.9, 133.4, 129.3, 126.9, 125.9, 125.6, 120.2, 120.0, 119.6, 112.0, 110.7, 54.7, 54.6, 48.6$ (2C, br. s), 47.0 (br. s),

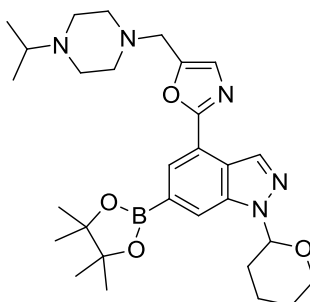
43.3 (br. s), 18.3. LCMS (Method A): $t_R = 0.74$ min, $[M+H]^+$ 612.4, (100% purity). HRMS: ($C_{31}H_{30}N_7O_7$) $[M+H]^+$ requires 612.2201, found $[M+H]^+$ 612.2180.

4-Fluorophenyl *5-(4-(5-(4-isopropylpiperazine-1-carbonyl)oxazol-2-yl)-1H-indazol-6-yl)-2-methoxynicotinate (68)*



To a stirred solution of 5-(4-(5-(4-isopropylpiperazine-1-carbonyl)oxazol-2-yl)-1H-indazol-6-yl)-2-methoxynicotinic acid **65** (100 mg, 0.204 mmol) in DMF (2 mL) was added HATU (85 mg, 0.22 mmol) and DIPEA (0.071 mL, 0.41 mmol). The mixture was stirred for 10 minutes at room temperature, before *p*-fluorophenol **50** (25 mg, 0.22 mmol) was added, and the reaction left to stir at room temperature for 3 h. The reaction was diluted with EtOAc (10 mL) and washed with aqueous LiCl solution (5%, 5 x 5 mL). The organics were dried through a hydrophobic frit, concentrated *in vacuo* and the residue purified by automated column chromatography on silica gel (0-30% EtOH:EtOAc, EtOAc). Desired fractions were combined, and the solvent removed *in vacuo* to give the product as an off-white solid (11 mg, 0.019 mmol, 9%). M.pt.: 181-184 °C. v_{max} (neat): 3130, 3055, 2964, 2876, 1720, 1629, 1505 cm^{-1} . 1H NMR (400 MHz, CHLOROFORM-*d*) $\delta = 8.77$ (1H, s), 8.69 (1H, d, $J = 2.7$ Hz), 8.63 (1H, d, $J = 2.7$ Hz), 8.16 (1H, s), 7.81 (1H, s), 7.74 (1H, s), 7.26 - 7.18 (2H, m), 7.18 - 7.08 (2H, m), 4.16 (3H, s), 3.89 (4H, br. s), 2.78 (1H, spt, $J = 6.6$ Hz), 2.70 - 2.59 (4H, m), 1.08 (6H, d, $J = 6.6$ Hz) (indazole N-H not seen). ^{13}C NMR (126 MHz, CHLOROFORM-*d*) $\delta = 163.2$, 162.6, 161.2, 160.4 (1C, d, $J = 245.1$ Hz), 157.5, 149.9, 146.5 (1C, d, $J = 3.7$ Hz), 144.7, 141.3, 140.5, 135.7, 135.4, 133.1, 129.1, 123.2 (2C, d, $J = 8.3$ Hz), 120.3, 120.0, 119.5, 116.2 (2C, d, $J = 23.1$ Hz), 112.9, 110.5, 54.7, 54.6, 48.6 (2C, br. s), 47.0 (br. s), 43.1 (br. s), 18.3. ^{19}F NMR (376 MHz, CHLOROFORM-*d*) $\delta = -116.66$ (1F, s). LCMS (Method A): $t_R = 0.76$ min, $[M+H]^+$ 585.5, (98% purity). HRMS: ($C_{31}H_{30}FN_6O_5$) $[M+H]^+$ requires 585.2256, found $[M+H]^+$ 585.2246.

5-((4-Isopropylpiperazin-1-yl)methyl)-2-(1-(tetrahydro-2H-pyran-2-yl)-6-(4,4,5,5-tetramethyl-1,3,2-dioxaborolan-2-yl)-1H-indazol-4-yl)oxazole (77)



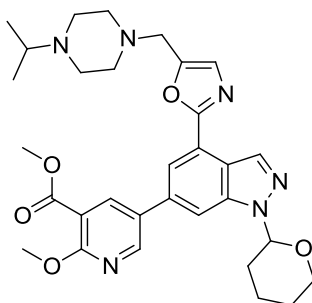
Zinc acetate conditions:

A heat gun-dried microwave vial was charged with zinc acetate (18 mg, 0.10 mmol) and purged with nitrogen. Anhydrous tetrahydrofuran (THF) (2 mL) and methyldiethoxysilane (0.5 mL, 3 mmol) were added and the mixture stirred at 65 °C for 30 min prior to the addition of (4-isopropylpiperazin-1-yl)(2-(1-(tetrahydro-2H-pyran-2-yl)-6-(4,4,5,5-tetramethyl-1,3,2-dioxaborolan-2-yl)-1H-indazol-4-yl)oxazol-5-yl)methanone **61** (549 mg, 1.00 mmol) in dry THF (1.5 mL) under nitrogen. The reaction was stirred at 65 °C for 60 h and then cooled to room temperature and stirred with NaOH (2 M, 5 mL) overnight. The product was extracted with EtOAc (3 x 5 mL). LCMS showed product in the organic layer, and boronic acid lost to the aqueous layer. The organics were dried through a hydrophobic frit, concentrated *in vacuo* and the product isolated by automated column chromatography on silica gel (0-25% MeOH:DCM, DCM). Desired fractions were combined and the solvent removed *in vacuo* to afford the product as a colourless oil (24 mg, 0.05 mmol, 5%). ν_{\max} (neat): 2971, 2935, 2815, 1487, 1448, 1391, 1143 cm^{-1} . ^1H NMR (600 MHz, CHLOROFORM-*d*) δ = 8.73 (1H, s), 8.29 (1H, s), 8.12 (1H, s), 7.15 (1H, s), 5.84 (1H, dd, J = 9.4, 2.8 Hz), 4.08 - 4.01 (1H, m), 3.80 (1H, m), 3.74 (2H, s), 2.84 (1H, spt, J = 6.2 Hz), 2.71 (7H, br. s), 2.68 - 2.57 (2H, m), 2.22 - 2.14 (1H, m), 2.11 - 2.03 (1H, m), 1.85 - 1.73 (2H, m), 1.69 - 1.63 (1H, m), 1.44 - 1.33 (12H, m), 1.10 (6H, d, J = 6.6 Hz). ^{13}C NMR (101 MHz, CHLOROFORM-*d*) δ = 161.2, 148.3, 139.9, 134.8, 127.6, 125.7, 122.9, 119.6, 118.5, 84.8, 84.2, 77.2, 67.6, 54.7, 52.3, 48.0, 29.6, 25.1, 24.9, 24.8, 22.7, 18.1. LCMS (Method A): t_{R} = 0.82 min, $[\text{M}+\text{H}^+]$ 536.6, (96% purity). HRMS: ($\text{C}_{29}\text{H}_{43}\text{O}_4\text{N}_5^{11}\text{B}$) $[\text{M}+\text{H}^+]$ requires 536.3403, found $[\text{M}+\text{H}^+]$ 536.3425.

RhH(CO)(PPh₃)₃ conditions:

To a flask containing (4-isopropylpiperazin-1-yl)(2-(1-(tetrahydro-2H-pyran-2-yl)-6-(4,4,5,5-tetramethyl-1,3,2-dioxaborolan-2-yl)-1H-indazol-4-yl)oxazol-5-yl)methanone **61** (93 mg, 0.17 mmol) and tris(triphenylphosphine)rhodium(I) carbonyl hydride (1.8 mg, 2.0 μmol) was added tetrahydrofuran (THF) (0.2 mL) and diphenylsilane (0.073 mL, 0.39 mmol). Effervescence was observed upon addition of the silane. The reaction was left to stir at room temperature for 17 h and then quenched by the addition of 1 mL EtOAc and 1 mL water. The layers were separated and the organics dried through a hydrophobic frit and concentrated *in vacuo*. The residue was purified by automated column chromatography on silica gel (0-20% MeOH:DCM, DCM). Desired fractions were combined and the solvent removed *in vacuo* to afford the product as a colourless gum (52 mg, 0.1 mmol, 57%). ν_{\max} (neat): 2967, 2931, 1451, 1390 cm⁻¹. ¹H NMR (400 MHz, CHLOROFORM-d) δ = 8.74 (1H, s), 8.30 (1H, s), 8.12 (1H, s), 7.14 (1H, s), 5.85 (1H, dd, *J* = 9.4, 2.6 Hz), 4.10 - 4.03 (1H, m), 3.85 - 3.77 (1H, m), 3.75 (2H, s), 2.73 - 2.56 (10H, m), 2.26 - 2.15 (1H, m), 2.12 - 2.03 (1H, m), 1.80 (2H, br. s), 1.73 - 1.65 (1H, m), 1.41 (12H, s), 1.05 (6H, d, *J* = 6.6 Hz). ¹³C NMR (126 MHz, CHLOROFORM-d) δ = 161.1, 148.6, 139.9, 134.8, 127.5, 125.7, 122.9, 119.7, 118.4, 84.8, 84.2, 67.7, 54.4, 53.1, 52.5, 48.5, 29.6, 25.1, 24.9, 24.9, 22.7, 18.6. LCMS (Method A): *t_R* = 0.89 min, [M+H⁺] 536.6, (100% purity). HRMS: (C₂₉H₄₃O₄N₅¹¹B) [M+H⁺] requires 536.3408, found [M+H⁺] 536.3409.

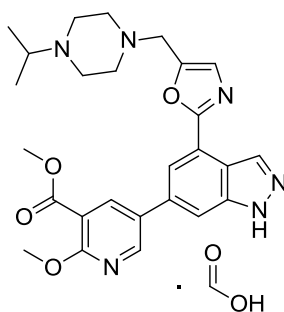
Methyl 5-(4-(5-((4-isopropylpiperazin-1-yl)methyl)oxazol-2-yl)-1-(tetrahydro-2H-pyran-2-yl)-1H-indazol-6-yl)-2-methoxynicotinate (63)



To a flask containing compound **62** (100 mg, 0.170 mmol) and tris(triphenylphosphine)rhodium(I) carbonyl hydride (1.8 mg, 2.0 μmol) was added THF (0.2 mL) and diphenylsilane (0.073 mL, 0.39 mmol). Effervescence was observed upon addition of the silane. The reaction was left to stir at room temperature. At 17 h, another portion of catalyst (2.0 mg, 2.2 μmol) and silane (0.075 mL, 0.40 mmol) were added. After a further 1.5 h, the reaction was diluted with 2 mL of diethyl ether and the product extracted to aqueous

HCl (1 M, 6 x 1 mL washings). The organic layer was discarded and the aqueous basified to pH 8 by the addition of sodium bicarbonate, and the product extracted with EtOAc (2 x 25 mL). The organic phases were combined, dried using a hydrophobic frit, concentrated *in vacuo* and the residue purified by automated column chromatography on silica gel (0-20% MeOH:DCM). Desired fractions were combined and the solvent removed *in vacuo* to afford the product as a brown gum (62 mg, 0.11 mmol, 64%). ν_{\max} (neat): 2954, 1728, 1468, 1420 cm^{-1} . $^1\text{H NMR}$ (400 MHz, CHLOROFORM- d) δ = 8.72 (1H, s), 8.67 (1H, d, J = 2.7 Hz), 8.51 (1H, d, J = 2.7 Hz), 8.07 (1H, d, J = 1.2 Hz), 7.82 - 7.78 (1H, m), 7.18 (1H, s), 5.84 (1H, dd, J = 8.9, 2.6 Hz), 4.13 (3H, s), 4.08 - 4.01 (1H, m), 3.97 (3H, s), 3.84 - 3.79 (1H, m), 3.78 (2H, s), 2.71 - 2.56 (9H, m), 2.25 - 2.11 (2H, m), 1.88 - 1.65 (4H, m), 1.05 (6H, d, J = 6.6 Hz). $^{13}\text{C NMR}$ (101 MHz, CHLOROFORM- d) δ = 165.46, 162.01, 160.61, 149.25, 149.10, 140.62, 140.24, 135.56, 134.59, 129.59, 127.56, 120.98, 120.83, 119.55, 113.85, 109.92, 85.54, 67.38, 54.44, 54.40, 53.07, 52.45, 52.43, 48.54, 29.43, 25.11, 22.42, 18.62 (two decimal places required to distinguish signals). LCMS (Method A): t_{R} = 0.78 min, $[\text{M}+\text{H}^+]$ 575.6, (100% purity). HRMS: ($\text{C}_{31}\text{H}_{39}\text{N}_6\text{O}_5$) $[\text{M}+\text{H}^+]$ requires 575.2976, found $[\text{M}+\text{H}^+]$ 575.2958.

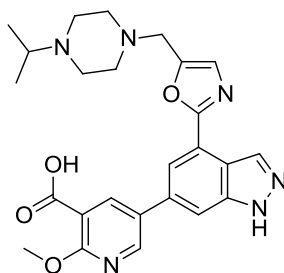
Methyl 5-(4-(5-((4-isopropylpiperazin-1-yl)methyl)oxazol-2-yl)-1H-indazol-6-yl)-2-methoxynicotinate, formic acid salt (58)



To a flask containing compound **63** (55 mg, 0.096 mmol) in anhydrous methanol (2 mL) under nitrogen was added chlorotrimethylsilane (TMSCl) (0.15 mL, 1.2 mmol). The reaction was stirred at 40 °C for 2 h. Triethylamine (0.164 mL, 1.17 mmol) was added to the vessel and the reaction cooled to room temperature. The solvent was removed *in vacuo* and the residue purified by automated column chromatography on silica gel, pretreated with triethylamine (0-15% MeOH:DCM). After evaporation of the desired fractions, the residue was further purified by MDAP (Method A). Desired fractions were combined and the solvent removed under a stream of nitrogen to afford the product as a white gum (42 mg, 0.08 mmol, 82%). ν_{\max} (neat): 3339, 2944, 1741, 1716, 1602, 1481 cm^{-1} . $^1\text{H NMR}$ (400 MHz, METHANOL- d_4) δ =

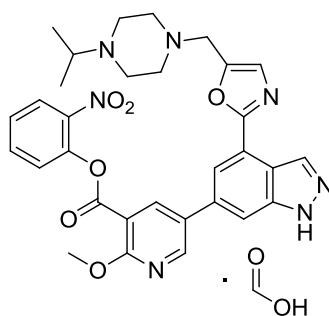
8.66 (1H, d, $J = 2.4$ Hz), 8.62 (1H, d, $J = 0.7$ Hz), 8.50 (1H, s), 8.46 (1H, d, $J = 2.7$ Hz), 8.01 (1H, d, $J = 1.2$ Hz), 7.85 (1H, s), 7.31 (1H, s), 4.06 (3H, s), 3.93 (3H, s), 3.90 (2H, s), 3.25 (1H, spt, $J = 6.4$ Hz), 3.13 (4H, br. s), 2.86 (4H, br. s), 1.27 (6H, d, $J = 6.6$ Hz) (indazole N-H not observed). ^{13}C NMR (126 MHz, METHANOL- d_4) $\delta = 169.9, 167.0, 163.4, 162.7, 150.3, 150.1, 143.1, 141.0, 136.8, 135.4, 130.6, 129.1, 121.5, 120.2, 120.1, 115.2, 111.5, 58.6, 54.9, 53.1, 52.4, 51.6, 49.6, 17.7$. LCMS (Method A): $t_R = 0.60$ min, $[\text{M}+\text{H}^+]$ 491.5, (100% purity). HRMS: ($\text{C}_{26}\text{H}_{31}\text{N}_6\text{O}_4$) $[\text{M}+\text{H}^+]$ requires 491.2401, found $[\text{M}+\text{H}^+]$ 491.2397.

5-(4-(5-((4-Isopropylpiperazin-1-yl)methyl)oxazol-2-yl)-1H-indazol-6-yl)-2-methoxynicotinic acid (64)



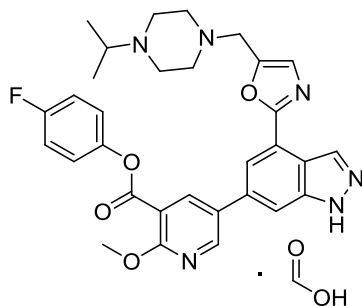
To a flask containing compound **63** (200 mg, 0.350 mmol) in anhydrous methanol (8 mL) under nitrogen was added TMSCl (0.45 mL, 3.5 mmol). The reaction was stirred at 40 °C for 16 h. Aqueous NaOH (2 M, 1.74 mL, 3.48 mmol) was then added slowly to neutralise the reaction, and the pH adjusted to pH 11 by the addition of more aqueous NaOH (2 M). The reaction was heated at 65 °C for 1 h, then cooled to room temperature and concentrated *in vacuo*. The residue was taken up in approximately 1:1 DMSO/water adjusted to pH 10 with ammonium bicarbonate and purified by automated reverse phase column chromatography on C18 silica gel (5-95% acetonitrile:water adjusted to pH 10 with ammonium bicarbonate). Desired fractions were collected and the solvent removed *in vacuo* to afford the product as a beige solid (153 mg, 0.321 mmol, 92%). M.pt.: 228-230 °C (decomp). ν_{max} (neat): 3122, 2945, 2831, 1742, 1604, 1580 cm^{-1} . ^1H NMR (400 MHz, DMSO- d_6) $\delta = 13.64$ (1H, br. s), 8.56 (1H, d, $J = 0.7$ Hz), 8.55 (1H, d, $J = 2.4$ Hz), 8.16 (1H, d, $J = 2.4$ Hz), 7.91 (1H, d, $J = 1.5$ Hz), 7.87 (1H, s), 7.32 (1H, s), 3.92 (3H, s), 3.74 (2H, s), 2.63 (1H, spt, $J = 6.4$ Hz), 0.96 (6H, d, $J = 6.6$ Hz) (carboxylic acid proton not seen, 8 piperazine H coincident with solvent peak, presence confirmed by HSQC). ^{13}C NMR (126 MHz, DMSO- d_6) $\delta = 167.3, 160.3, 159.8, 149.4, 144.9, 141.3, 137.0, 135.0, 133.4, 128.4, 127.3, 122.1, 119.5, 118.2, 117.8, 109.8, 53.6, 53.3, 52.3, 51.4, 47.8, 18.1$. LCMS (Method A): $t_R = 0.54$ min, $[\text{M}+\text{H}^+]$ 477.5, (100% purity). HRMS: ($\text{C}_{25}\text{H}_{29}\text{N}_6\text{O}_4$) $[\text{M}+\text{H}^+]$ requires 477.2245, found $[\text{M}+\text{H}^+]$ 477.2242.

2-Nitrophenyl *5-(4-(5-((4-isopropylpiperazin-1-yl)methyl)oxazol-2-yl)-1H-indazol-6-yl)-2-methoxynicotinate, formic acid salt (59)*



To a stirred solution of 5-(4-(5-((4-isopropylpiperazin-1-yl)methyl)oxazol-2-yl)-1H-indazol-6-yl)-2-methoxynicotinic acid **64** (40 mg, 0.084 mmol) in DMF (1 mL) was added HATU (35 mg, 0.092 mmol) and DIPEA (0.029 mL, 0.17 mmol). The mixture was stirred for 10 min at room temperature, before *o*-nitrophenol **52** (13 mg, 0.093 mmol) was added and the reaction left to stir at room temperature for 3 h. The reaction was purified, without workup, by MDAP (formic acid modifier). Desired fractions were combined, and the solvent removed under a stream of nitrogen to afford the product as an off-white gum (24 mg, 0.037 mmol, 44%). ν_{\max} (neat): 2928, 2853, 1756, 1603, 1528, 1476, 1346 cm^{-1} . $^1\text{H NMR}$ (400 MHz, CHLOROFORM-*d*) δ = 8.74 (1H, s), 8.73 - 8.71 (2H, m), 8.45 (s, 1H), 8.16 (1H, dd, J = 8.1, 1.5 Hz), 8.05 (1H, d, J = 1.2 Hz), 7.76 (1H, s), 7.72 (1H, dd, J = 7.8, 1.5 Hz), 7.49 - 7.43 (2H, m), 7.19 (1H, s), 4.15 (3H, s), 3.79 (2H, s), 3.35 (1H, spt, J = 6.6 Hz), 3.08 (4H, br. s), 2.92 (4H, br. s), 1.27 (6H, d, J = 6.6 Hz) (indazole N-H not observed). $^{13}\text{C NMR}$ (101 MHz, CHLOROFORM-*d*) δ = 166.9, 162.6, 162.1, 161.0, 150.5, 148.1, 144.1, 141.8, 141.3, 140.9, 135.3, 135.3, 134.8, 129.5, 128.0, 126.8, 125.9, 125.6, 120.7, 119.2, 116.3, 111.9, 109.9, 56.1, 54.6, 51.8, 49.4, 47.3, 16.9. LCMS (Method A): t_{R} = 0.73 min, $[\text{M}+\text{H}^+]$ 598.2, (96% purity). HRMS: ($\text{C}_{31}\text{H}_{32}\text{N}_7\text{O}_6$) $[\text{M}+\text{H}^+]$ requires 598.2409, found $[\text{M}+\text{H}^+]$ 598.2418.

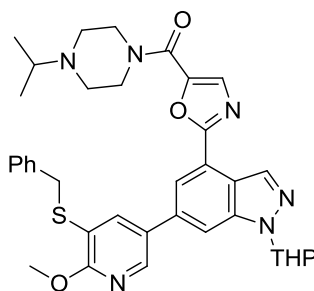
4-Fluorophenyl *5-(4-(5-((4-isopropylpiperazin-1-yl)methyl)oxazol-2-yl)-1H-indazol-6-yl)-2-methoxynicotinate, formic acid salt (60) (HATU Method)*



To a stirred solution of 5-(4-(5-((4-isopropylpiperazin-1-yl)methyl)oxazol-2-yl)-1H-indazol-6-yl)-2-methoxynicotinic acid **64** (50 mg, 0.11 mmol), in DMF (1 mL) was added HATU (44 mg, 0.12 mmol) and DIPEA (0.037 mL, 0.21 mmol). The reaction was left to stir at room temperature for 10 min prior to the addition of 4-fluorophenol **50** (13 mg, 0.12 mmol). The reaction was left to stir at room temperature for 1 h and then purified, without workup, by MDAP (formic acid modifier). Desired fractions were combined and the solvent removed *in vacuo* to afford the product as an off-white solid (14 mg, 0.023 mmol, 22%). M.pt.: 185-188 °C. ν_{\max} (neat): 2927, 2853, 1746, 1587, 1503, 1477 cm^{-1} . ^1H NMR (400 MHz, CHLOROFORM-*d*) δ = 8.74 (1H, s), 8.70 (1H, d, J = 2.7 Hz), 8.63 (1H, d, J = 2.4 Hz), 8.46 (s, 1H), 8.05 (1H, s), 7.74 (1H, s), 7.26 - 7.19 (3H, m), 7.16 - 7.08 (2H, m), 4.15 (3H, s), 3.80 (2H, s), 3.33 (1H, spt, J = 6.6 Hz), 3.07 (4H, br. s), 2.92 (4H, br. s), 1.26 (6H, d, J = 6.6 Hz) (indazole N-H not observed). ^{13}C NMR (101 MHz, CHLOROFORM-*d*) δ = 166.99, 162.44, 162.18 (1C, d, J = 239.9 Hz), 159.16, 159.11, 149.96, 148.15, 146.53 (1C, d, J = 3.7 Hz), 141.34, 140.52, 135.44, 135.35, 129.43, 128.00, 123.17 (2C, d, J = 8.1 Hz), 120.67, 119.36, 119.24, 116.14 (2C, d, J = 23.5 Hz), 112.91, 109.79, 56.01, 54.59, 51.88, 50.18, 47.28, 16.94 (two decimal places required to distinguish signals). ^{19}F NMR (376 MHz, CHLOROFORM-*d*) δ = -116.7 (1F, s). LCMS (Method A): t_{R} = 0.75 min, $[\text{M}+\text{H}^+]$ 571.2, (100% purity). HRMS: ($\text{C}_{31}\text{H}_{32}\text{FN}_6\text{O}_4$) $[\text{M}+\text{H}^+]$ requires 571.2464, found $[\text{M}+\text{H}^+]$ 571.2468.

Synthesis of Compounds Bearing an Electrophilic Sulfur Centre

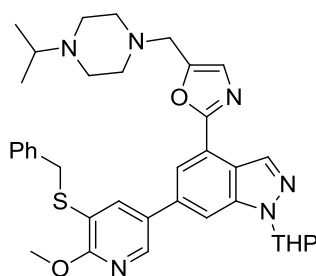
(2-(6-(5-(Benzylthio)-6-methoxypyridin-3-yl)-1-(tetrahydro-2H-pyran-2-yl)-1H-indazol-4-yl)oxazol-5-yl)(4-isopropylpiperazin-1-yl)methanone (**83**)



A microwave vial was charged with 3-(benzylthio)-5-chloro-2-methoxypyridine **82** (500 mg, 1.88 mmol), (4-isopropylpiperazin-1-yl)(2-(1-(tetrahydro-2H-pyran-2-yl)-6-(4,4,5,5-tetramethyl-1,3,2-dioxaborolan-2-yl)-1H-indazol-4-yl)oxazol-5-yl)methanone **61** (1.551 g, 2.820 mmol), sodium carbonate (658 mg, 6.21 mmol) and chloro(2-dicyclohexylphosphino-2',4',6'-triisopropyl-1,1'-biphenyl)[2-(2-aminoethyl)phenyl]palladium(II) (XPhos

palladacycle) (139 mg, 0.188 mmol). 1,4-Dioxane (10 mL) and water (2.5 mL) were added, the vial sealed and the reaction heated in the biotage microwave system at 130 °C for 1 h. The reaction was cooled to room temperature, filtered through celite, washed with methanol and concentrated *in vacuo*. The residue was partitioned between EtOAc (30 mL) and distilled water (30 mL). The layers were separated and the organics washed with NaOH (0.5 M, 3 x 10 mL), distilled water (2 x 10 mL) and brine (2 x 10 mL). The organics were dried through a hydrophobic frit, concentrated *in vacuo*, and the residue purified by automated column chromatography on silica gel (0-30% EtOH:EtOAc). Desired fractions were combined, and the solvent removed *in vacuo* to afford the product as a yellow foam (981 mg, 1.50 mmol, 80%). M.pt.: 69-74 °C. ν_{\max} (neat): 2964, 2873, 1627, 1455, 1415 cm^{-1} . ^1H NMR (400 MHz, CHLOROFORM-*d*) δ = 8.67 (1H, s), 8.31 (1H, d, J = 2.4 Hz), 8.05 (1H, d, J = 1.5 Hz), 7.78 - 7.72 (3H, m), 7.39 - 7.29 (4H, m), 7.27 - 7.21 (1H, m), 5.81 (1H, dd, J = 9.0, 2.7 Hz), 4.20 (2H, s), 4.10 (3H, s), 4.08 - 4.01 (1H, m), 3.90 (4H, br. s), 3.83 - 3.73 (1H, m), 2.77 (1H, spt, J = 6.6 Hz), 2.67 - 2.61 (4H, m), 2.28 - 2.10 (2H, m), 1.88 - 1.62 (4H, m), 1.08 (6H, d, J = 6.6 Hz). ^{13}C NMR (126 MHz, CHLOROFORM-*d*) δ = 161.3, 161.1, 157.4, 144.8, 142.7, 140.6, 137.3, 136.7, 136.4, 134.1, 133.5, 130.0, 129.0, 128.9, 128.6, 127.4, 120.7, 120.1, 119.8, 110.9, 85.5, 67.5, 54.5, 54.3, 48.6 (2C, br. s), 46.9 (1C, br. s), 43.0 (1C br. s), 36.8, 29.4, 25.1, 22.4, 18.4. LCMS (Method A): t_{R} = 0.99 min, $[\text{M}+\text{H}^+]$ 653.8, (100% purity). HRMS: ($\text{C}_{36}\text{H}_{41}\text{N}_6\text{O}_4\text{S}$) $[\text{M}+\text{H}^+]$ requires 653.2905, found $[\text{M}+\text{H}^+]$ 653.2935.

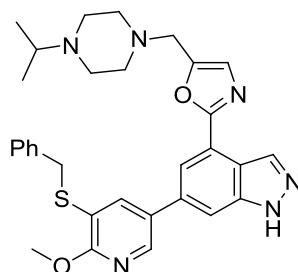
2-(6-(5-(Benzylthio)-6-methoxypyridin-3-yl)-1-(tetrahydro-2H-pyran-2-yl)-1H-indazol-4-yl)-5-((4-isopropylpiperazin-1-yl)methyl)oxazole (84)



To a flask containing (2-(6-(5-(benzylthio)-6-methoxypyridin-3-yl)-1-(tetrahydro-2H-pyran-2-yl)-1H-indazol-4-yl)oxazol-5-yl)(4-isopropylpiperazin-1-yl)methanone **83** (750 mg, 1.15 mmol) and tris(triphenylphosphine)rhodium(I) carbonyl hydride (13 mg, 0.014 mmol) was added THF (1.3 mL) and diphenylsilane (0.490 mL, 2.64 mmol). The reaction was left to stir at room temperature for 2.5 h. Additional aliquots of tris(triphenylphosphine)rhodium(I) carbonyl hydride (13 mg, 0.014 mmol) and diphenylsilane (0.245 mL, 1.32 mmol) were added

and the reaction mixture was stirred at room temperature for further 1.5 h. Upon completion of the reaction, the mixture was diluted with EtOAc (50 mL) and the product extracted to aqueous HCl (1 M, 6 x 15 mL). The organics were discarded, the aqueous basified to pH 8 by the addition of sodium hydroxide (2 M). The product was extracted to EtOAc (3 x 25 mL). The organic extracts were combined, dried through a hydrophobic frit, concentrated *in vacuo*, and the residue purified by automated column chromatography on silica gel (0-20% MeOH:DCM). Desired fractions were combined, and the solvent removed *in vacuo* to afford the product as a yellow solid (538 mg, 0.842 mmol, 73%). M.pt.: 62-66 °C. ν_{\max} (neat): 2941, 2856, 1586, 1455 cm^{-1} . ^1H NMR (400 MHz, CHLOROFORM-*d*) δ = 8.71 (1H, s), 8.32 (1H, d, J = 2.2 Hz), 7.97 (1H, d, J = 1.5 Hz), 7.77 (1H, d, J = 2.2 Hz), 7.66 (1H, s), 7.39 - 7.29 (4H, m), 7.26 - 7.22 (1H, m), 7.17 (1H, s), 5.80 (1H, dd, J = 9.2, 2.6 Hz), 4.20 (2H, s), 4.10 (3H, s), 4.08 - 4.00 (1H, m), 3.78 (2H, s), 2.72 - 2.56 (10H, m), 2.27 - 2.10 (2H, m), 1.89 - 1.60 (4H, m), 1.05 (6H, d, J = 6.6 Hz). ^{13}C NMR (101 MHz, CHLOROFORM-*d*) δ = 161.1, 160.7, 149.0, 142.8, 140.6, 137.5, 136.8, 136.3, 134.6, 130.3, 129.0, 128.6, 127.5, 127.4, 120.8, 120.7, 119.9, 119.7, 109.8, 85.5, 67.4, 54.4, 54.2, 53.1, 52.5, 48.6, 36.9, 29.4, 25.1, 22.5, 18.6. LCMS (Method A): t_{R} = 1.00 min, $[\text{M}+\text{H}^+]$ 639.6, (100% purity). HRMS: ($\text{C}_{36}\text{H}_{43}\text{N}_6\text{O}_3\text{S}$) $[\text{M}+\text{H}^+]$ requires 639.3112, found $[\text{M}+\text{H}^+]$ 639.3115.

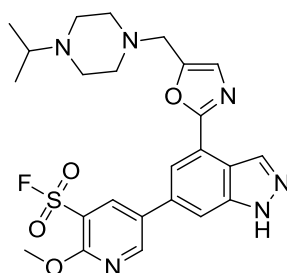
2-(6-(5-(Benzylthio)-6-methoxy-pyridin-3-yl)-1H-indazol-4-yl)-5-((4-isopropylpiperazin-1-yl)methyl)oxazole (85)



To a flask containing 2-(6-(5-(benzylthio)-6-methoxy-pyridin-3-yl)-1-(tetrahydro-2H-pyran-2-yl)-1H-indazol-4-yl)-5-((4-isopropylpiperazin-1-yl)methyl)oxazole **84** (525 mg, 0.822 mmol) in anhydrous methanol (15 mL) under nitrogen was added TMSCl (1.05 mL, 8.22 mmol). The reaction was stirred at 40 °C for 2 h. Sodium hydroxide (2 M, 4.11 mL, 8.22 mmol) was then added and the reaction cooled to room temperature and concentrated *in vacuo*. The residue was partitioned between EtOAc (25 mL) and water (25 mL). The pH of the aqueous was confirmed to be 10 prior to separation, and washing of the organic phase with distilled water (2 x 10 mL) and brine (1 x 10 mL). The organics were dried through a hydrophobic frit,

concentrated *in vacuo* and the residue purified by automated column chromatography on silica gel (0-20% MeOH:DCM). Desired fractions were combined and the solvent removed *in vacuo* to afford the product as a white solid (405 mg, 0.730 mmol, 89%). M.pt.: 214-217 °C. ν_{max} (neat): 2815, 1584, 1456, 1410 cm^{-1} . ^1H NMR (400 MHz, ACETIC ACID- d_4) δ = 8.78 (1H, s), 8.43 (1H, d, J = 2.2 Hz), 8.17 (1H, d, J = 1.2 Hz), 7.98 (1H, s), 7.95 (1H, d, J = 2.2 Hz), 7.62 (1H, s), 7.41 (2H, d, J = 7.1 Hz), 7.31 (2H, t, J = 7.5 Hz), 7.22 (1H, tt, J = 7.3, 1.5 Hz), 4.44 (2H, s), 4.27 (2H, s), 4.08 (3H, s), 3.65 - 3.49 (9H, m), 1.33 (6H, d, J = 6.8 Hz) (indazole N-H not seen). ^{13}C NMR (126 MHz, ACETIC ACID- d_4) δ = 162.49, 160.81, 144.04, 141.49, 141.17, 136.80, 136.77, 136.29, 133.53, 130.54, 129.61, 128.89, 128.48, 127.28, 121.65, 120.30, 119.53, 118.53, 111.39, 58.18, 54.02, 49.57, 48.39, 45.79, 35.77, 15.70 (two decimal places required to distinguish signals). LCMS (Method A): t_{R} = 0.81 min, $[\text{M}+\text{H}^+]$ 555.6, (100% purity). HRMS: ($\text{C}_{31}\text{H}_{35}\text{N}_6\text{O}_2\text{S}$) $[\text{M}+\text{H}^+]$ requires 555.2537, found $[\text{M}+\text{H}^+]$ 555.2529.

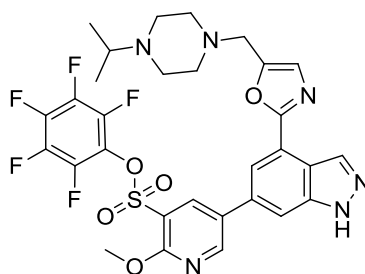
5-(4-(5-((4-Isopropylpiperazin-1-yl)methyl)oxazol-2-yl)-1H-indazol-6-yl)-2-methoxy-pyridine-3-sulfonyl fluoride (78)



To a stirred solution of 2-(6-(5-(benzylthio)-6-methoxy-pyridin-3-yl)-1H-indol-4-yl)-5-((4-isopropylpiperazin-1-yl)methyl)oxazole **85** (130 mg, 0.235 mmol) in acetonitrile (2.4 mL) and water (0.060 mL), acidified with acetic acid (0.090 mL, 1.6 mmol) and cooled to <10 °C was added 1,3-dichloro-5,5-dimethylhydantoin **86** (139 mg, 0.704 mmol) portionwise. The reaction was stirred in ice for 30 min, at which point the product had precipitated, and was isolated by filtration under vacuum. A sample of solid was reacted with morpholine, and LCMS showed $[\text{M}+\text{H}^+]$ 582.2, (79% pure) corresponding to the morpholine sulfonamide, indicating the presence of sulfonyl chloride **87**. 65 mg (0.12 mmol) of this solid was added to a stirring solution of potassium hydrogen fluoride (35 mg, 0.45 mmol), water (0.145 mL) and acetonitrile (0.725 mL). After 1 h, the reaction was quenched by the addition of sat. NaHCO_3 (1 mL) and EtOAc (2 mL) then stirred for 5 minutes. The layers were separated and the aqueous washed with EtOAc (2 x 2 mL). The organics were dried through a hydrophobic frit and concentrated *in vacuo* to afford the crude residue, which was purified by MDAP

(ammonium bicarbonate modifier). Desired fractions were combined, the volatile solvents removed *in vacuo* and the product extracted to DCM (3 x 10 mL washings). The organics were dried through a hydrophobic frit and concentrated *in vacuo* to afford the product as a colourless gum (12 mg, 0.023 mmol, 19%). ¹H NMR (400 MHz, CHLOROFORM-d) δ = 8.77 (1H, d, *J* = 2.5 Hz), 8.63 (1H, s), 8.53 (1H, d, *J* = 2.5 Hz), 7.74 (1H, s), 7.50 (1H, s), 7.31 (1H, s), 4.27 (3H, s), 3.88 (2H, s), 2.96 - 2.68 (9H, m), 1.11 (6H, d, *J* = 6.3 Hz), indazole N-H not observed. ¹⁹F{¹H} NMR (376 MHz, CHLOROFORM-d) δ = 59.22 (1F, s). LCMS (Method A): *t*_R = 1.12 min, [M+H⁺] 515.2 (96% purity). The compound was found to decompose prior to collection of remaining characterisation data.

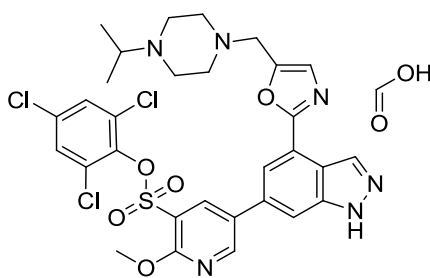
Perfluorophenyl 5-(4-(5-((4-isopropylpiperazin-1-yl)methyl)oxazol-2-yl)-1H-indazol-6-yl)-2-methoxypyridine-3-sulfonate (79)



To a stirred solution of 2-(6-(5-(benzylthio)-6-methoxypyridin-3-yl)-1H-indol-4-yl)-5-((4-isopropylpiperazin-1-yl)methyl)oxazole **85** (130 mg, 0.235 mmol) in acetonitrile (2.4 mL) and water (0.060 mL), acidified with acetic acid (0.090 mL, 1.6 mmol) and cooled to <10 °C was added 1,3-dichloro-5,5-dimethylhydantoin **86** (139 mg, 0.704 mmol) portionwise. The reaction was stirred in ice for 30 min, at which point the product had precipitated, and was isolated by filtration under vacuum. A sample of solid was reacted with morpholine, and LCMS showed [M+H⁺] 582.2, (79% pure) corresponding to the morpholine sulfonamide, indicating the presence of sulfonyl chloride **87**. 100 mg (0.188 mmol) of this solid was added to a stirring solution of pentafluorophenol (38 mg, 0.21 mmol) and triethylamine (0.079 mL, 0.57 mmol) in DCM (1 mL) at room temperature. After 2.5 h the reaction was concentrated *in vacuo*, and the residue purified by MDAP (formic acid modifier). Desired fractions were combined, and the volatile solvents removed *in vacuo*. DCM (10 mL) was then added, and the aqueous basified to pH 8 by the cautious addition of NH₄OH. The layers were separated, and the aqueous washed with DCM (3 x 10 mL). The organics were dried through a hydrophobic frit and concentrated *in vacuo* to afford the title product as a white solid (19 mg, 0.028 mmol, 15%). M.pt.: 158-161 °C (d). *v*_{max} (neat): 2964, 2831, 1599, 1517, 1490, 1385

cm⁻¹. ¹H NMR (400 MHz, DMSO-d₆) δ = 13.59 (1H, br. s.), 9.09 (1H, d, *J* = 2.4 Hz), 8.60 (1H, s), 8.53 (1H, d, *J* = 2.4 Hz), 8.03 (1H, s), 7.97 (1H, d, *J* = 1.5 Hz), 7.34 (1H, s), 4.13 (3H, s), 3.75 (2H, s), 2.73 - 2.67 (1H, m), 2.55 (8H, br. s.), 0.98 (6H, d, *J* = 6.6 Hz). ¹⁹F{¹H} NMR (376 MHz, DMSO-d₆) δ = -152.31 (2F, d, *J* = 17.3 Hz), -155.54 (1F, t, *J* = 24.3 Hz), -161.77 (2F, t, *J* = 20.8 Hz). ¹³C NMR (126 MHz, DMSO-d₆) δ = 159.7, 159.3, 153.0, 149.4, 141.0, 140.0, 133.7, 133.0, 129.5, 127.5, 119.7, 118.6, 118.1, 116.8, 111.0, 55.1, 54.4, 51.6, 51.1, 47.8, 17.7. Pentafluorophenol carbons not observable due to F-C coupling. LCMS (Method A): t_R = 0.86 min, [M+H⁺] 679.1 (99% purity). HRMS: (C₃₀H₂₈F₅N₆O₅S) [M+H⁺] requires 679.1757, found [M+H⁺] 679.1753.

2,4,6-Trichlorophenyl 5-(4-(5-((4-isopropylpiperazin-1-yl)methyl)oxazol-2-yl)-1H-indazol-6-yl)-2-methoxypyridine-3-sulfonate, formic acid salt (80)

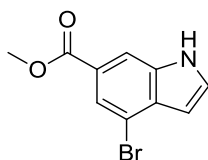


To a stirred solution of 2-(6-(5-(benzylthio)-6-methoxypyridin-3-yl)-1H-indol-4-yl)-5-((4-isopropylpiperazin-1-yl)methyl)oxazole **85** (75 mg, 0.14 mmol) in acetonitrile (1.35 mL) and water (0.034 mL), acidified with acetic acid (0.052 mL, 0.91 mmol) and cooled to <10 °C was added 1,3-dichloro-5,5-dimethylhydantoin **86** (54 mg, 0.27 mmol) portionwise. The reaction was left to stir in ice for 2 h, at which point the reaction was diluted with DCM (2 mL) and washed with sat. NaHCO₃ (2 x 1 mL) and brine (1 x 1 mL). The organics (containing sulfonyl chloride **87**) were dried through a hydrophobic frit into a stirring solution of 2,4,6-trichlorophenol (54 mg, 0.27 mmol) and triethylamine (0.057 mL, 0.41 mmol) in DCM (0.5 mL). The reaction was left to stir at room temperature for 30 min and then concentrated *in vacuo*. The residue was taken up in DMSO (1 mL) and purified by MDAP (formic acid modifier). Desired fractions were combined, and the solvent removed by nitrogen blowdown at room temperature to afford the title product as an off-white solid (13 mg, 0.018 mmol, 13%). M.pt.: 120-124 °C. ν_{max} (neat): 2942, 1727, 1596, 1558, 1482, 1385, 1184 cm⁻¹. ¹H NMR (400 MHz, CHLOROFORM-d) δ = 8.79 (1H, d, *J* = 2.5 Hz), 8.76 (1H, s), 8.44 (1H, d, *J* = 2.5 Hz), 8.43 (1H, s), 8.03 - 8.00 (1H, m), 7.71 (1H, s), 7.38 (2H, s), 7.21 (1H, s), 4.22 (3H, s), 3.80 (2H, s), 3.28 (1H, spt, *J* = 6.6 Hz), 3.03 (4H, br. s), 2.90 (4H, br. s), 1.26 (6H, d, *J* = 6.5 Hz), indazole N-H not observed. ¹³C NMR (126 MHz, CHLOROFORM-d) δ = 166.87, 160.70, 160.11, 151.49,

148.38, 142.55, 141.21, 138.72, 135.59, 134.44, 133.09, 130.76, 129.64, 129.18, 128.04, 121.00, 120.97, 119.60, 118.98, 109.86, 55.88, 55.17, 51.93, 50.36, 47.34, 17.06 (two decimal places required to distinguish signals). LCMS (Method A): $t_R = 0.89$ min, $[M+H]^+$ 692.7, (97% purity). HRMS: ($C_{30}H_{30}^{35}Cl_3N_6O_5S$) $[M+H]^+$ requires 691.1059, found $[M+H]^+$ 691.1052.

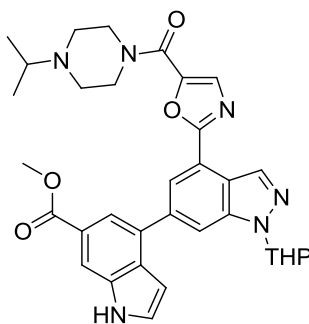
Synthesis of Activated Esters Containing the Indole Back-pocket Group

*Methyl 4-bromo-1H-indole-6-carboxylate*²³⁰ (**90**)



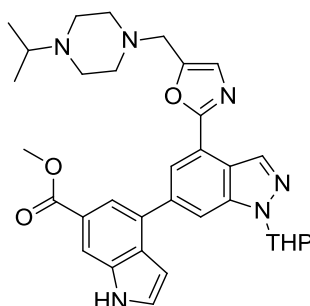
To a stirred solution of 4-bromo-1H-indole-6-carboxylic acid **89** (150 mg, 0.625 mmol) and $NaHCO_3$ (210 mg, 2.50 mmol) in DMF (3 mL) was added methyl iodide (0.340 mL, 5.44 mmol). The reaction was stoppered, and stirred at room temperature for 24 h. Distilled water (10 mL) was then added to the reaction mixture, forming a precipitate, which was extracted to EtOAc (3 x 20 mL). The organics were then washed with aq. LiCl solution (5%, 3 x 15 mL), dried through a hydrophobic frit and concentrated *in vacuo*. The residue was purified by automated column chromatography on silica gel (0-100% EtOAc:cyclohexane) to afford the title product as an off-white solid (149 mg, 0.586 mmol, 94%). M.pt.: 145-150 °C. ν_{max} (neat): 3291, 3090, 2945, 1687 cm^{-1} . 1H NMR (400 MHz, CHLOROFORM-*d*) $\delta = 8.61$ (1H, br. s), 8.14 - 8.10 (1H, m), 8.01 (1H, d, $J = 1.3$ Hz), 7.43 (1H, t, $J = 2.9$ Hz), 6.69 - 6.64 (1H, m), 3.95 (3H, s). ^{13}C NMR (101 MHz, CHLOROFORM-*d*) $\delta = 166.9, 135.1, 132.1, 127.8, 125.0, 123.7, 114.3, 112.7, 103.7, 52.2$. LCMS (Method A): $t_R = 1.10$ min, $[M+H]^+$ 253.9 and 255.9, (100% purity). HRMS: ($C_{10}H_9^{79}BrNO_2$) $[M+H]^+$ requires 253.9811, found $[M+H]^+$ 253.9814.

Methyl 4-(4-(5-(4-isopropylpiperazine-1-carbonyl)oxazol-2-yl)-1-(tetrahydro-2H-pyran-2-yl)-1H-indazol-6-yl)-1H-indole-6-carboxylate (**91**)



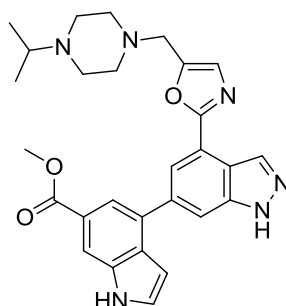
A flask was charged with (4-isopropylpiperazin-1-yl)(2-(1-(tetrahydro-2H-pyran-2-yl)-6-(4,4,5,5-tetramethyl-1,3,2-dioxaborolan-2-yl)-1H-indazol-4-yl)oxazol-5-yl)methanone **61** (240 mg, 0.437 mmol), methyl 4-bromo-1H-indole-6-carboxylate **90** (100 mg, 0.394 mmol), PdCl₂(dppf) (29 mg, 0.040 mmol), and Na₂CO₃ (125 mg, 1.18 mmol). 1,4-Dioxane (5 mL) and distilled water (1.25 mL) were added and the reaction stirred. The vessel was degassed and purged with nitrogen three times and then heated at 80 °C for 2 h. The reaction was cooled to room temperature, filtered through celite, and concentrated *in vacuo*. The residue was then partitioned between EtOAc (20 mL) and distilled water (20 mL). The layers were separated and the organics washed with aq. NaHCO₃ (3 x 10 mL), distilled water (1 x 10 mL) and brine (1 x 10 mL). The organics were then dried through a hydrophobic frit, concentrated *in vacuo*, and the residue purified by automated column chromatography on silica gel (0-50% EtOAc in (3:1) EtOH:cyclohexane). Desired fractions were combined, and the solvent removed *in vacuo* to afford the product as a brown gum. This was triturated with diisopropyl ether, and the solvent removed *in vacuo* to afford the title product as an off-white solid (190 mg, 0.318 mmol, 81%). M.pt.: 148 - 151 °C (d). ν_{\max} (neat): 3264, 2965, 1710, 1618, 1526, 1435 cm⁻¹. ¹H NMR (600 MHz, CHLOROFORM-d) δ = 8.94 (1H, br. s.), 8.73 (1H, s), 8.33 (1H, d, *J* = 1.1 Hz), 8.22 - 8.20 (1H, m), 8.04 (1H, s), 8.00 (1H, d, *J* = 1.1 Hz), 7.80 (1H, s), 7.44 (1H, t, *J* = 2.8 Hz), 6.80 - 6.72 (1H, m), 5.86 (1H, dd, *J* = 9.4, 2.4 Hz), 4.06 (1H, d, *J* = 11.4 Hz), 3.97 (3H, s), 3.95 - 3.83 (3H, m), 3.82 - 3.74 (1H, m), 2.76 (1H, spt, *J* = 6.6 Hz), 2.70 - 2.58 (5H, m), 2.24 - 2.12 (2H, m), 1.86 - 1.73 (3H, m), 1.71 - 1.64 (1H, m), 1.07 (6H, d, *J* = 6.6 Hz). ¹³C NMR (151 MHz, CHLOROFORM-d) δ = 167.9, 161.5, 157.5, 144.8, 140.6, 139.2, 135.7, 134.2, 133.9, 133.1, 130.0, 128.2, 124.1, 122.7, 121.0, 120.7, 119.2, 113.2, 112.9, 102.3, 85.5, 67.5, 54.6, 52.1, 48.7 (2C, br. s), 46.8 (br. s), 43.1 (br. s), 29.5, 25.1, 22.5, 18.4. LCMS (Method A): *t*_R = 0.78 min, [M+H⁺] 597.3, (98% purity). HRMS: (C₃₃H₃₇N₆O₅) [M+H⁺] requires 597.2820, found [M+H⁺] 597.2814.

Methyl 4-(4-(5-((4-isopropylpiperazin-1-yl)methyl)oxazol-2-yl)-1-(tetrahydro-2H-pyran-2-yl)-1H-indazol-6-yl)-1H-indole-6-carboxylate (92)



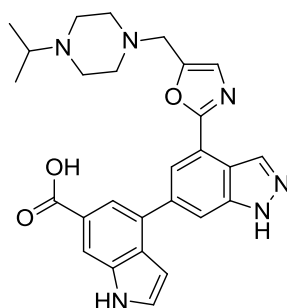
To a flask containing methyl 4-(4-(5-(4-isopropylpiperazine-1-carbonyl)oxazol-2-yl)-1-(tetrahydro-2H-pyran-2-yl)-1H-indazol-6-yl)-1H-indole-6-carboxylate **91** (190 mg, 0.318 mmol) and tris(triphenylphosphine)rhodium(I) carbonyl hydride (3.8 mg, 4.1 μ mol) was added THF (1 mL) and then diphenylsilane (0.136 mL, 0.732 mmol). Effervescence was observed upon addition of the silane. The reaction was left to stir at room temperature. A murky brown suspension formed after 10 min of stirring, which was loosened by the addition of THF (0.5 mL). Further equivalents of silane (1.4 mL) and rhodium catalyst (4 mg) were added with THF (1 mL) at 7 and 23 h to force completion. After a total reaction time of 27 h, the reaction was diluted with EtOAc and transferred to a separating funnel. The product was extracted to aq. HCl (1 M, 3 x 15 mL), and the organic layer discarded. The pH of the aqueous was adjusted to 7 by the addition of sat. NaHCO₃, and then 9 by the careful addition of aq. NaOH (2 M). The product was then extracted to EtOAc (3 x 15 mL), and the organics were dried through a hydrophobic frit and concentrated *in vacuo*. The residue was purified by automated column chromatography on silica gel (0-30% EtOH:EtOAc). Desired fractions were combined, and the solvent removed *in vacuo* to afford the title product as an off-white solid (123 mg, 0.211 mmol, 66%). M.pt.: 180 - 185 °C (decomp). ν_{\max} (neat): 2931, 2831, 1703 cm^{-1} . ¹H NMR (400 MHz, CHLOROFORM-*d*) δ = 8.81 (1H, br. s.), 8.76 (1H, s), 8.27 - 8.23 (1H, m), 8.20 (1H, s), 8.02 (1H, d, *J* = 1.3 Hz), 7.97 (1H, s), 7.44 (1H, t, *J* = 2.9 Hz), 7.18 (1H, s), 6.80 - 6.74 (1H, m), 5.84 (1H, dd, *J* = 9.2, 2.1 Hz), 4.09 - 4.01 (1H, m), 3.98 (3H, s), 3.82 - 3.78 (1H, m), 3.77 (2H, s), 2.81 - 2.57 (10H, m), 2.25 - 2.11 (2H, m), 1.89 - 1.59 (3H, m), 1.06 (6H, d, *J* = 6.5 Hz). ¹³C NMR (126 MHz, CHLOROFORM-*d*) δ = 168.0, 161.0, 148.7, 140.6, 139.1, 135.6, 134.6, 133.5, 130.1, 128.1, 127.5, 124.1, 121.7, 121.0, 120.6, 120.2, 113.0, 111.9, 102.5, 85.4, 67.5, 54.5, 52.7, 52.3, 52.1, 48.3, 29.5, 25.1, 22.5, 18.4. LCMS (Method A): *t_R* = 0.76 min, [M+H⁺] 583.4, (95% purity). HRMS: (C₃₃H₃₉N₆O₄) [M+H⁺] requires 583.3027, found [M+H⁺] 583.3024.

Methyl 4-(4-(5-((4-isopropylpiperazin-1-yl)methyl)oxazol-2-yl)-1H-indazol-6-yl)-1H-indole-6-carboxylate (94)



To a heat-gun-dried flask containing methyl 4-(4-(5-((4-isopropylpiperazin-1-yl)methyl)oxazol-2-yl)-1-(tetrahydro-2H-pyran-2-yl)-1H-indazol-6-yl)-1H-indole-6-carboxylate **92** (100 mg, 0.172 mmol) in anhydrous methanol (2 mL) under nitrogen was added TMSCl (0.219 mL, 1.72 mmol). The reaction was stirred at 40 °C for 38 h, cooled to room temperature, neutralised with Et₃N (0.239 mL, 1.72 mmol), and concentrated *in vacuo*. The residue was partitioned between EtOAc (15 mL) and distilled water (15 mL). The solid was filtered off, and washed with further distilled water (15 mL) and EtOAc (15 mL). The layers were separated, and the organics washed with sat. NaHCO₃ (2 x 15 mL). The organics were combined in methanol with the solids, and concentrated *in vacuo*. The residue was then purified by automated reverse-phase column chromatography on C18 silica gel (5-95% MeCN + 0.1% NH₃:10 mM ammonium bicarbonate adjusted to pH 10 with ammonia). Desired fractions were combined, and the solvent removed *in vacuo* to afford the title product as a white solid (46 mg, 0.092 mmol, 54%). M.pt.: 140-143 °C. v_{\max} (neat): 3167, 2969, 2839, 1690 cm⁻¹. ¹H NMR (400 MHz, DMSO-d₆) δ = 13.35 (1H, br. s), 11.81 (1H, br. s), 8.61 (1H, s), 8.16 (1H, br. s.), 8.05 (1H, s), 7.95 (1H, s), 7.81 (1H, s), 7.74 (1H, d, *J* = 2.0 Hz), 7.32 (1H, s), 6.69 (1H, d, *J* = 2.3 Hz), 3.90 (3H, s), 3.73 (2H, s), 2.64 - 2.35 (m), 0.93 (6H, d, *J* = 6.5 Hz) (eight piperazine signals and expected isopropyl septet signal (2.65-2.35 (m)) obscured by solvent signal; their presence was confirmed by HSQC and HMBC correlations). ¹³C NMR (126 MHz, DMSO-d₆) δ = 167.1, 159.9, 149.5, 141.3, 137.9, 135.8, 133.5, 132.2, 130.2, 129.3, 127.2, 122.5, 119.5, 119.3, 118.3, 117.1, 113.1, 111.7, 100.6, 53.5, 52.6, 51.9, 51.5, 47.9, 18.2. LCMS (Method A): *t*_R = 0.61 min, [M+H⁺] = 499.3, (100% purity). HRMS: (C₂₈H₃₁N₆O₃) [M+H⁺] requires 499.2452, found [M+H⁺] 499.2470.

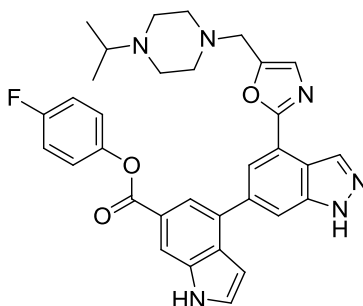
4-(4-(5-((4-Isopropylpiperazin-1-yl)methyl)oxazol-2-yl)-1H-indazol-6-yl)-1H-indole-6-carboxylic acid (93)



To a heat gun-dried flask under nitrogen was added methyl 4-(4-(5-((4-isopropylpiperazin-1-yl)methyl)oxazol-2-yl)-1-(tetrahydro-2H-pyran-2-yl)-1H-indazol-6-yl)-1H-indole-6-

carboxylate **92** (700 mg, 1.20 mmol) in anhydrous methanol (15 mL) and TMSCl (1.54 mL, 12.1 mmol). The reaction was stirred at 40 °C for 38 h, and then aq. NaOH (2 M) was added to adjust the pH to >11. The reaction was then heated to 65 °C for a further 24 h, cooled to room temperature and concentrated *in vacuo*. The residue was then purified by automated reverse-phase column chromatography on C18 silica gel (5-95% MeCN + 0.1% NH₃:10 mM ammonium bicarbonate adjusted to pH 10 with ammonia). Desired fractions were combined, the solvent removed *in vacuo* and the solid dried in a vacuum oven at 40 °C overnight to afford the title product as an off-white solid (554 mg, 1.14 mmol, 95%). M.pt.: 283-289 °C (decomp.) ν_{\max} (neat): 3176, 1588, 1547, 1389, 1342 cm⁻¹. IR shifts indicated zwitterion (1547 COO⁻).²⁹⁵ ¹H NMR (400 MHz, DMSO-d₆) δ = 13.54 (1H, br. s), 11.58 (1H, br. s.), 8.59 (1H, d, *J* = 1.0 Hz), 8.10 (1H, s), 8.08 (1H, d, *J* = 1.3 Hz), 7.96 (1H, s), 7.85 (1H, d, *J* = 1.3 Hz), 7.58 (1H, t, *J* = 2.8 Hz), 7.31 (1H, s), 6.66 - 6.62 (1H, m), 3.73 (2H, s), 2.64 - 2.35 (m), 0.92 (6H, d, *J* = 6.5 Hz) (eight piperazine signals and expected isopropyl septet signal (2.64-2.35 (m)) obscured by solvent signal; their presence was confirmed by HSQC and HMBC correlations; the carboxylic acid proton was not observed.) ¹³C NMR (126 MHz, DMSO-d₆) δ = 169.2, 160.0, 149.4, 141.2, 138.8, 136.1, 133.4, 131.0, 128.3, 127.5, 127.2, 120.3, 119.7, 119.1, 118.0, 112.8, 111.4, 109.5, 100.1, 53.5, 52.5, 51.5, 47.9, 18.2. LCMS (Method A): *t_R* = 0.54 min, [M+H⁺] 485.3, (100% purity). HRMS: (C₂₇H₂₉N₆O₃) [M+H⁺] requires 485.2296, found [M+H⁺] 485.2272.

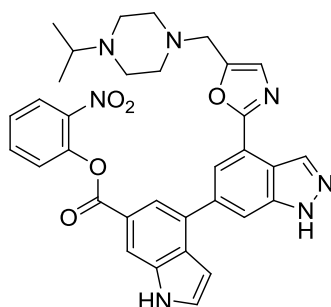
4-Fluorophenyl 4-(4-(5-((4-isopropylpiperazin-1-yl)methyl)oxazol-2-yl)-1H-indazol-6-yl)-1H-indole-6-carboxylate (**95**)



4-(4-(5-((4-Isopropylpiperazin-1-yl)methyl)oxazol-2-yl)-1H-indazol-6-yl)-1H-indole-6-carboxylic acid **93** (50 mg, 0.10 mmol), *p*-fluorophenol (18 mg, 0.16 mmol), and PyBOP (59 mg, 0.11 mmol) were stirred in DMF (0.75 mL) at room temperature. DIPEA (0.036 mL, 0.21 mmol) was then added dropwise to the stirring reaction and the reaction left to stir at room temperature. After 19 h, the reaction was purified directly, without workup, by MDAP (ammonium bicarbonate modifier). Desired fractions were combined, and the volatile

solvents removed *in vacuo*. The pH of the remaining aqueous was adjusted to >10 with aq. NH₄OH, and the product extracted to DCM (5 x 10 mL). The organics were dried through a hydrophobic frit and concentrated *in vacuo* to afford the title product as an off-white solid (14 mg, 0.024 mmol, 24%). M.pt.: 138-145 °C. ν_{\max} (neat): 2924, 1728, 1502, 1174 cm⁻¹. ¹H NMR (400 MHz, CHLOROFORM-d) δ = 8.90 (1H, br. s), 8.79 (1H, d, *J* = 1.0 Hz), 8.32 - 8.28 (1H, m), 8.19 (1H, d, *J* = 1.0 Hz), 8.07 (1H, d, *J* = 1.3 Hz), 7.86 - 7.82 (1H, m), 7.45 (1H, t, *J* = 2.8 Hz), 7.26 - 7.21 (2H, m), 7.20 (1H, s), 7.16 - 7.09 (2H, m), 6.76 - 6.72 (1H, m), 3.80 (2H, s), 2.77 - 2.57 (9H, m), 1.05 (6H, d, *J* = 6.3 Hz), indazole N-H not observed. ¹⁹F{¹H} NMR (376 MHz, CHLOROFORM-d) δ = -117.69 (1F, s). ¹³C NMR (126 MHz, CHLOROFORM-d) δ = 166.1, 161.2, 160.1 (1C, d, *J* = 215.5 Hz), 148.7, 147.0 (1C, d, *J* = 3.2 Hz), 141.1, 139.1, 135.7, 135.6, 133.5, 130.6, 128.5, 127.6, 123.3 (2C, d, *J* = 8.3 Hz), 123.0, 121.4, 121.3, 120.2, 119.2, 116.1 (2C, d, *J* = 23.6 Hz), 113.6, 111.3, 102.6, 54.4, 52.9, 52.4, 48.5, 18.5. LCMS (Method A): *t*_R = 0.77 min, [M+H⁺] 579.2, (99% purity). HRMS: (C₃₃H₃₂FN₆O₃) [M+H⁺] requires 579.2514, found [M+H⁺] 579.2518.

2-Nitrophenyl 4-(4-(5-((4-isopropylpiperazin-1-yl)methyl)oxazol-2-yl)-1H-indazol-6-yl)-1H-indole-6-carboxylate (96)



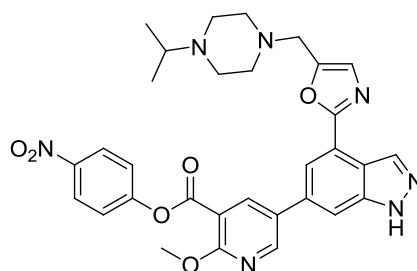
4-(4-(5-((4-Isopropylpiperazin-1-yl)methyl)oxazol-2-yl)-1H-indazol-6-yl)-1H-indole-6-carboxylic acid **93** (50 mg, 0.10 mmol) *o*-nitrophenol (22 mg, 0.16 mmol), and PyBOP (59 mg, 0.11 mmol) were stirred in DMF (0.75 mL) at room temperature. DIPEA (0.036 mL, 0.21 mmol) was then added dropwise to the stirring reaction and the reaction left to stir at room temperature. After 45 min, the reaction was purified by MDAP. Purification with ammonium bicarbonate modifier was unsuccessful, and a second purification by MDAP (formic acid modifier) was required. Desired fractions were combined, and the volatile solvents removed *in vacuo*. The pH of the remaining aqueous was adjusted to >10 with aq. NH₄OH, and the product extracted to DCM (5 x 10 mL). The organics were dried through a hydrophobic frit

and concentrated *in vacuo* to afford the title product as a yellow solid (13 mg, 0.021 mmol, 21%). M.pt.: 139-146 °C. ν_{\max} (neat): 2925, 1731, 1529, 1347 cm^{-1} . ^1H NMR (400 MHz, CHLOROFORM- d) δ = 8.87 (1H, br. s), 8.79 (1H, s), 8.33 (1H, s), 8.19 (1H, s), 8.16 (1H, d, J = 7.8 Hz), 8.06 (1H, s), 7.86 (1H, s), 7.72 (1H, t, J = 7.1 Hz), 7.51 - 7.41 (3H, m), 7.19 (1H, s), 6.79 (1H, s), 3.80 (2H, s), 2.80 - 2.64 (9H, m), 1.07 (6H, d, J = 6.5 Hz) (indazole N-H not observed). ^{13}C NMR (126 MHz, CHLOROFORM- d) δ = 165.1, 160.9, 148.6, 144.6, 142.2, 141.1, 139.0, 135.8, 135.6, 134.6, 133.6, 130.9, 128.9, 127.7, 126.4, 125.8, 125.6, 122.0, 121.6, 121.3, 120.2, 119.3, 114.1, 111.4, 102.7, 54.6, 52.5, 52.3, 48.3, 18.4. LCMS (Method A): t_{R} = 0.76 min, $[\text{M}+\text{H}^+]$ 606.2, (97% purity). HRMS: ($\text{C}_{33}\text{H}_{32}\text{N}_7\text{O}_5$) $[\text{M}+\text{H}^+]$ requires 606.2459, found $[\text{M}+\text{H}^+]$ 606.2464.

Synthesis of Activated Esters with Varying Electronic Properties

The esters were synthesised from the parent carboxylic acid **64**, the synthesis of which is detailed above.

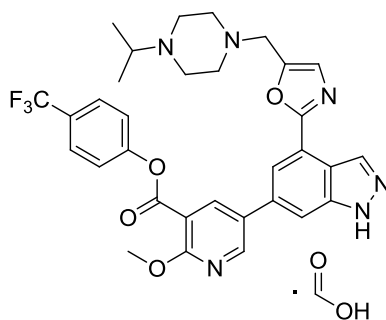
4-Nitrophenyl **5-(4-(5-((4-isopropylpiperazin-1-yl)methyl)oxazol-2-yl)-1H-indazol-6-yl)-2-methoxynicotinate (99)**



HATU (96 mg, 0.25 mmol), compound **64** (100 mg, 0.210 mmol) and DIPEA (0.073 mL, 0.42 mmol) were stirred in DMF (1.5 mL) at room temperature for 10 min prior to the addition of 4-nitrophenol (44 mg, 0.32 mmol). The reaction was then left to stir at room temperature. After 1 h, the reaction was diluted to 2 mL with DMSO and purified by MDAP (Method B). Desired fractions were combined, concentrated *in vacuo* and then dried fully using a Vapourtec V10 to afford a yellow solid. The sample was taken up in DMSO (1 mL) and purified further by MDAP (Method D). Desired fractions were dried under flowing nitrogen at 40 °C overnight to afford the product as a TFA salt. The sample was partitioned between DCM (2 mL) and distilled water (2 mL). Saturated aqueous NaHCO_3 was added dropwise to adjust the pH to 10, and the product was extracted to the organic layer. The aqueous was extracted further with 3 x 2 mL DCM. The organics were then dried through a hydrophobic frit,

concentrated by nitrogen blowdown and dried further in a vacuum oven at 40 °C for 2 h to afford the product as a yellow solid (17 mg, 0.028 mmol, 14% yield). M.pt.: 146-149 °C. ν_{\max} (neat): 2964, 2816, 1754, 1522, 1477, 1345 cm^{-1} . ^1H NMR (400 MHz, CHLOROFORM- d) δ = 8.75 - 8.71 (2H, m), 8.67 (1H, d, J = 3.0 Hz), 8.35 (2H, d, J = 9.6 Hz), 8.01 (1H, d, J = 1.0 Hz), 7.68 (1H, s), 7.48 (2H, d, J = 9.1 Hz), 7.20 (1H, s), 4.18 (3H, s), 3.81 (2H, s), 2.72 (9H, br. s), 1.07 (6H, d, J = 5.5 Hz) (indazole N-H not observed). ^{13}C NMR (151 MHz, CHLOROFORM- d) δ = 162.6, 162.3, 160.6, 155.5, 150.6, 149.0, 145.6, 141.2, 140.8, 135.8, 135.4, 129.7, 127.8, 125.3, 122.7, 120.9, 119.5, 119.2, 112.1, 109.3, 54.7, 54.4, 52.9, 52.3, 48.5, 18.5. LCMS (Method A): t_{R} = 0.76 min, $[\text{M}+\text{H}^+]$ 598.2, (100% purity). HRMS: ($\text{C}_{31}\text{H}_{32}\text{N}_7\text{O}_6$) $[\text{M}+\text{H}^+]$ requires 598.2409, found $[\text{M}+\text{H}^+]$ 598.2406.

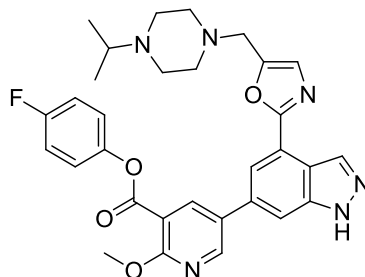
4-(Trifluoromethyl)phenyl 5-(4-(5-((4-isopropylpiperazin-1-yl)methyl)oxazol-2-yl)-1H-indazol-6-yl)-2-methoxynicotinate, formic acid salt (100)



4-(Trifluoromethyl)phenol (51 mg, 0.32 mmol), PyBOP (120 mg, 0.231 mmol) and compound **64** (100 mg, 0.210 mmol) were stirred in DMF (1.5 mL) at room temperature. DIPEA (0.073 mL, 0.42 mmol) was then added dropwise to the stirring reaction and the reaction left to stir at room temperature. After 3 h, the reaction was diluted to 3 mL and the product purified directly, without workup, by MDAP (Method C). Desired fractions were combined and the solvent removed by nitrogen blowdown at 40 °C. The solid was taken up in DMSO (1 mL) and further purified by MDAP (Method B). Desired fractions were combined, and the solvent removed by nitrogen blowdown to the product as a white solid (55 mg, 0.083 mmol, 39% yield). M.pt.: 98-105 °C (decomp.) ν_{\max} (neat): 2967, 2830, 1733, 1601, 1572, 1478, 1322 cm^{-1} . ^1H NMR (400 MHz, DMSO- d_6) δ = 13.56 (1H, br. s), 8.93 (1H, d, J = 2.4 Hz), 8.77 (1H, d, J = 2.4 Hz), 8.60 (1H, s), 8.17 (1H, s), 8.03 - 8.01 (2H, m), 7.89 (2H, d, J = 8.5 Hz), 7.60 (2H, d, J = 8.5 Hz), 7.34 (1H, s), 4.07 (3H, s), 3.74 (2H, s), 2.63 (1H, spt, J = 6.4 Hz), 0.94 (6H, d, J = 6.4 Hz) (piperazine signals obscured by DMSO peak, confirmed by HSQC and HMBC correlations). $^{19}\text{F}\{\text{H}\}$ NMR (376 MHz, DMSO- d_6) δ = -60.59 (3F, s). ^{13}C NMR (126 MHz, DMSO- d_6) δ = 163.8,

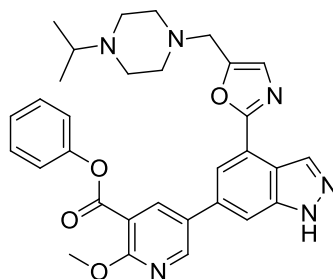
162.6, 161.9, 160.2, 153.9, 150.6, 150.0, 140.9, 134.5, 134.1, 129.5, 127.8, 127.4 (2C, q, $J = 3.7$ Hz), 127.2 (1C, $J = 32.4$ Hz), 124.5 (1C, q, $J = 271.9$ Hz), 123.6, 120.2, 118.9, 118.5, 116.1, 112.9, 110.9, 54.8, 54.2, 52.7, 51.8, 48.3, 18.5. LCMS (Method A): $t_R = 0.85$ min, $[M+H]^+$ 621.2, (100% purity). HRMS: ($C_{32}H_{32}F_3N_6O_4$) $[M+H]^+$ requires 621.2432, found $[M+H]^+$ 621.2429.

4-Fluorophenyl **5-(4-(5-((4-isopropylpiperazin-1-yl)methyl)oxazol-2-yl)-1H-indazol-6-yl)-2-methoxynicotinate (60)** (PyBOP method)



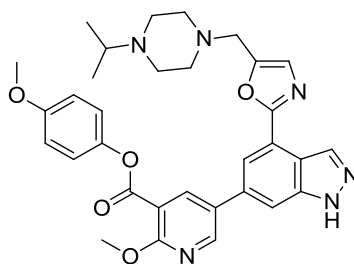
Compound **64** (100 mg, 0.210 mmol), 4-fluorophenol (35 mg, 0.32 mmol) and PyBOP (120 mg, 0.231 mmol) were stirred in DMF (1.5 mL) at room temperature. DIPEA (0.073 mL, 0.42 mmol) was then added dropwise to the stirring reaction and the reaction left to stir at room temperature. After 10 min, the reaction was diluted to 3 mL with DMSO, and purified directly, without workup by MDAP (Method C). Desired fractions were combined, and the volatile solvents removed *in vacuo*. The pH of the remaining aqueous was adjusted to >10 with aq. NH_4OH , and the product extracted to DCM (5 x 10 mL). The organic phases were combined, dried using a hydrophobic frit, concentrated *in vacuo* and dried in a vacuum oven at 40 °C for 1 h to afford the product as an off-white solid (55 mg, 0.096 mmol, 46% yield). M.pt.: 151-156 °C. ν_{max} (neat): 3366, 2925, 2806, 1736, 1507, 1479, 1418 cm^{-1} . 1H NMR (400 MHz, CHLOROFORM- d) $\delta = 8.74$ (1H, s), 8.70 (1H, d, $J = 2.5$ Hz), 8.64 (1H, d, $J = 2.5$ Hz), 8.01 (1H, d, $J = 1.0$ Hz), 7.68 - 7.67 (1H, m), 7.26 - 7.21 (2H, m), 7.19 (1H, s), 7.16 - 7.10 (2H, m), 4.17 (3H, s), 3.80 (2H, s), 2.77 - 2.59 (9H, m), 1.06 (6H, d, $J = 6.5$ Hz). $^{19}F\{H\}$ NMR (376 MHz, CHLOROFORM- d) $\delta = -117.16$ (1F, s). ^{13}C NMR (126 MHz, CHLOROFORM- d) $\delta = 163.3$, 162.5, 160.6, 160.4 (1C, d, $J = 244.6$ Hz), 150.0, 148.9, 146.5 (1C, d, $J = 2.8$ Hz), 141.1, 140.6, 135.7, 135.5, 129.5, 127.7, 123.2 (2C, d, $J = 8.3$ Hz), 120.8, 119.4, 119.1, 116.2 (2C, d, $J = 23.1$ Hz), 112.9, 109.3, 54.6, 54.4, 52.9, 52.3, 48.5, 18.6. LCMS (Method A): $t_R = 0.77$ min, $[M+H]^+$ 571.1, (99% purity). HRMS: ($C_{31}H_{32}FN_6O_4$) $[M+H]^+$ requires 571.2464, found $[M+H]^+$ 571.2470.

Phenyl 5-(4-(5-((4-isopropylpiperazin-1-yl)methyl)oxazol-2-yl)-1H-indazol-6-yl)-2-methoxynicotinate (101)



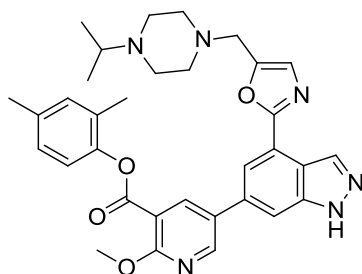
Compound **64** (100 mg, 0.210 mmol), phenol (30 mg, 0.32 mmol) and PyBOP (120 mg, 0.231 mmol) and were stirred in DMF (1.5 mL) at room temperature. DIPEA (0.073 mL, 0.42 mmol) was then added dropwise to the stirring reaction and the reaction left to stir at room temperature. After 5 min, the reaction was diluted to 3 mL with DMSO, and purified directly, without workup by MDAP (Method C). Desired fractions were combined, and the volatile solvents removed *in vacuo*. The pH of the remaining aqueous was adjusted to >10 with aq. NH₄OH, and the product extracted to DCM (5 x 10 mL). The organic phases were combined, dried using a hydrophobic frit, and concentrated *in vacuo* to afford the product as an off-white solid (29 mg, 0.052 mmol, 25% yield). M.pt.: 128-136 °C. ν_{\max} (neat): 3352, 2925, 2813, 1729, 1477 cm⁻¹. ¹H NMR (400 MHz, CHLOROFORM-d) δ = 8.73 (1H, d, *J* = 1.0 Hz), 8.69 (1H, d, *J* = 2.5 Hz), 8.65 (1H, d, *J* = 2.5 Hz), 8.00 (1H, d, *J* = 1.3 Hz), 7.66 (1H, t, *J* = 1.0 Hz), 7.49 - 7.42 (2H, m), 7.32 - 7.27 (3H, m), 7.19 (1H, s), 4.17 (3H, s), 3.80 (2H, s), 2.78 - 2.56 (9H, m), 1.06 (6H, d, *J* = 6.5 Hz). ¹³C NMR (126 MHz, DMSO-d₆) δ = 163.30, 162.47, 160.60, 150.75, 149.82, 148.88, 141.15, 140.60, 135.62, 135.51, 129.49, 129.45, 127.72, 126.03, 121.76, 120.77, 119.35, 119.11, 113.16, 109.28, 54.57, 54.45, 52.81, 52.29, 48.52, 18.56 (two decimal places required to distinguish signals). LCMS (Method A): *t_R* = 0.73 min, [M+H⁺] 553.2, (100% purity). HRMS: (C₃₁H₃₃N₆O₄) [M+H⁺] requires 553.2558, found [M+H⁺] 553.2557.

4-Methoxyphenyl 5-(4-(5-((4-isopropylpiperazin-1-yl)methyl)oxazol-2-yl)-1H-indazol-6-yl)-2-methoxynicotinate (103)



Compound **64** (100 mg, 0.210 mmol), 4-methoxyphenol (39 mg, 0.31 mmol) and PyBOP (120 mg, 0.231 mmol) were stirred in DMF (1.5 mL) at room temperature. DIPEA (0.073 mL, 0.42 mmol) was then added dropwise to the stirring reaction and the reaction left to stir at room temperature. After 1 h, the reaction was diluted to 3 mL with DMSO, and purified directly, without workup, by MDAP (Method C). Desired fractions were combined, and the volatile solvents removed *in vacuo*. The pH of the remaining aqueous was adjusted to >10 with aq. NH₄OH, and the product extracted to DCM (5 x 10 mL). The organics were dried through a hydrophobic frit, concentrated *in vacuo* and dried in a vacuum oven at 40 °C overnight to afford the product as an off-white solid (22 mg, 0.038 mmol, 18% yield). M.pt.: 167-173 °C. ν_{\max} (neat): 3351, 2924, 2853, 2809, 1730, 1508 cm⁻¹. ¹H NMR (400 MHz, CHLOROFORM-d) δ = 8.72 (1H, d, *J* = 0.8 Hz), 8.68 (1H, d, *J* = 2.5 Hz), 8.64 (1H, d, *J* = 2.5 Hz), 7.99 (1H, d, *J* = 1.3 Hz), 7.67 - 7.64 (1H, m), 7.19 (1H, s), 7.19 (2H, d, *J* = 9.1 Hz), 6.96 (2H, d, *J* = 9.1 Hz), 4.16 (3H, s), 3.84 (3H, s), 3.80 (2H, s), 2.77 - 2.59 (9H, m), 1.06 (6H, d, *J* = 6.5 Hz). ¹³C NMR (126 MHz, CHLOROFORM-d) δ = 163.7, 162.4, 160.6, 157.4, 149.7, 148.9, 144.2, 141.1, 140.6, 135.6, 135.5, 129.4, 127.7, 122.5, 120.8, 119.3, 119.1, 114.5, 113.3, 109.3, 55.6, 54.6, 54.4, 52.8, 52.3, 48.5, 18.6. LCMS (Method A): *t_R* = 0.73 min, [M+H⁺] 583.6, (98% purity). HRMS: (C₃₂H₃₅N₆O₅) [M+H⁺] requires 583.2663, found [M+H⁺] 583.2681.

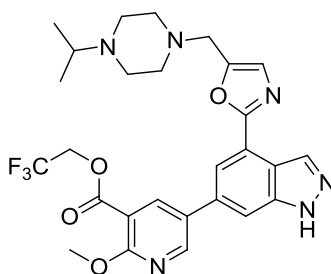
2,4-Dimethylphenyl 5-(4-(5-((4-isopropylpiperazin-1-yl)methyl)oxazol-2-yl)-1H-indazol-6-yl)-2-methoxynicotinate (102)



Compound **64** (100 mg, 0.210 mmol), 2,4-dimethylphenol (0.039 mL, 0.32 mmol) and PyBOP (120 mg, 0.231 mmol) and were stirred in DMF (1.5 mL) at room temperature. DIPEA (0.073 mL, 0.42 mmol) was then added dropwise to the stirring reaction and the reaction left to stir at room temperature. After 2 h, the reaction was diluted to 3 mL, and purified directly, without workup, by MDAP (Method C). Desired fractions were combined, and the volatile solvents removed *in vacuo*. The pH of the remaining aqueous was adjusted to >10 with aq. NH₄OH, and the product extracted to DCM (5 x 10 mL). The organic phases were combined, dried using a hydrophobic frit, and concentrated *in vacuo* and dried in a vacuum oven at 40

°C overnight to afford the product as an off-white solid (14 mg, 0.024 mmol, 12% yield). M.pt.: 183-189 °C. ν_{\max} (neat): 3345, 2923, 2853, 1728 cm^{-1} . ^1H NMR (500 MHz, CHLOROFORM- d) δ = 10.89 (1H, br. s), 8.72 (1H, s), 8.69 (1H, d, J = 2.7 Hz), 8.65 (1H, d, J = 2.7 Hz), 7.99 (1H, s), 7.66 (1H, s), 7.19 (1H, s), 7.10 (1H, s), 7.07 (2H, s), 4.16 (3H, s), 3.80 (2H, s), 2.78 - 2.57 (9H, m), 2.35 (3H, s), 2.27 (3H, s), 1.06 (6H, d, J = 6.3 Hz). ^{13}C NMR (126 MHz, CHLOROFORM- d) δ = 163.5, 162.4, 160.6, 149.7, 148.9, 147.2, 141.2, 140.6, 135.8, 135.7, 135.6, 131.8, 129.8, 129.5, 127.7, 127.5, 121.7, 120.8, 119.4, 119.1, 113.4, 109.3, 54.5, 54.4, 52.9, 52.3, 48.5, 20.9, 18.6, 16.3. LCMS (Method A): t_{R} = 0.82 min, $[\text{M}+\text{H}^+]$ 581.2 (100% purity). HRMS: ($\text{C}_{33}\text{H}_{37}\text{N}_6\text{O}_4$) $[\text{M}+\text{H}^+]$ requires 581.2871, found $[\text{M}+\text{H}^+]$ 581.2870.

2,2,2-Trifluoroethyl 5-(4-(5-((4-isopropylpiperazin-1-yl)methyl)oxazol-2-yl)-1H-indazol-6-yl)-2-methoxynicotinate (104)

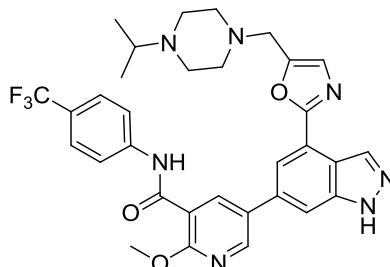


5-(4-(5-((4-Isopropylpiperazin-1-yl)methyl)oxazol-2-yl)-1H-indazol-6-yl)-2-methoxynicotinic acid **64** (100 mg, 0.210 mmol), 2,2,2-trifluoroethanol (0.023 mL, 0.32 mmol) and PyBOP (120 mg, 0.231 mmol) and were stirred in DMF (1.5 mL) at room temperature. DIPEA (0.073 mL, 0.42 mmol) was then added dropwise to the stirring reaction and the reaction left to stir at room temperature. After 30 min, the reaction was purified directly, without workup by MDAP (ammonium bicarbonate modifier). Desired fractions were combined, and the volatile solvents removed *in vacuo*. The pH of the remaining aqueous was adjusted to >10 with aq. NH_4OH , and the product extracted to DCM (5 x 10 mL). The organics were dried through a hydrophobic frit and concentrated *in vacuo* to afford the title product as an off-white solid (22 mg, 0.039 mmol, 19%). M.pt.: 119-125 °C. ν_{\max} (neat): 3131, 2925, 2816, 1749, 1725, 1606, 1481 cm^{-1} . ^1H NMR (400 MHz, CHLOROFORM- d) δ = 8.73 (1H, d, J = 1.0 Hz), 8.68 (1H, d, J = 2.8 Hz), 8.49 (1H, d, J = 2.8 Hz), 7.97 (1H, d, J = 1.3 Hz), 7.64 (1H, s), 7.20 (1H, s), 4.75 (2H, q, J = 8.3 Hz), 4.15 (3H, s), 3.81 (2H, s), 2.78 - 2.58 (9H, m), 1.06 (6H, d, J = 6.5 Hz) (indazole N-H not observed). $^{19}\text{F}\{^1\text{H}\}$ NMR (376 MHz, CHLOROFORM- d) δ = -73.88 (1F, s). ^{13}C NMR (126 MHz, CHLOROFORM- d) δ = 163.0, 162.4, 160.5, 150.3, 148.9, 141.2, 140.4, 135.7, 135.4, 129.5, 127.7, 120.9, 123.1 (1C, q, J = 276.5 Hz), 119.4, 119.1, 112.0, 109.2, 60.9 (1C, q, J = 37.0

Hz), 54.6, 54.4, 52.8, 52.3, 48.5, 18.6. LCMS (Method A): $t_R = 0.70$ min, $[M+H]^+$ 559.6, (97% purity). HRMS: $(C_{27}H_{30}F_3N_6O_4)$ $[M+H]^+$ requires 559.2275, found $[M+H]^+$ 559.2272.

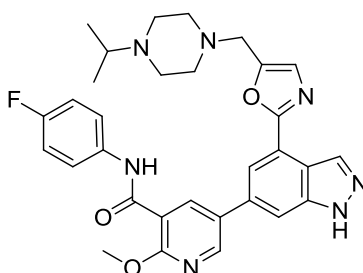
Synthesis of Amide Equivalents of the Activated Esters

5-(4-(5-((4-isopropylpiperazin-1-yl)methyl)oxazol-2-yl)-1H-indazol-6-yl)-2-methoxy-N-(4-(trifluoromethyl)phenyl)nicotinamide (106)



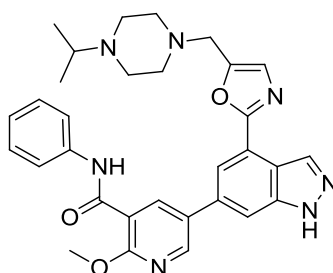
5-(4-(5-((4-isopropylpiperazin-1-yl)methyl)oxazol-2-yl)-1H-indazol-6-yl)-2-methoxynicotinic acid **64** (30 mg, 0.063 mmol), 4-(trifluoromethyl)aniline (0.012 ml, 0.094 mmol) and PyBOP (36.0 mg, 0.069 mmol) were stirred in *N,N*-dimethylformamide (DMF) (0.5 ml) at room temperature. DIPEA (0.022 ml, 0.126 mmol) was then added dropwise to the stirring reaction and the reaction left to stir at room temperature. After 3 h, the reaction was concentrated under flowing nitrogen at 40 °C, and the reaction mixture loaded onto an SCX column. Impurities were washed off with methanol, and the crude product was eluted with a solution of ammonia in methanol. The eluted fractions were concentrated, and then purified by MDAP (ammonium bicarbonate modifier). Desired fractions were combined and concentrated *in vacuo* to afford the product as an off-white gum (4.0 mg, 6.5 μ mol, 10%). ν_{max} (neat): 3367, 2968, 2817, 1678, 1602, 1541, 1471, 1323 cm^{-1} . 1H NMR (600 MHz, CHLOROFORM-*d*) $\delta = 11.05$ (1H, br. s), 10.04 (1H, s), 8.87 (1H, d, $J = 2.6$ Hz), 8.71 (1H, s), 8.64 (1H, d, $J = 2.6$ Hz), 7.98 (1H, s), 7.85 (2H, d, $J = 8.3$ Hz), 7.69 - 7.64 (3H, m), 7.22 (1H, s), 4.29 (3H, s), 3.81 (2H, s), 2.91 - 2.45 (9H, m), 1.07 (6H, d, $J = 6.4$ Hz). ^{13}C NMR (151 MHz, CHLOROFORM-*d*) $\delta = 161.93, 160.57, 159.74, 148.89, 148.66, 141.18, 141.00, 140.78, 135.66, 135.33, 131.23, 127.76, 126.35$ (2C, q, $J = 3.6$ Hz), 126.35 (1C q, $J = 33.0$ Hz), 124.10 (1C, q, $J = 271.5$ Hz), 120.81, 120.10, 119.46, 119.06, 115.65, 109.36, 54.88, 54.48, 52.82, 52.30, 48.51, 18.53 (two decimal places required to distinguish signals). ^{19}F NMR (376 MHz, CHLOROFORM-*d*) $\delta = -62.13$ (1F, s). LCMS (Method A): $t_R = 0.82$ min, $[M+H]^+$ 620.1, (94% purity). HRMS: $(C_{32}H_{33}N_7O_3F_3)$ $[M+H]^+$ requires 620.2597, found $[M+H]^+$ 620.2596.

N-(4-Fluorophenyl)-5-(4-(5-((4-isopropylpiperazin-1-yl)methyl)oxazol-2-yl)-1H-indazol-6-yl)-2-methoxynicotinamide (107)



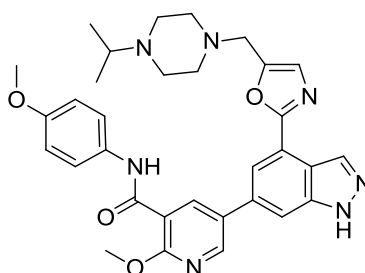
5-(4-(5-((4-Isopropylpiperazin-1-yl)methyl)oxazol-2-yl)-1H-indazol-6-yl)-2-methoxynicotinic acid **64** (50 mg, 0.11 mmol), 4-fluoroaniline (0.015 mL, 0.16 mmol) and PyBOP (66 mg, 0.13 mmol) were stirred in DMF (0.5 mL) at room temperature. DIPEA (0.037 mL, 0.21 mmol) was then added dropwise to the stirring reaction and the reaction left to stir at room temperature. After 1.5 h, the reaction was diluted with EtOAc (15 mL) and washed with distilled water (10 mL) and brine (3 x 10 mL). The organics were dried through a hydrophobic frit and concentrated *in vacuo*. The residue was then purified by MDAP (ammonium bicarbonate modifier). Desired fractions were combined, and the solvent removed by nitrogen blow-down at 40 °C. The compound was desalted by partitioning between distilled water (5 mL) and EtOAc (5 mL). The pH of the aqueous was adjusted to 10 with aq. NaOH (2 M) and the product extracted to the organic layer. The aqueous was extracted with further EtOAc washes (3 x 10 mL) and the organics dried through a hydrophobic frit and concentrated *in vacuo* to afford the title product as an off-white solid (16 mg, 0.028 mmol, 27%). M.pt.: 146-150 °C. ν_{\max} (neat): 2930, 2815, 1649, 1547, 1510 cm^{-1} . ^1H NMR (400 MHz, CHLOROFORM-*d*) δ = 9.83 (1H, s), 8.85 (1H, d, J = 2.5 Hz), 8.68 (1H, d, J = 1.0 Hz), 8.60 (1H, d, J = 2.5 Hz), 7.93 (1H, d, J = 1.0 Hz), 7.72 - 7.65 (2H, m), 7.62 (1H, s), 7.21 (1H, s), 7.13 - 7.05 (2H, m), 4.26 (3H, s), 3.81 (2H, s), 2.82 - 2.58 (9H, m), 1.06 (6H, d, J = 6.5 Hz), indazole N-H not observed. $^{19}\text{F}\{^1\text{H}\}$ NMR (376 MHz, CHLOROFORM-*d*) δ = -117.55 (1F, s). ^{13}C NMR (126 MHz, CHLOROFORM-*d*) δ = 160.7 (1C, d, J = 241.4 Hz), 160.6, 160.5, 158.6, 148.7, 148.3, 141.1, 140.6, 135.5, 135.3, 133.9 (1C, d, J = 4.6 Hz), 131.1, 127.8, 122.3 (2C, d, J = 7.4 Hz), 120.6, 119.3, 118.9, 115.8, 115.7 (2C, d, J = 22.2 Hz), 109.3, 54.8, 54.4, 52.8, 52.3, 48.5, 18.6. LCMS (Method A): t_{R} = 0.74 min, $[\text{M}+\text{H}^+]$ 570.3, (100% purity). HRMS: ($\text{C}_{31}\text{H}_{33}\text{FN}_7\text{O}_3$) $[\text{M}+\text{H}^+]$ requires 570.2623, found $[\text{M}+\text{H}^+]$ 570.2639.

5-(4-(5-((4-Isopropylpiperazin-1-yl)methyl)oxazol-2-yl)-1H-indazol-6-yl)-2-methoxy-N-phenylnicotinamide (108)



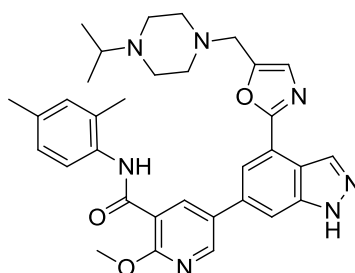
5-(4-(5-((4-Isopropylpiperazin-1-yl)methyl)oxazol-2-yl)-1H-indazol-6-yl)-2-methoxynicotinic acid **64** (50 mg, 0.11 mmol), aniline (0.014 mL, 0.16 mmol) and PyBOP (66 mg, 0.13 mmol) were stirred in DMF (0.5 mL) at room temperature. DIPEA (0.037 mL, 0.21 mmol) was then added dropwise to the stirring reaction and the reaction left to stir at room temperature. After 1.5 h, the reaction was purified directly, without workup, by MDAP (ammonium bicarbonate modifier). Desired fractions were combined, and the solvent removed by nitrogen blowdown at 40 °C. The compound was desalted by partitioning between distilled water (5 mL) and EtOAc (5 mL). The pH of the aqueous was adjusted to 10 with aq. NaOH (2 M) and the product extracted to the organic layer. The aqueous was extracted with further EtOAc washes (3 x 10 mL) and the organics dried through a hydrophobic frit and concentrated *in vacuo* to afford the title product as an off-white solid (17 mg, 0.031 mmol, 29%). M.pt.: 133-141 °C. ν_{max} (neat): 2954, 2807, 1673, 1599, 1541, 1470 cm^{-1} . ^1H NMR (400 MHz, CHLOROFORM-*d*) δ = 9.87 (1H, s), 8.87 (1H, d, J = 2.5 Hz), 8.70 (1H, d, J = 1.0 Hz), 8.61 (1H, d, J = 2.8 Hz), 7.97 (1H, d, J = 1.3 Hz), 7.73 (2H, dd, J = 8.6, 1.2 Hz), 7.67 - 7.63 (1H, m), 7.41 (2H, t, J = 7.9 Hz), 7.22 - 7.15 (2H, m), 4.27 (3H, s), 3.81 (2H, s), 2.81 - 2.56 (9H, m), 1.08 - 1.01 (6H, m) (indazole N-H not observed). ^{13}C NMR (126 MHz, CHLOROFORM-*d*) δ = 161.6, 160.6, 159.8, 148.8, 148.2, 141.1, 140.6, 137.9, 135.5, 135.4, 131.0, 129.1, 127.7, 124.6, 120.7, 120.5, 119.4, 119.0, 116.1, 109.3, 54.7, 54.4, 52.8, 52.3, 48.5, 18.6. LCMS (Method A): t_{R} = 0.73 min, $[\text{M}+\text{H}^+]$ 552.4, (99% purity). HRMS: ($\text{C}_{31}\text{H}_{34}\text{N}_7\text{O}_3$) $[\text{M}+\text{H}^+]$ requires 552.2718, found $[\text{M}+\text{H}^+]$ 552.2702.

5-(4-(5-((4-Isopropylpiperazin-1-yl)methyl)oxazol-2-yl)-1H-indazol-6-yl)-2-methoxy-N-(4-methoxyphenyl)nicotinamide (110)



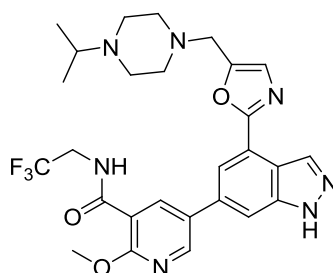
5-(4-(5-((4-Isopropylpiperazin-1-yl)methyl)oxazol-2-yl)-1H-indazol-6-yl)-2-methoxynicotinic acid **64** (50 mg, 0.11 mmol), *p*-methoxyaniline (0.014 mL, 0.16 mmol) and PyBOP (66 mg, 0.13 mmol) were stirred in DMF (0.5 mL) at room temperature. DIPEA (0.037 mL, 0.21 mmol) was then added dropwise to the stirring reaction and the reaction left to stir at room temperature. After 1.5 h, the reaction was purified directly, without workup, by MDAP (ammonium bicarbonate modifier). Desired fractions were combined, and the solvent removed by nitrogen blowdown at 40 °C. The compound was desalted by partitioning between distilled water (5 mL) and EtOAc (5 mL). The pH of the aqueous was adjusted to 10 with aq. NaOH (2 M) and the product extracted to the organic layer. The aqueous was extracted with further EtOAc washes (3 x 10 mL) and the organics dried through a hydrophobic frit and concentrated *in vacuo* to afford the title product as an off-white solid (38 mg, 0.065 mmol, 62%). M.pt.: 106-110 °C. ν_{\max} (neat): 2959, 2816, 1659, 1600, 1544, 1510, 1470 cm^{-1} . ^1H NMR (400 MHz, CHLOROFORM-*d*) δ = 9.75 (1H, s), 8.86 (1H, d, J = 2.5 Hz), 8.70 (1H, d, J = 0.8 Hz), 8.60 (1H, d, J = 2.5 Hz), 7.97 (1H, d, J = 1.3 Hz), 7.66 - 7.65 (1H, m), 7.63 (2H, d, J = 9.1 Hz), 7.20 (1H, s), 6.94 (2H, d, J = 9.1 Hz), 4.26 (3H, s), 3.84 (3H, s), 3.80 (2H, s), 2.79 - 2.60 (9H, m), 1.06 (6H, d, J = 6.5 Hz), indazole N-H not observed. ^{13}C NMR (126 MHz, CHLOROFORM-*d*) δ = 161.4, 160.6, 159.8, 156.7, 148.8, 148.0, 141.1, 140.5, 135.4, 131.1, 131.0, 127.7, 122.2, 120.6, 119.3, 119.0, 116.1, 114.8, 114.2, 109.4, 55.5, 54.7, 54.5, 52.8, 52.3, 48.5, 18.6. LCMS (Method A): t_{R} = 0.73 min, $[\text{M}+\text{H}^+]$ 582.3, (98% purity). HRMS: ($\text{C}_{32}\text{H}_{36}\text{N}_7\text{O}_4$) $[\text{M}+\text{H}^+]$ requires 582.2823, found $[\text{M}+\text{H}^+]$ 582.2806.

N-(2,4-Dimethylphenyl)-5-(4-(5-((4-isopropylpiperazin-1-yl)methyl)oxazol-2-yl)-1H-indazol-6-yl)-2-methoxynicotinamide (109)



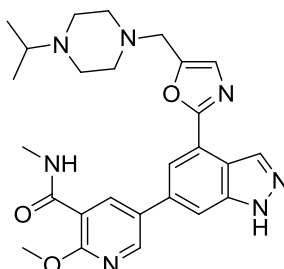
5-(4-(5-((4-Isopropylpiperazin-1-yl)methyl)oxazol-2-yl)-1H-indazol-6-yl)-2-methoxynicotinic acid **64** (50 mg, 0.11 mmol), 2,4-dimethylaniline (0.019 mL, 0.16 mmol) and PyBOP (66 mg, 0.13 mmol) were stirred in DMF (0.5 mL) at room temperature. DIPEA (0.037 mL, 0.21 mmol) was then added dropwise to the stirring reaction and the reaction left to stir at room temperature. After 1.5 h, the reaction was purified directly, without workup, by MDAP (ammonium bicarbonate modifier). Desired fractions were combined, and the solvent removed by nitrogen blowdown at 40 °C. The compound was desalted by partitioning between distilled water (5 mL) and EtOAc (5 mL). The pH of the aqueous layer was adjusted to 10 with aq. NaOH (2 M) and the product extracted to the organic layer. The aqueous layer was extracted with further EtOAc washes (3 x 10 mL) and the organics dried through a hydrophobic frit and concentrated *in vacuo* to afford the title product as an off-white solid (22 mg, 0.038 mmol, 36%). M.pt.: 132-138 °C. ν_{\max} (neat): 2964, 2815, 1669, 1600, 1540, 1470 cm^{-1} . ^1H NMR (400 MHz, CHLOROFORM-*d*) δ = 9.80 (1H, s), 8.90 (1H, d, J = 2.5 Hz), 8.70 (1H, s), 8.61 (1H, d, J = 2.5 Hz), 8.14 (1H, d, J = 8.1 Hz), 7.97 (1H, d, J = 1.0 Hz), 7.66 (1H, s), 7.21 (1H, s), 7.13 - 7.04 (2H, m), 4.26 (3H, s), 3.80 (2H, s), 2.80 - 2.58 (9H, m), 2.37 (3H, s), 2.34 (3H, s), 1.06 (6H, d, J = 6.5 Hz), indazole N-H not observed. ^{13}C NMR (126 MHz, CHLOROFORM-*d*) δ = 161.4, 160.6, 159.8, 148.7, 148.0, 141.1, 140.7, 135.5, 135.4, 134.4, 133.8, 131.1, 131.0, 127.9, 127.7, 127.4, 122.1, 120.6, 119.3, 119.0, 116.3, 109.4, 54.7, 54.4, 52.8, 52.3, 48.5, 20.9, 18.6, 17.9. LCMS (Method A): t_{R} = 0.82 min, $[\text{M}+\text{H}^+]$ 580.4, (100% purity). HRMS: ($\text{C}_{33}\text{H}_{38}\text{N}_7\text{O}_3$) $[\text{M}+\text{H}^+]$ requires 580.3031, found $[\text{M}+\text{H}^+]$ 580.3024.

5-(4-(5-((4-Isopropylpiperazin-1-yl)methyl)oxazol-2-yl)-1H-indazol-6-yl)-2-methoxy-N-(2,2,2-trifluoroethyl)nicotinamide (111)



5-(4-(5-((4-Isopropylpiperazin-1-yl)methyl)oxazol-2-yl)-1H-indazol-6-yl)-2-methoxynicotinic acid **64** (50 mg, 0.11 mmol), 2,2,2-trifluoroethanamine (0.025 mL, 0.32 mmol) and PyBOP (66 mg, 0.13 mmol) were stirred in DMF (0.5 mL) at room temperature. DIPEA (0.037 mL, 0.21 mmol) was then added dropwise to the stirring reaction and the reaction left to stir at room temperature. After 1 h, the sample was purified directly, without workup, by MDAP (ammonium bicarbonate modifier). Desired fractions were combined, and the solvent removed *in vacuo* to afford the title product as an off-white solid (39 mg, 0.070 mmol, 67%). M.pt.: 137-146 °C. ν_{\max} (neat): 2964, 2818, 1667, 1539, 1473 cm^{-1} . ^1H NMR (400 MHz, CHLOROFORM-*d*) δ = 11.04 (1H, br. s), 8.83 (1H, d, J = 2.5 Hz), 8.70 (1H, d, J = 1.0 Hz), 8.62 (1H, d, J = 2.5 Hz), 8.32 (1H, t, J = 6.2 Hz), 7.96 (1H, d, J = 1.3 Hz), 7.64 (1H, s), 7.21 (1H, s), 4.29 - 4.14 (5H, m), 3.80 (2H, s), 2.80 - 2.57 (9H, m), 1.06 (6H, d, J = 6.5 Hz). $^{19}\text{F}\{^1\text{H}\}$ NMR (376 MHz, CHLOROFORM-*d*) δ = -72.19 (1F, s). ^{13}C NMR (126 MHz, CHLOROFORM-*d*) δ = 164.2, 160.5, 160.1, 148.8, 148.6, 141.1, 140.8, 135.6, 135.3, 130.9, 127.7, 124.2 (1C, q, J = 278.4 Hz), 120.7, 119.4, 119.0, 114.6, 109.3, 54.7, 54.4, 52.8, 52.3, 48.5, 41.1 (1C, q, J = 34.2 Hz), 18.6. LCMS (Method A): t_{R} = 0.66 min, $[\text{M}+\text{H}^+]$ 558.3, (99% purity). HRMS: ($\text{C}_{27}\text{H}_{31}\text{F}_3\text{N}_7\text{O}_3$) $[\text{M}+\text{H}^+]$ requires 558.2435, found $[\text{M}+\text{H}^+]$ 558.2412.

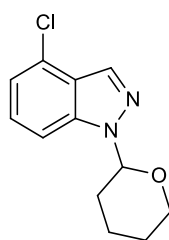
5-(4-(5-((4-Isopropylpiperazin-1-yl)methyl)oxazol-2-yl)-1H-indazol-6-yl)-2-methoxy-N-methylnicotinamide (112)



5-(4-(5-((4-Isopropylpiperazin-1-yl)methyl)oxazol-2-yl)-1H-indazol-6-yl)-2-methoxynicotinic acid **64** (50 mg, 0.11 mmol), methylamine (2.0 M in THF) (0.079 mL, 0.16 mmol) and PyBOP (66 mg, 0.13 mmol) were stirred in DMF (0.5 mL) at room temperature. DIPEA (0.037 mL, 0.210 mmol) was then added dropwise to the stirring reaction and the reaction left to stir at room temperature. A further 0.2 mL of methylamine solution was added after 16 h, and then at 25 h a further 66 mg PyBOP, 0.1 mL methylamine solution and 0.037 mL DIPEA were added. Full conversion was observed after a total of 41 h. The product was then isolated, without workup, by MDAP and further automated reverse-phase column chromatography (ammonium bicarbonate modifier). Desired fractions were combined, and the volatile solvents removed *in vacuo*. The pH of the remaining aqueous layer was then confirmed to be 10, and the product extracted to DCM (3 x 15 mL). The organics were dried through a hydrophobic frit and concentrated *in vacuo* to afford the title compound as a white solid (13 mg, 0.027 mmol, 25%). M.pt.: 179-184 °C. ν_{\max} (neat): 3417, 3221, 2925, 2806, 1658, 1643, 1542, 1470 cm^{-1} . ^1H NMR (400 MHz, CHLOROFORM-*d*) δ = 11.26 (1H, br. s), 8.85 (1H, d, J = 2.5 Hz), 8.71 (1H, s), 8.59 (1H, d, J = 2.8 Hz), 8.03 - 7.94 (2H, m), 7.68 (1H, s), 7.20 (1H, s), 4.19 (3H, s), 3.79 (2H, s), 3.11 (3H, d, J = 5.0 Hz), 2.77 - 2.58 (9H, m), 1.06 (6H, d, J = 6.5 Hz). ^{13}C NMR (126 MHz, CHLOROFORM-*d*) δ = 164.4, 160.6, 160.2, 148.8, 147.7, 141.2, 140.4, 135.6, 135.5, 130.7, 127.7, 120.6, 119.3, 119.1, 115.7, 109.5, 54.5, 52.8, 52.3, 48.5, 29.7, 26.8, 18.6. LCMS (Method A): t_{R} = 0.54 min, $[\text{M}+\text{H}^+]$ 490.2, (100% purity). HRMS: ($\text{C}_{26}\text{H}_{32}\text{N}_7\text{O}_3$) $[\text{M}+\text{H}^+]$ requires 490.2561, found $[\text{M}+\text{H}^+]$ 490.2553.

Synthesis of Azido Probe 131

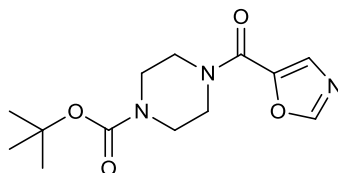
4-Chloro-1-(tetrahydro-2H-pyran-2-yl)-1H-indazole (134)



A solution of 4-chloro-1H-indazole **132** (5 g, 33 mmol) in EtOAc (50 mL) was stirred under nitrogen. 3,4-Dihydro-2H-pyran **133** (6.0 mL, 66 mmol) was then added, followed by trifluoroacetic acid (0.505 mL, 6.55 mmol), and the reaction mixture was heated to reflux. After 2.5 h the reaction was cooled to room temperature, triethylamine (0.936 mL, 6.72 mmol) was then added, and the reaction stirred at room temperature for 20 min.

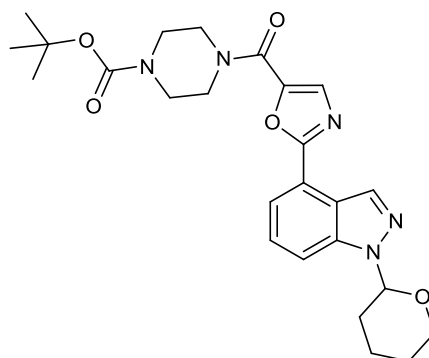
Crystallisation was attempted using IPA and water, heating at 65 °C and cooling slowly, without success – no crystal formed. The volatiles were then removed *in vacuo*, and the product extracted with EtOAc (3 x 25 mL). The organics were dried using a hydrophobic frit, and concentrated *in vacuo* to afford an oil, which crystallised overnight in the freezer. The solids were broken with a spatula, and then dried on a high-vacuum line for 3 h to afford the product as an off-white solid (7.67 g, 32.4 mmol, 99% yield). M.pt.: 64-68 °C. ν_{\max} (neat): 2970, 2949, 2854, 1613, 1497, 1447, 1418, 1173 cm^{-1} . ^1H NMR (400 MHz, CHLOROFORM-*d*) δ = 8.11 (1H, s), 7.55 - 7.49 (1H, m), 7.28 - 7.35 (1H, m), 7.19 - 7.14 (1H, m), 5.73 (1H, dd, J = 9.3, 2.8 Hz), 4.07 - 3.98 (1H, m), 3.80 - 3.70 (1H, m), 2.63 - 2.50 (1H, m), 2.23 - 2.04 (2H, m), 1.85 - 1.63 (3H, m). ^{13}C NMR (101 MHz, CHLOROFORM-*d*) δ = 140.5, 132.4, 127.1, 126.6, 124.0, 120.9, 108.9, 85.7, 67.4, 29.4, 25.1, 22.4. LCMS (method A): t_{R} = 1.22 min, $[\text{M}+\text{H}^+]$ 237.2, (100% purity). HRMS: ($\text{C}_{12}\text{H}_{14}\text{ClN}_2\text{O}$) $[\text{M}+\text{H}^+]$ requires 237.0795, found $[\text{M}+\text{H}^+]$ 237.0788.

***tert*-Butyl 4-(oxazole-5-carbonyl)piperazine-1-carboxylate (137)**



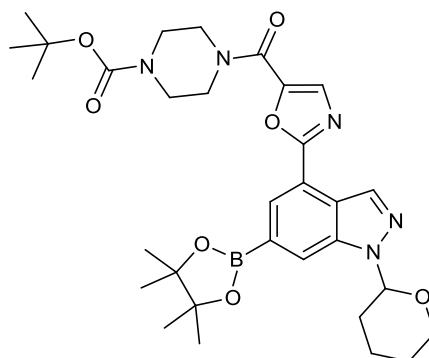
To a suspension of oxazole-5-carboxylic acid **135** (2.50 g, 22.1 mmol) in EtOAc (45 mL) under nitrogen was added DIPEA (7.72 ml, 44.2 mmol) and then propylphosphonic anhydride solution (T3P[®]) (50% wt in EtOAc) (15.8 mL, 26.5 mmol). *tert*-Butyl piperazine-1-carboxylate **136** (6.18 g, 33.2 mmol) was then added and the reaction stirred at room temperature for 30 min. The reaction mixture was then diluted with EtOAc (20 mL), and washed sequentially with NaOH (2 M aq, 25 mL), HCl (2 M aq, 25 mL), and brine (25 mL). The organics were dried using a hydrophobic frit and concentrated *in vacuo* to afford a yellow oil, which was dried under high vacuum overnight to afford the product as a pale yellow solid (5.51 g, 19.6 mmol, 89% yield). M.pt. 135-138 °C. ν_{\max} (neat): 3096, 2975, 2933, 2860, 1700, 1683, 1611, 1427 cm^{-1} . ^1H NMR (400 MHz, CHLOROFORM-*d*) δ = 7.96 (1H, s), 7.62 (1H, s), 3.80 - 3.72 (4H, m), 3.56 - 3.50 (4H, m), 1.49 (9H, s). ^{13}C NMR (101 MHz, CHLOROFORM-*d*) δ = 157.3, 154.3, 151.4, 144.9, 131.8, 80.4, 46.0 (2C, br. s), 43.4 (2C, br. s), 28.3. LCMS (method A): t_{R} = 0.77 min, $[\text{M}+\text{Na}^+]$ 304.0, (100% purity). HRMS: ($\text{C}_8\text{H}_{12}\text{N}_3\text{O}_2$) $[\text{M}+\text{H}-\text{Boc}]$ requires 182.0930, found $[\text{M}+\text{H}-\text{Boc}]$ 182.0932; ($\text{C}_{13}\text{H}_{19}\text{N}_3\text{O}_4\text{Na}$) $[\text{M}+\text{Na}^+]$ requires 304.1273, found $[\text{M}+\text{Na}^+]$ 304.1273.

tert-Butyl 4-(2-(1-(tetrahydro-2H-pyran-2-yl)-1H-indazol-4-yl)oxazole-5-carbonyl) piperazine-1-carboxylate (**138**)



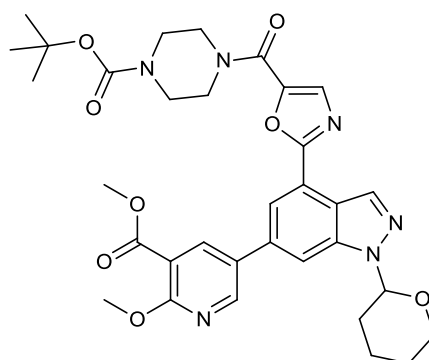
Palladium(II) chloride (42 mg, 0.24 mmol) and dicyclohexyl(2',4',6'-triisopropyl-[1,1'-biphenyl]-2-yl)phosphane (XPhos) (0.242 g, 0.507 mmol) were suspended in cyclopentyl methyl ether (CPME) (15 mL). Compound **134** (2.00 g, 8.45 mmol), compound **137** (2.43 g, 8.64 mmol) and potassium carbonate (1.98 g, 14.3 mmol) were added, and rinsed into the flask with CPME (2 mL). A solution of pivalic acid (0.586 mL, 5.05 mmol) dissolved in CPME (2 mL) was added, followed by a rinse with CPME (3 mL). The flask was degassed under vacuum and refilled with nitrogen three times, then heated to 110 °C for 15 h. The reaction was then cooled to room temperature, filtered through celite with EtOAc (25 mL) and the combined solution washed with water (2 x 25 mL) and brine (2 x 25 mL). The organics were dried using a hydrophobic frit and concentrated *in vacuo*. The residue was then purified by automated column chromatography on silica gel (0-100% EtOAc in cyclohexane). Desired fractions were combined, and the solvent removed *in vacuo* to afford the product as an off-white solid (3.24 g, 6.73 mmol, 80% yield). M.pt.: 154-159 °C. ν_{\max} (neat) 3122, 2975, 2928, 1690, 1633, 1420, 1249, 1164 cm^{-1} . ^1H NMR (400 MHz, CHLOROFORM-*d*) δ = 8.68 (1H, s), 7.94 (1H, d, J = 7.1 Hz), 7.78 - 7.82 (2H, m), 7.51 (1H, dd, J = 8.3, 7.3 Hz), 5.81 (1H, dd, J = 9.1, 2.5 Hz), 4.08 - 3.99 (1H, m), 3.93 - 3.73 (5H, m), 3.63 - 3.55 (4H, m), 2.67 - 2.54 (1H, m), 2.26 - 2.08 (2H, m), 1.89 - 1.65 (3H, m), 1.51 (9H, s). ^{13}C NMR (101 MHz, CHLOROFORM-*d*) δ = 161.7, 157.8, 154.5, 144.4, 140.0, 134.4, 134.1, 126.2, 121.5, 121.2, 119.2, 113.6, 85.6, 80.5, 67.4, 43.7, 29.4, 28.4, 25.1, 22.4 (2C of piperazine not observed due to broadening, expected at ~46 ppm from piperazine fragment **137**). 43.7 ppm peak confirmed in HSQC). LCMS (method A): t_{R} = 1.24 min, $[\text{M}+\text{Na}^+]$ 504.2, (99% purity). HRMS: ($\text{C}_{25}\text{H}_{32}\text{N}_5\text{O}_5$) $[\text{M}+\text{H}^+]$ requires 482.2403, found $[\text{M}+\text{H}^+]$ 482.2402.

tert-Butyl 4-(2-(1-(tetrahydro-2H-pyran-2-yl)-6-(4,4,5,5-tetramethyl-1,3,2-dioxaborolan-2-yl)-1H-indazol-4-yl)oxazole-5-carbonyl)piperazine-1-carboxylate (139)



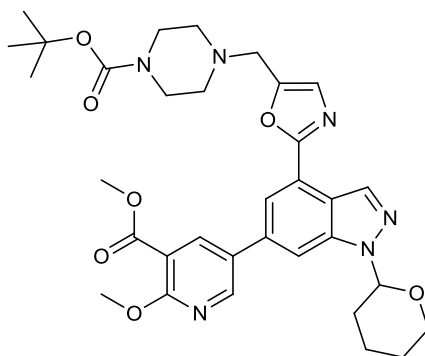
Pinacolborane (2.26 ml, 15.6 mmol) was added to a purple stirred solution of compound **138** (3.00 g, 6.23 mmol), 3,4,7,8-tetramethyl-1,10-phenanthroline (74 mg, 0.31 mmol) and (1,5-cyclooctadiene)(methoxy)iridium(I) dimer (41 mg, 0.062 mmol) in tetrahydrofuran (13 ml) at room temperature. The solution turned green, and was heated to reflux for 18 h. The reaction was then cooled to room temperature, quenched with IPA (16 mL), and concentrated *in vacuo*. The residue was then stirred in IPA (35 mL) at 50 °C for 3.5 h to afford deborylation of the diborylated side-product. The sample was then concentrated to approximately 2/3 volume *in vacuo*, cooled slowly to room temperature, and then cooled further in ice. The solid was isolated by filtration, washed with IPA, and dried under flowing air for 1 h to afford the product as an off-white solid (3.24 g, 5.33 mmol, 86% yield). M.pt.: 146-149 °C. v_{\max} (neat): 2970, 2928, 2860, 1694, 1611, 1421, 1365 cm^{-1} . ^1H NMR (400 MHz, CHLOROFORM-*d*) δ = 8.70 (1H, s), 8.37 (1H, s), 8.19 (1H, s), 7.79 (1H, s), 5.86 (1H, dd, J = 9.6, 2.5 Hz), 4.11 - 4.03 (1H, m), 3.91 - 3.77 (5H, m), 3.65 - 3.54 (4H, m), 2.72 - 2.58 (1H, m), 2.27 - 2.15 (1H, m), 2.14 - 2.03 (1H, m), 1.89 - 1.64 (3H, m), 1.51 (9H, s), 1.41 (12H, s). ^{13}C NMR (101 MHz, CHLOROFORM-*d*) δ = 161.9, 157.9, 154.5, 144.3, 139.9, 134.2, 134.1, 126.9, 123.0, 119.7, 118.5, 84.9, 84.4, 80.5, 67.6, 43.3, 29.6, 28.4, 25.3, 24.9, 22.6 (2C of piperazine not observed due to broadening, expected at ~46 ppm from piperazine fragment **137**). 43.3 ppm peak confirmed in HSQC). LCMS (method A): t_{R} = 1.48 min, $[\text{M}+\text{H}^+]$ 608.2, (75% total area); hydrolysed Bpin observed at 1.07 min $[\text{M}+\text{H}^+]$ = 526.1, (25% total area), one product by NMR. HRMS: ($\text{C}_{25}\text{H}_{33}\text{BN}_5\text{O}_7$) $[\text{M}+\text{H}-\text{pinacol}]$ requires 526.2473, found $[\text{M}+\text{H}-\text{pinacol}]$ 526.2480. $\text{C}_{31}\text{H}_{43}\text{BN}_5\text{O}_7$ $[\text{M}+\text{H}^+]$ requires 608.3256, found 608.3250.

tert-Butyl 4-(2-(6-(6-methoxy-5-(methoxycarbonyl)pyridin-3-yl)-1-(tetrahydro-2H-pyran-2-yl)-1H-indazol-4-yl)oxazole-5-carbonyl)piperazine-1-carboxylate (**140**)



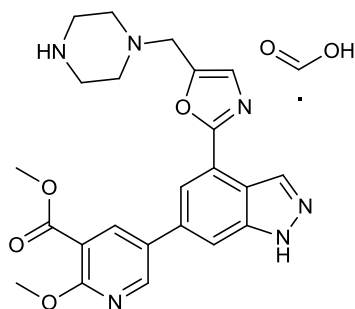
A flask was charged with compound **139** (1.36 g, 2.24 mmol), compound **37** (500 mg, 2.03 mmol), PdCl₂(dppf) (0.149 g, 0.203 mmol), and Na₂CO₃ (0.646 g, 6.10 mmol). 1,4-Dioxane (27 mL) and water (6.75 mL) were added and the reaction stirred. The vessel was degassed and purged with nitrogen three times and then heated at 80 °C for 30 min. The reaction was then cooled to room temperature, filtered through celite, and concentrated *in vacuo*. The residue was then partitioned between EtOAc (25 mL) and water (15 mL). The layers were separated, and the organics washed with distilled water (15 mL) and brine (2 x 15 mL). The organics were dried using a hydrophobic frit and concentrated *in vacuo*. The residue was purified by automated reverse-phase chromatography on C18 silica gel (5-95% MeCN in water, 0.1% formic acid modifiers). Desired fractions were combined, and the volatile solvents removed *in vacuo*. The compound was then extracted to DCM (3 x 10 mL), dried using a hydrophobic frit and concentrated *in vacuo* to a brown oil. The compound was precipitated from DCM (2 mL) with cyclohexane, and isolated by vacuum filtration to afford the product as an off-white solid (914 mg, 1.41 mmol, 70% yield). M.pt.: 126-132 °C. v_{\max} (neat): 2928, 2865, 1697, 1629, 1419 cm⁻¹. ¹H NMR (400 MHz, CHLOROFORM-d) δ = 8.68 (1H, s), 8.66 (1H, d, J = 2.45 Hz), 8.49 (1H, d, J = 2.45 Hz), 8.13 (1H, d, J = 0.98 Hz), 7.88 (1H, s), 7.79 (1H, s), 5.86 (1H, dd, J = 9.05, 2.69 Hz), 4.14 (3H, s), 4.09 - 4.01 (1H, m), 3.98 (3H, s), 3.90 - 3.76 (5H, m), 3.62-3.55 (4H, m), 2.69-2.57 (1H, m), 2.27-2.11 (2H, m), 1.90-1.67 (3H, m), 1.50 (9H, s). ¹³C NMR (101 MHz, CHLOROFORM-d) δ = 165.4, 162.1, 161.4, 157.8, 154.4, 149.2, 144.6, 140.7, 140.2, 135.7, 134.0, 133.9, 129.2, 120.9, 120.6, 119.8, 114.0, 111.2, 85.6, 80.6, 67.4, 54.5, 52.5, 43.7, 29.4, 28.4, 25.1, 22.3 (2C of piperazine not observed due to broadening, expected at ~46 ppm from piperazine fragment **137**, 43.7 peak confirmed in HSQC). LCMS (method A): t_R = 1.35 min, [M+H⁺] 647.1, (96% purity). HRMS: (C₃₃H₃₉N₆O₈) [M+H⁺] requires 647.2829, found [M+H⁺] 647.2825.

tert-Butyl 4-((2-(6-(6-methoxy-5-(methoxycarbonyl)pyridin-3-yl)-1-(tetrahydro-2H-pyran-2-yl)-1H-indazol-4-yl)oxazol-5-yl)methyl)piperazine-1-carboxylate (141)



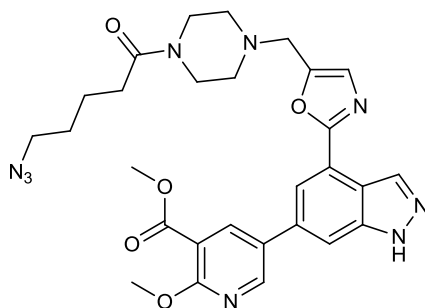
To a flask containing compound **140** (750 mg, 1.16 mmol) and tris(triphenylphosphine)rhodium(I) carbonyl hydride (16 mg, 0.017 mmol) was added THF (1.16 mL) and then diphenylsilane (0.525 mL, 2.83 mmol) dropwise. Effervescence was observed upon addition of the silane. The flask was stoppered, and the reaction was left to stir at room temperature for 30 min. The solvent was then removed by nitrogen blowdown, and the product recrystallised from boiling IPA. The solids were isolated by filtration affording the product as an off-white solid (520 mg, 0.822 mmol, 71% yield). M.pt.: 142-147 °C. ν_{\max} (neat): 2959, 2860, 1729, 1694, 1456, 1420 cm^{-1} . ^1H NMR (400 MHz, CHLOROFORM-*d*) δ = 8.72 (1H, d, J = 1.0 Hz), 8.67 (1H, d, J = 2.4 Hz), 8.51 (1H, d, J = 2.9 Hz), 8.08 (1H, d, J = 1.5 Hz), 7.81 (1H, d, J = 1.0 Hz), 7.18 (1H, s), 5.84 (1H, dd, J = 9.0, 2.7 Hz), 4.14 (3H, s), 4.09 - 4.01 (1H, m), 3.98 (3H, s), 3.85 - 3.79 (1H, m), 3.77 (2H, s), 3.48 (4H, t, J = 5.4 Hz), 2.69 - 2.58 (1H, m), 2.54 (4H, t, J = 4.6 Hz), 2.27 - 2.12 (2H, m), 1.90 - 1.66 (3H, m), 1.46 (9H, s). ^{13}C NMR (101 MHz, CHLOROFORM-*d*) δ = 165.51, 162.03, 160.75, 154.66, 149.26, 148.82, 140.67, 140.24, 135.59, 134.54, 129.56, 127.62, 120.89, 120.84, 119.58, 113.88, 110.05, 85.56, 79.74, 67.37, 54.45, 52.59, 52.57, 52.46, 42.97, 29.43, 28.41, 25.11, 22.39 (two decimal places required to distinguish signals. 52.56 and 42.97 peaks identified by HSQC and HMBC only). LCMS (method A): t_{R} = 0.95 min, $[\text{M}+\text{H}^+]$ 633.4, (97% purity). HRMS: ($\text{C}_{33}\text{H}_{41}\text{N}_6\text{O}_7$) $[\text{M}+\text{H}^+]$ requires 633.3037, found $[\text{M}+\text{H}^+]$ 633.3033.

Methyl 2-methoxy-5-(4-(5-(piperazin-1-ylmethyl)oxazol-2-yl)-1H-indazol-6-yl)nicotinate formate (142)



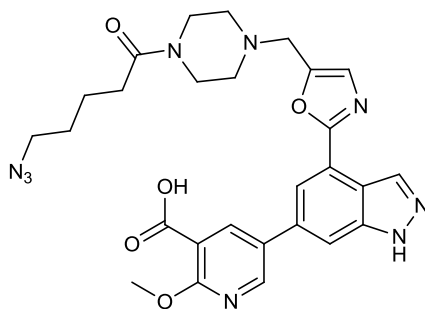
To a flask containing compound **141** (550 mg, 0.869 mmol) in anhydrous methanol (10 mL) under nitrogen was added TMSCl (1.1 mL, 8.6 mmol). The reaction was stirred at 50 °C for 14 h. The reaction was then cooled to room temperature, and the solid isolated by filtration. The solid was taken up in water, and purified by automated reverse-phase chromatography on C18 silica gel (5-95% MeCN in water with 0.1% formic acid modifiers). Desired fractions were combined and concentrated to afford a clear gum, which was turned over to solid with agitation in MeCN. The solvent was removed by nitrogen blowdown, and the solid dried in a vacuum oven at 40 °C overnight to afford the product as an off-white solid (279 mg, 0.564 mmol, 65% yield). M.pt.: 137-141 °C. v_{\max} (neat): 3331, 2949, 2833, 2472, 1715, 1567, 1478 cm^{-1} . ^1H NMR (400 MHz, DMSO- d_6) δ = 8.81 (1H, d, J = 2.5 Hz), 8.60 (1H, s), 8.47 (1H, d, J = 2.5 Hz), 8.28 (1H, s), 7.96 (2H, s), 7.37 (1H, s), 4.01 (3H, s), 3.87 (3H, s), 3.80 (2H, s), 2.92 (4H, t, J = 5.0 Hz), 2.58 (4H, t, J = 4.5 Hz). ^{13}C NMR (101 MHz, DMSO- d_6) δ = 164.8, 164.6, 160.8, 159.9, 149.0, 148.8, 141.2, 139.3, 134.1, 133.5, 128.8, 127.6, 119.6, 118.4, 117.9, 113.9, 110.3, 54.0, 52.3, 51.3, 50.3, 43.6. LCMS (method A) t_{R} = 0.55 min, $[\text{M}+\text{H}^+]$ 449.0, (93% purity). HRMS: ($\text{C}_{23}\text{H}_{25}\text{N}_6\text{O}_4$) $[\text{M}+\text{H}^+]$ requires 449.1937, found $[\text{M}+\text{H}^+]$ 449.1938.

Methyl 5-(4-(5-((4-(5-azidopentanoyl)piperazin-1-yl)methyl)oxazol-2-yl)-1H-indazol-6-yl)-2-methoxynicotinate (144)



HATU (115 mg, 0.303 mmol), DIPEA (0.070 ml, 0.40 mmol) and 5-azidopentanoic acid **143** (43 mg, 0.30 mmol) were stirred at room temperature in DMF (0.5 mL) for 10 min. Compound **142** (100 mg, 0.202 mmol) and DIPEA (0.070 ml, 0.401 mmol) in DMF (0.5 mL) was then added and the reaction stirred at room temperature for 1.5 h. The reaction was then purified directly, without workup, by MDAP (method A). Desired fractions were combined, concentrated *in vacuo*, and dried in a vacuum oven at 40 °C for 2 h to afford the product as a white solid (67 mg, 0.12 mmol, 58% yield). M.pt. not recorded due to azide. ν_{\max} (neat): 3197, 2941, 2864, 2823, 2093, 1730, 1715, 1629, 1605 cm^{-1} . ^1H NMR (400 MHz, CHLOROFORM- d) δ = 10.61 (1H, br. s), 8.78 (1H, s), 8.65 (1H, d, J = 2.5 Hz), 8.49 (1H, d, J = 3.0 Hz), 8.08 (1H, d, J = 1.5 Hz), 7.73 (1H, s), 7.21 (1H, s), 4.13 (3H, s), 3.97 (3H, s), 3.80 (2H, s), 3.70 (2H, t, J = 4.8 Hz), 3.53 (2H, t, J = 4.8 Hz), 3.30 (2H, t, J = 6.5 Hz), 2.59 (4H, q, J = 5.0 Hz), 2.36 (2H, t, J = 7.1 Hz), 1.78 - 1.64 (4H, m). ^{13}C NMR (101 MHz, CHLOROFORM- d) δ = 179.29, 170.77, 165.44, 162.07, 160.86, 149.09, 148.60, 140.16, 135.87, 129.25, 127.75, 120.80, 119.58, 119.39, 119.36, 113.92, 109.48, 54.48, 52.82, 52.51, 52.48, 52.41, 51.21, 45.39, 41.49, 32.48, 28.53, 22.34 (two decimal places required to distinguish signals). LCMS (method B): t_{R} = 1.00 min, $[\text{M}+\text{H}^+]$ 574.1 (100% purity). HRMS: ($\text{C}_{28}\text{H}_{32}\text{N}_9\text{O}_5$) $[\text{M}+\text{H}^+]$ requires 574.2526, found $[\text{M}+\text{H}^+]$ 574.2525.

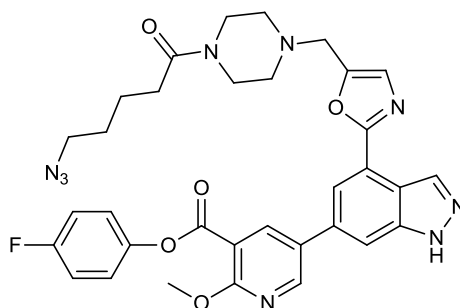
5-(4-(5-((4-(5-Azidopentanoyl)piperazin-1-yl)methyl)oxazol-2-yl)-1H-indazol-6-yl)-2-methoxynicotinic acid (145)



Compound **144** (60 mg, 0.11 mmol) and lithium hydroxide (25 mg, 1.0 mmol) were stirred at room temperature in THF (400 μL), methanol (100 μL), and water (100 μL) for 1.5 h. The reaction mixture was then purified directly by automated column chromatography on C18 silica gel (5-50% MeCN in 10 mM ammonium bicarbonate). Desired fractions were combined, concentrated *in vacuo*, and dried in a vacuum oven overnight to afford the product as a white solid (55 mg, 0.098 mmol, 94% yield). M.pt. not recorded due to azide. ν_{\max} (neat): 3199, 2928, 2869, 2818, 2093, 1717, 1606, 1573 cm^{-1} . ^1H NMR (600 MHz, DMSO- d_6) δ 8.56 (1H, d,

$J = 0.7$ Hz), 8.46 (1H, d, $J = 2.6$ Hz), 8.10 (1H, d, $J = 2.6$ Hz), 7.91 (1H, d, $J = 1.1$ Hz), 7.85 (1H, s), 7.34 (1H, s), 3.89 (3H, s), 3.79 (2H, s), 3.50 - 3.43 (4H, m), 3.29 (2H, t, $J = 7.0$ Hz), 2.49 - 2.47 (2H, m), 2.46 - 2.42 (2H, m), 2.30 (2H, t, $J = 7.0$ Hz), 1.55 - 1.48 (4H, m) (2.49-2.47 peak for piperazine 2H obscured by DMSO, presence and connectivity confirmed by HSQC and HMBC correlations; indazole N-H and acid COOH protons not observed). ^{13}C NMR (151 MHz, DMSO- d_6) δ 170.2, 167.9, 160.1, 160.0, 149.0, 143.6, 141.4, 136.4, 135.2, 133.3, 128.4, 127.5, 124.7, 119.4, 118.1, 117.8, 109.8, 53.1, 52.3, 51.8, 51.2, 50.4, 44.8, 40.9, 31.5, 27.8, 21.9. LCMS (method B): $t_R = 0.63$ min, $[\text{M}+\text{H}^+]$ 560.3, (100% purity). HRMS: ($\text{C}_{27}\text{H}_{30}\text{N}_9\text{O}_5$) $[\text{M}+\text{H}^+]$ requires 560.2370, found $[\text{M}+\text{H}^+]$ 560.2371.

4-Fluorophenyl 5-(4-(5-((4-(5-azidopentanoyl)piperazin-1-yl)methyl)oxazol-2-yl)-1H-indazol-6-yl)-2-methoxynicotinate (131)



Compound **145** (45 mg, 0.080 mmol), PyBOP (46 mg, 0.088 mmol), and 4-fluorophenol (14 mg, 0.13 mmol) were stirred in DMF (0.5 mL). DIPEA (0.028 mL, 0.16 mmol) was then added dropwise, and the reaction stirred at room temperature for 2 h. Another equivalent of 4-fluorophenol (14 mg, 0.13 mmol) was added, and the reaction stirred for an additional hour. The reaction was then purified directly, without workup, by MDAP (method A). Desired fractions were combined and concentrated *in vacuo* to afford the product as an off-white solid (8.5 mg, 0.013 mmol, 16% yield). M.pt. not recorded due to azide. ν_{max} (neat): 2934, 2097, 1756, 1626, 1504, 1477 cm^{-1} . ^1H NMR (600 MHz, CHLOROFORM- d) δ 8.79 (1H, s), 8.71 (1H, d, $J = 2.6$ Hz), 8.64 (1H, d, $J = 2.6$ Hz), 8.10 (1H, d, $J = 1.5$ Hz), 7.76 (1H, s), 7.25 - 7.19 (3H, m), 7.16 - 7.08 (2H, m), 4.16 (3H, s), 3.80 (2H, s), 3.72 - 3.67 (2H, m), 3.55 - 3.48 (2H, m), 3.29 (2H, t, $J = 6.8$ Hz), 2.64 - 2.54 (4H, m), 2.36 (2H, t, $J = 7.3$ Hz), 1.76 - 1.69 (2H, m), 1.68 - 1.62 (2H, m). ^{13}C NMR (151 MHz, CHLOROFORM- d) δ 170.8, 163.4, 162.5, 160.8, 160.4 (1C, d, $J = 244.9$ Hz), 150.0, 148.6, 146.5 (1C, d, $J = 2.8$ Hz), 141.3, 140.6, 135.7, 135.6, 129.4, 127.8, 123.1 (2C, d, $J = 8.3$ Hz), 120.9, 119.4, 119.3, 116.2 (2C, d, $J = 23.8$ Hz), 112.9, 109.6, 54.6,

52.8, 52.5, 52.4, 51.2, 45.4, 41.5, 32.5, 28.5, 22.3. $^{19}\text{F}\{\text{H}\}$ NMR (376 MHz, CHLOROFORM-d) δ -116.60 (1F, s). LCMS (method B): $t_{\text{R}} = 1.17$ min, $[\text{M}+\text{H}^+]$ 654.4, (99% purity). HRMS: ($\text{C}_{33}\text{H}_{33}\text{FN}_9\text{O}_5$) $[\text{M}+\text{H}^+]$ requires 654.2589, found $[\text{M}+\text{H}^+]$ 654.2582.

7 – References

- (1) Singh, J.; Petter, R. C.; Baillie, T. A.; Whitty, A. *Nat. Rev. Drug Discov.* **2011**, *10*, 307–317.
 - (2) Lei, J.; Zhou, Y.; Xie, D.; Zhang, Y. *J. Am. Chem. Soc.* **2015**, *137*, 70–73.
 - (3) Waxman, D. J.; Strominger, J. L. *Annu. Rev. Biochem.* **1983**, *52*, 825–869.
 - (4) Yocum, R. R.; Rasmussen, J. R.; Strominger, J. L. *J. Biol. Chem.* **1980**, *255*, 3977–3986.
 - (5) Bradshaw, J. M.; McFarland, J. M.; Paavilainen, V. O.; Bisconte, A.; Tam, D.; Phan, V. T.; Romanov, S.; Finkle, D.; Shu, J.; Patel, V.; Ton, T.; Li, X.; Loughhead, D. G.; Nunn, P. A.; Karr, D. E.; Gerritsen, M. E.; Funk, J. O.; Owens, T. D.; Verner, E.; Brameld, K. A.; Hill, R. J.; Goldstein, D. M.; Taunton, J. *Nat. Chem. Biol.* **2015**, *11*, 525–531.
 - (6) Lee, C. U.; Grossmann, T. N. *Angew. Chem. Int. Ed.* **2012**, *51*, 8699–8700.
 - (7) Barf, T.; Kaptein, A. *J. Med. Chem.* **2012**, *55*, 6243–6262.
 - (8) Baillie, T. A. *Angew. Rev.* **2016**, *55*, 2–17.
 - (9) Mah, R.; Thomas, J. R.; Shafer, C. M. *Bioorg. Med. Chem. Lett.* **2014**, *24*, 33–39.
 - (10) Bauer, R. A. *Drug Discov. Today* **2015**, *20*, 1061–1073.
 - (11) Petter, R.; Jewell, C. F.; Lee, K.; Medikonda, A. P.; Niu, D.; Qiao, L.; Singh, J.; Zhu, Z. Ligand-Directed Covalent Modification of Protein. WO2011/082285 A1, 2011.
 - (12) González-Bello, C. *ChemMedChem* **2016**, *11*, 22–30.
 - (13) Hossam, M.; Lasheen, D. S.; Abouzid, K. A. M. *Arch. Pharm. Chem. Life Sci.* **2016**, *349*, 1–21.
 - (14) Kalgutkar, A. S.; Dalvie, D. K. *Expert Opin. Drug Discov.* **2012**, *7*, 561–581.
 - (15) Park, B. K.; Boobis, A.; Clarke, S.; Goldring, C. E. P.; Jones, D.; Kenna, J. G.; Lambert, C.; Lavery, H. G.; Naisbitt, D. J.; Nelson, S.; Nicoll-Griffith, D. A.; Obach, R. S.; Routledge, P.; Smith, D. A.; Tweedie, D. J.; Vermeulen, N.; Williams, D. P.; Wilson, I. D.; Baillie, T. A. *Nat. Rev. Drug Discov.* **2011**, *10*, 292–306.
-

-
- (16) Zimmermann, A. E.; Katona, B. G. *Pharmacother. J. Hum. Pharmacol. Drug Ther.* **1997**, *17*, 308–326.
- (17) Yusuf, S.; Zhao, F.; Mehta, S. R.; Chrolavicius, S.; Tognoni, G.; Fox, K. K. *N. Engl. J. Med.* **2001**, *345*, 494–502.
- (18) Olbe, L.; Carlsson, E.; Lindberg, P. *Nat. Rev. Drug Discov.* **2003**, *2*, 132–139.
- (19) Topol, E. J.; Schork, N. J. *Nat. Med.* **2011**, *17*, 40–41.
- (20) Sanderson, K. *Nat. Rev. Drug Discov.* **2013**, *12*, 649–651.
- (21) Singh, J.; Petter, R. C.; Kluge, A. F. *Curr. Opin. Chem. Biol.* **2010**, *14*, 475–480.
- (22) Adeniyi, A. A.; Muthusamy, R.; Soliman, M. E. *Expert Opin. Drug Discov.* **2016**, *11*, 79–90.
- (23) United States Food and Drug Administration. Afatinib
<http://www.fda.gov/Drugs/InformationOnDrugs/ApprovedDrugs/ucm360574.htm>
(accessed Jan 7, 2014).
- (24) United States Food and Drug Administration. FDA approves Imbruvica for rare blood cancer
<http://www.fda.gov/NewsEvents/Newsroom/PressAnnouncements/ucm374761.htm>
(accessed Jan 7, 2014).
- (25) Pan, Z.; Scheerens, H.; Li, S.-J.; Schultz, B. E.; Sprengeler, P. A.; Burrill, L. C.; Mendonca, R. V.; Sweeney, M. D.; Scott, K. C. K.; Grothaus, P. G.; Jeffery, D. A.; Spoerke, J. M.; Honigberg, L. A.; Young, P. R.; Dalrymple, S. A.; Palmer, J. T. *ChemMedChem* **2007**, *2*, 58–61.
- (26) Stevens, K. L.; Alligood, K. J.; Alberti, J. G. B.; Caferro, T. R.; Chamberlain, S. D.; Dickerson, S. H.; Dickson, H. D.; Emerson, H. K.; Griffin, R. J.; Hubbard, R. D.; Keith, B. R.; Mullin, R. J.; Petrov, K. G.; Gerding, R. M.; Reno, M. J.; Rheault, T. R.; Rusnak, D. W.; Sammond, D. M.; Smith, S. C.; Uehling, D. E.; Waterson, A. G.; Wood, E. R. *Bioorg. Med. Chem. Lett.* **2009**, *19*, 21–26.
- (27) Landi, L.; Cappuzzo, F. *Transl. Lung Cancer Res.* **2013**, *2*, 40–49.
-

-
- (28) Overkleeft, H. S.; Liu, N.; Hoogendoorn, S.; van der Kar, B.; Kaptein, A.; Barf, T.; Driessen, C.; Filippov, D.; van der Marel, G. a; van der Stelt, M. *Org. Biomol. Chem.* **2015**, *13*, 5147–5157.
- (29) Zeng, M.; Lu, J.; Li, L.; Feru, F.; Quan, C.; Gero, T. W.; Ficarro, S. B.; Xiong, Y.; Ambrogio, C.; Paranal, R. M.; Catalano, M.; Shao, J.; Wong, K.-K.; Marto, J. A.; Fischer, E. S.; Jänne, P. A.; Scott, D. A.; Westover, K. D.; Gray, N. S. *Cell Chem. Biol.* **2017**, 1005–1016.
- (30) Müller, M. P.; Jeganathan, S.; Heidrich, A.; Campos, J.; Goody, R. S. *Sci. Rep.* **2017**, *7*, 1–11.
- (31) McGregor, L. M.; Jenkins, M. L.; Kerwin, C.; Burke, J. E.; Shokat, K. M. *Biochemistry* **2017**, *56*, 3178–3183.
- (32) Kwiatkowski, N.; Zhang, T.; Rahl, P. B.; Abraham, B. J.; Reddy, J.; Ficarro, S. B.; Dastur, A.; Amzallag, A.; Ramaswamy, S.; Tesar, B.; Jenkins, C. E.; Hannett, N. M.; McMillin, D.; Sanda, T.; Sim, T.; Kim, N. D.; Look, T.; Mitsiades, C. S.; Weng, A. P.; Brown, J. R.; Benes, C. H.; Marto, J. A.; Young, R. A.; Gray, N. S. *Nature* **2014**, *511*, 616–620.
- (33) Zhang, T.; Kwiatkowski, N.; Olson, C. M.; Dixon-Clarke, S. E.; Abraham, B. J.; Greifengberg, A. K.; Ficarro, S. B.; Elkins, J. M.; Liang, Y.; Hannett, N. M.; Manz, T.; Hao, M.; Bartkowiak, B.; Greenleaf, A. L.; Marto, J. A.; Geyer, M.; Bullock, A. N.; Young, R. A.; Gray, N. S. *Nat. Chem. Biol.* **2016**, *12*, 876–884.
- (34) Ratcliffe, S. J.; Yi, T.; Khandekar, S. S. *J. Biomol. Screen.* **2007**, *12*, 126–132.
- (35) Lagoutte, R.; Patouret, R.; Winssinger, N. *Curr. Opin. Chem. Biol.* **2017**, *39*, 54–63.
- (36) Dagher, J.-P.; Zambaldo, C.; Abegg, D.; Barluenga, S.; Tallant, C.; Müller, S.; Adibekian, A.; Winssinger, N. *Angew. Chem. Int. Ed.* **2015**, *54*, 6057–6061.
- (37) Patricelli, M. P.; Szardenings, A. K.; Liyanage, M.; Nomanbhoy, T. K.; Wu, M.; Weissig, H.; Aban, A.; Chun, D.; Tanner, S.; Kozarich, J. W. *Biochemistry* **2007**, *46*, 350–358.
- (38) Liu, Q.; Kirubakaran, S.; Hur, W.; Niepel, M.; Westover, K.; Thoreen, C. C.; Wang, J.; Ni, J.; Patricelli, M. P.; Vogel, K.; Riddle, S.; Waller, D. L.; Traynor, R.; Sanda, T.; Zhao, Z.; Kang, S. A.; Zhao, J.; Look, A. T.; Sorger, P. K.; Sabatini, D. M.; Gray, N. S. *J. Biol. Chem.* **2012**, *287*, 9742–9752.
-

-
- (39) Patricelli, M. P.; Nomanbhoy, T. K.; Wu, J.; Brown, H.; Zhou, D.; Zhang, J.; Jagannathan, S.; Aban, A.; Okerberg, E.; Herring, C.; Nordin, B.; Weissig, H.; Yang, Q.; Lee, J. D.; Gray, N. S.; Kozarich, J. W. *Chem. Biol.* **2011**, *18*, 699–710.
- (40) Liu, Y.; Patricelli, M. P.; Cravatt, B. F. *Proc. Natl. Acad. Sci.* **1999**, *96*, 14694–14699.
- (41) Cognetta, A. B.; Niphakis, M. J.; Lee, H.-C.; Martini, M. L.; Hulce, J. J.; Cravatt, B. F. *Chem. Biol.* **2015**, *22*, 928–937.
- (42) Hacker, S. M.; Backus, K. M.; Lazear, M. R.; Forli, S.; Correia, B. E.; Cravatt, B. F. *Nat. Chem.* **2017**, *9*, 1181–1190.
- (43) Lin, S.; Yang, X.; Jia, S.; Weeks, A. M.; Hornsby, M.; Lee, P. S.; Nichiporuk, R. V.; Iavarone, A. T.; Wells, J. A.; Toste, F. D.; Chang, C. J. *Science* **2017**, *355*, 597–602.
- (44) Backus, K. M.; Correia, B. E.; Lum, K. M.; Forli, S.; Horning, B. D.; González-Páez, G. E.; Chatterjee, S.; Lanning, B. R.; Teijaro, J. R.; Olson, A. J.; Wolan, D. W.; Cravatt, B. F. *Nature* **2016**, *534*, 570–574.
- (45) Dubinsky, L.; Krom, B. P.; Meijler, M. M. *Bioorg. Med. Chem.* **2012**, *20*, 554–570.
- (46) Lum, K. M.; Sato, Y.; Beyer, B. A.; Plaisted, W. C.; Anglin, J. L.; Lairson, L. L.; Cravatt, B. F. *ACS Chem. Biol.* **2017**, *12*, 2671–2681.
- (47) Parker, C. G.; Galmozzi, A.; Wang, Y.; Correia, B. E.; Sasaki, K.; Joslyn, C. M.; Kim, A. S.; Cavallaro, C. L.; Lawrence, R. M.; Johnson, S. R.; Narvaiza, I.; Saez, E.; Cravatt, B. F. *Cell* **2017**, *168*, 527–541.
- (48) Pan, S.; Jang, S.-Y.; Wang, D.; Liew, S. S.; Li, Z.; Lee, J.-S.; Yao, S. Q. *Angew. Chem. Int. Ed.* **2017**, *56*, 11816–11821.
- (49) Copeland, R. A. *Enzymes: A Practical Introduction to Structure, Mechanism and Data Analysis*, 2nd ed.; John Wiley & Sons Inc.: New York, NY, USA, 2000; Vol. 7.
- (50) Bissantz, C.; Kuhn, B.; Stahl, M. *J. Med. Chem.* **2010**, *53*, 5061–5084.
- (51) Johnson, D. S.; Weerapana, E.; Cravatt, B. F. *Future Med. Chem.* **2010**, *2*, 949–964.
- (52) Cravatt, B. F.; Wright, A. T.; Kozarich, J. W. *Annu. Rev. Biochem.* **2008**, *77*, 383–414.
-

-
- (53) Schwartz, P. A.; Kuzmic, P.; Solowiej, J.; Bergqvist, S.; Bolanos, B.; Almaden, C.; Nagata, A.; Ryan, K.; Feng, J.; Dalvie, D.; Kath, J. C.; Xu, M.; Wani, R.; Murray, B. W. *Proc. Natl. Acad. Sci.* **2014**, *111*, 173–178.
- (54) Powers, J. C.; Asgian, J. L.; Ekici, Ö. D.; James, K. E. *Chem. Rev.* **2002**, *102*, 4639–4750.
- (55) Hunkapiller, M. W.; Smallcombe, S. H.; Whitaker, D. R.; Richards, J. H. *J. Biol. Chem.* **1973**, *248*, 8306–8308.
- (56) Isom, D. G.; Castaneda, C. A.; Cannon, B. R.; Garcia-Moreno E., B. *Proc. Natl. Acad. Sci.* **2011**, *108*, 5260–5265.
- (57) Grimsley, G. R.; Scholtz, J. M.; Pace, C. N. *Protein Sci.* **2009**, *18*, 247–251.
- (58) Weerapana, E.; Wang, C.; Simon, G. M.; Richter, F.; Khare, S.; Dillon, M. B. D.; Bachovchin, D. A.; Mowen, K.; Baker, D.; Cravatt, B. F. *Nature* **2010**, *468*, 790–795.
- (59) Bar-Peled, L.; Kemper, E. K.; Suciu, R. M.; Vinogradova, E. V; Backus, K. M.; Horning, B. D.; Paul, T. A.; Ichu, T.; Svensson, R. U.; Olucha, J.; Chang, M. W.; Kok, B. P.; Zhu, Z.; Ihle, N. T.; Dix, M. M.; Jiang, P.; Hayward, M. M.; Saez, E.; Shaw, R. J.; Cravatt, B. F. *Cell* **2017**, *171*, 696–709.
- (60) Lanning, B. R.; Whitby, L. R.; Dix, M. M.; Douhan, J.; Gilbert, A. M.; Hett, E. C.; Johnson, T. O.; Joslyn, C.; Kath, J. C.; Niessen, S.; Roberts, L. R.; Schnute, M. E.; Wang, C.; Hulce, J. J.; Wei, B.; Whiteley, L. O.; Hayward, M. M.; Cravatt, B. F. *Nat. Chem. Biol.* **2014**, *10*, 760–767.
- (61) Miller, R. M.; Paavilainen, V. O.; Krishnan, S.; Sera, I. M.; Taunton, J. *J. Am. Chem. Soc.* **2013**, *135*, 5298–5301.
- (62) Nacht, M.; Qiao, L.; Sheets, M. P.; Martin, T. S.; Labenski, M.; Mazdiyasni, H.; Karp, R.; Zhu, Z.; Chaturvedi, P.; Bhavsar, D.; Niu, D.; Westlin, W.; Petter, R. C.; Medikonda, A. P.; Singh, J. *J. Med. Chem.* **2013**, *56*, 712–721.
- (63) Kathman, S. G.; Xu, Z.; Statsyuk, A. V. *J. Med. Chem.* **2014**, *57*, 4969–4974.
- (64) Roush, W. R.; Gwaltney, S. L.; Cheng, J.; Scheidt, K. A.; McKerrow, J. H.; Hansell, E. *J. Am. Chem. Soc.* **1998**, *120*, 10994–10995.
-

-
- (65) Suh, E. H.; Liu, Y.; Connelly, S.; Genereux, J. C.; Wilson, I. A.; Kelly, J. W. *J. Am. Chem. Soc.* **2013**, *135*, 17869–17880.
- (66) Jost, C.; Nitsche, C.; Scholz, T.; Roux, L.; Klein, C. D. *J. Med. Chem.* **2014**, *57*, 7590–7599.
- (67) Ebbrell, D. J.; Madden, J. C.; Cronin, M. T. D.; Schultz, T. W.; Enoch, S. J. *Chem. Res. Toxicol.* **2016**, *29*, 1073–1081.
- (68) Flanagan, M. E.; Abramite, J. A.; Anderson, D. P.; Aulabaugh, A.; Dahal, U. P.; Gilbert, A. M.; Li, C.; Montgomery, J.; Oppenheimer, S. R.; Ryder, T.; Schu, B. P.; Uccello, D. P.; Walker, G. S.; Wu, Y.; Brown, M. F.; Chen, J. M.; Hayward, M. M.; Noe, M. C.; Obach, R. S.; Philippe, L.; Shanmugasundaram, V.; Shapiro, M. J.; Starr, J.; Stroh, J.; Che, Y. *J. Med. Chem.* **2014**, *57*, 10072–10079.
- (69) Cee, V. J.; Volak, L. P.; Chen, Y.; Bartberger, M. D.; Tegley, C.; Arvedson, T.; McCarter, J.; Tasker, A. S.; Fotsch, C. *J. Med. Chem.* **2015**, *58*, 9171–9178.
- (70) Lonsdale, R.; Burgess, J.; Colclough, N.; Davies, N. L.; Lenz, E. M.; Orton, A. L.; Ward, R. A. *J. Chem. Inf. Model.* **2017**, *57*, 3124–3137.
- (71) Schmidt, T. C.; Welker, A.; Rieger, M.; Sahu, P. K.; Sotriffer, C. A.; Schirmeister, T.; Engels, B. *ChemPhysChem* **2014**, *15*, 3226–3235.
- (72) Krenske, E. H.; Petter, R. C.; Houk, K. N. *J. Org. Chem.* **2016**, *81*, 11726–11733.
- (73) Marino, S. M.; Gladyshev, V. N. *J. Mol. Biol.* **2010**, *404*, 902–916.
- (74) Clayden, J.; Greeves, N.; Warren, S. In *Organic Chemistry*; Oxford University Press: Oxford, 2012; pp 498–527.
- (75) Kung, A.; Chen, Y.-C.; Schimpl, M.; Ni, F.; Zhu, J.; Turner, M.; Molina, H.; Overman, R.; Zhang, C. *J. Am. Chem. Soc.* **2016**, *138*, 10554–10560.
- (76) Avery, C. a.; Pease, R. J.; Smith, K.; Boothby, M.; Buckley, H. M.; Grant, P. J.; Fishwick, C. W. G. *Eur. J. Med. Chem.* **2015**, *98*, 49–53.
- (77) Greenbaum, D.; Medzihradzky, K. F.; Burlingame, A.; Bogyo, M. *Chem. Biol.* **2000**, *7*, 569–581.
-

-
- (78) Adam, G. C.; Sorensen, E. J.; Cravatt, B. F. *Nat. Biotechnol.* **2002**, *20*, 805–809.
- (79) Adam, G. C.; Cravatt, B. F.; Sorensen, E. J. *Chem. Biol.* **2001**, *8*, 81–95.
- (80) Smith, M. E. B.; Caspersen, M. B.; Robinson, E.; Morais, M.; Maruani, A.; Nunes, J. P. M.; Nicholls, K.; Saxton, M. J.; Caddick, S.; Baker, J. R.; Chudasama, V. *Org. Biomol. Chem.* **2015**, *13*, 7946–7949.
- (81) ElSohly, A. M.; MacDonald, J. I.; Hentzen, N. B.; Aanei, I. L.; El Muslemay, K. M.; Francis, M. B. *J. Am. Chem. Soc.* **2017**, *139*, 3767–3773.
- (82) Shannon, D. A.; Weerapana, E. *Curr. Opin. Chem. Biol.* **2015**, *24*, 18–26.
- (83) Shannon, D. A.; Banerjee, R.; Webster, E. R.; Bak, D. W.; Wang, C.; Weerapana, E. *J. Am. Chem. Soc.* **2014**, *136*, 3330–3333.
- (84) Krishnan, S.; Miller, R. M.; Tian, B.; Mullins, R. D.; Jacobson, M. P.; Taunton, J. *J. Am. Chem. Soc.* **2014**.
- (85) Serafimova, I. M.; Pufall, M. A.; Krishnan, S.; Duda, K.; Cohen, M. S.; Maglathlin, R. L.; McFarland, J. M.; Miller, R. M.; Frödin, M.; Taunton, J. *Nat. Chem. Biol.* **2012**, *8*, 471–476.
- (86) Staub, I.; Sieber, S. A. *J. Am. Chem. Soc.* **2008**, *130*, 13400–13409.
- (87) Böttcher, T.; Sieber, S. A. *Angew. Chem. Int. Ed.* **2008**, *47*, 4600–4603.
- (88) Shannon, D. A.; Gu, C.; McLaughlin, C. J.; Kaiser, M.; van der Hoorn, R. A. L.; Weerapana, E. *ChemBioChem* **2012**, *13*, 2327–2330.
- (89) Adibekian, A.; Martin, B. R.; Chang, J. W.; Hsu, K. L.; Tsuboi, K.; Bachovchin, D. A.; Speers, A. E.; Brown, S. J.; Spicer, T.; Fernandez-Vega, V.; Ferguson, J.; Hodder, P. S.; Rosen, H.; Cravatt, B. F. *J. Am. Chem. Soc.* **2012**, *134*, 10345–10348.
- (90) Ahn, K.; Johnson, D. S.; Mileni, M.; Beidler, D.; Long, J. Z.; McKinney, M. K.; Weerapana, E.; Sadagopan, N.; Liimatta, M.; Smith, S. E.; Lazerwith, S.; Stiff, C.; Kamtekar, S.; Bhattacharya, K.; Zhang, Y.; Swaney, S.; Van Becelaere, K.; Stevens, R. C.; Cravatt, B. F. *Chem. Biol.* **2009**, *16*, 411–420.
- (91) Bandyopadhyay, A.; Gao, J. *Curr. Opin. Chem. Biol.* **2016**, *34*, 110–116.
-

-
- (92) Gu, C.; Shannon, D. A.; Colby, T.; Wang, Z.; Shabab, M.; Kumari, S.; Villamor, J. G.; McLaughlin, C. J.; Weerapana, E.; Kaiser, M.; Cravatt, B. F.; Van Der Hoorn, R. A. L. *Chem. Biol.* **2013**, *20*, 541–548.
- (93) Hett, E. C.; Xu, H.; Geoghegan, K. F.; Gopalsamy, A.; Kyne, R. E.; Menard, C. A.; Narayanan, A.; Parikh, M. D.; Liu, S.; Roberts, L.; Robinson, R. P.; Tones, M. A.; Jones, L. H. *ACS Chem. Biol.* **2015**, *10*, 1094–1098.
- (94) Weerapana, E.; Simon, G. M.; Cravatt, B. F. *Nat. Chem. Biol.* **2008**, *4*, 405–407.
- (95) Martín-Gago, P.; Fansa, E. K.; Winzker, M.; Murarka, S.; Janning, P.; Schultz-Fademrecht, C.; Baumann, M.; Wittinghofer, A.; Waldmann, H. *Cell Chem. Biol.* **2017**, *24*, 589–597.
- (96) Pettinger, J.; Jones, K.; Cheeseman, M. D. *Angew. Chem. Int. Ed.* **2017**, *56*, 15200–15209.
- (97) Dahal, U.; Gilbert, A.; Obach, R.; Chen, J.; Garcia-Irizarry, C.; Schuff, B.; Starr, J.; Uccello, D.; Young, J. *Med. Chem. Commun.* **2016**, *7*, 864–872.
- (98) Zhao, Q.; Ouyang, X.; Wan, X.; Gajiwala, K. S.; Kath, J. C.; Jones, L. H.; Burlingame, A. L.; Taunton, J. J. *Am. Chem. Soc.* **2017**, *139*, 680–685.
- (99) Grimster, N. P.; Connelly, S.; Baranczak, A.; Dong, J.; Krasnova, L. B.; Sharpless, K. B.; Powers, E. T.; Wilson, I. A.; Kelly, J. W. *J. Am. Chem. Soc.* **2013**, *135*, 5656–5668.
- (100) Narayanan, A.; Jones, L. H. *Chem. Sci.* **2015**, *6*, 2650–2659.
- (101) Fadeyi, O. O.; Hoth, L. R.; Choi, C.; Feng, X.; Gopalsamy, A.; Hett, E. C.; Kyne, R. E.; Robinson, R. P.; Jones, L. H. *ACS Chem. Biol.* **2017**, *12*, 2015–2020.
- (102) Baranczak, A.; Liu, Y.; Connelly, S.; Du, W. H.; Greiner, E. R.; Genereux, J. C.; Wiseman, R. L.; Eisele, Y. S.; Bradbury, N. C.; Dong, J.; Noodleman, L.; Sharpless, K. B.; Wilson, I. A.; Encalada, S. E.; Kelly, J. W. *J. Am. Chem. Soc.* **2015**, *137*, 7404–7414.
- (103) Mukherjee, H.; Debreczeni, J.; Breed, J.; Tentarelli, S.; Aquila, B.; Dowling, J. E.; Whitty, A.; Grimster, N. P. *Org. Biomol. Chem.* **2017**, *15*, 9685–9695.
- (104) Pettinger, J.; Bihan, Y.-V. Le; Widya, M.; Montfort, R. L. M. Van; Jones, K.; Cheeseman,
-

- (105) Larraufie, M.-H.; Yang, W. S.; Jiang, E.; Thomas, A. G.; Slusher, B. S.; Stockwell, B. R. *Bioorg. Med. Chem. Lett.* **2015**, *25*, 4787–4792.
- (106) Bell, I. M.; Stirdivant, S. M.; Ahern, J.; Culberson, J. C.; Darke, P. L.; Dinsmore, C. J.; Drakas, R. A.; Gallicchio, S. N.; Graham, S. L.; Heimbrook, D. C.; Hall, D. L.; Hua, J.; Kett, N. R.; Kim, A. S.; Kornienko, M.; Kuo, L. C.; Munshi, S. K.; Quigley, A. G.; Reid, J. C.; Trotter, B. W.; Waxman, L. H.; Williams, T. M.; Zartman, C. B. *Biochemistry* **2005**, *44*, 9430–9440.
- (107) Akçay, G.; Belmonte, M. A.; Aquila, B.; Chuaqui, C.; Hird, A. W.; Lamb, M. L.; Rawlins, P. B.; Su, N.; Tentarelli, S.; Grimster, N. P.; Su, Q. *Nat. Chem. Biol.* **2016**, *12*, 931–936.
- (108) Choi, S.; Connelly, S.; Reixach, N.; Wilson, I. A.; Kelly, J. W. *Nat. Chem. Biol.* **2010**, *6*, 133–139.
- (109) Ward, C. C.; Kleinman, J. I.; Nomura, D. K. *ACS Chem. Biol.* **2017**, *12*, 1478–1483.
- (110) Anderson, K. E.; To, M.; Olzmann, J. A.; Nomura, D. K. *ACS Chem. Biol.* **2017**, *12*, 2522–2528.
- (111) Cesco, S. De; Kurian, J.; Dufresne, C.; Mittermaier, A. K.; Moitessier, N. *Eur. J. Med. Chem.* **2017**, *138*, 96–114.
- (112) London, N.; Miller, R. M.; Krishnan, S.; Uchida, K.; Irwin, J. J.; Eidam, O.; Gibold, L.; Cimermančič, P.; Bonnet, R.; Shoichet, B. K.; Taunton, J. *Nat. Chem. Biol.* **2014**, *10*.
- (113) Duong-Ly, K. C.; Peterson, J. R. *Curr. Protoc. Pharmacol.* **2013**, *60*, 2.9.1-2.9.14.
- (114) Cantley, L. L. C. *Science* **2002**, *296*, 1655–1657.
- (115) Hanks, S. K.; Hunter, T. *J. Fed. Am. Soc. Exp. Biol.* **1995**, *9*, 576–596.
- (116) Manning, G.; Whyte, D. B.; Martinez, R.; Hunter, T.; Sudarsanam, S. *Science* **2002**, *298*, 1912–1934.
- (117) Scheeff, E. D.; Bourne, P. E. *PLoS Comput. Biol.* **2005**, *1*, 359–381.
- (118) Knight, Z. A.; Shokat, K. M. *Chem. Biol.* **2005**, *12*, 621–637.
-

-
- (119) Burnett, G.; Kennedy, E. P. *J. Biol. Chem.* **1954**, *211*, 969–980.
- (120) Cohen, P. *Nat. Cell Biol.* **2002**, *4*, E127–E130.
- (121) Editorial. *Nat. Rev. Drug Discov.* **2004**, *3*, 985.
- (122) Tamaokia, T.; Nomotoa, H.; Takahashia, I.; Kato, Y.; Morimoto, M.; Tomita, F. *Biochem. Biophys. Res. Commun.* **1986**, *135*, 397–402.
- (123) Yaish, P.; Gazit, A.; Gilon, C.; Levitzki, A. *Science* **1988**, *242*, 933–935.
- (124) Cohen, P. *Curr. Opin. Chem. Biol.* **1999**, *3*, 459–465.
- (125) Druker, B. J.; Talpaz, M.; Resta, D. J.; Peng, B.; Buchdunger, E.; Ford, J. M.; Lydon, N. B.; Kantarjian, H.; Capdeville, R.; Ohno-Jones, S.; Sawyers, C. L. *N. Engl. J. Med.* **2001**, *344*, 1031–1037.
- (126) Kaelin Jr, W. G. *Sci. STKE* **2004**, *225*, pe12-pe12.
- (127) Chabner, B. A. *Oncologist* **2001**, *6*, 230–232.
- (128) Fabbro, D.; Cowan-Jacob, S. W.; Moebitz, H. *Br. J. Pharmacol.* **2015**, *172*, 2675–2700.
- (129) Wu, P.; Nielsen, T. E.; Clausen, M. H. *Drug Discov. Today* **2016**, *21*, 5–10.
- (130) Niessen, S.; Dix, M. M.; Barbas, S.; Hayward, M. M.; Kath, J. C.; Cravatt, B. F.; Niessen, S.; Dix, M. M.; Barbas, S.; Potter, Z. E.; Lu, S.; Brodsky, O. *Cell Chem. Biol.* **2017**, *24*, 1–13.
- (131) Tan, L.; Akahane, K.; McNally, R.; Reyskens, K. M. S. ; Ficarro, S. B.; Liu, S.; Herter-Sprie, G. S.; Koyama, S.; Pattison, M. J.; Labella, K. M.; Johannessen, L.; Akbay, E. A.; Wong, K.-K.; Frank, D. A.; Marto, J. A.; Look, T. A.; Arthur, S.; Eck, M. J.; Gray, N. S. *J. Med. Chem.* **2015**, *58*, 6589–6606.
- (132) Tan, L.; Wang, J.; Tanizaki, J.; Huang, Z.; Aref, A. R.; Rusan, M.; Zhu, S.-J.; Zhang, Y.; Ercan, D.; Liao, R. G.; Capelletti, M.; Zhou, W.; Hur, W.; Kim, N.; Sim, T.; Gaudet, S.; Barbie, D. a; Yeh, J.-R. J.; Yun, C.-H.; Hammerman, P. S.; Mohammadi, M.; Jänne, P. a; Gray, N. S. *Proc. Natl. Acad. Sci.* **2014**, *111*, E4869–E4877.
- (133) Ward, R. A.; Colclough, N.; Challinor, M.; Debreczeni, J.; Eckersley, K.; Fairley, G.;
-

-
- Feron, L.; Flemington, V.; Graham, M. A.; Greenwood, R.; Hopcroft, P.; Howard, T. D.; James, M.; Jones, C. D.; Jones, C. R.; Renshaw, J.; Roberts, K.; Snow, L.; Tonge, M.; Yeung, K. *J. Med. Chem.* **2015**, *58*, 4690–4801.
- (134) Liu, Q.; Sabnis, Y.; Zhao, Z.; Zhang, T.; Buhrlage, S. J.; Jones, L. H.; Gray, N. S. *Chem. Biol.* **2013**, *20*, 146–159.
- (135) Zhang, J.; Yang, P. L.; Gray, N. S. *Nat. Rev. Cancer* **2009**, *9*, 28–39.
- (136) Leproult, E.; Barluenga, S.; Moras, D.; Wurtz, J.-M.; Winssinger, N. *J. Med. Chem.* **2011**, *54*, 1347–1355.
- (137) Zhao, Z.; Liu, Q.; Bliven, S.; Xie, L.; Bourne, P. E. *J. Med. Chem.* **2017**, *60*, 2879–2889.
- (138) Carrera, A. C.; Alexandrov, K.; Roberts, T. M. *Proc. Natl. Acad. Sci.* **1993**, *90*, 442–446.
- (139) Whitman, M.; Downes, C. P.; Keeler, M.; Keller, T.; Cantley, L. *Nature* **1988**, *332*, 644–646.
- (140) Walker, E. H.; Perisic, O.; Ried, C.; Stephens, L.; Williams, R. L. *Nature* **1999**, *402*, 313–320.
- (141) Vanhaesebroeck, B.; Whitehead, M. A.; Piñeiro, R. *J. Mol. Med.* **2016**, *94*, 5–11.
- (142) Ghigo, A.; Damilano, F.; Braccini, L.; Hirsch, E. *BioEssays* **2010**, *32*, 185–196.
- (143) Gunn, R. M.; Hailes, H. C. *J. Chem. Biol.* **2008**, *1*, 49–62.
- (144) Vanhaesebroeck, B.; Stephens, L.; Hawkins, P. *Nat. Rev. Mol. Cell Biol.* **2012**, *13*, 195–203.
- (145) Wymann, M. P.; Marone, R. *Curr. Opin. Cell Biol.* **2005**, *17*, 141–149.
- (146) Amzel, L. M.; Huang, C.; Mandelker, D.; Lengauer, C.; Gabelli, S. B.; Vogelstein, B. *Nat. Rev. Cancer* **2008**, *8*, 665–669.
- (147) Koyasu, S. *Nat. Immunol.* **2003**, *4*, 313–319.
- (148) Okkenhaug, K.; Bilancio, A.; Farjot, G.; Priddle, H.; Sancho, S.; Peskett, E.; Pearce, W.; Meek, S. E.; Salpekar, A.; Waterfield, M. D.; Smith, A. J. H.; Vanhaesebroeck, B. *Science* **2002**, *297*, 1031–1034.
-

-
- (149) Puri, K. D.; Doggett, T. A.; Douangpanya, J.; Hou, Y.; Tino, W. T.; Wilson, T.; Graf, T.; Clayton, E.; Turner, M.; Hayflick, J. S.; Diacovo, T. G. *Blood* **2004**, *103*, 3448–3456.
- (150) Rommel, C.; Camps, M.; Ji, H. *Nat. Rev. Immunol.* **2007**, *7*, 191–201.
- (151) Fruman, D. A.; Chiu, H.; Hopkins, B. D.; Bagrodia, S.; Cantley, L. C.; Abraham, R. T. *Cell* **2017**, *170*, 605–635.
- (152) Samuels, Y.; Wang, Z.; Bardelli, A.; Silliman, N.; Ptak, J.; Szabo, S.; Yan, H.; Gazdar, A.; Powell, S. M.; Riggins, G. J.; Willson, J. K. V.; Markowitz, S.; Kinzler, K. W.; Vogelstein, B.; Velculescu, V. E. *Science* **2004**, *304*, 554.
- (153) Jia, S.; Liu, Z.; Zhang, S.; Liu, P.; Zhang, L.; Lee, S. H.; Zhang, J.; Signoretti, S.; Loda, M.; Roberts, T. M.; Zhao, J. J. *Nature* **2008**, *454*, 776–780.
- (154) Bi, L.; Okabe, I.; Bernard, D. J.; Wynshaw-Boris, A.; Nussbaum, R. L. *J. Biol. Chem.* **1999**, *274*, 10963–10968.
- (155) Bi, L.; Okabe, I.; Bernard, D. J.; Nussbaum, R. L. *Mamm. Genome* **2002**, *13*, 169–172.
- (156) Hirsch, E.; Katanaev, V. L.; Garlanda, C.; Azzolino, O.; Pirola, L.; Silengo, L.; Sozzani, S.; Mantovani, A.; Altruda, F.; Wymann, M. *Science* **2000**, *287*, 1049–1053.
- (157) Marone, R.; Cmiljanovic, V.; Giese, B.; Wymann, M. P. *Biochim. Biophys. Acta* **2008**, *1784*, 159–185.
- (158) Rowan, W. C.; Smith, J. L.; Affleck, K.; Amour, A. *Biochem. Soc. Trans.* **2012**, *40*, 240–245.
- (159) Clayton, E.; Bardi, G.; Bell, S. E.; Chantry, D.; Downes, C. P.; Gray, A.; Humphries, L. A.; Rawlings, D.; Reynolds, H.; Vigorito, E.; Turner, M. *J. Exp. Med.* **2002**, *196*, 753–763.
- (160) Holgate, S. T.; Wenzel, S.; Postma, D. S.; Weiss, S. T.; Renz, H.; Sly, P. D. *Nat. Rev. Dis. Prim.* **2015**, *1*, 1–22.
- (161) Wu, S.; Luo Howard, H.; Wang, H.; Zhao, W.; Hu, Q.; Yang, Y. *Biochem. Biophys. Res. Commun.* **2016**, 6–11.
- (162) Bunnage, M. E.; Chekler, E. L. P.; Jones, L. H. *Nat. Chem. Biol.* **2013**, *9*, 195–199.
-

-
- (163) Down, K.; Amour, A.; Baldwin, I. R.; Cooper, A. W. J.; Deakin, A. M.; Felton, L. M.; Guntrip, S. B.; Hardy, C.; Harrison, Z. A.; Jones, K. L.; Jones, P.; Keeling, S. E.; Le, J.; Livia, S.; Lucas, F.; Lunniss, C. J.; Parr, N. J.; Robinson, E.; Rowland, P.; Smith, S.; Thomas, D. A.; Vitulli, G.; Washio, Y.; Hamblin, J. N. *J. Med. Chem.* **2015**, *58*, 7381–7399.
- (164) Knight, Z. A.; Shokat, K. M. *Biochem. Soc. Trans.* **2007**, *35*, 245–249.
- (165) Berndt, A.; Miller, S.; Williams, O.; Le, D. D.; Houseman, B. T.; Pacold, J. I.; Gorrec, F.; Hon, W.-C.; Liu, Y.; Rommel, C.; Gaillard, P.; Rückle, T.; Schwarz, M. K.; Shokat, K. M.; Shaw, J. P.; Williams, R. L. *Nat. Chem. Biol.* **2010**, *6*, 117–124.
- (166) Knight, Z. A.; Chiang, G. G.; Alaimo, P. J.; Kenski, D. M.; Ho, C. B.; Coan, K.; Abraham, R. T.; Shokat, K. M. *Bioorg. Med. Chem.* **2004**, *12*, 4749–4759.
- (167) Alaimo, P. J.; Knight, Z. A.; Shokat, K. M. *Bioorg. Med. Chem.* **2005**, *13*, 2825–2836.
- (168) Matte, A.; Tari, L. W.; Delbaere, L. T. *Structure* **1998**, *6*, 413–419.
- (169) Burriss, H. A.; Patel, M. R.; Lanasa, M. C.; Brander, D.; Connor, O. A. O.; Deng, C.; Gutierrez, M.; Jones, S. F.; Kuhn, J. G.; Miskin, H. P.; Sportelli, P.; Vakkalanka, S.; Flinn, I. In *19th Congress of the European Hematology Association*; Milan, Italy, 2014.
- (170) Lannutti, B. J.; Meadows, S. A.; Herman, S. E. M.; Kashishian, A.; Steiner, B.; Johnson, A. J.; Byrd, J. C.; Tyner, J. W.; Loriaux, M. M.; Deininger, M.; Druker, B. J.; Puri, K. D.; Ulrich, R. G.; Giese, N. A. *Blood* **2011**, *117*, 591–594.
- (171) United States Food and Drug Administration. FDA approves Zydelig for three types of blood cancers
<http://www.fda.gov/NewsEvents/Newsroom/PressAnnouncements/ucm406387.htm> (accessed Nov 11, 2014).
- (172) Somoza, J. R.; Koditek, D.; Villaseñor, A. G.; Novikov, N.; Wong, M. H.; Liclican, A.; Xing, W.; Lagpacan, L.; Wang, R.; Schultz, B. E.; Papalia, G. A.; Samuel, D.; Lad, L.; McGrath, M. E. *J. Biol. Chem.* **2015**, *290*, 8439–8446.
- (173) Knight, Z. A.; Gonzalez, B.; Feldman, M. E.; Zunder, E. R.; Goldenberg, D. D.; Williams, O.; Loewith, R.; Stokoe, D.; Balla, A.; Toth, B.; Balla, T.; Weiss, W. A.; Williams, R. L.;
-

Shokat, K. M. *Cell* **2006**, *125*, 733–747.

- (174) Amour, A.; Barton, N.; Cooper, A. W. J.; Inglis, G.; Jamieson, C.; Luscombe, C. N.; Morrell, J.; Peace, S.; Perez, D.; Rowland, P.; Tame, C.; Uddin, S.; Vitulli, G.; Wellaway, N. *J. Med. Chem.* **2016**, *59*, 7239–7251.
- (175) Sutherlin, D. P.; Baker, S.; Bisconte, A.; Blaney, P. M.; Brown, A.; Chan, B. K.; Chantry, D.; Castanedo, G.; Depledge, P.; Goldsmith, P.; Goldstein, D. M.; Hancox, T.; Kaur, J.; Knowles, D.; Kondru, R.; Lesnick, J.; Lucas, M. C.; Lewis, C.; Murray, J.; Nadin, A. J.; Nonomiya, J.; Pang, J.; Pegg, N.; Price, S.; Reif, K.; Safina, B. S.; Salphati, L.; Staben, S.; Seward, E. M.; Shuttleworth, S.; Sohal, S.; Sweeney, Z. K.; Ultsch, M.; Waszkowycz, B.; Wei, B. *Bioorg. Med. Chem. Lett.* **2012**, *22*, 4296–4302.
- (176) Furet, P.; Guagnano, V.; Fairhurst, R. A.; Imbach-Weese, P.; Bruce, I.; Knapp, M.; Fritsch, C.; Blasco, F.; Blanz, J.; Aichholz, R.; Hamon, J.; Fabbro, D.; Caravatti, G. *Bioorg. Med. Chem. Lett.* **2013**, *23*, 3741–3748.
- (177) Peace, S.; Ingliss, G.; Hobbs, H. Unpublished Work.
- (178) Brian, P. W.; Curtis, P. J.; Hemming, H. G.; Norris, G. L. F. *Trans. Br. Mycol. Soc.* **1957**, *40*, 365–368.
- (179) Walker, E. H.; Pacold, M. E.; Perisic, O.; Stephens, L.; Hawkins, P. T.; Wymann, M. P.; Williams, R. L. *Mol. Cell* **2000**, *6*, 909–919.
- (180) Powis, G.; Bonjouklian, R.; Berggren, M. M.; Gallegos, A.; Abraham, R.; Ashendel, C.; Zalkow, L.; Matter, W. F.; Dodge, J.; Grindey, G.; Vlahos, C. J. *Cancer Res.* **1994**, *54*, 2419–2423.
- (181) Waterfield, M. D.; Panayotou, G.; Wymann, M. P.; Bulgarelli-Leva, G.; Zvelebil, M. J.; Pirola, L.; Vanhaesebroeck, B. *Mol. Cell. Biol.* **1996**, *16*, 1722–1733.
- (182) Pirola, L.; Zvelebil, M. J.; Bulgarelli-Leva, G.; Van Obberghen, E.; Waterfield, M. D.; Wymann, M. P. *J. Biol. Chem.* **2001**, *276*, 21544–21554.
- (183) Yuan, H.; Barnes, K. R.; Weissleder, R.; Cantley, L.; Josephson, L. *Chem. Biol.* **2007**, *14*, 321–328.
- (184) Vanhaesebroeck, B.; Leever, S. J.; Ahmadi, K.; Timms, J.; Katso, R.; Driscoll, P. C.;
-

-
- Woscholski, R.; Parker, P. J.; Waterfield, M. D. *Annu. Rev. Biochem.* **2001**, *70*, 535–602.
- (185) Liu, Y.; Jiang, N.; Wu, J.; Dai, W.; Rosenblum, J. S. *J. Biol. Chem.* **2007**, *282*, 2505–2511.
- (186) Elling, R. A.; Fucini, R. V.; Romanowski, M. J. *Acta Crystallogr. D. Biol. Crystallogr.* **2008**, *D64*, 909–918.
- (187) Ihle, N. T.; Williams, R.; Chow, S.; Chew, W.; Berggren, M. I.; Paine-Murrieta, G.; Minion, D. J.; Halter, R. J.; Wipf, P.; Abraham, R.; Kirkpatrick, L.; Powis, G. *Mol. Cancer Ther.* **2004**, *3*, 763–772.
- (188) Howes, A. L.; Chiang, G. G.; Lang, E. S.; Ho, C. B.; Powis, G.; Vuori, K.; Abraham, R. T. *Mol. Cancer Ther.* **2007**, *6*, 2505–2514.
- (189) Koul, D.; Shen, R.; Kim, Y.; Kondo, Y.; Lu, Y.; Bankson, J.; Ronen, S. M.; Kirkpatrick, D. L.; Powis, G.; Yung, W. K. A. *Neuro. Oncol.* **2010**, *12*, 559–569.
- (190) Sundstrom, T. J.; Anderson, A. C.; Wright, D. L. *Org. Biomol. Chem.* **2009**, *7*, 840–850.
- (191) Yu, K.; Lucas, J.; Zhu, T.; Zask, A.; Gaydos, C.; Toral-Barza, L.; Gu, J.; Li, F.; Chaudhary, I.; Cai, P.; Lotvin, J.; Petersen, R.; Ruppen, M.; Fawzi, M.; Ayril-Kaloustian, S.; Skotnicki, J.; Mansour, T.; Frost, P.; Gibbons, J. *Cancer Biol. Ther.* **2005**, *4*, 538–545.
- (192) A Phase II Study of PX-866 in Patients With Recurrent or Metastatic Castration Resistant Prostate Cancer
<https://clinicaltrials.gov/ct2/show/NCT01331083?term=PX-866&rank=6> (accessed Dec 17, 2014).
- (193) Cheng, Y.-C.; Prusoff, W. H. *Biochem. Pharmacol.* **1973**, *22*, 3099–3108.
- (194) Burgi, H. B.; Dunitz, J. D.; Lehn, J. M.; Wipff, G. *Tetrahedron* **1974**, *30*, 1563–1572.
- (195) Steglich, W.; Neises, B. *Angew. Chem. Int. Ed.* **1978**, *17*, 522–523.
- (196) Iwasawa, T.; Wash, P.; Gibson, C.; Rebek, J. Jr. *Tetrahedron* **2007**, *63*, 6506–6511.
- (197) Danehy, J. P.; Noel, C. J. *J. Am. Chem. Soc.* **1960**, *82*, 2511–2515.
- (198) In *CRC Handbook of Chemistry and Physics*; Haynes, W. M., Ed.; CRC Press Taylor &
-

- (199) Connors, K. A.; Bender, M. L. *J. Org. Chem.* **1961**, *26*, 2498–2504.
- (200) Yang, W.; Drueckhammer, D. G. *J. Am. Chem. Soc.* **2001**, *123*, 11004–11009.
- (201) Yang, W. Y.; Drueckhammer, D. G. *Org. Lett.* **2000**, *2*, 4133–4136.
- (202) Maude, A. B.; Williams, A. J. *Chem. Soc. Perkin Trans. 2* **1997**, 179–184.
- (203) Bream, R. N.; Hayler, J. D.; Ironmonger, A. G.; Szeto, P.; Webb, M. R.; Wheelhouse, K. M. P.; Willacy, R. D. Processes to make indazole derivatives, 2016.
- (204) Kuwano, R.; Takahashi, M.; Ito, Y. *Tetrahedron Lett.* **1998**, *39*, 1017–1020.
- (205) Ironmonger, A.; Bream, R.; Roberts, A. Unpublished Work, 2014.
- (206) Zhou, S.; Junge, K.; Addis, D.; Das, S.; Beller, M. *Angew. Chem. Int. Ed.* **2009**, *48*, 9507–9510.
- (207) Das, S.; Addis, D.; Junge, K.; Beller, M. *Chem. Eur. J.* **2011**, *17*, 12186–12192.
- (208) Das, S.; Addis, D.; Zhou, S.; Junge, K.; Beller, M. *J. Am. Chem. Soc.* **2010**, *132*, 1770–1771.
- (209) Larcombe-McDouall, J.; Buttell, N.; Harrison, N.; Wray, S. *J. Physiol.* **1999**, *518*, 783–790.
- (210) Gribble, F. M.; Loussouarn, G.; Tucker, S. J.; Zhao, C.; Nichols, C. G.; Ashcroft, F. M. *J. Biol. Chem.* **2000**, *275*, 30046–30049.
- (211) Davis, A.; Ward, S. E. In *The Handbook of Medicinal Chemistry: Principles and Practice*; The Royal Society of Chemistry: Cambridge, 2014; pp 544–545.
- (212) Khandekar, S. S. *J. Biomol. Screen.* **2005**, *10*, 447–455.
- (213) Gushwa, N. N.; Kang, S.; Chen, J.; Taunton, J. *J. Am. Chem. Soc.* **2012**, *134*, 20214–20217.
- (214) Ruiz-Larrea, F.; Vicendo, P.; Yaish, P.; End, P.; Panayotou, G.; Fry, M. J.; Morgan, S. J.; Thompson, A.; Parker, P. J.; Waterfield, M. D.; Page, T. *Biochem. J.* **1993**, *290*, 609–
-

- (215) Dong, J.; Krasnova, L.; Finn, M. G.; Sharpless, K. B. *Angew. Chem. Int. Ed.* **2014**, *53*, 9430–9448.
- (216) Miller, R. M.; Taunton, J. *Methods Enzymol.* **2014**, *548*, 93–116.
- (217) Brouwer, A. J.; Jonker, A.; Werkhoven, P.; Kuo, E.; Li, N.; Gallastegui, N.; Kemmink, J.; Florea, B. I.; Groll, M.; Overkleeft, H. S.; Liskamp, R. M. J. *J. Med. Chem.* **2012**, *55*, 10995–11003.
- (218) Brouwer, A. J.; Ceylan, T.; Jonker, A. M.; van der Linden, T.; Liskamp, R. M. J. *Bioorg. Med. Chem.* **2011**, *19*, 2397–2406.
- (219) Brouwer, A. J.; Ceylan, T.; Linden, T. V. D.; Liskamp, R. M. J. *Tetrahedron Lett.* **2009**, *50*, 3391–3393.
- (220) Wilden, J. D.; Judd, D. B.; Caddick, S. *Tetrahedron Lett.* **2005**, *46*, 7637–7640.
- (221) Wilden, J. D.; Geldeard, L.; Lee, C. C.; Judd, D. B.; Caddick, S. *Chem. Commun* **2007**, 1074–1076.
- (222) Caddick, S.; Wilden, J. D.; Bush, H. D.; Wadman, S. N.; Judd, D. B. *Org. Lett.* **2002**, *4*, 2549–2551.
- (223) Caddick, S.; Wilden, J. D.; Judd, D. B. *Chem. Commun.* **2005**, 2727–2728.
- (224) Yan, L.; Bertarelli, D. C. G.; Hayallah, A. M.; Meyer, H.; Klotz, K.-N.; Müller, C. E. *J. Med. Chem.* **2006**, *49*, 4384–4391.
- (225) Yan, L.; Müller, C. E. *J. Med. Chem.* **2004**, *47*, 1031–1043.
- (226) Gupta, B.; Sharma, R.; Singh, N.; Karpichev, Y.; Satnami, M. L.; Ghosh, K. K. *J. Phys. Org. Chem.* **2013**, *26*, 632–642.
- (227) Pu, Y. M.; Christesen, A.; Ku, Y. Y. *Tetrahedron Lett.* **2010**, *51*, 418–421.
- (228) Larson, J. W.; McMahon, T. B. *J. Am. Chem. Soc.* **1982**, *104*, 5848–5849.
- (229) Nielsen, M. K.; Ugaz, C. R.; Li, W.; Doyle, A. G. *J. Am. Chem. Soc.* **2015**, *197*, 9571–9574.
-

-
- (230) Spink, E.; Ding, D.; Peng, Z.; Boudreau, M. A.; Leemans, E.; Lastochkin, E.; Song, W.; Lichtenwalter, K.; O'Daniel, P. I.; Testero, S. A.; Pi, H.; Schroeder, V. A.; Wolter, W. R.; Antunes, N. T.; Suckow, M. A.; Vakulenko, S.; Chang, M.; Mobashery, S. *J. Med. Chem.* **2015**, *58*, 1380–1389.
- (231) Kovacic, P.; Somanathan, R. *J. Appl. Toxicol.* **2014**, *34*, 810–824.
- (232) Hansch, C.; Leo, A.; Taft, R. W. *Chem. Rev.* **1991**, *91*, 165–195.
- (233) Charter, N. W.; Kauffman, L.; Singh, R. A. J.; Eglen, R. M. *J. Biomol. Screen.* **2006**, *11*, 390–399.
- (234) Strelow, J. M. *SLAS Discov.* **2017**, *22*, 3–20.
- (235) Copeland, R. A. In *Methods of Biochemical Analysis*; Wiley: New Jersey, 2005; Vol. 46.
- (236) Zaro, B. W.; Whitby, L. R.; Lum, K. M.; Cravatt, B. F. *J. Am. Chem. Soc.* **2016**, *138*, 15841–15844.
- (237) Steen, H.; Mann, M. *Nat. Rev. Mol. Cell Biol.* **2004**, *5*, 699–711.
- (238) Ting, L.; Rad, R.; Gygi, S. P.; Haas, W. *Nat. Methods* **2011**, *8*, 937–940.
- (239) Bantscheff, M.; Eberhard, D.; Abraham, Y.; Bastuck, S.; Boesche, M.; Hobson, S.; Mathieson, T.; Perrin, J.; Raida, M.; Rau, C.; Reader, V.; Sweetman, G.; Bauer, A.; Bouwmeester, T.; Hopf, C.; Kruse, U.; Neubauer, G.; Ramsden, N.; Rick, J.; Kuster, B.; Drewes, G. *Nat. Biotechnol.* **2007**, *25*, 1035–1044.
- (240) Lemeer, S.; Zörgiebel, C.; Ruprecht, B.; Kohl, K.; Kuster, B. *J. Proteome Res.* **2013**, *12*, 1723–1731.
- (241) Esbroeck, A. C. M. van; Janssen, A. P. A.; Cognetta, A. B.; Ogasawara, D.; Shpak, G.; Kroeg, M. Van Der; Kantae, V.; Baggelaar, M. P.; Vrij, F. M. S. De; Deng, H.; Allarà, M.; Fezza, F.; Lin, Z.; Wel, T. Van Der; Soethoudt, M.; Mock, E. D.; Dulk, H. Den; Baak, I. L.; Florea, B. I.; Hendriks, G.; Petrocellis, L. De; Overkleeft, H. S.; Hankemeier, T.; Zeeuw, C. I. De; Marzo, V. Di; Maccarrone, M.; Cravatt, B. F.; Kushner, S. A.; Stelt, M. van der. *Science* **2017**, *356*, 1084–1087.
- (242) Kolb, H. C.; Finn, M. G.; Sharpless, K. B. *Angew. Chem. Int. Ed.* **2001**, *40*, 2004–2021.
-

-
- (243) Mckay, C. S.; Finn, M. G. *Chem. Biol.* **2014**, *21*, 1075–1101.
- (244) Prescher, J. A.; Bertozzi, C. R. *Nat. Chem. Biol.* **2005**, *1*, 13–21.
- (245) Rostovtsev, V. V.; Green, L. G.; Fokin, V. V.; Sharpless, K. B. *Angew. Chem. Int. Ed.* **2002**, *41*, 2596–2599.
- (246) Presolski, S. I.; Hong, V.; Cho, S.-H.; Finn, M. G. *J. Am. Chem. Soc.* **2010**, *132*, 14570–14576.
- (247) Jewett, J. C.; Bertozzi, C. R. *Chem. Soc. Rev.* **2010**, *39*, 1272–1279.
- (248) Oliveira, B. L.; Guo, Z.; Bernardes, G. J. L. *Chem. Soc. Rev.* **2017**, *46*, 4895–4950.
- (249) Speers, A. E.; Cravatt, B. F. *Chem. Biol.* **2014**, *128*, 189–190.
- (250) Burke, E. G.; Gold, B.; Hoang, T. T.; Raines, R. T.; Schomaker, J. M. *J. Am. Chem. Soc.* **2017**, *139*, 8029–8037.
- (251) Rutkowska, A.; Thomson, D. W.; Vappiani, J.; Werner, T.; Mueller, K. M.; Dittus, L.; Krause, J.; Muelbaier, M.; Bergamini, G.; Bantscheff, M. *ACS Chem. Biol.* **2016**, *11*, 2541–2550.
- (252) Blackman, M. L.; Royzen, M.; Fox, J. M. *J. Am. Chem. Soc.* **2008**, *130*, 13518–13519.
- (253) Larsen, M. a.; Hartwig, J. F. *J. Am. Chem. Soc.* **2014**, *136*, 4287–4299.
- (254) Tsuchiya, S.; Yamabe, M.; Yamaguchi, Y.; Kobayashi, Y.; Konno, T.; Tada, K. *Int. J. Cancer* **1980**, *26*, 171–176.
- (255) Bosshart, H.; Heinzelmann, M. *Ann. Transl. Med.* **2016**, *4*, 438–442.
- (256) Qin, Z. *Atherosclerosis* **2012**, *221*, 2–11.
- (257) Feng, Y.; Zhang, N.; Jacobs, K. M.; Jiang, W.; Yang, L. V.; Li, Z.; Zhang, J.; Lu, J. Q.; Hu, X. H. *Cytom. Part A* **2014**, *85*, 817–826.
- (258) Yu, X.; Long, Y. C.; Shen, H. M. *Autophagy* **2015**, *11*, 1711–1728.
- (259) Klaeger, S.; Gohlke, B.; Perrin, J.; Gupta, V.; Heinzlmeir, S.; Helm, D.; Qiao, H.; Bergamini, G.; Handa, H.; Savitski, M. M.; Bantscheff, M.; Médard, G.; Preissner, R.;
-

-
- Kuster, B. *ACS Chem. Biol.* **2016**, *11*, 1245–1254.
- (260) Cahn, A.; Hamblin, J. N.; Begg, M.; Wilson, R.; Dunsire, L.; Sriskantharajah, S.; Montembault, M.; Leemereise, C. N.; Galinanes-Garcia, L.; Watz, H.; Kirsten, A. M.; Fuhr, R.; Hessel, E. M. *Pulm. Pharmacol. Ther.* **2017**, *46*, 69–77.
- (261) Kazmi, F.; Hensley, T.; Pope, C.; Funk, R. S.; Loewen, G. J.; Buckley, D. B.; Parkinson, A. *Drug Metab. Dispos.* **2013**, *41*, 897–905.
- (262) Dittus, L.; Werner, T.; Muelbaier, M.; Bantscheff, M. *ACS Chem. Biol.* **2017**, *12*, 2515–2521.
- (263) Yee, M. C.; Fas, S. C.; Stohlmeyer, M. M.; Wandless, T. J.; Cimprich, K. A. *J. Biol. Chem.* **2005**, *280*, 29053–29059.
- (264) Liu, Y.; Shreder, K. R.; Gai, W.; Corral, S.; Ferris, D. K.; Rosenblum, J. S. *Chem. Biol.* **2005**, *12*, 99–107.
- (265) Farrar, M. A.; Schreiber, R. D. *Annu. Rev. Immunol.* **1993**, *11*, 571–611.
- (266) Fitzgerald, P.; Eugene, M. C.; Clarke, G.; Scully, P.; Barry, S.; Eamonn, M. M. Q.; Shanahan, F.; Cryan, J.; Dinan Timothy, G. *Neurogastroenterol. Motil.* **2008**, *20*, 1291–1297.
- (267) Grip, O.; Janciauskiene, S. *PLoS One* **2009**, *4*, 1–6.
- (268) Ghosh, T. K.; Mickelson, D. J.; Solberg, J. C.; Lipson, K. E.; Inglefield, J. R.; Alkan, S. S. *Int. Immunopharmacol.* **2007**, *7*, 1111–1121.
- (269) Selvin, P. R. *Nat. Struct. Biol.* **2000**, *7*, 730–734.
- (270) Clegg, R. M. *Curr. Opin. Biotechnol.* **1995**, *6*, 103–110.
- (271) Forster, T. *Discuss. Faraday Soc.* **1959**, *27*, 1–6.
- (272) Prevo, B.; Peterman, E. J. G. *Chem. Soc. Rev.* **2014**, *43*, 1144–1155.
- (273) Sekar, R. B.; Periasamy, A. *J. Cell Biol.* **2003**, *160*, 629–633.
- (274) Yan, Y.; Marriott, G. *Curr. Opin. Chem. Biol.* **2003**, *7*, 635–640.
-

-
- (275) Gray, A.; Olsson, H.; Batty, I. H.; Priganica, L.; Downes, C. P. *Anal. Biochem.* **2003**, *313*, 234–245.
- (276) Washburn, M. P.; Wolters, D.; Yates III, J. R. *Nat. Biotechnol.* **2001**, *19*, 242–247.
- (277) Megger, D. A.; Pott, L. L.; Ahrens, M.; Padden, J.; Bracht, T.; Kuhlmann, K.; Eisenacher, M.; Meyer, H. E.; Sitek, B. *Biochim. Biophys. Acta* **2014**, *1844*, 967–976.
- (278) Thompson, A.; Schäfer, J.; Kuhn, K.; Kienle, S.; Schwarz, J.; Schmidt, G.; Neumann, T.; Hamon, C. *Anal. Chem.* **2003**, *75*, 1895–1904.
- (279) McAlister, G. C.; Huttlin, E. L.; Haas, W.; Ting, L.; Jedrychowski, M. P.; Rogers, J. C.; Kuhn, K.; Pike, I.; Grothe, R. A.; Blethrow, J. D.; Gygi, S. P. *Anal. Chem.* **2012**, *84*, 7469–7478.
- (280) Werner, T.; Becher, I.; Sweetman, G.; Doce, C.; Savitski, M. M.; Bantscheff, M. *Anal. Chem.* **2012**, *84*, 7188–7194.
- (281) Dayon, L.; Hainard, A.; Licker, V.; Turck, N.; Kuhn, K.; Hochstrasser, D. F.; Burkhard, P. R.; Sanchez, J. C. *Anal. Chem.* **2008**, *80*, 2921–2931.
- (282) Saveliev, S.; Bratz, M.; Zubarev, R.; Szapacs, M.; Budamgunta, H.; Urh, M. *Nat. Methods* **2013**, *10*, i–ii.
- (283) Olsen, J. V.; Ong, S.-E.; Mann, M. *Mol. Cell. Proteomics* **2004**, *3*, 608–614.
- (284) Werner, T.; Sweetman, G.; Savitski, M. F.; Mathieson, T.; Bantscheff, M.; Savitski, M. M. *Anal. Chem.* **2014**, *86*, 3594–3601.
- (285) Tian, C.; Sun, R.; Liu, K.; Fu, L.; Liu, X.; Zhou, W.; Yang, Y.; Yang, J. *Cell Chem. Biol.* **2017**, *24*, 1416–1427.
- (286) Kabsch, W. *Acta Crystallogr. D. Biol. Crystallogr.* **2010**, *D66*, 125–132.
- (287) Evans, P. R.; Murshudov, G. N. *Acta Crystallogr. D. Biol. Crystallogr.* **2013**, *D69*, 1204–1214.
- (288) Winn, M. D.; Ballard, C. C.; Cowtan, K. D.; Dodson, E. J.; Emsley, P.; Evans, P. R.; Keegan, R. M.; Krissinel, E. B.; Leslie, A. G. W.; McCoy, A.; McNicholas, S. J.; Murshudov, G. N.; Pannu, N. S.; Potterton, E. A.; Powell, H. R.; Read, R. J.; Vagin, A.;
-

Wilson, K. S. *Acta Crystallogr. D. Biol. Crystallogr.* **2011**, *D67*, 235–242.

- (289) Emsley, P.; Lohkamp, B.; Scott, W. G.; Cowtan, K. *Acta Crystallogr. D. Biol. Crystallogr.* **2010**, *D66*, 486–501.
- (290) Bricogne, G.; Blanc, E.; Brandl, M.; Flensburg, C.; Keller, P.; Paciorek, W.; Roversi, P.; Sharff, A.; Smart, O. S.; Vonrhein, C.; Womack, T. O. BUSTER, (Global Phasing Ltd. Cambridge, UK, 2016).
- (291) Farrant, R. D.; Hollerton, J. C.; Lynn, S. M.; Provera, S.; Sidebottom, P. J.; Upton, R. J. *Magn. Reson. Chem.* **2010**, *48*, 753–762.
- (292) Gong, E. Y. In *Antiviral Methods and Protocols (Methods in Molecular Biology)*; Springer, 2013; pp 59–78.
- (293) Erra, S. M.; Carrascal, R. M.; Taltavull, M. J.; Caturla, J. J. F.; Bernal, A. F. J.; Pages, S. L. M.; Mir, C. M.; Casals, C. G.; Hernandez, O. M. B. Pyrrolotriazinone derivatives as pi3k inhibitors. WO 2014060432 A1, April 24, 2014.
- (294) Hadida, R. S.; Grootenhuys, P. D. J.; Zhou, J.; Bear, B.; Miller, M.; McCartney, J. Modulators of cftr. WO2008141119 A2, November 20, 2008.
- (295) Pretsch, E.; Simon, W.; Seibl, J.; Clerc, T. In *Tables of Spectral Data for Structure Determination of Organic Compounds*; Fresenius, W., Huber, J. F. K., Pungor, E., Rechnitz, G. A., Simon, W., West, T. S., Eds.; Springer-Verlag: Berlin, 1989; p 1175.

Appendix

Selectively Targeting the Kinome-Conserved Lysine of PI3K δ as a General Approach to Covalent Kinase Inhibition

Samuel E. Dalton,^{†,‡} Lars Dittus,[§] Daniel A. Thomas,[‡] Máire A. Convery,[‡] Joao Nunes,[‡] Jacob T. Bush,[‡] John P. Evans,[‡] Thilo Werner,[§] Marcus Bantscheff,[§] John A. Murphy,[†] and Sebastien Campos^{*,‡,§}

[†]Department of Pure and Applied Chemistry, WestCHEM, University of Strathclyde, 295 Cathedral Street, Glasgow G1 1XL, U.K.

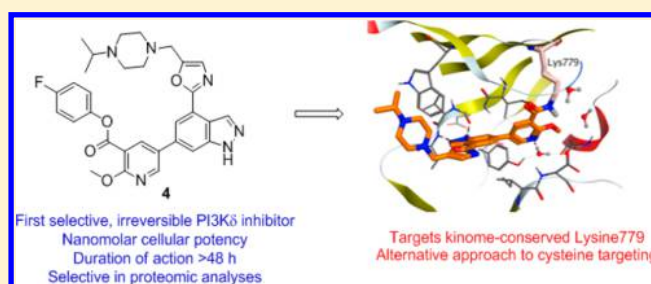
[‡]Medicines Research Centre, GlaxoSmithKline, Gunnels Wood Road, Stevenage, Hertfordshire SG1 2NY, U.K.

[§]Cellzome GmbH, a GSK company, Meyerhofstraße 1, Heidelberg 69117, Germany

Supporting Information

ABSTRACT: Selective covalent inhibition of kinases by targeting poorly conserved cysteines has proven highly fruitful to date in the development of chemical probes and approved drugs. However, this approach is limited to ~200 kinases possessing such a cysteine near the ATP-binding pocket. Herein, we report a novel approach to achieve selective, irreversible kinase inhibition, by targeting the conserved catalytic lysine residue. We have illustrated our approach by developing selective, covalent PI3K δ inhibitors that exhibit nanomolar potency in cellular assays, and a duration of action

>48 h in CD4+ T cells. Despite conservation of the lysine residue throughout the kinome, the lead compound shows high levels of selectivity over a selection of lipid and protein kinases in biochemical assays, as well as covalent binding to very few off-target proteins in live-cell proteomic studies. We anticipate this approach could offer a general strategy, as an alternative to targeting non-conserved cysteines, for the development of selective covalent kinase inhibitors.



INTRODUCTION

The clinical successes of ibrutinib¹ and afatinib² have prompted a resurgence of interest in covalent drug discovery.^{3,4} Covalent inhibitors can possess the advantages of increased potency, prolonged duration of action, decoupled pharmacodynamics and pharmacokinetics, and, often, require less frequent and lower doses.^{4,5}

In the kinase field, researchers commonly target cysteine residues for covalent inhibition.⁶ Targeted residues are often “non-catalytic and poorly conserved”⁷ to maximize selectivity, and mitigate the risk of off-target covalent interactions.^{4,5,7,8} However, only ~200 of over 500 human kinases have been mapped with a cysteine in the vicinity of the ATP pocket, and <50 have been demonstrated to covalently engage with inhibitors, restricting the scope of this strategy.^{6,9–11} We chose to challenge this general approach by investigating the potential to selectively and irreversibly target the kinome-conserved lysine residue.¹² Covalent conjugation with lysine is far less common, due to its protonation state, and therefore poorer nucleophilicity under physiological conditions.¹³ Nonetheless, interest in this nucleophile is rapidly gaining traction in the scientific community.^{14–18}

The heterodimeric lipid kinase phosphoinositide 3-kinase delta (PI3K δ)^{19,20} has been targeted specifically over the related PI3K α , β and γ isoforms for the treatment of a variety of diseases.^{21,22} A number of selective reversible PI3K δ small molecule inhibitors have entered clinical trials, with Zydelig

recently obtaining FDA approval as a second-line treatment for relapsed follicular B-cell non-Hodgkin lymphoma, and relapsed chronic lymphocytic leukemia.^{23–25} More recently, drug developers have targeted PI3K δ for the treatment of inflammatory conditions such as asthma, chronic obstructive pulmonary disease (COPD), rheumatoid arthritis and activated PI3K δ syndrome.^{21,26–32}

To our knowledge, a selective covalent PI3K δ inhibitor has not yet been disclosed, and there is no obvious isoform specific nucleophilic residue to target around the ATP binding site. Irreversible pan-PI3K inhibitors have been investigated previously, based on the fungal antibiotic wortmannin.^{33–35} These compounds target the conserved lysine^{12,36,37} for the covalent reaction, but are poorly selective.³⁵ Promiscuous kinase probes that covalently bind to this residue,^{38–41} have also been developed and commercialized, however methods of selectively targeting this lysine in specific kinases have not yet been reported.

Herein we describe the development of the first selective, irreversible PI3K δ inhibitor, which reacts with the conserved catalytic lysine (Lys779 in PI3K δ numbering). Selectivity was achieved through optimization of the reversible interactions in formation of the initial enzyme–inhibitor complex, while the rate of the covalent reaction with the protein remained constant.

Received: August 22, 2017

Published: December 12, 2017

The targeted lysine residue is present throughout the kinome, hence we anticipate that this strategy could provide an alternative general approach for the development of selective irreversible kinase inhibitors.

RESULTS AND DISCUSSION

Design of Lysine-Targeting Inhibitors. Clinical candidate **1** was identified as a suitable starting point due to its potency profile, and reversible interaction between the sulfonamide and Lys779.²³ We replaced the *cis*-dimethylmorpholine with the more basic, more soluble piperazine moiety²³ and hypothesized that substitution of the sulfonamide for an electrophilic functional group could afford covalent inhibitors (Figure 1). *In silico* modeling suggested that activated esters⁴²

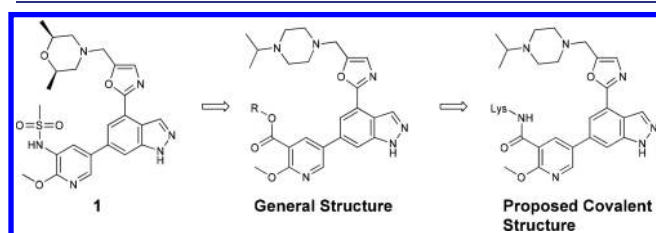


Figure 1. Generalized design principles for development of selective, irreversible PI3K δ inhibitors.

would be tolerated in a reversible enzyme–inhibitor complex with PI3K δ . Furthermore, the model of the covalently bound amide adduct that would form from these inhibitors did not reveal any obvious conformational issues (Figure S1).

Activated Esters Potently Engage PI3K δ in Enzyme and Cellular Assays. A selection of phenolic esters were synthesized, and their potencies at PI3K α , β , γ and δ were assessed using purified recombinant proteins via homogeneous time-resolved fluorescence (HTRF) assays.²³ Additionally, these compounds were tested in a phenotypic human-whole blood (hWB) assay, measuring reduction in interferon gamma (IFN γ) secretion after treatment with T-cell stimulating antibody, CytoStim, as a readout for PI3K δ engagement²³ (Table 1).

Esters 2–7 potently inhibited PI3K δ in isolated enzyme assays with pIC₅₀ values ranging from micromolar (ester 7), to sub-nanomolar (ester 2), confirming that the phenolic ester motifs were tolerated in the ATP binding pocket of the kinase. Furthermore, these data suggested a general trend that PI3K δ potency of the inhibitors improved with the electron withdrawing ability of the R group attached to the ester, although the very high PI3K δ activity of **2** was achieved at the expense of selectivity. The 4-trifluoromethylphenol ester **3** is an exception to this trend. Its relatively strong electron withdrawing effect (σ_p = 0.78, 0.54, 0.06, and –0.27 for NO₂, CF₃, F, and OMe substituents, respectively)⁴³ did not enhance the PI3K δ potency compared to the electron neutral phenol **5**. The decreased potency of 2,4-dimethylphenol ester **7** may have arisen from clash between the 2-methyl group and the kinase, or steric hindrance to nucleophilic attack at the carbonyl. Compounds **3** to **5** showed the best profiles in this analysis, with biochemical potencies on-par with wortmannin **10**, and selectivity comparable to the FDA-approved PI3K δ drug, Zydelig²⁴ **11**. Furthermore, compounds **3**–**5** provided good levels of inhibitory activity in the hWB assay (~10 nM), supporting engagement of PI3K δ in cells, and were at least 15-fold more potent than **10** and **11** in this assay. It is worth noting that

Table 1. Compounds 2–9 Inhibit PI3K δ in Biochemical and Cellular Assays

compd	pIC ₅₀ ^a				hWB IFN γ pIC ₅₀ ^b
	δ	α	β	γ	
1	9.1	6.3	6.2	6.3	8.5
2	9.2 ^c	8.2 ^c	7.2 ^c	5.8 ^c	N.T.
3	8.3	5.6	5.1	4.6	8.1
4	8.1	5.5	5.3	4.8	7.9
5	8.2	5.6	5.4	4.9	7.9
6	7.3	4.8	4.9	5.0	7.4
7	6.4	5.1	4.8	5.0	6.9
8	7.4	5.0	<4.5	<4.5	7.0
9	7.9	4.9	4.7	4.8	5.0
10 wortmannin	8.3	8.1	8.0	8.2	6.7
11 Zydelig	8.1	5.0	5.8	6.6	6.7

^aBiochemical pIC₅₀ data for all inhibitors at all four PI3K isoforms (measured after 1 h at K_M(ATP) using HTRF assays). ^bPhenotypic hWB pIC₅₀ derived from measuring levels of IFN γ after stimulation with CytoStim (20 h incubation, free compound concentrations are not available). Data for pan-covalent PI3K inhibitor wortmannin **10**, and FDA approved PI3K δ selective, reversible inhibitor Zydelig **11** derived from these assays are also shown. ^cCompound found to be particularly unstable in DMSO, results reported from N = 2 only. N.T.: Compound not tested due to instability of the DMSO 10 mM stock solution. All compounds were tested a minimum of three times in HTRF and hWB assays, with the exception of compounds **2**, **8** and **9** (Table S1).

covalent inhibition is a time-dependent process, and the pIC₅₀ values would be expected to vary with time. The biochemical assays were read-out at 1 h in all cases, and the hWB assay at 20 h to provide consistency for data analysis.

Protein Mass Spectrometry and Reactivity Assessments Indicated the Potential for Site-Specific Nucleophilic Trapping by a Lysine Residue. After 5 min incubation of recombinant PI3K δ with **4** (2:1 molar ratio of **4**:PI3K δ), we observed formation of a single adduct by intact protein liquid chromatography–mass spectrometry (LCMS). Compared to untreated protein, this mass shift was consistent with the addition of **4**, and loss of 4-fluorophenol. Repeating this assay with 10 mol equiv of **4**, and 20 h incubation showed no additional adduct formation. Pre-incubation of PI3K δ with 10 equiv of the potent ATP-competitive reversible inhibitor²³ **12** prevented formation of the covalent adduct, suggesting covalent modification occurred in the ATP binding site. Carboxylic acid **9** showed no evidence of covalent bond formation in this experiment, implying that the phenolic ester was required for the covalent reaction. These results suggested that **4** was covalently, and specifically, binding to the ATP binding site of PI3K δ (Figure 2a).

Reactivity analysis showed that **4** was stable to hydrolysis and reaction with *N*-Boc lysine under physiological conditions (phosphate buffer, pH 7.4, 37 °C), but upon deprotonation of the lysine smooth amide bond formation was observed (Figures S2 and S3). Together with the mass spectrometry data

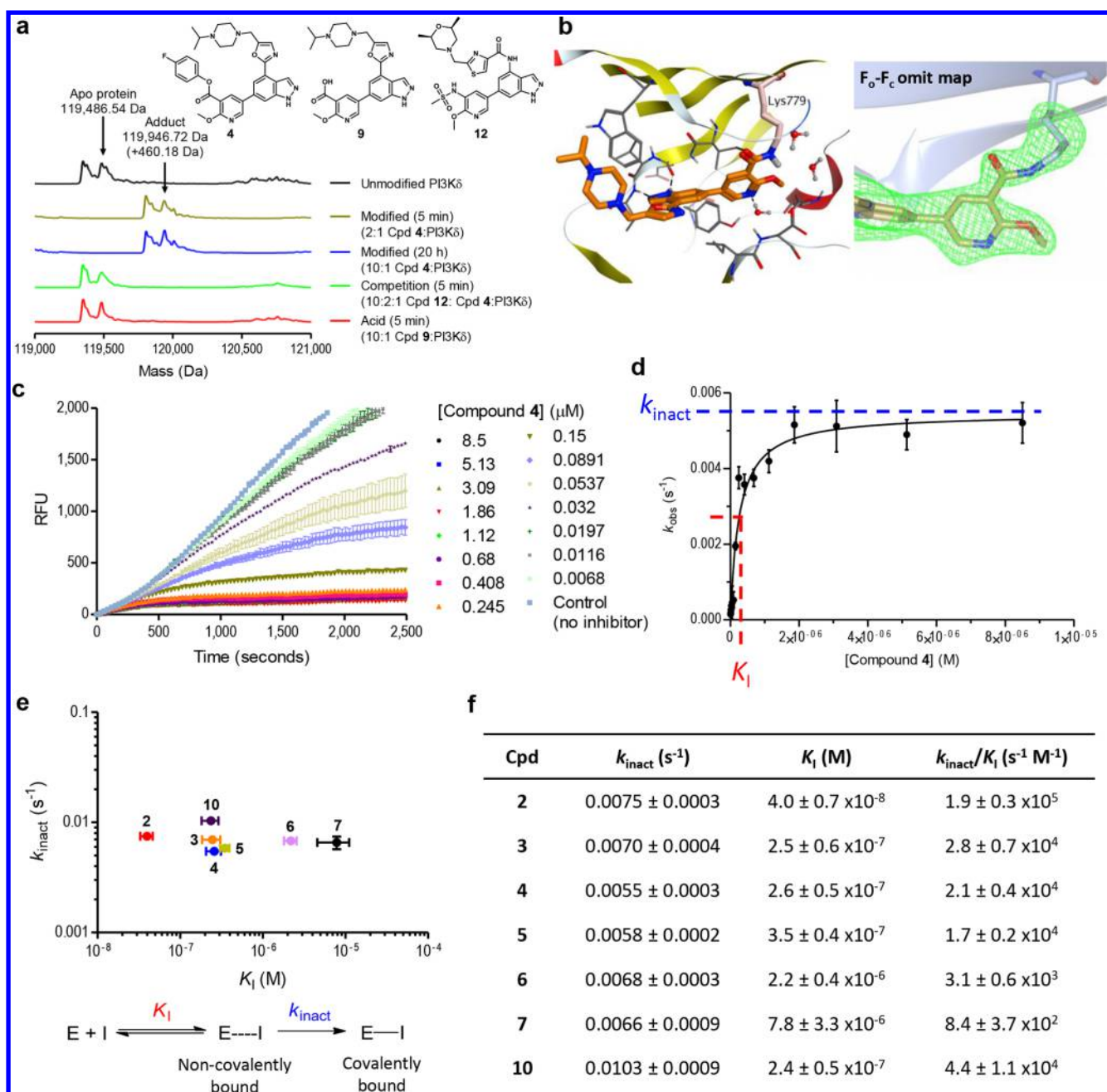


Figure 2. Compounds 2–7 covalently inactivate PI3K δ by amide bond formation to Lys779, with potency dependent on reversible recognition. (a) Protein mass spectrometry. Top to bottom: apo protein; protein treated with 2 equiv of 4, analyzed at 5 min; protein treated with 10 equiv of 4 overnight; protein pretreated with 10 equiv of 12 for 15 min, prior to addition of 2 equiv of 4, and analyzed at 5 min; protein incubated with 10 equiv of 9 and analyzed at 5 min. (b) Left: Crystal structure of 4 after overnight soaking with PI3K δ crystals (PDB: 6EYZ). Right: $F_0 - F_c$ omit map is shown in green at 2.7 rmsd, with Lys799 side-chain and ligand coordinates removed, showing clear electron density from Lys779 onto the ligand. (c) Raw time-course data for 4. Concentrations are shown after correction for absolute stock concentration using quantitative NMR (Table S5). (d) Plot of derived k_{obs} from (b) vs concentration of inhibitor to derive K_I and k_{inact} . (e) Plot of derived k_{inact} vs K_I for all 6 esters, and wortmannin.^{4,46} (f) Table of k_{inact} , K_I , and k_{inact}/K_I values. Kinetic measurements were performed in triplicate, and data are shown as the mean \pm s.e.m.

suggesting that a single, specific modification occurred in the active site of PI3K δ , we proposed that this bond could be forming with the conserved lysine.

Confirmation of Lys779 as the Nucleophilic Residue.

After overnight soaking of pre-grown murine PI3K δ crystals^{20,23} with 4, we observed a covalently bound adduct between the inhibitor and the targeted lysine residue (Figure 2b) by X-ray crystallography. Continuous electron density was seen between Lys779 and the carbonyl of the ester, and there was no evidence

for the phenolic group being present, consistent with formation of an amide bond. Methyl ester 8 showed a reversibly bound adduct (Figure S4), consistent with the reduced reactivity of this ester (Figure S2). The remainder of the compound satisfied the desired hydrogen bonding interactions between the indazole and hinge residues Val828 and Glu826, as well as occupying the selectivity region next to Trp760 with the basic amine.^{23,44}

Time-Course Experiments To Determine k_{inact} and K_I . Using the commercially available ADP Quest assay kit⁴⁵ we

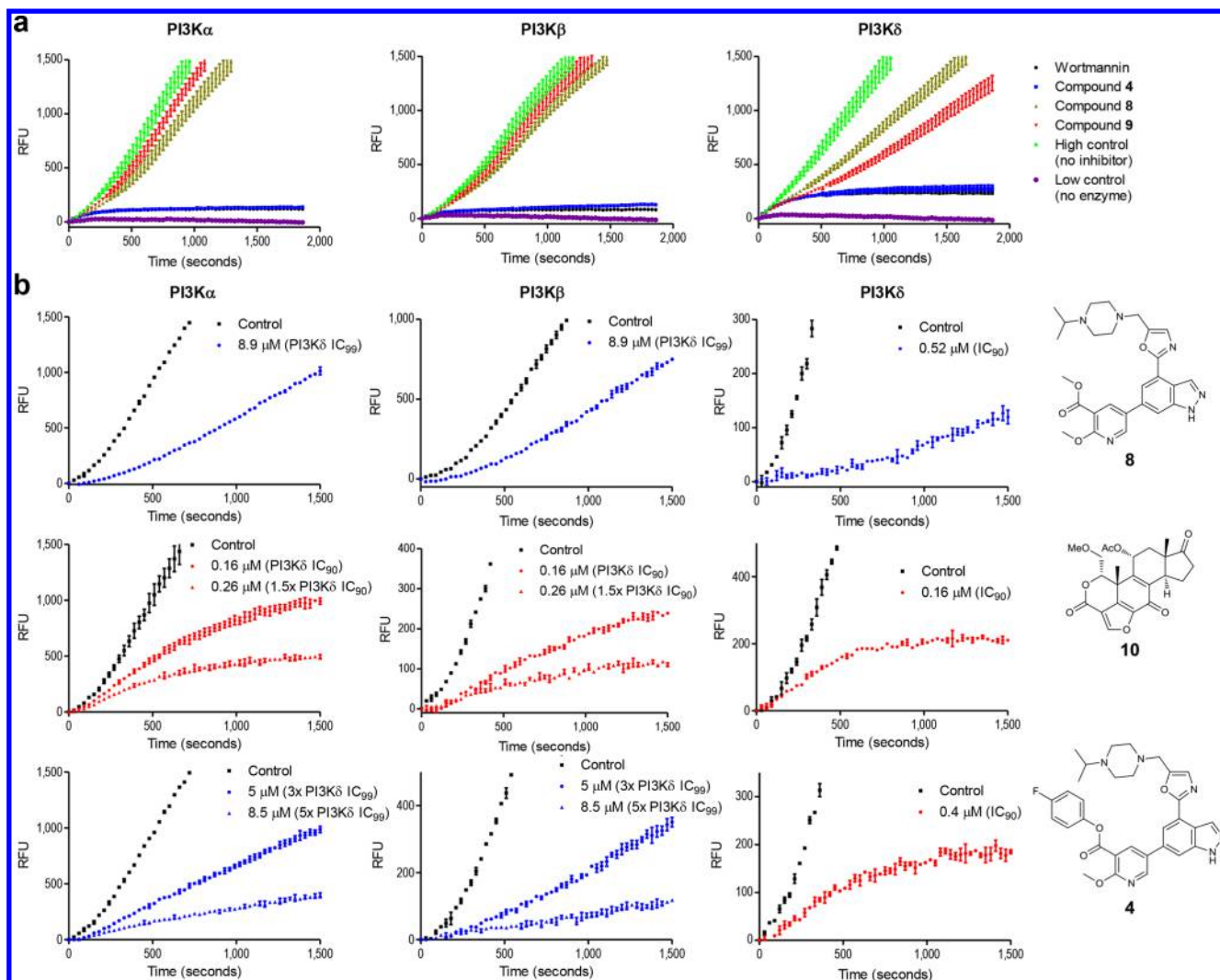


Figure 3. 4 does not covalently inhibit PI3K α and β up to 5x PI3K δ IC₉₉ with cellular concentrations of ATP. (a) Jump dilutions conducted at PI3K α (left), PI3K β (middle) and PI3K δ (right) in the absence of competing ATP. Covalent inactivation of all three kinases was observed under these conditions by 4. Inhibitor assays were conducted in triplicate and controls in duplicate. Results are plotted as mean \pm s.e.m. (b) Kinetic plots of the inhibition over time under saturating ATP conditions (1 mM). Linear plots (blue) relative to no-inhibitor controls (black) are typical of reversible inhibitors. Nonlinear plots (red) relative to no-inhibitor controls (black) are typical of slow-binding inhibitors (confirmed to be irreversible by jump dilution experiments in (a)). The top row depicts reversible ester 8, showing linear progress at IC₉₀ at PI3K δ , and at PI3K α and β at the PI3K δ IC₉₉. Middle row depicts irreversible inactivation of all three kinases by wortmannin at IC₉₀ for PI3K δ (1.5x PI3K δ IC₉₀ curves are also shown). Bottom row shows selective ester 4, exhibiting covalent inhibition at PI3K δ at IC₉₀, and reversible inhibition at PI3K α and β at 3x and 5x PI3K δ IC₉₉. Assays were conducted in duplicate, and results are shown as mean \pm s.e.m.

derived the concentration of inhibitor required for half of the maximum rate of covalent bond formation (K_I), the rate constant for irreversible inactivation (k_{inact}) and the second order rate constant typically used to characterize irreversible inhibitors (k_{inact}/K_I) (Figure 2f).^{4,46–48} Full analyses for esters 2–7 and 10, including equations used, are detailed in the Supporting Information.

All six esters exhibited non-linear reaction progress curves (Figure 2c and Figure S7) indicating time-dependent inhibition of PI3K δ , consistent with covalent inactivation. The k_{inact}/K_I ranking obtained from the replot method correlated well with the potencies obtained from the PI3K δ biochemical and hWB assays (Table 1 and Figure S7). The kinetic data were visualized by plotting k_{inact} as a function of K_I , as described by Schwartz et al. (Figure 2e).⁴⁹ This representation clearly showed that similar k_{inact} values were found for all six esters (1.4-fold difference across the series), but K_I differences spanned 2 orders of

magnitude, from 40 nM (compound 2) to 7.8 μ M (compound 6) (195-fold difference, Figure 2f). This indicated that the electronic nature of the phenolate leaving group (i.e., pK_a value), and therefore expected chemical reactivity/leaving group ability, does not correlate with the rate of the covalent inactivation in this system. Rather, there is a correlation with K_I , suggesting a more complex mechanism than the traditional two-step scheme depicted in Figure 2e. The differences in pIC₅₀ between the esters in our biochemical assay must therefore be dictated by reversible interactions in formation of the initial enzyme–inhibitor complex and not the rate of the covalent reaction. We have proposed a reaction mechanism supporting these data, invoking additional steps to explain the dependence of K_I on pK_a (supplementary discussion and Scheme S1). Finally, our prior analysis of the chemical reactivity of 4 (Figures S2 and S3) showed it to be inert to nucleophilic substitution under physiological conditions. This suggested that the elevated

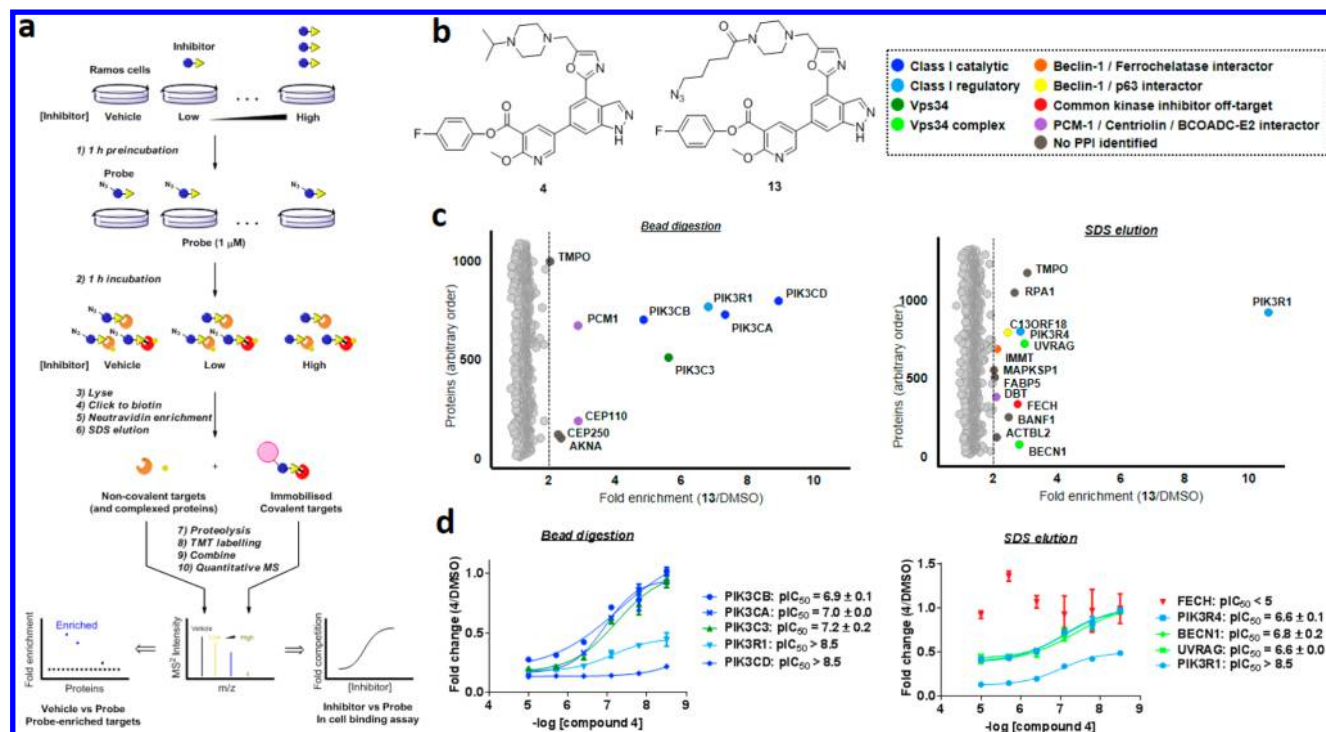


Figure 4. Chemoproteomic analysis identifies targets of 4 in human cells. (a) General assay design. (b) Structures of 4 and 13, and key for graphs below. (c) The scatter plots display proteins enriched with neutravidin beads after clicking a biotin moiety to proteins labeled *in situ* with probe 13 (1 μM) relative to vehicle control. Proteins were accessed by enzymatic bead digestion or SDS elution from the bead. The dotted lines represent 2-fold enrichment (13/DMSO) and proteins with >2-fold enrichment are deemed specific targets of 13, and are labeled by their entrez gene ID. (d) Dose–response curves for competition of 13 binding to specifically enriched targets after pretreatment of cells for 1 h with 4. Binding curves and resulting pIC_{50} values are shown for proteins enriched >2-fold. With the exception of FECH, values are not plotted if no binding curve could be fitted using GraphPad Prism 7.03. The values represented are the average \pm s.e.m. from two biological replicates. In (c) and (d), data were filtered with the criteria that quantified unique peptide matches >1 and quantified unique peptide to spectra matches >2. Proteins were required to be identified and quantified in both replicates to be included in the analysis, and data are plotted as the mean of the TMT label ratios (MS^2) per protein.

reactivity observed in these kinetic analyses was occurring specifically in the protein, and that the local microenvironment around Lys779 may be contributing to an increased reactivity of this residue, rendering it hyper-reactive.^{16,37,50,51}

Selectivity, Despite the Conserved Lysine, Is Driven by Reversible Interactions. To assess off-target covalent binding, jump dilution and kinetic measurements at two closely related PI3K isoforms (α and β) were carried out with 4. All three enzymes were inactivated in the jump dilution experiment without competing ATP indicating that 4 could covalently inhibit PI3K α , β and δ at high pre-incubation concentrations (Table S3), without a competing ligand (Figure 3a). As controls, the experiment was performed with covalent pan-PI3K inhibitor 10, and reversibly bound ester analogues 8 and 9. 10 showed covalent inactivation of all three kinases, whereas 8 and 9 showed the expected regeneration of enzyme activity after dilution, consistent with a reversible mode of inhibition (Figure 3a and Table S4).

However, in the kinetic analysis with competing ATP (1 mM), linear reaction progressions were observed at PI3K α and β at all tested concentrations (Table S6). The gradient of these plots decreased with increasing concentration of inhibitor, consistent with a rapid onset of inhibition. The absence of the slow-binding nonlinear phase we had observed at PI3K δ suggested no covalent binding was occurring at these kinases under these conditions. Indeed, for ester 4, the kinetics at PI3K δ reflected 10, while the kinetics at PI3K α and β reflected the

reversibly bound methyl ester 8 (Figure 3b). This absence of apparent covalent adduct formation at PI3K α and β was seen up to 8.5 μM of 4, ~ 5 times the PI3K δ IC_{99} ($= 1.59 \mu\text{M}$) under these conditions. Reprocessing the raw data along the time axis allowed derivation of IC_{50} values every 30 s over this time window. These plots showed a time-dependent decrease in IC_{50} at PI3K δ , but not at PI3K α and β for 4 (Figure S8), supporting selective covalent inhibition in this assay. 4 also exhibited excellent selectivity against a panel of 10 lipid kinases and 140 protein kinases (Tables S7 and S8).

These kinetic and jump dilution analyses revealed a concentration window where 4 covalently inactivated PI3K δ , but not highly homologous isoforms of the same family, despite the conserved nature of the nucleophilic amino acid. Upon saturating the ATP binding site with high concentrations of inhibitor, in the absence of competing ATP, covalent inactivation does occur. However, in a cell-like environment, covalent inactivation of PI3K α and β is unlikely to occur up to 5 \times the PI3K δ IC_{99} . Consistent with our earlier observation that potency differences between the esters at PI3K δ was governed by reversible interactions, this selectivity must also arise from differences in the initial reversible binding interactions (K_i) with these kinases.

Chemoproteomics Revealed 4 To Be Selective for PI3K δ in Live Cells. Azido probe 13 was synthesized, and retained potency at PI3K δ in the biochemical HTRF assay ($\text{pIC}_{50} = 7.6$). At 1 μM , it was shown to covalently modify a

protein with a molecular weight consistent with PI3K δ in THP-1 monocyte lysates by in-gel fluorescence after strain-promoted azide–alkyne cycloaddition click reaction (SPAAC) with dibenzocyclooctyne-conjugated-Cy5 dye (DBCO-Cy5), and SDS-PAGE separation. Co-elution of PI3K δ with the Cy5 signal was confirmed by immunostaining with p110 δ antibody after transfer to PVDF membranes (Figure S9).⁵² Furthermore, the Cy5 fluorescence signal was gradually ablated in the presence of increasing concentrations of **4**, with a pIC₅₀ of 7.5, suggesting potent engagement of PI3K δ by **4** in complex cell lysates.

Protein targets of probe **13** in Ramos cells were then identified by a quantitative mass spectrometry-based chemoproteomics method using tandem mass tag (TMT) labeling (Figure 4a), based on related experiments by Lanning et al.⁵³ and Niessen et al.⁵⁴ Cells were treated with either vehicle or **13** at 1 μ M for 1 h, lysed, and proteins bound by **13** were enriched with neutravidin beads after SPAAC reaction with a DBCO–biotin conjugate. Non-covalently bound proteins were expected to be predominantly eluted with SDS, whereas covalent targets should only be detected after on-bead proteolysis.

Comparison to vehicle-treated cells identified 22 out of ~1000 identified proteins that were specifically enriched >2-fold by *in situ* treatment with **13** (Figure 4c and supplementary data set). Of those 22 proteins, eight were exclusively identified after direct proteolysis, including the class I catalytic subunits of PI3K δ (gene ID PIK3CD), PI3K α (gene ID PIK3CA), PI3K β (gene ID PIK3CB), and the class III PI3K protein Vps34 (gene ID PIK3C3), suggesting these proteins as covalent targets of **13**. In contrast, the Vps34 regulatory subunits⁵⁵ PI3K regulatory subunit 4 (gene ID PIK3R4), Beclin-1 (gene ID BECN1), p63 (gene ID UVRAG), mitofilin (gene ID IMMT), and protein RUBCNL-like (gene ID C13ORF18) as well as the common kinase inhibitor off-target ferrochelatase⁵⁶ (gene ID FECH), were only found in the SDS eluates. The possibility to elute those proteins from the capturing matrix with SDS buffer implicates those proteins as reversible binders of **13**, or proteins in complexes with enriched targets. The PI3K regulatory subunit α (gene ID PIK3R1) was identified in the bead digest fraction as well as in the SDS eluates. Signal abundances of detected tryptic peptides (MS¹ intensities) indicated a 3- to 4-fold higher abundance in the SDS fraction than in the bead digests. This suggests major, but incomplete, elution of this known interactor of class I catalytic PI3K subunits²⁶ with the applied conditions.

To accurately assess off-target interactions of **4**, we derived dose–response curves from competing the binding to **13** by pretreatment with concentrations of **4** ranging from 10 μ M to 3.2 nM for 1 h (Figure 4d). For the specifically enriched proteins exclusively found in the bead digests, we calculated pIC₅₀ values for PI3K δ , PI3K α , PI3K β , and Vps34 to be >8.5, 7.0, 6.9, and 7.2, respectively. This indicates that irreversible binding of PI3K δ to **13** can be competed by **4** with >20-fold selectivity at the used incubation conditions. For the proteins identified exclusively in the SDS fraction, we determined reasonable binding curves for Beclin-1, p63, and PI3K regulatory subunit 4. All resulted in very similar pIC₅₀ values (pIC_{50,BECN1} = 6.8; pIC_{50,UVRAG} = 6.6; pIC_{50,PIK3R4} = 6.6). Binding curves were incomplete for those proteins (maximal competition by 10 μ M compound ca. 50%), suggesting they were interacting with a known complex partner,⁵⁵ rather than being true targets of the compound. A similar effect might be observed for PI3K regulatory subunit α for which a pIC₅₀ value >8.5 was determined. As a complex partner of PI3K α , PI3K β , and PI3K δ ,²⁶ the determined apparent dose-dependent competition

may result from a combination of competitive binding to any of these PI3K proteins. Within the tested concentration range, mitofilin, ferrochelatase, and protein RUBCNL-like, (as well as the remaining proteins that were specifically enriched with **13**) did not show strong competition of binding by **4**, suggesting low affinity binding.

These chemoproteomic data support minimal off-target binding by **4** in human cells. Coupled with our selectivity hypothesis and kinase panel investigations above (Figure 3 and Tables S7 and S8), we propose **4** to be a highly selective irreversible inhibitor of PI3K δ at concentrations below 1 μ M.

Cellular Washout Studies Suggest an Extended Duration of Action. CD4+ T cells were incubated with **4** or **12** (hWB pIC₅₀ = 7.9) for 2 h, then washed and incubated for a further 48 h before stimulation with α CD3 and measurement of IFN γ release. **4** showed sustained depletion of IFN γ secretion 48 h after washout, without cytotoxic effects (Figure S10), whereas regeneration of IFN γ secretion was observed for **12** (Figure 5).

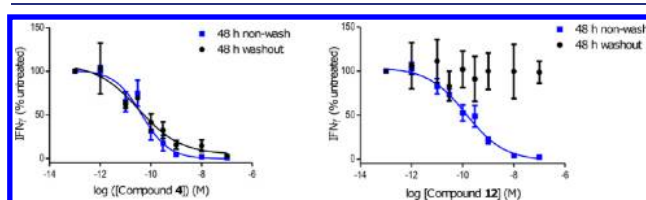


Figure 5. Inhibitor **4** showed a prolonged duration of action, up to at least 48 h in CD4+ T cells. Cellular washout studies conducted in CD4+ T cells isolated from hWB. Cells were treated with inhibitors for 2 h, washed, and stimulated with α CD3 to induce IFN γ release, measured after 48 h. Left: Covalent compound **4** showed a clear sustained duration of action (black circles) 48 h after washing. Right: Reversible compound **12** showed a clear disruption of the inhibition profile (black circles) 48 h after washing. The experiment was repeated using 5 donors (for each donor: $N = 3$ replicates for washout, and $N = 2$ replicates for non-wash condition), and results are depicted as mean \pm s.e.m. Non-washed curves showing the dose–response after 48 h are shown in blue.

These results, taken together with the data presented above, suggest that inhibition of PI3K δ could be sustained for at least 48 h using an irreversible targeting approach, with no cytotoxic effect. It is worth noting, however, that cellular accumulation of dibasic piperazines could also be a contributing factor to the duration of action for this series of compounds.^{57,58}

CONCLUSION

Selective covalent inhibition relies on a two step process of reversible binding and then covalent inactivation.^{4,5} Here, we have demonstrated that selectivity in formation of the initial enzyme–inhibitor complex is the crucial factor for achieving potent, selective covalent inhibition of conserved residues. Kinetic studies indicated that the electronics, and expected chemical reactivities, of the electrophilic esters did not affect the rate of covalent bond formation with the enzyme, k_{inact} . The observed variation in potency of the esters at PI3K δ (Table 1) therefore arose from the reversible binding steps of the inhibitors, due to electronic changes in the phenolic group, reflected by K_i . Furthermore, through kinetic studies at PI3K α , β , and δ we determined that there was a reasonable concentration range at which covalent inhibition of PI3K δ could be achieved, without covalent inactivation of related enzymes. This was confirmed by chemoproteomic studies with **13** *in situ* which suggested minimal off-target binding of **4**, and a

>20-fold selectivity window for covalent modification of PI3K δ , despite conservation of the targeted lysine residue and presence of other reactive moieties.

As a more general approach, variation of the electrophilic center to affect reversible binding could be exploited for fine-tuning of the potency, selectivity, and physicochemical properties of inhibitors for irreversible drug discovery programmes. By maintaining a constant k_{inact} across a series of electrophilic esters, this provides an orthogonal approach to established EGFR and Janus Kinase (JAK) inhibitors that vary the k_{inact} to improve the drug profile.^{8,59} Furthermore, a common method for enzymes to develop resistance to covalent inhibitors targeting poorly conserved cysteines is by point mutation of the modified residue.⁶⁰ A similar resistance mechanism would not be applicable to the strategy we have developed, as mutation of the catalytic lysine would render the kinase inactive.⁶¹ Finally, the potential lability of these esters could impart kinetic selectivity *in vivo*. Zaro et al. recently described how the proteome-wide selectivity of ibrutinib improved when a fumarate ester was incorporated into the covalent warhead. They attributed this to hydrolysis of the metabolically labile ester, affording an inert 1,4-unsaturated carboxylate.⁶² Carboxylic acid **9** formed in our case is poorly active in the cellular assay ($\text{pIC}_{50} = 5.0$, Table 1), and inert to covalent bond formation by mass-spectrometry (Figure 2a), suggesting a similar mechanism could be observed here.

By modification of a known reversible inhibitor,²³ we have developed a series of esters which selectively and covalently inhibit PI3K δ . In addition to the excellent selectivity profile, our lead compound **4** showed ~ 10 nM activity in the hWB phenotypic inflammatory cytokine response assay, and extended duration of action (>48 h), in cellular washout studies. Owing to the importance of PI3K δ as a target for inflammation and oncology, this selective, covalent PI3K δ inhibitor could have applications in the development of long-acting therapeutics.

Prior studies have shown that the targeted conserved lysine reacts covalently with promiscuous probes possessing reactive warheads.^{38–41} We therefore envisage that this approach could be orthogonal to non-conserved cysteine targeting, and applicable across the kinome. By this method, researchers may be able to generate selective covalent chemical probes of any chosen kinase, which could provide tools to vastly improve the understanding of human biology in diseased states.

■ ASSOCIATED CONTENT

Supporting Information

The Supporting Information is available free of charge on the ACS Publications website at DOI: 10.1021/jacs.7b08979.

Biological methods, synthetic methods and characterization, supplementary Figures S1–S10, Tables S1–S8, and Schemes S1–S3, mass spectrometry tables, and additional discussions (PDF)

Supplementary data set (XLSX)

■ AUTHOR INFORMATION

Corresponding Author

*sebastien.x.campos@gsk.com

ORCID

Marcus Bantscheff: 0000-0002-8343-8977

John A. Murphy: 0000-0003-3136-0845

Sebastien Campos: 0000-0003-1717-5918

Notes

The authors declare no competing financial interest.

■ ACKNOWLEDGMENTS

We thank the GlaxoSmithKline/University of Strathclyde Industrial PhD programme for funding this work. We also thank D. House for providing revisions of the manuscript, J.N. Hamblin and V. Patel for intellectual discussions, and N. Barton, C. Chitty, P. Francis, L. Gordon, N. Hodnett, S. Kumper, S.M. Lynn, J.E. Rowedder, E. Sherriff and H. Taylor for technical assistance and discussion.

■ REFERENCES

- (1) Kim, E. S.; Dhillon, S. *Drugs* **2015**, *75*, 769–776.
- (2) Hossam, M.; Lasheen, D. S.; Abouzid, K. A. M. *Arch. Pharm.* **2016**, *349*, 573–593.
- (3) Bradshaw, J. M.; McFarland, J. M.; Paavilainen, V. O.; Bisconte, A.; Tam, D.; Phan, V. T.; Romanov, S.; Finkle, D.; Shu, J.; Patel, V.; Ton, T.; Li, X.; Loughhead, D. G.; Nunn, P. A.; Karr, D. E.; Gerritsen, M. E.; Funk, J. O.; Owens, T. D.; Verner, E.; Brameld, K. A.; Hill, R. J.; Goldstein, D. M.; Taunton, J. *Nat. Chem. Biol.* **2015**, *11*, 525–531.
- (4) Singh, J.; Petter, R. C.; Baillie, T. A.; Whitty, A. *Nat. Rev. Drug Discovery* **2011**, *10*, 307–317.
- (5) Baillie, T. A. *Angew. Chem., Int. Ed.* **2016**, *55*, 13408–13421.
- (6) Liu, Q.; Sabnis, Y.; Zhao, Z.; Zhang, T.; Buhrlage, S. J.; Jones, L. H.; Gray, N. S. *Chem. Biol.* **2013**, *20*, 146–159.
- (7) Mah, R.; Thomas, J. R.; Shafer, C. M. *Bioorg. Med. Chem. Lett.* **2014**, *24*, 33–39.
- (8) Nacht, M.; Qiao, L.; Sheets, M. P.; St. Martin, T.; Labenski, M.; Mazdiyasi, H.; Karp, R.; Zhu, Z.; Chaturvedi, P.; Bhavsar, D.; Niu, D.; Westlin, W.; Petter, R. C.; Medikonda, A. P.; Singh, J. *J. Med. Chem.* **2013**, *56*, 712–721.
- (9) Zhang, J.; Yang, P. L.; Gray, N. S. *Nat. Rev. Cancer* **2009**, *9*, 28–39.
- (10) Leproult, E.; Barluenga, S.; Moras, D.; Wurtz, J.-M.; Winsinger, N. *J. Med. Chem.* **2011**, *54*, 1347–1355.
- (11) Zhao, Z.; Liu, Q.; Bliven, S.; Xie, L.; Bourne, P. E. *J. Med. Chem.* **2017**, *60*, 2879–2889.
- (12) Carrera, A. C.; Alexandrov, K.; Roberts, T. M. *Proc. Natl. Acad. Sci. U. S. A.* **1993**, *90*, 442–446.
- (13) Dahal, U.; Gilbert, A.; Obach, R.; Chen, J.; Garcia-Irizarry, C.; Schuff, B.; Starr, J.; Uccello, D.; Young, J.; Flanagan, M. E. *MedChemComm* **2016**, *7*, 864–872.
- (14) Akçay, G.; Belmonte, M. A.; Aquila, B.; Chuaqui, C.; Hird, A. W.; Lamb, M. L.; Rawlins, P. B.; Su, N.; Tentarelli, S.; Grimster, N. P.; Su, Q. *Nat. Chem. Biol.* **2016**, *12*, 931–936.
- (15) Ancombe, E.; Meschini, E.; Mora-vidal, R.; Stephen, R.; Endicott, J. A.; Griffin, R. J. *Chem. Biol.* **2015**, *22*, 1159–1164.
- (16) Hacker, S. M.; Backus, K. M.; Lazear, M. R.; Forli, S.; Correia, B. E.; Cravatt, B. F. *Nat. Chem.* **2017**, *9*, 1181–1190.
- (17) Pettinger, J.; Jones, K.; Cheeseman, M. D. *Angew. Chem., Int. Ed.* **2017**, *56*, 15200–15209.
- (18) Pettinger, J.; Le Bihan, Y.-V.; Widya, M.; van Montfort, R. L. M.; Jones, K.; Cheeseman, M. D. *Angew. Chem., Int. Ed.* **2017**, *56*, 3536–3540.
- (19) Cantley, L. L. *C. Science* **2002**, *296*, 1655–1657.
- (20) Berndt, A.; Miller, S.; Williams, O.; Le, D. D.; Houseman, B. T.; Pacold, J. I.; Gorrec, F.; Hon, W.-C.; Liu, Y.; Rommel, C.; Gaillard, P.; Rückle, T.; Schwarz, M. K.; Shokat, K. M.; Shaw, J. P.; Williams, R. L. *Nat. Chem. Biol.* **2010**, *6*, 117–124.
- (21) Stark, A.-K.; Sriskantharajah, S.; Hessel, E. M.; Okkenhaug, K. *Curr. Opin. Pharmacol.* **2015**, *23*, 82–91.
- (22) Fruman, D. A.; Chiu, H.; Hopkins, B. D.; Bagrodia, S.; Cantley, L. C.; Abraham, R. T. *Cell* **2017**, *170*, 605–635.
- (23) Down, K.; Amour, A.; Baldwin, I. R.; Cooper, A. W. J.; Deakin, A. M.; Felton, L. M.; Guntrip, S. B.; Hardy, C.; Harrison, Z. A.; Jones, K. L.; Jones, P.; Keeling, S. E.; Le, J.; Livia, S.; Lucas, F.; Lunniss, C. J.; Parr, N. J.; Robinson, E.; Rowland, P.; Smith, S.; Thomas, D. A.; Vitulli, G.; Washio, Y.; Hamblin, J. N. *J. Med. Chem.* **2015**, *58*, 7381–7399.

- (24) Somoza, J. R.; Koditek, D.; Villaseñor, A. G.; Novikov, N.; Wong, M. H.; Liclican, A.; Xing, W.; Laggapan, L.; Wang, R.; Schultz, B. E.; Papalia, G. A.; Samuel, D.; Lad, L.; McGrath, M. E. *J. Biol. Chem.* **2015**, *290*, 8439–8446.
- (25) Liu, P.; Cheng, H.; Roberts, T. M.; Zhao, J. J. *Nat. Rev. Drug Discovery* **2009**, *8*, 627–644.
- (26) Vanhaesebroeck, B.; Whitehead, M. A.; Piñeiro, R. *J. Mol. Med.* **2016**, *94*, 5–11.
- (27) Rowan, W. C.; Smith, J. L.; Affleck, K.; Amour, A. *Biochem. Soc. Trans.* **2012**, *40*, 240–245.
- (28) Rommel, C.; Camps, M.; Ji, H. *Nat. Rev. Immunol.* **2007**, *7*, 191–201.
- (29) Koyasu, S. *Nat. Immunol.* **2003**, *4*, 313–319.
- (30) Ghigo, A.; Damilano, F.; Braccini, L.; Hirsch, E. *BioEssays* **2010**, *32*, 185–196.
- (31) Okkenhaug, K.; Bilancio, A.; Farjot, G.; Priddle, H.; Sancho, S.; Peskett, E.; Pearce, W.; Meek, S. E.; Salpekar, A.; Waterfield, M. D.; Smith, A. J. H.; Vanhaesebroeck, B. *Science* **2002**, *297*, 1031–1034.
- (32) Puri, K. D.; Doggett, T. A.; Douangpanya, J.; Hou, Y.; Tino, W. T.; Wilson, T.; Graf, T.; Clayton, E.; Turner, M.; Hayflick, J. S.; Diacovo, T. G. *Blood* **2004**, *103*, 3448–3456.
- (33) Norman, B. H.; Shih, C.; Toth, J. E.; Ray, J. E.; Dodge, J. a.; Johnson, D. W.; Rutherford, P. G.; Schultz, R. M.; Worzalla, J. F.; Vlahos, C. J. *J. Med. Chem.* **1996**, *39*, 1106–1111.
- (34) Waterfield, M. D.; Panayotou, G.; Wymann, M. P.; Bulgarelli-Leva, G.; Zvelebil, M. J.; Pirola, L.; Vanhaesebroeck, B. *Mol. Cell. Biol.* **1996**, *16*, 1722–1733.
- (35) Hong, D. S.; Bowles, D. W.; Falchook, G. S.; Messersmith, W. A.; George, G. C.; O'Bryant, C. L.; Vo, A. C. H.; Klucher, K.; Herbst, R. S.; Eckhardt, S. G.; Peterson, S.; Hausman, D. F.; Kurzrock, R.; Jimeno, A. *Clin. Cancer Res.* **2012**, *18*, 4173–4182.
- (36) Walker, E. H.; Pacold, M. E.; Perisic, O.; Stephens, L.; Hawkins, P. T.; Wymann, M. P.; Williams, R. L. *Mol. Cell* **2000**, *6*, 909–919.
- (37) Miller, R. M.; Taunton, J. *Methods Enzymol.* **2014**, *548*, 93–116.
- (38) Patricelli, M. P.; Nomanbhoy, T. K.; Wu, J.; Brown, H.; Zhou, D.; Zhang, J.; Jagannathan, S.; Aban, A.; Okerberg, E.; Herring, C.; Nordin, B.; Weissig, H.; Yang, Q.; Lee, J. D.; Gray, N. S.; Kozarich, J. W. *Chem. Biol.* **2011**, *18*, 699–710.
- (39) Cravatt, B. F.; Wright, A. T.; Kozarich, J. W. *Annu. Rev. Biochem.* **2008**, *77*, 383–414.
- (40) Zhao, Q.; Ouyang, X.; Wan, X.; Gajiwala, K. S.; Kath, J. C.; Jones, L. H.; Burlingame, A. L.; Taunton, J. *J. Am. Chem. Soc.* **2017**, *139*, 680–685.
- (41) Patricelli, M. P.; Szardenings, A. K.; Liyanage, M.; Nomanbhoy, T. K.; Wu, M.; Weissig, H.; Aban, A.; Chun, D.; Tanner, S.; Kozarich, J. W. *Biochemistry* **2007**, *46*, 350–358.
- (42) Choi, S.; Connelly, S.; Reixach, N.; Wilson, I. A.; Kelly, J. W. *Nat. Chem. Biol.* **2010**, *6*, 133–139.
- (43) Hansch, C.; Leo, A.; Taft, R. W. *Chem. Rev.* **1991**, *91*, 165–195.
- (44) Sutherlin, D. P.; Baker, S.; Bisconte, A.; Blaney, P. M.; Brown, A.; Chan, B. K.; Chantry, D.; Castanedo, G.; Depledge, P.; Goldsmith, P.; Goldstein, D. M.; Hancox, T.; Kaur, J.; Knowles, D.; Kondru, R.; Lesnick, J.; Lucas, M. C.; Lewis, C.; Murray, J.; Nadin, A. J.; Nonomiya, J.; Pang, J.; Pegg, N.; Price, S.; Reif, K.; Safina, B. S.; Salphati, L.; Staben, S.; Seward, E. M.; Shuttleworth, S.; Sohal, S.; Sweeney, Z. K.; Ultsch, M.; Waszkowycz, B.; Wei, B. *Bioorg. Med. Chem. Lett.* **2012**, *22*, 4296–4302.
- (45) Charter, N. W.; Kauffman, L.; Singh, R. A. J.; Eglen, R. M. *J. Biomol. Screening* **2006**, *11*, 390–399.
- (46) Copeland, R. A. *Enzymes: A Practical Introduction to Structure, Mechanism and Data Analysis*; Wiley: New York, 2000; Chap. 10.
- (47) Kitz, R.; Wilson, B. *J. Biol. Chem.* **1962**, *237*, 3245–3249.
- (48) Strelow, J. M. *SLAS Discovery* **2017**, *22*, 3–20.
- (49) Schwartz, P. A.; Kuzmic, P.; Solowiej, J.; Bergqvist, S.; Bolanos, B.; Almaden, C.; Nagata, A.; Ryan, K.; Feng, J.; Dalvie, D.; Kath, J. C.; Xu, M.; Wani, R.; Murray, B. W. *Proc. Natl. Acad. Sci. U. S. A.* **2014**, *111*, 173–178.
- (50) Weerapana, E.; Wang, C.; Simon, G. M.; Richter, F.; Khare, S.; Dillon, M. B. D.; Bachovchin, D. A.; Mowen, K.; Baker, D.; Cravatt, B. F. *Nature* **2010**, *468*, 790–795.
- (51) Backus, K. M.; Correia, B. E.; Lum, K. M.; Forli, S.; Horning, B. D.; González-Páez, G. E.; Chatterjee, S.; Lanning, B. R.; Teijaro, J. R.; Olson, A. J.; Wolan, D. W.; Cravatt, B. F. *Nature* **2016**, *534*, 570–574.
- (52) Rutkowska, A.; Thomson, D. W.; Vappiani, J.; Werner, T.; Mueller, K. M.; Dittus, L.; Krause, J.; Muelbaier, M.; Bergamini, G.; Bantscheff, M. *ACS Chem. Biol.* **2016**, *11*, 2541–2550.
- (53) Lanning, B. R.; Whitby, L. R.; Dix, M. M.; Douhan, J.; Gilbert, A. M.; Hett, E. C.; Johnson, T. O.; Joslyn, C.; Kath, J. C.; Niessen, S.; Roberts, L. R.; Schnute, M. E.; Wang, C.; Hulce, J. J.; Wei, B.; Whiteley, L. O.; Hayward, M. M.; Cravatt, B. F. *Nat. Chem. Biol.* **2014**, *10*, 760–767.
- (54) Niessen, S.; Dix, M. M.; Barbas, S.; Potter, Z. E.; Lu, S.; Brodsky, O.; Planken, S.; Behenna, D.; Almaden, C.; Gajiwala, K. S.; Ryan, K.; Ferre, R.; Lazear, M. R.; Hayward, M. M.; Kath, J. C.; Cravatt, B. F. *Cell Chem. Biol.* **2017**, *24*, 1388–1400.
- (55) Yu, X.; Long, Y. C.; Shen, H. M. *Autophagy* **2015**, *11*, 1711–1728.
- (56) Klaeger, S.; Gohlke, B.; Perrin, J.; Gupta, V.; Heinzlmeir, S.; Helm, D.; Qiao, H.; Bergamini, G.; Handa, H.; Savitski, M. M.; Bantscheff, M.; Médard, G.; Preissner, R.; Kuster, B. *ACS Chem. Biol.* **2016**, *11*, 1245–1254.
- (57) Cahn, A.; Hamblin, J. N.; Beggs, M.; Wilson, R.; Dunsire, L.; Srisankarajah, S.; Montembault, M.; Leemereise, C. N.; Galinanes-Garcia, L.; Watz, H.; Kirsten, A. M.; Fuhr, R.; Hessel, E. M. *Pulm. Pharmacol. Ther.* **2017**, *46*, 69–77.
- (58) Kazmi, F.; Hensley, T.; Pope, C.; Funk, R. S.; Loewen, G. J.; Buckley, D. B.; Parkinson, A. *Drug Metab. Dispos.* **2013**, *41*, 897–905.
- (59) Thorarensen, A.; Dowty, M. E.; Banker, M. E.; Juba, B. M.; Jussif, J.; Lin, T.; Vincent, F.; Czerwinski, R. M.; Casimiro-Garcia, A.; Unwalla, R.; Trujillo, J. I.; Liang, S.; Balbo, P.; Che, Y.; Gilbert, A. M.; Brown, M. F.; Hayward, M.; Montgomery, J.; Leung, L.; Yang, X.; Soucy, S.; Hegen, M.; Coe, J.; Langille, J.; Vajdos, F. F.; Chrencik, J. E.; Telliez, J.-B. *J. Med. Chem.* **2017**, *60*, 1971–1993.
- (60) Engel, J.; Lategahn, J.; Rauh, D. *ACS Med. Chem. Lett.* **2016**, *7*, 2–5.
- (61) Iyer, G. H.; Moore, M. J.; Taylor, S. S. *J. Biol. Chem.* **2005**, *280*, 8800–8807.
- (62) Zaro, B. W.; Whitby, L. R.; Lum, K. M.; Cravatt, B. F. *J. Am. Chem. Soc.* **2016**, *138*, 15841–15844.